GNGTS 2024

APPLIED GEOPHYSICS FOR ENERGY, ENVIRONMENT AND NEW TECHNOLOGIES

Session 3.2

Near surface geophysics

Convenors of the session:

***Emanuele Forte* – eforte@units.it**
***Chiara Colombero* – chiara.colombero@polito.it**
***Michele Cercato* – michele.cercato@uniroma1.it**

Contributions recommended for this session:

- **Innovative geophysical techniques;**
- **Quantitative data integration;**
- **Geophysical data processing;**
- **Geophysical modeling;**
- **Time-lapse geophysical approaches;**
- **Geophysics for hydrogeological properties and hydrological dynamics (Hydrogeophysics);**
- **Geophysics for biological interactions (Biogeophysics);**
- **Geophysics for cultural heritage (Archaeogeophysics);**
- **Geophysics for environmental risks (Environmental Geophysics);**
- **Geophysics for applied geology and engineering (Engineering Geophysics).**

There is a growing need to quantitatively characterize the near surface and related anthropic structures, providing a reliable estimate of their geometric, mechanical and hydraulic characteristics through the use of high-resolution, environmentally and economically sustainable techniques.
This session is open to contributions that illustrate methodological innovations, processing methods, case studies and applications of different geophysical methods, typically at high resolution, in all the above mentioned fields.

Applicability of cheap and lightweight magnetic sensors to geophysical exploration

F. Accomando[1] and G. Florio[1]

[1] Dipartimento di Scienze della Terra, dell'Ambiente e delle Risorse – Università di Napoli "Federico II", Italia.

In recent years, there was a notable technological advancement in geophysical sensors. In the case of magnetometry, several sensors were used having the common feature to be miniaturized and lightweight, thus idoneous to be carried by UAV in drone-borne magnetometric surveys. Moreover, such sensors have the common feature to be very cheap, so that it is in principle very easy to have the resources to combine two or three of them to form gradiometers. Nonetheless, another common feature is that their sensitivity ranges from 0.1 to about 200 nT, thus not comparable to that of alkali vapor, standard flux-gate or even proton magnetometers. However, their low-cost, small volume and weight remain as very interesting features of these sensors. In this communication, we want to explore the range of applications of small tri-axial magnetometers commonly used for attitude determination in several devices. We compare the results of ground-based surveys performed with conventional geophysical instruments with those obtained using these sensors.

Corresponding author: filippo.accomando@unina.it

Exploring rockfall precursors through unsupervised deep-learning clustering analysis

G.M. Adinolfi [1] , C. Comina [1], S.C. Vinciguerra [1]

[1] *Department of Earth Sciences, University of Turin, Turin, Italy*

Studying rock mass stability is greatly enhanced by the powerful tool of seismic monitoring. This technique allows for continuous recording, making it easier to analyse spatiotemporal activity related to gravitational instabilities. Seismic monitoring is essential for detecting and assessing damage and cracking processes as precursors to macroscopic failures.

In this research, we present initial findings from seismic monitoring conducted at a test site where a rockfall occurred shortly after deploying a small-aperture array of three seismic stations, covering approximately 100 meters. These stations were equipped with a tri-axial velocimetric sensor and data-loggers sampling at 250 Hz. The specific focus of the seismic array was to survey potential instabilities originating from structural weaknesses, including deformation bands, joints, and lithological contacts. The installation of the site-specific seismic array preceded a rockfall event by about a month. The rockfall occurred at the lithological contact between folded gneisses and a unit of dolomitic limestones, predominantly composed of dolomites and dolomitic saccharoid marbles. The seismic signature of the rockfall persisted for approximately 10 seconds, and spectral analysis revealed the occurrence of multiple sub-episodes of slip triggered by the initial rupture.

No apparent correlations between precursory activity and the rockfall occurrence were identified through traditional seismological approaches. In response to this challenge, we applied a recently developed unsupervised deep-learning method for clustering signals in continuous multichannel seismic time series. This method combines a deep scattering network for automatic feature extraction with a Gaussian mixture model for clustering. Our successful application of this approach led to the identification of seismic signals associated with the rockfall, encompassing various slip episodes, along with their initiation and propagation. Additionally, we detected precursory activity occurring approximately 2 hours before the rockfall, consistently identified through the clustering analysis (Fig. 1).

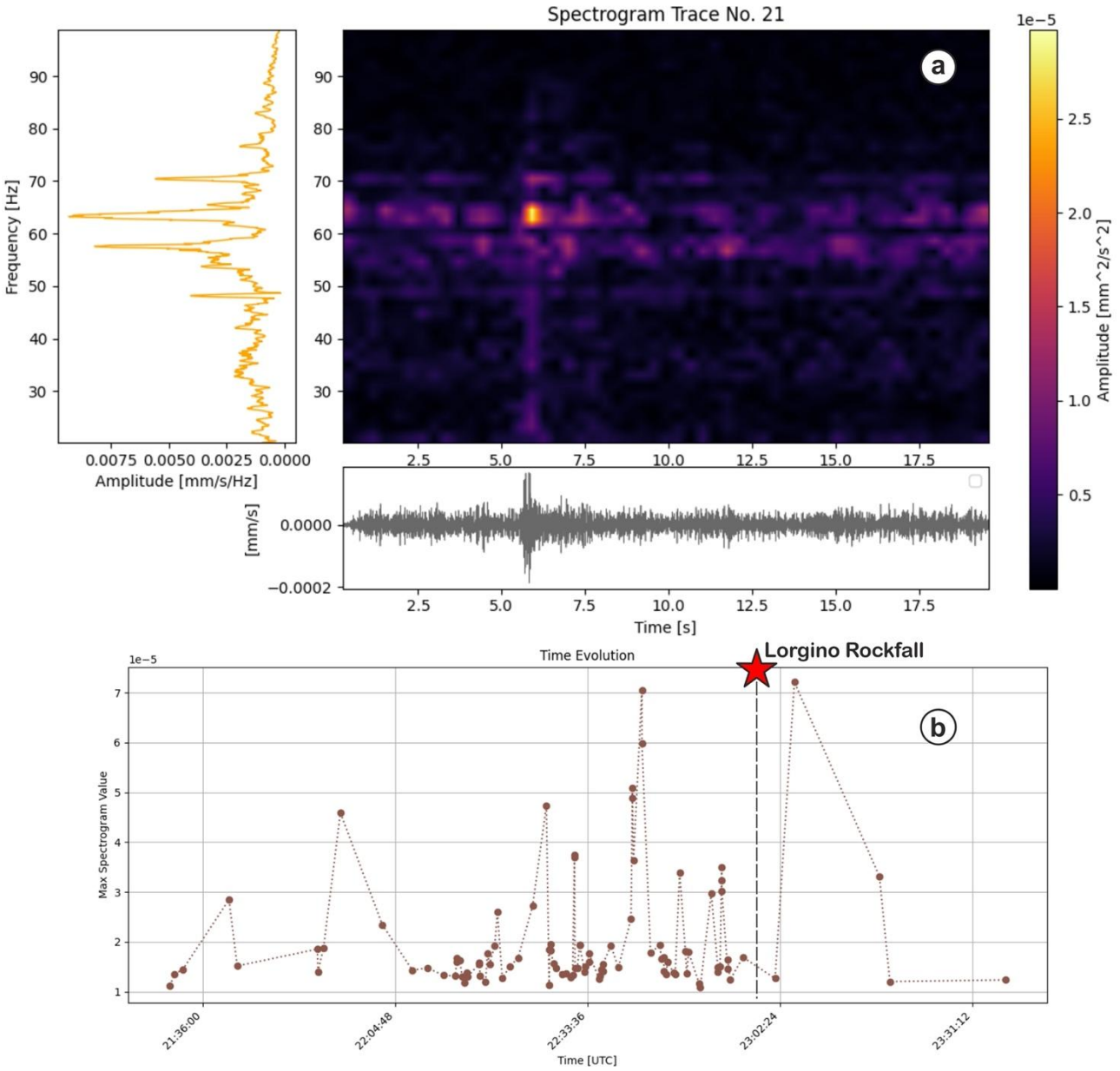

Figure 1 a) Example of time-frequency analysis for a precursory event. b) Amplitude vs time of precursory seismic signals

Preliminary results indicate a slow initiation process, potentially linked to a precursory nucleation phase driven by an intermittent preparatory process before the large stick–slip acceleration accompanying the rock mass failure. Despite their low amplitude and absence of direct visibility in raw seismic records, these signals were effectively discerned through the deep learning analysis.

References

Seydoux, L., Balestriero, R., Poli, P., Hoop, M. D., Campillo, M., & Baraniuk, R.; 2020: *Clustering earthquake signals and background noises in continuous seismic data with unsupervised deep learning.* Nature communications, 11(1), 3972.

Corresponding author: guidomaria.adinolfi@unito.it

Combined 3D surface wave and refraction analysis around the Scrovegni Chapel in Padua, Italy

I. Barone[1], M. Pavoni[1], J. T. F. Ting[1], J. Boaga[1,3], G. Cassiani[1,3], D. Dupuy[4], R. Deiana[2,3]

[1] Università degli Studi di Padova, Dipartimento di Geoscienze, Padova
[2] Università degli Studi di Padova, Dipartimento dei Beni Culturali, Padova
[3] Università degli Studi di Padova, Centro Interdipartimentale di Ricerca Studio e Conservazione dei Beni Archeologici, Architettonici e Storico-Artistici (CIBA), Padova
[4] Geo2x SA, Yverdon-les-Bains, Svizzera

The Scrovegni Chapel in Padua (Italy) is part of the Padua UNESCO World Heritage site since 2021. The chapel hosts a worldwide famous fresco cycle of Giotto dating back to the 14th century, and it is located in a complex archaeological area hosting remains of several periods. In particular, the façade of the chapel stands on the remains of the elliptical middle wall of a Roman amphitheatre. Many aspects are still unclear, especially regarding the interconnection between the two monuments and the presence of buried radial walls of the amphitheatre in that area (Deiana et al., 2018).

Following the previous studies from Barone et al. 2022 and Barone et al. 2023, a new active seismic data acquisition has been carried out using 28 source locations and 188 seismic nodes, placed all around the chapel on a regular grid of 3 m spacing in both spatial directions (Fig. 1). The new survey area partially overlaps the previously investigated areas. The source used is a weight drop with a 50 kg mass falling from a height of approximately 2 m. Each shot was repeated twice to increase the signal-to-noise ratio. A combination of single-component (1C) and three-component (3C) nodes was used. Although only the vertical component was considered for the analyses described hereinafter, the 3C recordings were used to study the seismic waves ellipticity.

The same shot records have been analysed with two different methods: surface wave tomography and first arrival traveltime tomography. As for the surface wave analysis, the same procedure used in Barone et al. 2022 was used, including: preliminary analysis for modes identification, pseudo 2D f-k filtering to remove higher-modes and backscattering, phase unwrapping, traveltime extraction and Eikonal tomography (Lin et al. 2009). The outcome of this procedure consists in a series of phase velocity maps, each referring to a different frequency of analysis between 10 Hz and 50 Hz. Autospectrum gradient maps were also computed, which reflect sudden amplitude changes due to abrupt lateral velocity variations.

The 3D first arrival traveltime tomography (Heincke et al. 2006) included the picking of the first breaks for all 3D gathers and inversion through the software GEOGIGA (Technology Corp.). Some preliminary analysis was needed in order to find the optimum parameters for inversion, including the generation of synthetic 2D and pseudo 3D models. Picking of first break times for the real 3D dataset was done manually and revealed the most time-consuming processing step, due to the high level of urban noise polluting the data.

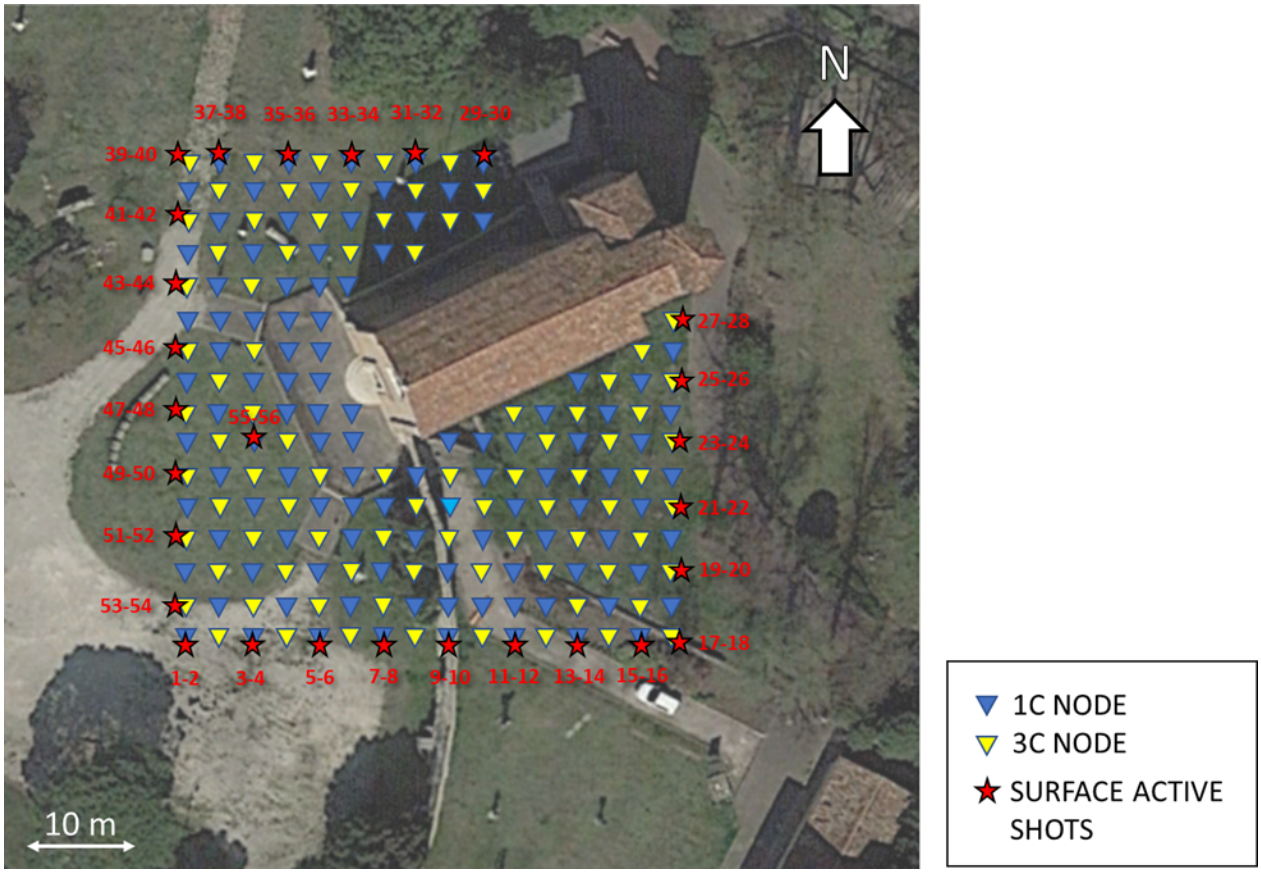

Fig. 1 – Acquisition scheme for the dense 3D seismic survey. 1C and 3D seismic nodes are represented as blue and yellow triangles, respectively, while active source locations are represented as red stars.

The phase velocity maps, the autospectrum gradient maps and the 3D Vp model from first arrival traveltime tomography reveal the same velocity anomalies, corresponding to known archaeological features such as the walls of the Roman amphitheatre and probable reinforced concrete structures built during the Second World War in order to protect the chapel. A low-velocity area in the south-western side of the study area, already mapped in Barone et al. 2022 and Barone et al. 2023, is clearly visible. Finally, a high-velocity area in the eastern side is also imaged, whose origin is uncertain and that will need further investigations.

In conclusion, this study demonstrates that a combined surface wave and refraction analysis using dense 3D seismic data can be helpful for archaeological prospection. Despite the noisy urban context, the limited number of sensors (with respect to our previous studies) and the non-optimum geophone spacing, especially for surface wave analysis, a spatial resolution of a few

meters was obtained. Further work will include depth inversion of phase velocity maps, in order to obtain a pseudo-3D Vs model.

Acknowledgments

This study, made possible by the willingness and support of the Culture Office of the Municipality of Padua, was funded under the agreement between the Veneto Regional Secretariat of the Italian Ministry of Culture (MiC) and the CIBA Interdepartmental Research Center of the University of Padua under the umbrella of WCRI SYCURI.

References

Barone, I., Cassiani, G., Ourabah, A., Boaga, J., Pavoni, M. and Deiana, R.; 2022: Surface wave tomography using dense 3D data around the Scrovegni Chapel in Padua, Italy. Scientific Reports, v. 12, 11806. doi: 10.1038/s41598-022-16061-1

Barone, I., Cassiani, G., Ourabah, A., Boaga, J., Pavoni, M. and Deiana, R.; 2023: Integrating controlled-source and ambient noise seismic measures for archaeological prospection: the Scrovegni Chapel case. Geophysical Journal International, v. 232, pp. 1944–1956. doi: 10.1093/gji/ggac432

Deiana, R.; 2018: L'importanza dell'approccio multidisciplinare: considerazioni a valle del progetto dell'Università di Padova sulla Cappella degli Scrovegni. In La Cappella degli Scrovegni nell'anfiteatro romano di Padova: nuove ricerche e questioni irrisolte, Padova University Press.

Heincke, B., Maurer, H., Green, A. G., Willenberg, H., Spillmann, T. and Burlini, L.; 2006: Characterizing an unstable mountain slope using shallow 2D and 3D seismic tomography, GEOPHYSICS, v. 71, n.6, B241-B256.

Lin, F.C., Ritzwoller, M.H. and Snieder, R.; 2009: Eikonal tomography: surface wave tomography by phase front tracking across a regional broad-band seismic array. Geophysical Journal International, v. 177, pp. 1091-1110. doi: 10.1111/j.1365-246X.2009.04105.

Corresponding author: ilaria.barone@unipd.it

P-and S-velocity 3D model for the characterisation of the subsurface beneath the village of Arquata del Tronto

G. Böhm[1], A. Affatato[1], L. Baradello[1], G. Brancatelli[1], E. Forlin[1], F. Meneghini[1]

[1] National Institute of Oceanography and Applied Geophysics – OGS (Italy)

1. Introduction

The 2016-2017 seismic sequence in the Central Apennines has, once again, demonstrated the importance of different seismic effects in complex geological contexts at short distances (e.g., valleys filled with soft sediments, hilltops, complex buried geometries). The severe damage reported by ancient settlements located on the top of a rocky hill, as in the case of Arquata del Tronto, has underlined the need to define an accurate three-dimensional numerical model (topography, seismo-stratigraphic, geomechanical, geotechnical characteristics, etc.) in order to best model the local seismic response through appropriate numerical simulations.
This work describes the results of a high-resolution reflection seismic acquisition (P-wave and S-wave) carried out at the Arquata del Tronto (AP) site for the geophysical characterization of the subsurface, as part of the public intervention "Progetto di suolo (terrazzamenti)" in the historic centre of Arquata del Tronto (AP). The final product of this study was a 3D velocity model obtained by the travel time tomography of the picked first break from the acquired seismic survey.

2. Seismic acquisition

The seismic survey made at this site consists of 3 separate lines (Fig. 1).
The acquisition of Line 1 (source spacing 4 m, group spacing 2 m), was carried out in 3 phases, using the electrodynamic vibrator (ELVIS VII) with 20-220 Hz, 10 seconds sweep as the source:
- with the P source and P geophones (10 Hz);
- with the S source oriented at an angle of 5° N (corresponding to the average strike direction of the outcropping formations) and the S geophones (14 Hz single component geophones oriented at the same angle of 5° N), called SA;
- with the S source oriented at an angle of 95° N (perpendicular to the strike direction) and the S geophones (single component geophones oriented at the same angle of 95° N), called SB.
Line 2 (source spacing 4 m, group spacing 2 m), was acquired with the shotgun as the source and the P geophones.
Line 3 (source spacing 8 m, group spacing 4 m), was acquired in 2 stages using the P-source ELVIS VII (20-220 Hz, 10 s sweep) and S-source MiniVib IVI T-2500 (20-200 Hz, 10 s sweep):
- with the P source and P geophones;
- with the S source aligned perpendicular to the local direction of the line and the S geophones (single component geophones, all oriented at an angle of 5° N);

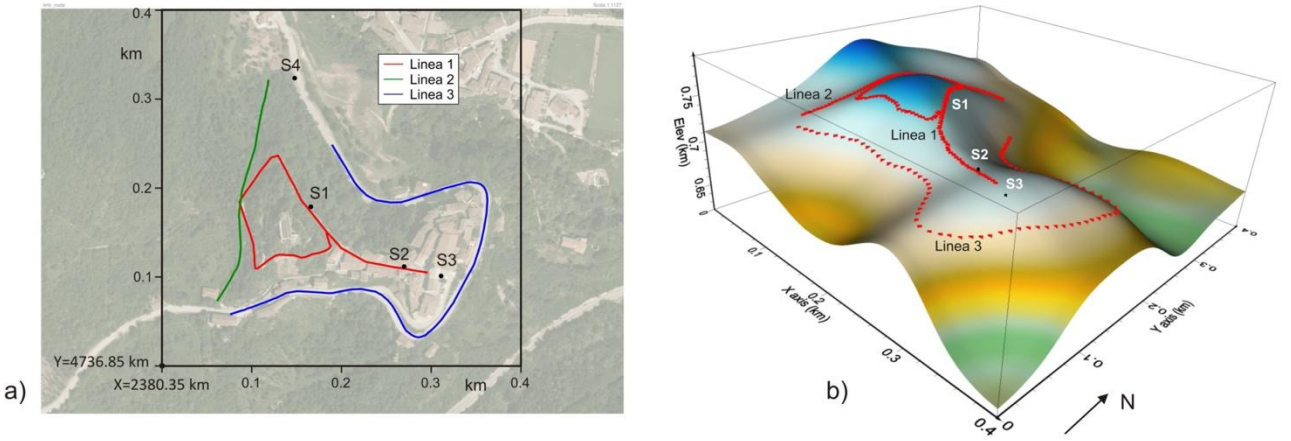

Fig. 1 – a) Location of the 3 seismic lines and the area used for the tomographic model (black rectangle) with the aerial image of the Arquata del Tronto area in transparency. The black dots represent the locations of the wells drilled in the area (S1, S2, S3 and S4). The coordinates of the lower right vertex are given in the Monte Mario/Italy Zone 2 reference system B) 3D view of the line positions with respect to the topography of the area.

3. 3D velocity model

All 3 seismic lines were taken into account in the reconstruction of the 3D velocity model (Figg. 2, 3). All coordinates (referred to Monte Mario/Italy zone 2, in the Gauss-Boaga projection) were referenced to an X=0 Y=0 origin, which corresponds to the point X=2380.35 km and Y=4736.85 km (Fig. 1).

The Cat3D software developed by OGS was used for the inversion of the arrival times. The tomographic method used for these data is based on a ray tracing algorithm (Böhm et al., 1999) for the direct model and the iterative method SIRT (Simultaneous Iterative Reconstruction Technique) (Stewart, 1991) for the travel time inversion. In addition, a model optimization technique based on the staggered grid method (Vesnaver and Böhm, 2000) was applied, which increases the resolution of the final inversion model by summing multiple tomographic solutions obtained from a well-conditioned (low null space) base grid shifted in the X and Y directions, while preserving the reliability of the tomographic solution proper to the base grid.

In general, the acquired seismic data showed the presence of coherent noise (air waves, ground roll, diffractions), which in some cases was relevant, especially in the acquisitions with S waves source. This is partly due to the presence of loose sediments or filling material below the surface (especially in the area of the old village) and the presence of walls, ditches and scarps close to the survey lines, which sometimes led to interference in the data caused by reflected and/or refracted lateral arrivals from these elements.

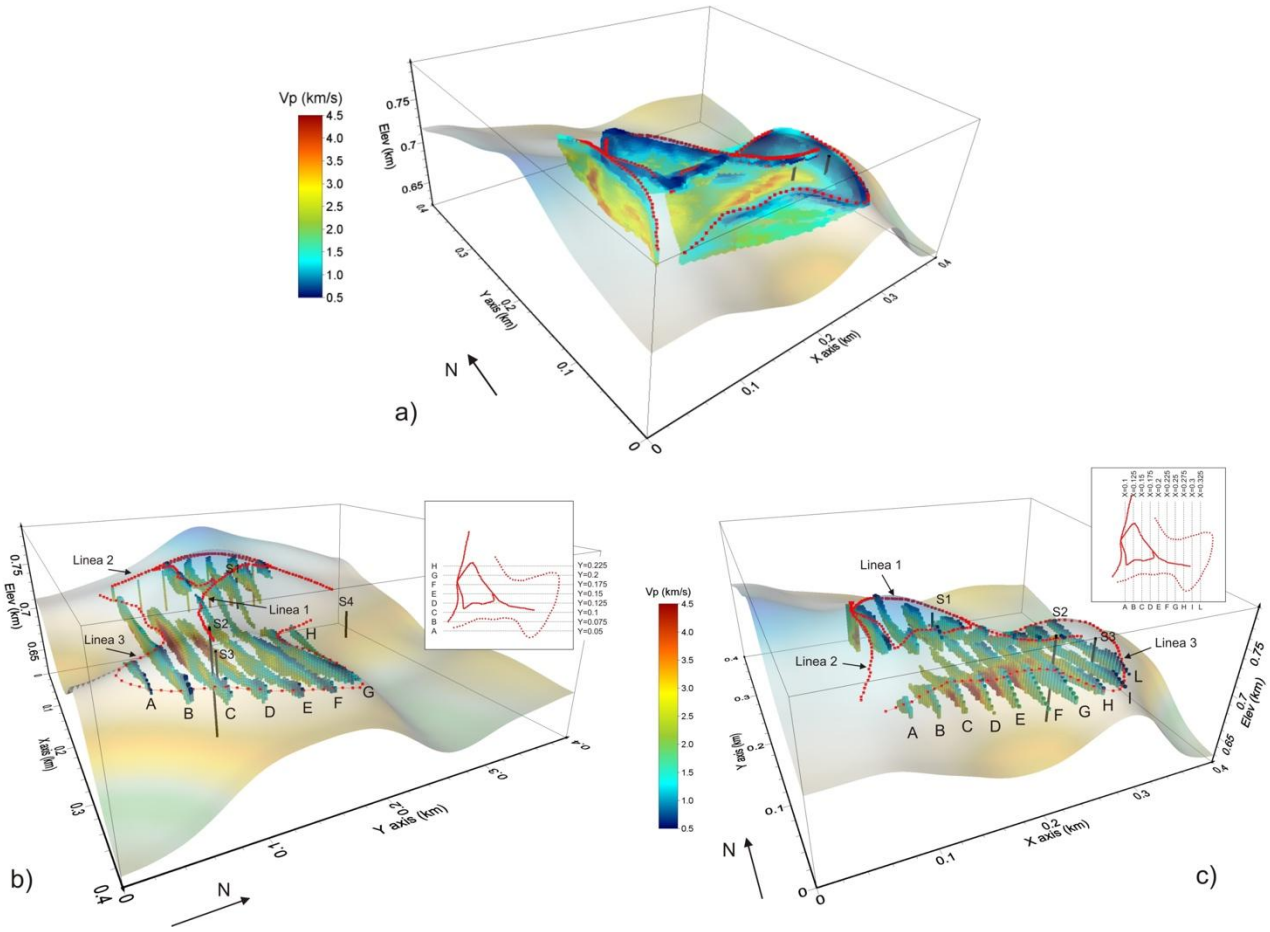

Fig. 2 – Complete 3D Vp model from the travel time tomography of the three lines. a) 3D view. b) Vertical sections extracted along the east-west direction and spaced 25 m apart (see map top right). c) Vertical sections extracted along the north-south direction and spaced 25 m apart (see map top right).

For each line, we inverted the travel times of the first arrivals , which were treated as related to diving waves in the ray tracing used for the inversion.

The resolution of the final tomographic models for Lines 1 and 2 is 2.5 m both in horizontal and vertical directions, starting from a base grid of 10x10 m (horizontally), while for Line 3, the resolution of the final velocity model is 5 m (horizontally) per 2.5 m (vertically), starting from a base grid of 15x15 m (horizontally).

For each inversion, the reliability of the tomographic solution was checked by analysing the time residuals (difference between the observed travel times and those calculated on the final model). In all instances of inversions based on the P times, root mean square (rms) values for the time residuals were approximately 3.5% in relation to the observed times. This corresponds to about 2.3 ms for Line 1, 3.1% with 1.3 ms for Line 2, and 1.6% along with 1.5 ms for Line 3 (which exhibited the lowest residuals).

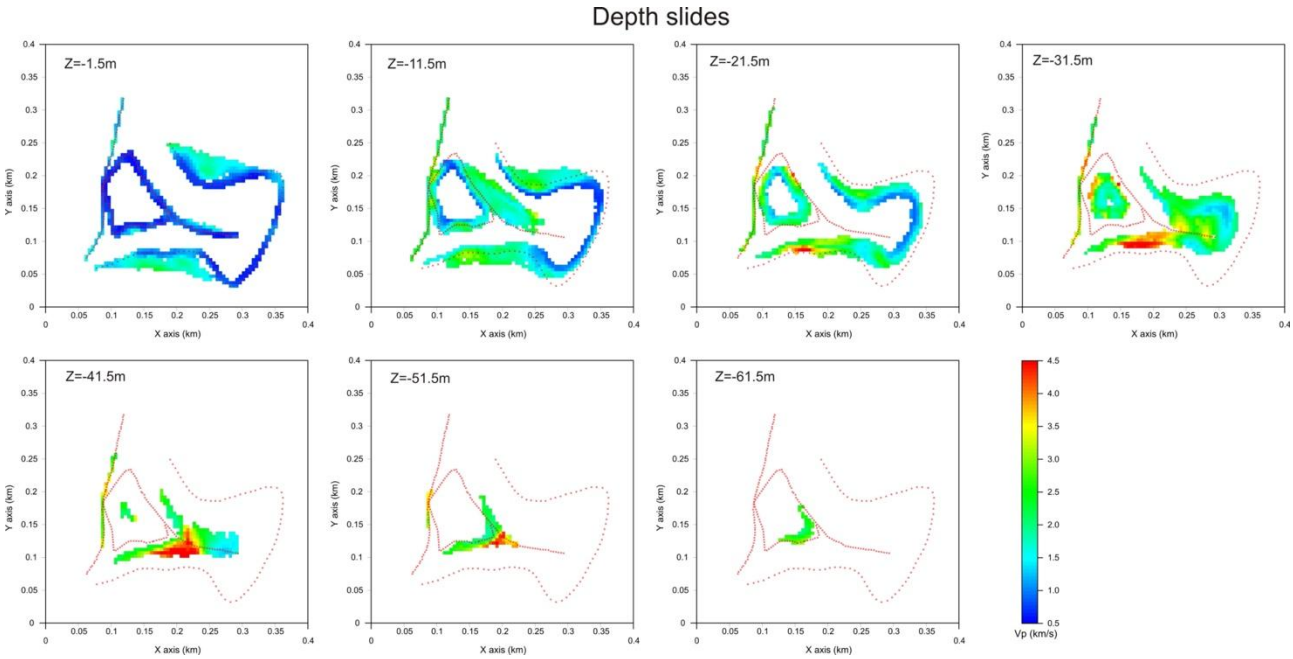

Fig. 3 – Horizontal slices corresponding to different depths of the final 3D tomographic P velocity model. The Z coordinate denotes the depth in relation to the corresponding topographic elevation.

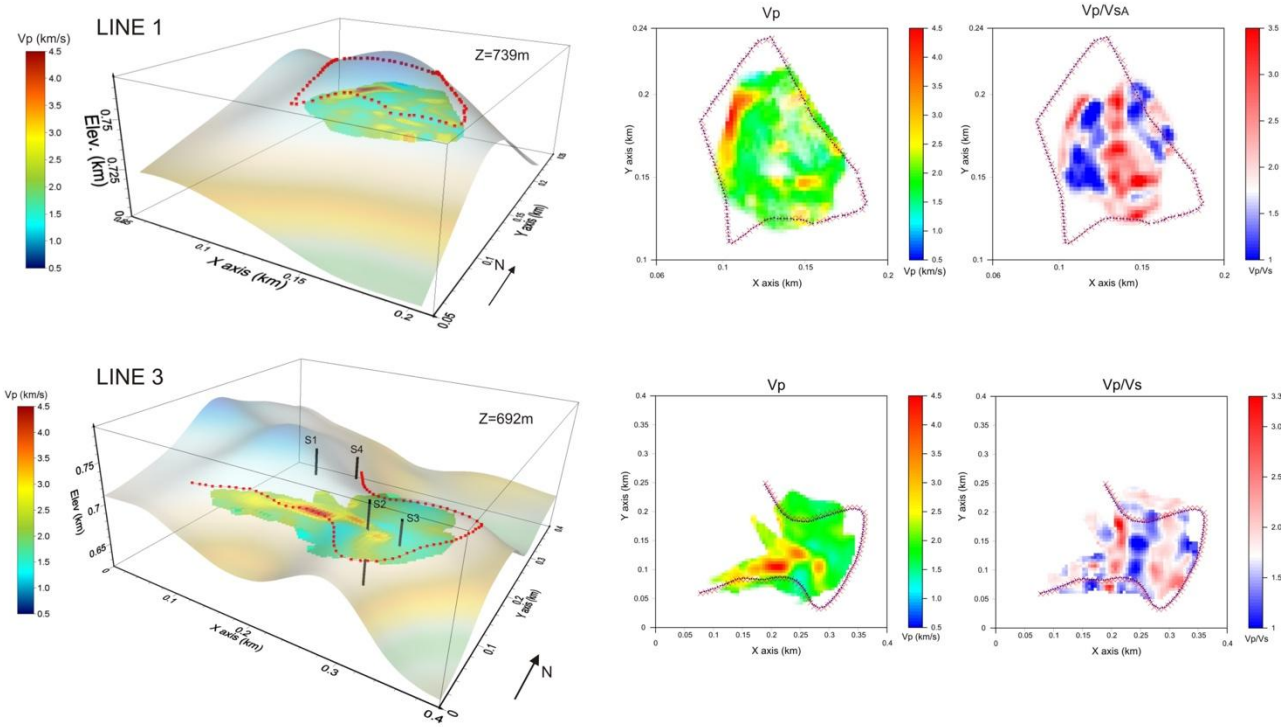

Fig. 4 – Horizontal sections of velocity volume corresponding to Z = 0.739 m (Line 1) and Z = 692 m (Line 3) for P velocity and Vp/Vs ratio.

4. Results and conclusions

In the surveyed area, there exist regions with elevated P velocities ranging between 3.5 and 4.5 km/s, extending to relatively shallow depths, even beneath Line 2. Conversely, in other zones,

heightened P velocities are observed primarily in the southernmost part of the hill, approximately 30 meters below the topographic surface. Notably, the structure directly beneath the centre of the old village exhibits comparatively lower P velocities. The region enclosed by the perimeter of Line 1 displays a heterogeneous distribution of P and S velocities, with the exception of the high-velocity zone on the western side, aligning with the elevated velocities detected beneath Line 2. Regarding S velocities, the reliability of the inversion is compromised by increased noise compared to P data, exacerbated by lateral events interfering with the first break signals used for inversion. Despite these challenges, an analysis of the Vp/Vs ratio maps (Fig. 4) reveals a discernible pattern showcasing alternating low and high values, following bands oriented in a north-south direction. This pattern broadly corresponds to the strike values of subsurface formations identified in the area.

Acknowledgments

The authors thank the entire OGS acquisition group for the professional level demonstrated in the tough acquisition task, the Marche Region Special Reconstruction Office (USR) for the permission to publish these data and results, Prof. Carlo G. Lai (Eucentre Foundation, Pavia), Prof. Alessandro Pagliaroli and Prof. Alberto Pizzi of the University of Chieti for their advice and valuable suggestions.

References

Böhm G., Rossi G., Vesnaver A.; 1999: Minimum-time ray tracing for 3-D irregular grids. Journal of seismic exploration, 8, 117-131.

Stewart R.; 1991: Exploration Seismic Tomography: Fundamentals. Course note series, vol. 3, S. N. Domenico, Editor. SEG - Society of Exploration Geophysicists.

DOI: https://doi.org/10.1190/1.9781560802372.

Vesnaver A., Böhm G.; 2000: Staggered or adapted grids for seismic tomography? The Leading Edge 19(9), 944-950. DOI: https://doi.org/10.1190/1.1438762.

Corresponding author: gbohm@ogs.it

Monitoring of the saline wedge in the Po di Goro river.

P. Boldrin[1], E. Ferrari[1], F. Droghetti[1], A. Bondesan[2], E. Rizzo[1]

[1] *University of Ferrara (Dipartimento di Fisica e Scienze della Terra, Ferrara, Italy)*
[2] *Consorzio di Bonifica di Ferrara (Italy)*

Keywords: salt wedge intrusion, EM, climate change, tides

Seawater intrusion in coastal aquifers is a worldwide problem caused, among other factors, by aquifer overexploitation related to human activities, such as irrigation and drinking water supply, and the reduction in natural groundwater recharge due to climate change [1]. In order to prevent or limit the degradation of both surface water and groundwater quality due to saltwater contamination, research studies have been conducted to gain a comprehensive understanding of the issue, identify fundamental parameters, and assess possible corrective measures.

The territory of the Po Delta is characterized by minimal slopes and it is largely situated below sea level. The elevation profile of the territory significantly influences land management. The morphological characteristics of the Po Delta make the largest Italian wetland particularly unstable and very fragile when subjected to human pressure. Only the application of careful policies concerning coastal defence, flood mitigation, anthropogenic subsidence reduction and salt wedge intrusion control will allow reduction of the present or predicted negative effects [2].

In order to detect the salinity of the water river, a probe system that measure the water conductivity (EC) is necessary. Typical monitoring system for EC data involves moving boat acquisitions, which depict a low resolution of the salt wedge detection. Moreover, long rivers are not suitable for point acquisition approach as they require long acquisition times. To overcome these limitations, geophysical methods could appear as a good alternative for fast mapping and detailed resolution. Taking in account these aspects, a monitoring research activity was applied along the Po di Goro River by geophysical method. In detail, a FDEM system was used to carry out the in-phase and out-phase components, in order to obtain the ECa distribution along the river. The geophysical monitoring began in summer 2022 [3], during the last salt wedge crisis along the Po River, and continued this summer. The first results of the Summer 2022 data set highlighted the saline wedge intrusion, on the contrary the Summer 2023 data set showed that saline intrusion was absent in the same investigated area. Anyway, the acquired data during last summer permitted to observe the influence of the tide on the advance and retreat of the salt wedge along the river (Fig.1). The results highlight the significant potential of the proposed geophysical

approach to monitor the salt wedge phenomenon during the warmer periods with increased drought but also on a daily basis due to the influence of tides.

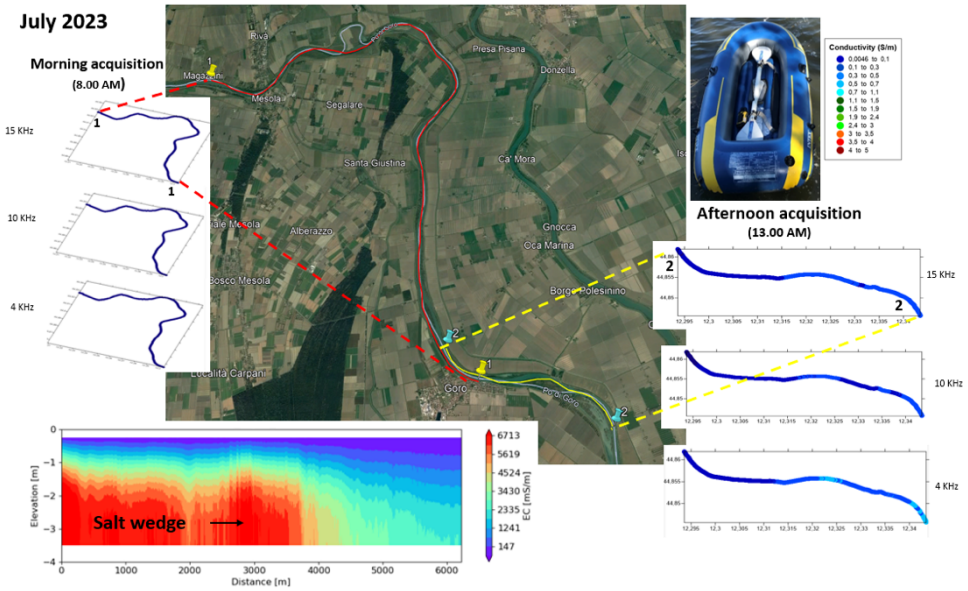

Fig.1: The map shows the pathway of the acquisitions. The acquisitions carried out in two different times of the day along part of Po di Goro (15 Km). During the morning (8.00 AM) when there was low tide and during the afternoon (13.00 PM) when there was a peak of maximum tide. The two paths have an overlap of about 1.5 Km. The different EMs were performed using different frequency of Profiler. It was located on a inflatable boat pulled by a kayak.

References

[1] Crestani E., Camporese M., Belluco E., Bouchedda A., Gloaguen E., Salandin P.; 2022: Large-Scale Physical Modeling of Salt-Water Intrusion. Water. https://doi.org/10.3390/w14081183

[2] Umberto S. Corbau C.; 2009: A review of the Delta Po evolution (Italy) related to climatic changes and human impacts. Geomorphology. http://dx.doi.org/10.1016/j.geomorph.2008.11.004

[3] Boldrin P., Bondesan A., Droghetti F, Ferrari E., Fornasari G., Neri F., Rizzo E.; 2023: DC and FDEM monitoring of the salt wedge on the Po di Goro river (Italy). Atti del 41° Convegno Nazionale del GNGTS.

Corresponding author: bldpla4@unife.it , enzo.rizzo@unife.it

Deep Electric Resistivity Tomography (DERT) on the Cazzaso Landslide

A. Bratus[1], F. Agliardi[2], O. Araujo[3], G.B. Crosta[2], G. Dattola[2], R.G. Francese[3], P. Frattini[2], M. Giorgi[1], F. Kranitz[4], S. Picotti[1]

[1] OGS – Istituto Nazionale di Oceanografia e di geofisica Sperimentale, Trieste, Italia.
[2]DISAT – Dipartimento di Scienze dell'Ambiente e della terra, Università degli Studi Milano – Bicocca, Milano, Italia.
[3]SCVSA - Dipartimento di Scienze Chimiche, della Vita e della Sostenibilità Ambientale, Università di Parma, Parma, Italia.
[4]Servizio Geologico, Regione Autonoma Friuli Venezia Giulia, Trieste, Italia.

Introduction

The Cazzaso landslide affects the eastern slope of Mt. Diverdalce, in the central part of the Fusea - Cazzaso - Sezza plateau, on the orographic right of the But River valley (Tolmezzo, Udine).
The complexity geological and geomorphological setting in which the landslide developed motivated the Geological Survey of the Autonomous Region of Friuli Venezia Giulia to collaborate with the OGS (National Institute of Oceanography and Experimental Geophysics), to better constrain the hydrogeological instability phenomena associated to the Cazzaso landslide by using cutting edge geophysical techniques. The resulting geophysical model of the subsoil was then exploited to study the landslide instability by the Department of Environment and Earth Sciences (DISAT) of the Bicocca University of Milan.

Geological, geomorphological and landslide settings

The Cazzaso landslide complex, reported since 1807 and reactivated as of October 1851, displaced the entire Cazzaso village up to 24 m causing the destruction of some buildings (Zuliani et al., 2021). Currently, three landslide perimeters are defined in the Italian landslide inventory (IFFI) (Trigila and Iadanza, 2007): two translational slides and one complex landslide.
Rock outcropping in the area belong to the sedimentary sequence of the Late Triassic Raibl group (Carnic). The Raibl group, between the formation of the Schlern and the Main Dolomite, consists of a very heterogeneous lithological succession, including black limestone and red sandstone, lastroid limestone, quaternary surface deposits of both morainic and slope origin, characterized by high heterogeneity.
The sequence is cut into multiple blocks by a complex network of major faults associated to the Sauris line, the most important structural feature in central-western Carnic Alps, whose main branch leads the Permo-Werfen to cover the Carnic (Carulli, 2006).
The Local geomorphology is substantially defined by the structural and lithological characteristics, which were shaped by glacial, river and gravitational activity, determining today's morphological appearance.

The Cazzaso landslide complex shows three markedly distinct sectors, with different morphological characteristics, notwithstanding the main morphogenetic agents (tectonic activity, glacial action, gravitational phenomena) are the same.
The western sector, higher in altitude, includes the large area dissected by the landslide movement. The morphology of this area is characterized by the presence of an upper slope with constant inclination and regular profile, morphologically interrupted by a well-delineated 30-m high detachment scarp, which delimits the landslide body that extends below this scarp.
The central part of the slope is occupied a morainic shelf on which the Cazzaso village stands, characterized by a slight slope towards E and locally interrupted by escarpments, which has its eastern limit at the increase in slope gradient.
The eastern part of the slope has a regular course, of medium acclivity, with outcropping rocky substratum that progressively connects with the deposits of the valley floor.

The geoelectric survey

The purpose of the geoelectric prospecting campaign was to contribute to the construction of a conceptual model of the landslide. The use of high-power transmitters (Rizzo and Gianpaolo, 2019) is a further expansion of the Electrical Resistivity Tomography (ERT) delivering a larger depth of exploration so that the method is often indicated as Deep ERT (DERT) (Bocchia et al., 2021). The survey was made using new generation instrumentation and was divided into two phases (Fig 1).

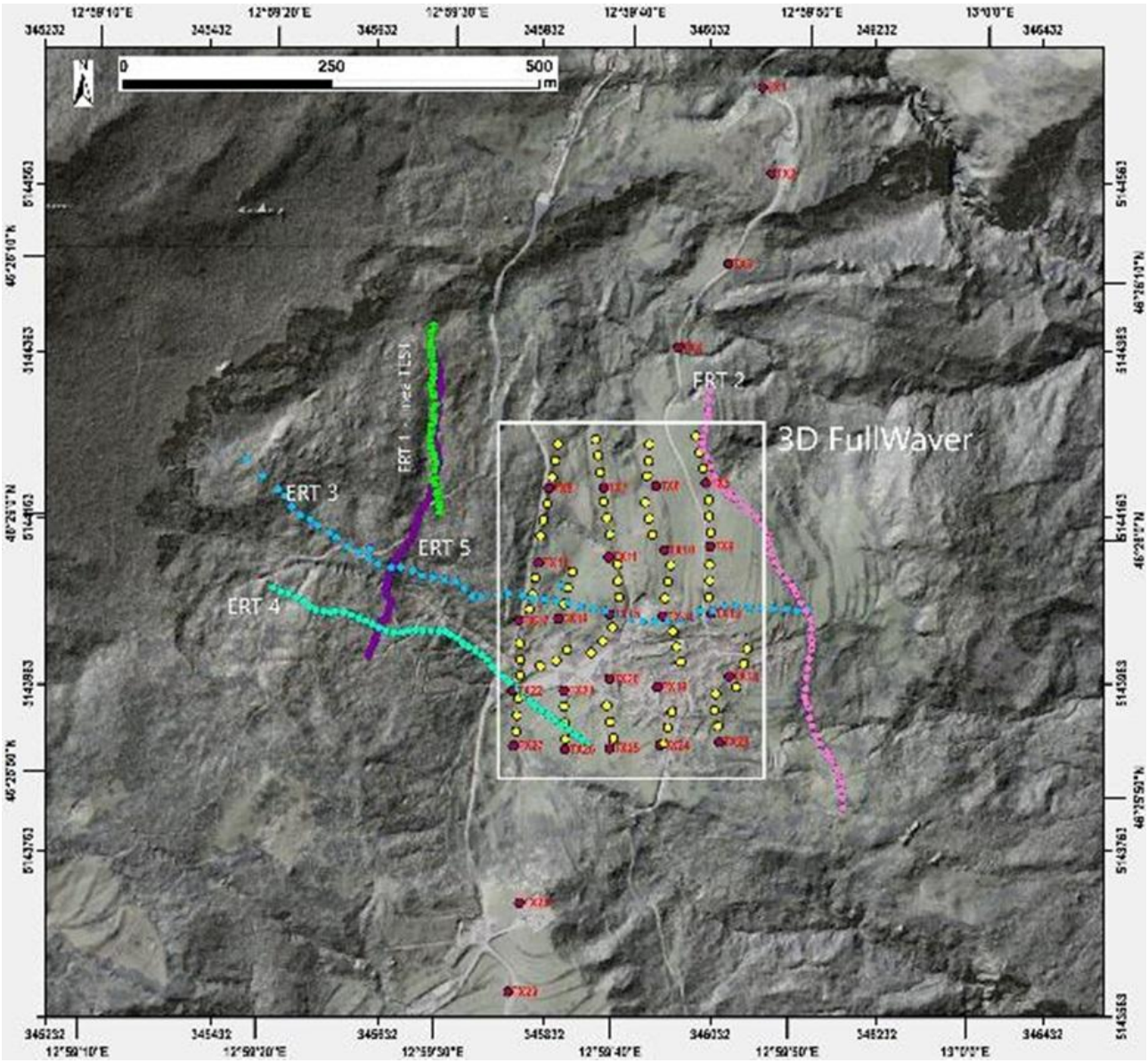

Fig 1 Layout of the MS and FW profiles in the area of the Cazzaso landslide.

In the first phase, a Multi-Source (MS) Wireless Data Acquisition was used. MS introduced a new approach for collecting DERT data (LaBrecque et al., 2013). The MS resistivity-meter has the peculiarity to control transmitting (Tx) and receiving (Rx) dipoles with short, isolated wires. It is a modular system based on stand-alone units remotely controlled via radio signals. Modularity eases the use of the system, but the real innovative and most important feature is its capability of injecting current simultaneously with different dipoles.

The campaign operations were preceded by a survey design phase which allowed to optimize the acquisition geometries. Moreover, a preliminary ERT test allowed to analyze the geophysical response of the subsurface. Then, 4 DERT lines were acquired: 2 lines transverse to the landslide (approximately in the N-S direction), and 2 longitudinal lines (approximately in the E-W direction). This arrangement enabled the investigation of both the western sector and the central sector of the slope.

16 MS units were used for a total of 48 electrodes placed on the ground. All the surveys were carried out adopting a in-line quadrupole acquisition geometry, with both single- and simultaneous multi-source (2 Tx and 4 Tx) transmitters (Bocchia et al., 2021). Further supplementary acquisitions

were carried out with the Tx/Rx dipoles translated at variable distances, internally to the line, according to a "pseudo-gradient" geometry.
In the second phase three-dimensional DERT survey was performed on the central part of the slope using the FullWaver system (Leite et al., 2017; Gance et al., 2021).
The FullWaver devices (Iris Instruments) have been designed for the measurement of resistivity, Induced Polarization and Self Potential on large 3D surfaces with complex topography. Depending on the size of the area to investigate, many V-FullWaver devices can be located on the surface of investigation, performing a continuous measurement. In the meantime, the operator moves a transmitter and the I-FullWaver on the same surface, to perform different current injections according to the survey geometry.
In our case 27 V-FullWaver were used, with a current transmission system TIPIX 3000 capable of injecting current up to 13 A.
The energization patterns were the following. A first set of 29 transmissions consists of a fixed pole A (labelled as TX 1) and a second transmitter B moving from TX2 to TX29, where the dipole aperture reaches the maximum value of about 1100 m. This acquisition sequence was followed by a backward energization scheme with the pole A fixed in TX29 and the pole B moving from TX28 to TX1. The combination of these dipole transmission patterns allowed to acquire different type of electrode arrays: dipole-dipole type, when the transmission dipole is very far from the receiving dipole; pole-dipole type, when the mobile transmitter B is close to the receiving dipole; gradient type, when both transmitters A and B are external and away from the receiving dipole.

Data Processing and inversion

ERT data processing and inversion were carried out by using the ERTLab Studio software (Fischanger et al., 2013), modified to manage both MS and FW measurements.
The application of the two methodologies produced a robust dataset where the 2D MS data and the 3D FW data are in good agreement. The maximum investigation depth, of about 110 - 120 m, has been reached by the FullWaver system under the village of Cazzaso.
The inversion algorithm is based smoothness-constrained least squares approach under the Occam assumptions and consists in minimizing the differences between calculated and measured difference of potentials (Fischanger et al., 2013).

Data Interpretation

In agreement with the geological setting, the measured physical parameters of the subsoil have been interpreted by assuming the landslide body composed by four main formations: inconsistent material; prevalence of sandstone, calcarenites; prevalence of shale and silt; dark stratified limestone and dolomite.
The interpretation of the DERT sections describes some important peculiarities, the most evident is the presence of a deep and large resistive body ascribable to the dolomite formation that increases towards the south and constitutes a barrier to the more conductive materials of the western and more steep part of the slope (fig 2).

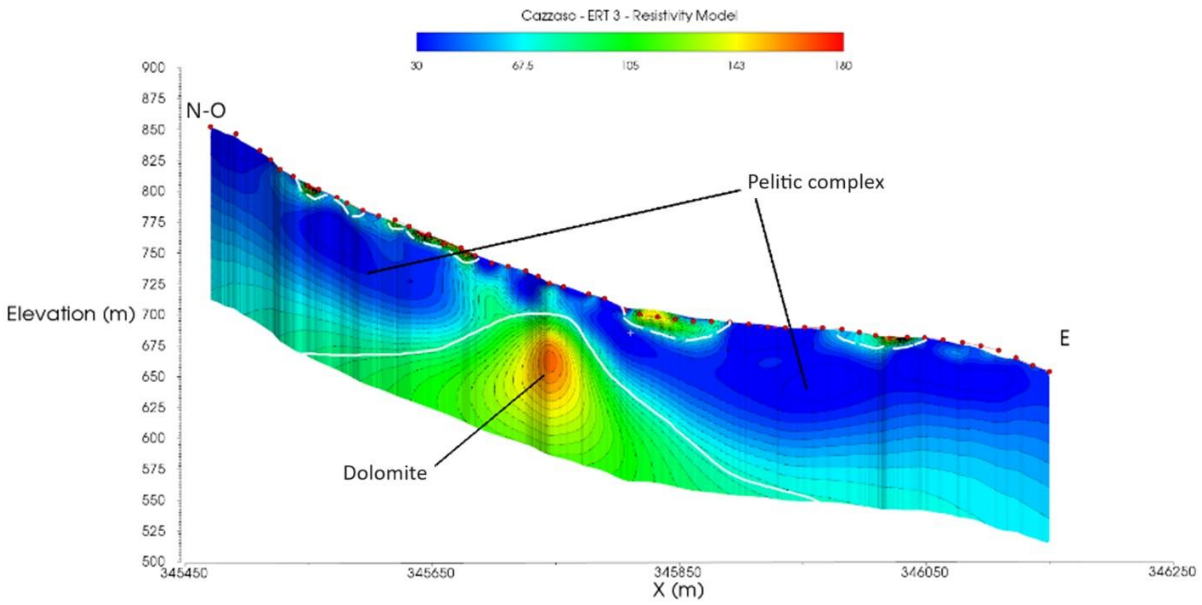

Fig 2 Resistivity model of the ERT3 line, in the transverse direction respect to the landslide.

The availability of three-dimensional resistivity model and of the of the chargeability distribution of the subsoil, up to a depth of about 100 m below the surface, has highlighted the main lithological, hydrogeological and geo-geological characteristics, identifying in detail the geometries of the conductive pelitic complex and of the surface separating this formation by the dolomite. (Fig 3)

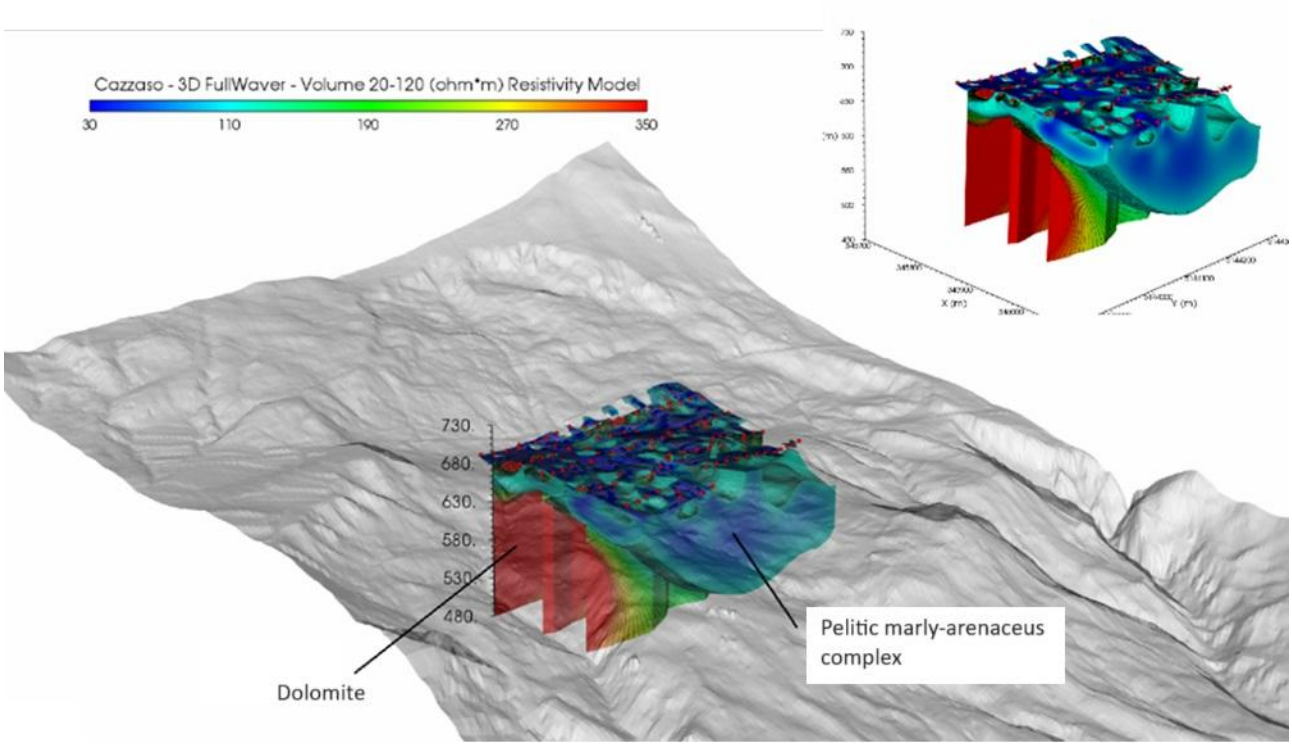

Fig 3 Resistivity volume (20 - 120 Ωm) extracted from the FullWaver cube showing the whole conductive pelitic complex and the contact between this and the dolomite.

Conclusions

The use and integrated application of innovative geophysical prospecting methodologies allowed to acquire high quality resistivity datasets, thus granting an adequate resolution even in the deepest parts of the investigated subsoil. This allowed to obtain imaging of the subsoil up to depths greater than 100 m from the surface, i.e. the depth of lithological and structural features directly constraining the development of the main Cazzaso landslide.

The geophysical models of the subsoil derived from the DERT profiles were capitalized by the study of the landslide by the University of Milano – Bicocca that drew important conclusions about the instability phenomena in the area of Cazzaso. The two slope areas, western with a higher slope, and central that refers to the terrace on which the Cazzaso village stands, are affected by phenomena of different types. The upper part of the landslide is more superficial and characterized by rapid phenomena with evolution in some cases such as to give significant displacements. The second part of is a slower and more continuous deep-seated landslide, probably with a superficial component superimposed on a very deep one that is still not well evaluated.

References

Bocchia, F., Francese, R. G., Giorgi, M., Fischanger, F., Picotti, S.; 2021: The impact of multiple transmitters on signal strength in Deep Electrical Resistivity Tomography data: an experiment in the Vajont valley (north-eastern Italy). Bulletin of Geophysics and Oceanography, Vol. 62, n. 4, pp. 687-706.

Carulli, G.B.; 2006: Note Illustrative della Carta Geologica del Friuli Venezia Giulia, Scala 1:150000; Regione Autonoma Friuli Venezia Giulia, Direzione Centrale Ambiente e Lavori Pubblici, Servizio Geologico Regionale; SELCA: Milano, Italy, pp. 1–44.

Fischanger, F., Morelli, G., Ranieri, G., Santarato, G. & Occhi, M.; 2013: 4d cross-borehole electrical resistivity tomography to control resin injection for ground stabilization: a case history in Venice (Italy), Near Surf. Geophys., 11(1), 41–50.

Gance, J., Leite, O., Lajaunie, M., Susanto, K., Truffert, C., Maillard, O., Bertrand, C., Ferhat, G., and Malet, J.-P.; 2021: Dense 3D electrical resistivity tomography to understand complex deep landslide structures, EGU General Assembly 2021, online, 19–30 Apr 2021, EGU21-14522, https://doi.org/10.5194/egusphere-egu21-14522.

LaBrecque D.J., Morelli G., Fischanger F., Lamoureux P. and Brigham R.; 2013: Field trials of the multi-source approach for resistivity and induced polarization data acquisition. In: Abstracts, AGU Fall Meeting, American Geophysical Union, San Francisco, CA, USA, NS34A-03

Leite, O., Truffert, C., Gance, J., Texier, B., Bernard, J.; 2017: A New Distributed and Cable Less System For Large 3D Electrical Resistivity Ert And Induced Polarization Tomography, 9th Congress of the Balkan Geophysical Society, Nov 2017, Volume 2017, p.1 – 5.

Rizzo E. and Giampaolo V.; 2019: New deep electrical resistivity tomography in the High Agri Valley basin (Basilicata, southern Italy). Geomatics, Nat. Hazards and Risk, 10, 197-218, doi: 10.1080/19475705.2018.1520150

Triglia, A., Iadanza, C.; 2007: “Il Progetto IFFI - Metodologia, risultati e rapporti regionali” Rapporto sulle frane in Italia, (APAT, Roma).

Zuliani, D.; Tunini, L.; DiTraglia, F.; Chersich, M.; Curone, D.; 2022: Cost-Effective, Single-Frequency GPS Network as a Tool for Landslide Monitoring. Sensors, 22, 3526. https://doi.org/10.3390/s22093526.

Corresponding author: abratus@ogs.it

What does the seismic record of a World War II bomb-explosion look like? observations from a controlled detonation in 26 november 2023 near Ferrara, Italy

Authors: *F. Brighenti[1], A. Garcia[2], R. Caputo [1]*

[1]Dipartimento di Fisica e Scienze della Terra, Università degli Studi di Ferrara, Italy
[2]Istituto Nazionale di Geofisica e Vulcanologia, Sezione di Bologna, Bologna, Italy

During restoration operations at the former Convent of San Benedetto in Corso Porta Po, in Ferrara (Italy), an unexploded aeroplane bomb from War World II (WWII) was found on the first floor of the church (see e.g., press release from the Prefecture (Prefettura - Ufficio territoriale del Governo di Ferrara 2023). In the morning of 26 November 2023 the bomb was removed from this location and later, at 14:19 (UTC), a controlled detonation of the war device was performed in a cave about 7 km NW of the city. The cave where the explosion occurred is located in an area in which a local seismic monitoring network, the SNet4Fer 3.0, operates for monitoring microseismicity around the Casaglia geothermal field (Fig. 1). SNet4Fer 3.0 is an evolution of the previous SNet4Fer 2.0 network, which is still in operation, and represents an improvement of the monitoring capabilities of the anthropogenic activities that can potentially induce seismicity in the geothermal field (Abu Zeid et al., 2017). Both networks are operated by the University of Ferrara.

The NetFer 3.0 network consists of 7 seismic stations, each equipped with a surface accelerometer and a three-component, 2 Hz borehole seismometer (with the exception of station FEM0, which has a broadband borehole seismometer), all located 148 m below ground level. In addition, the NetFer 2.0 network consists of five stations equipped with single-component (with the exception of the PONT station, which has a three-component instrument) borehole seismometers located at depths ranging from 12 to 57 m below ground level.

Figure 2 shows some examples of the seismic records of the bomb explosion; in the records it is possible to distinguish relatively, weak P and S phase arrivals as well as the seismic trace of the airwave from the airblast. Despite the energy of the explosions being relatively low, if compared to earthquakes, the records in the nearby stations can provide interesting data for different analyses as e.g., for studying the anatomy of the records, for performing forensic analyses related with the equivalent charge of the war device, and also for checking the installation of the borehole instrumentation. In this work, we present some preliminary analyses of the seismic records of this explosion.

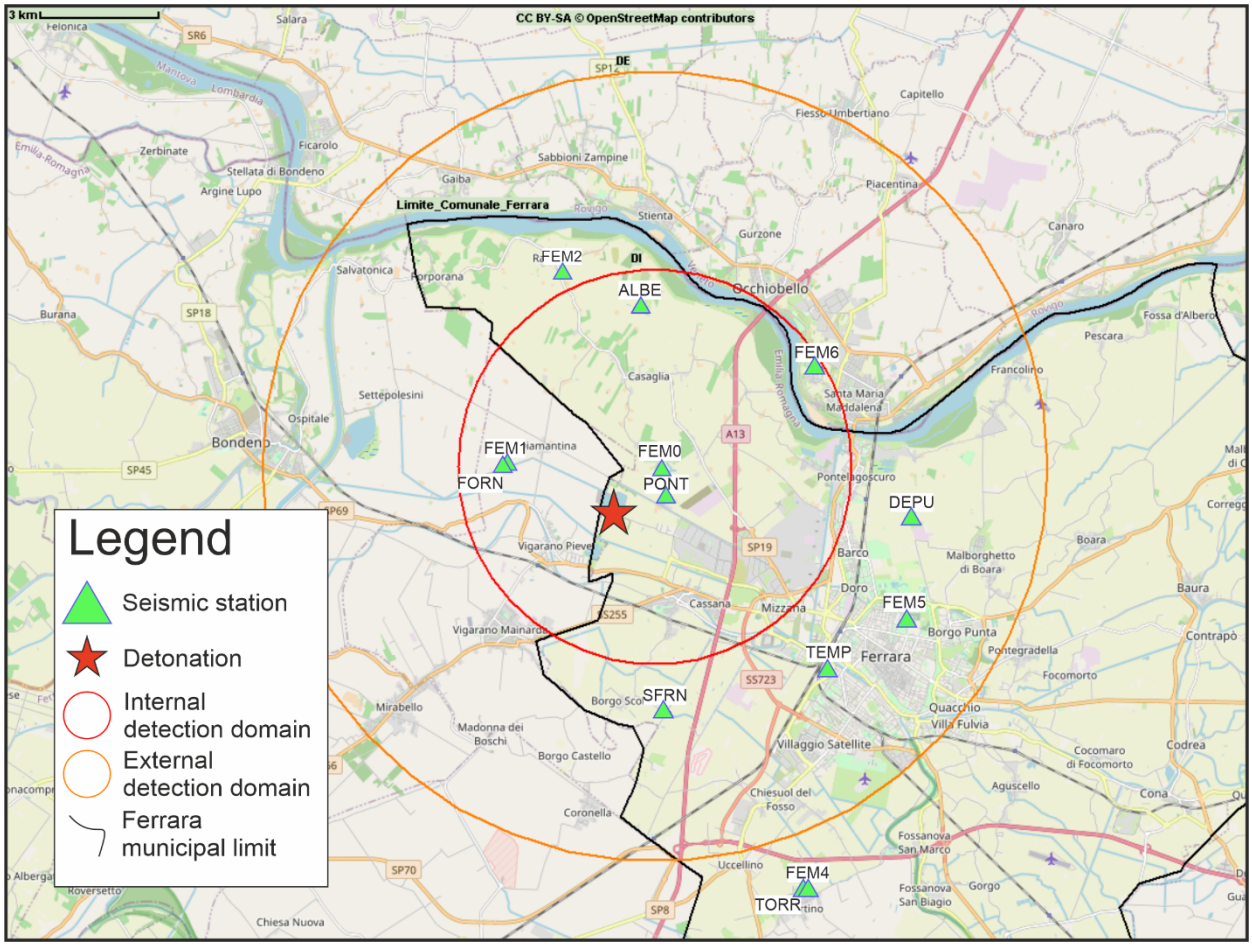

Figure 1: SNet4Fer 2.0/3.0 seismic networks (green triangles). The red star represents the point where the WWII bomb was detonated; the circles represent the internal (red) and external (orange) monitoring domains of the Casaglia geothermal field.

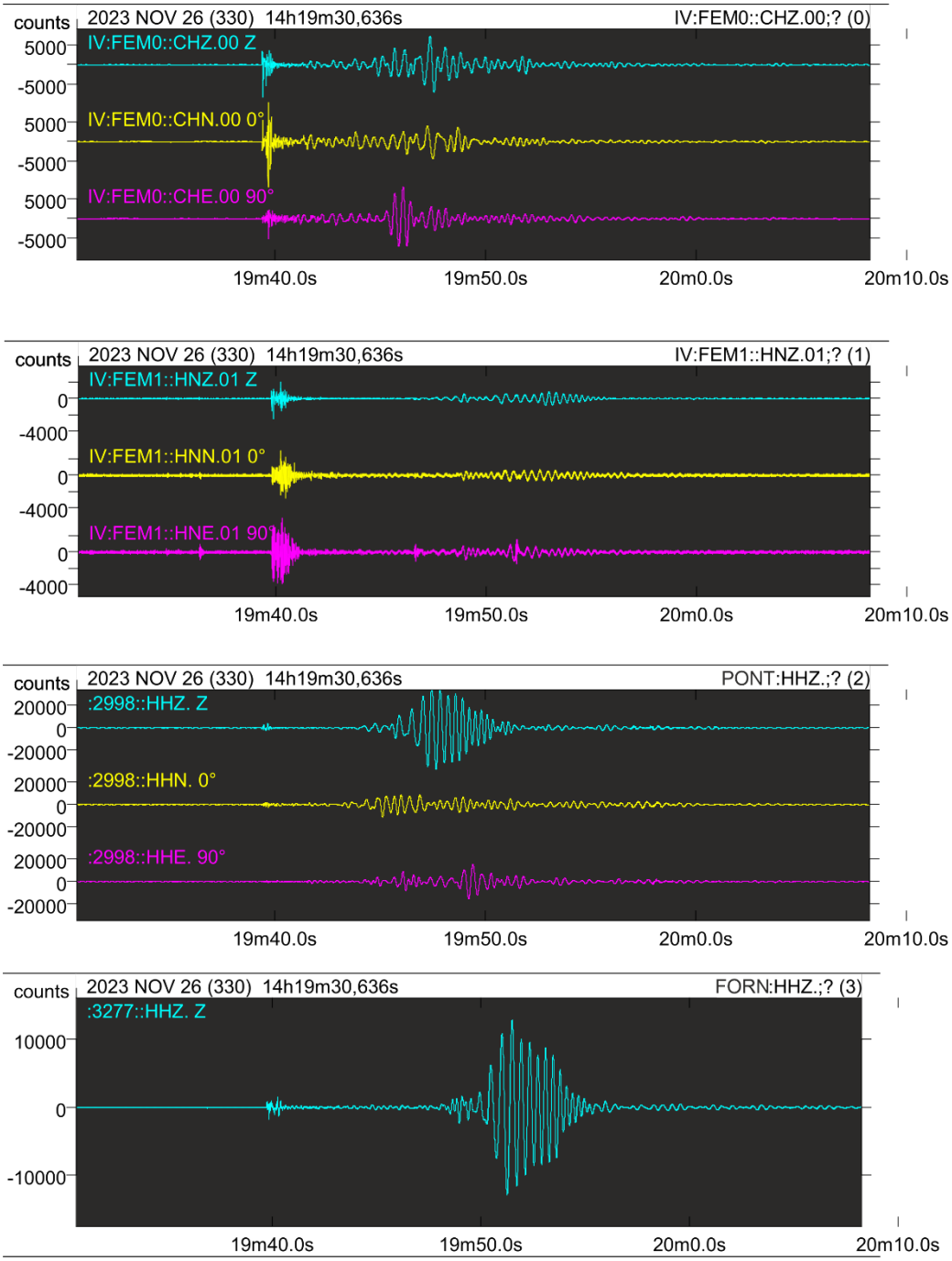

Figure 2. Examples of the bomb explosion seismograms recorded in stations from the SNet4Fer network. The first two panels show the 3-component records in the SNet4Fer 3.0 stations FEM0 and FEM1 (the seismograms are from the borehole sensors). The third and fourth panels show the records of two NetFer2.0 stations: PONT (3 components) and FORN stations (1 component).

References

Abu Zeid, N., Dall'olio, L., Bignardi, S., and Santarato, G., (2017). “Past, present and future improvements of the efficiency of the local seismic network of the geothermal reservoir of Casaglia, Ferrara (North Italy)”. 19th EGU General Assembly, 23-28 April, 2017, Vienna, Proceedings, 19172.

Prefettura - Ufficio territoriale del Governo di Ferrara (2023). Comunicato stampa del 26 novembre 2023. Link: https://www.prefettura.it/ferrara/contenuti/Neutralizzato_l_ordigno_bellico_inesploso_rinvenuto_nell_ex_convento_di_san_benedetto-18065660.htm (last accessed: 15 december 2023).

Corresponding author fabio.brighenti@unife.it

GPR investigations in the Santa Maria di Vezzolano rectory (AT)

M.F. Alberghina[1,2], V. Barberis[3], P. Capizzi[4], G. Comello[3], G. Milazzo[3], S. Schiavone[2]

[1] Department of Biology, Ecology and Earth Sciences (DiBEST), University of Calabria, Ponte P. Bucci, Cubo 12b, II Piano 87036, Arcavacata di Rende (CS), Italy

[2] S.T.Art-Test di S. Schiavone & C sas, via Stovigliai, 88 93015 Niscemi (CL), Italy,

[3] Regional Directorate of Piedmont Museums, Ministry of Culture, Via Accademia delle Scienze, 5, 10123 Torino (TO), Italy, valentina.barberis@cultura.gov.it

[4] Department of Earth and Marine Sciences (DiSTeM), University of Palermo,Via Archirafi 26 90123 Palermo (PA), Italy

The rectory of Santa Maria di Vezzolano in Albugnano (Asti, Italy) was founded in 1095 AD. Between the 12th and 13th centuries the structure experienced its period of maximum magnificence, followed by a phase of progressive decline which lasted until 1800. In 1937 the complex was handed under the management of the Italian State and is now part of the cultural heritage sites of the Regional Directorate of Piedmont Museums, peripheral institute of the Ministry of Culture.

Among the non-invasive investigations, geophysical methodologies were conducted to deepen the knowledge of any architectural elements under the pavement not yet detected. In particular, ground penetrating radar (GPR) investigations (fig. 1) with a 200/600 MHz multi-channel antenna were carried out on the internal flooring of the church and in the area in front of the façade to identify cavities, discontinuities or underground architectural structures. Ground Penetrating Radar (Conyers and Leckebusch, 2010; Goodman and Piro, 2013) is today a consolidated method widely used for diagnostics and research in archaeological prospecting and in other fields of cultural heritage (Deiana et al., 2018; Cozzolino et al., 2020; Capizzi et al., 2021).

All GPR profiles were carried out with an interdistance of 50 centimeters and acquired using the Georadar instrumentation of IDS – Engineering dei Sistemi S.p.a. – RIS MF HI-MOD model, equipped with a 200/600 MHz dual frequency antenna. The investigation depths were estimated considering an average electromagnetic wave propagation velocity of 0.1 m/ns. This average value was obtained from the slopes of the reflection hyperbolas present in the data. Each profile has been processed to eliminate coherent and inconsistent noise present in the original data. After processing the data with ReflexW software (Sandmeier, 2016) trying to eliminate both coherent and inconsistent noise, we proceeded with the analysis and interpretation in relation to the purposes envisaged by the study. For simplicity of graphic representation of the processed data, it was chosen to display the interpretative models of the investigated volume, in terms of normalized reflected amplitude. For each of the four areas investigated (central nave, side nave, portion in front of the Jubè, external area) a 3D model was built, using a code implemented in Matlab for the

construction of the data matrix and the Voxler application (Golden Software) for the graphic rendering. For the spatial interpolation the Inverse Distance Weighting algorithm (Shepard, 1968) was applied, which uses a weighted average based on the distance of the points from the observation point.

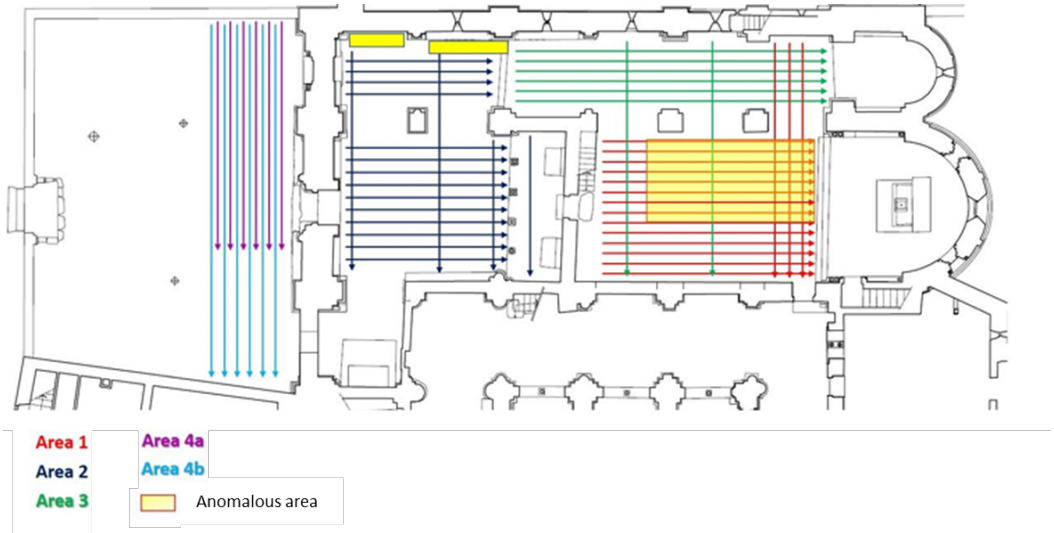

Fig. 1 – Location of the ground penetrating radar profiles.

All GPR profiles were carried out with an interdistance of 50 centimeters and acquired using the Georadar instrumentation of IDS – Engineering dei Sistemi S.p.a. – RIS MF HI-MOD model, equipped with a 200/600 MHz dual frequency antenna. The investigation depths were estimated considering an average electromagnetic wave propagation velocity of 0.1 m/ns. This average value was obtained from the slopes of the reflection hyperbolas present in the data. Each profile has been processed to eliminate coherent and inconsistent noise present in the original data. After processing the data with ReflexW software (Sandmeier, 2016) trying to eliminate both coherent and inconsistent noise, we proceeded with the analysis and interpretation in relation to the purposes envisaged by the study. For simplicity of graphic representation of the processed data, it was chosen to display the interpretative models of the investigated volume, in terms of normalized reflected amplitude. For each of the four areas investigated (central nave, side nave, portion in front of the Jubè, external area) a 3D model was built, using a code implemented in Matlab for the construction of the data matrix and the Voxler application (Golden Software) for the graphic rendering. For the spatial interpolation the Inverse Distance Weighting algorithm (Shepard, 1968) was applied, which uses a weighted average based on the distance of the points from the observation point.

The georadar survey carried out for a total of 54 profiles identified anomalies attributable to possible buried structures (fig. 2). In particular, some anomalies are compatible with the presence of crypts/burials in the central nave in the area near the main altar and, at greater depth (about 3 m) an anomaly in the initial part of the nave, near the Jubé. The latter is confirmed by another anomaly identified at the same depth on the opposite side of the arches. Some anomalies have also been identified in the side nave at a depth of approximately 2 m compatible with pre-existing architectural structures. As regards the external portion, the ground penetrating radar survey did

not reveal any other underground structures other than those already known from previous excavations (Crosetto, 2011).

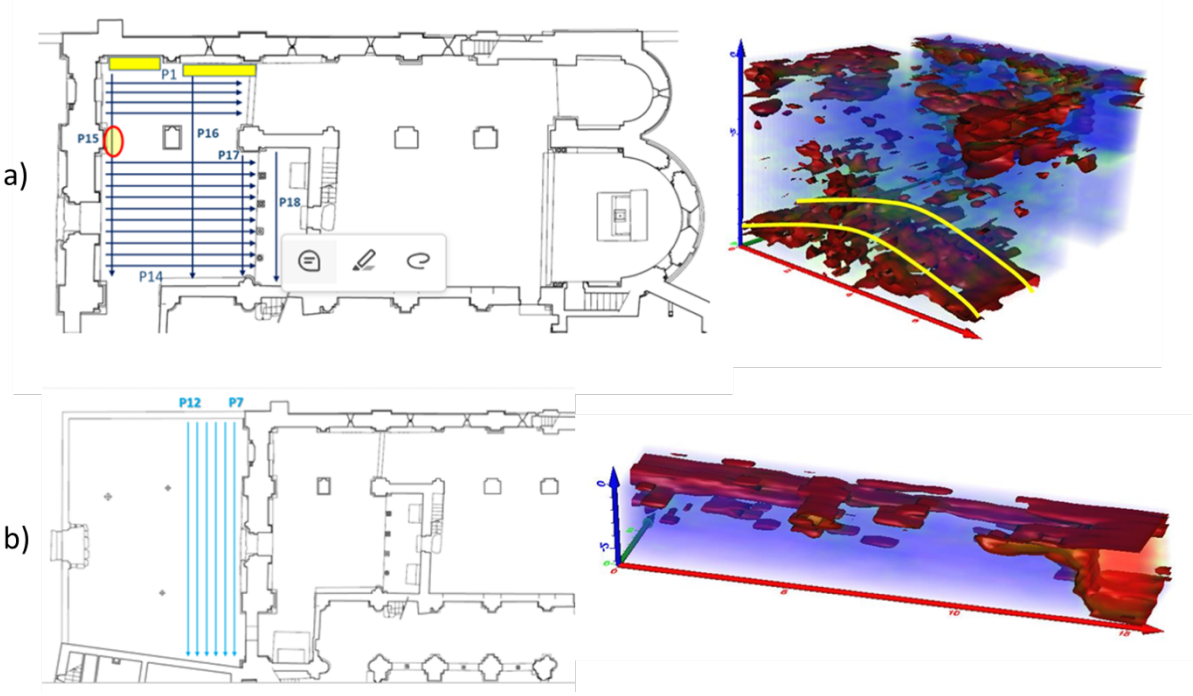

Fig. 2 – Partially GPR results for the area 2 (a) and the area 4b (b).

References

Capizzi P., Marrone M., Aleo Nero C., Bonfardeci A., Canzoneri A., Carollo A., Martorana R, Romano F. (2021) Georadar investigations in the Church of San Paolo (San Giacomo dei Militari, Palermo). Near Surface Geoscience 2021 – Bordeaux, France, 29 August – 2 September 2021, 1-5, https://doi.org/10.3997/2214-4609.202120203

Conyers LB, Leckebusch J (2010) Geophysical Archaeology Research Agendas for the Future: Some Ground penetrating Radar Examples. Archaeological Prospection, 17(2), 117-123. https://doi.org/10.1002/arp.379

Cozzolino, M., Di Giovanni, E., Gentile, V., Mauriello, P., Pizzano, N. (2020) Ground-Penetrating Radar Survey for the Study of the Church of Saint Cosma in Helerito (Tagliacozzo, L'Aquila, Italy). Geosciences, 10(6), 244. https://doi.org/10.3390/geosciences10060244

Crosetto, A., (2011) Santa Maria di Vezzolano: nuovi dati storici. In titolo volume Palazzo Carignano Torino.

Deiana R, Leucci G, Martorana R (2018) New Perspectives on Geophysics for Archaeology: A Special Issue. Surveys in Geophysics, 39(6), 1035–1038. https://doi.org/10.1007/s10712-018-9500-4

Goodman D, Piro S (2013) GPR Remote Sensing in Archaeology. Springer, 9. https://doi.org/10.1007/978-3-642-31857-3

Sandmeier, K.J. (2016) ReflexW Version 8.1. Program for Processing of Seismic, Acoustic or Electromagnetic Reflection, Refraction and Transmission Data. Software Manual, Karlsruhe, Germany.

Shepard, D. (1968) A two-dimensional interpolation function for irregularly-spaced data. Proc. 23rd National Conference ACM, ACM, 517-524.

Corresponding author: patrizia.capizzi@unipa.it

Identification of archaeological features using *Machine Learning* techniques applied to electromagnetic data

A. Capozzoli [1], E. Piegari [1], F. Cella [2], M. La Manna [1], V. Paoletti [1]

[1] Dipartimento di Scienze della Terra, dell'Ambiente e delle Risorse, Università degli Studi di Napoli Federico II, Naples, Italy

[2] Dipartimento di Scienze e Tecnologie, Università di Camerino, Camerino, Italy

Introduction

Over the past decades, geophysical investigations in the archaeological field have been recognized as an important tool for identifying target areas and planning dig works (e.g., Cella et al., 2015; Di Maio et al., 2016; El Qadi et al., 2019 and references therein). Indeed, they allow exploration of evermore extended surfaces with a significant reduction in costs associated with excavation campaigns. One of the geophysical prospecting methods with the highest values of the benefit-cost ratio is the frequency domain electromagnetic method (FDEM). This method allows obtaining quick information on both the electrical and magnetic properties of the investigated volumes from the measurements of the two components of the EM field. However, correlations between the maps of such components are commonly found only by visual inspection (e.g., Everett, 2013). The aim of the present study is to realize integrated maps of the two EM components in the attempt to obtain automatic identification of the target areas.

Material and methods

We analyze the electromagnetic (EM) data acquired in 2012 at the archaeological site of Torre Galli (Vibo Valentia, Calabria, Italy) where a magnetic study and two digs were previously conducted (Cella & Fedi, 2015). We apply the K-Means clustering algorithm to three FDEM dataset, one for each of the operating frequencies (5 kHz, 10 kHz and 15 kHz), in order to retrieve information about potential areas of interest at different depths. The K-means algorithm is an unsupervised Machine Learning technique grouping data with similar characteristics in a predefined number of clusters (e.g., Bhattacharya, 2021). We use two approaches to identify the optimal number of clusters for the specific problem. Specifically, we compute the Silhouette coefficient and apply the Elbow method to the partitions of data in the parameter space defined by the two components of the EM field. Then, we map in the real space the optimal clusters obtained for each analysed datasets and compare our results with the outcome of magnetic prospection.

Results

From the cluster analysis applied to the EM data for two operating frequencies (5 kHz, 10 kHz), it turns out that the Silhouette coefficient always identifies an optimal number of clusters, smaller than that from the Elbow method. In other words, optimal clusters validated by the Silhouette coefficient correspond to areas in the archaeological site that are much larger than those identified by the Elbow method. Looking at the clusters of major interest for archaeological studies, which are characterized by the highest values of magnetic susceptibility and electrical resistivity, it is found that groups from the Silhouette validation analysis can contain up to three of the optimal clusters identified by the Elbow method. However, in some cases the clusters from both the Elbow method and Silhouette coefficient agree in the identification of potential target areas, i.e., where the presence of a ditch is inferred. We stress that all the anomalous areas identified by the analysis of magnetic data fall within the areas of potential interest for the archaeological excavation operations identified by the present clustering analysis. Hence, the proposed approach shows that the application of unsupervised machine learning techniques to FDEM data is promising in improving the efficiency of this method making it more attractive for archaeological research.

References

Bhattacharya, S.; 2021: A Primer on Machine Learning in Subsurface Geosciences, 1, 1–172.

Cella, F., Fedi, M.; 2015: High-resolution geophysical 3D imaging for archaeology by magnetic and EM data: the case of the iron age settlement of Torre Galli, Southern Italy. Surveys in Geophysics, 36(6), 831-850.

Cella, F., Paoletti, V., Florio, G., Fedi, M.; 2015: Characterizing elements of urban planning in Magna Graecia using geophysical techniques: the case of Tirena (Southern Italy). Archaeological Prospection, 22(3), 207-219.

Di Maio, R., La Manna, M., Piegari, E.; 2016: 3D reconstruction of buried structures from magnetic, electromagnetic and ERT data: Example from the archaeological site of Phaistos (Crete, Greece). Archaeological Prospection, 23, 3-13.

El-Qady, G., Metwaly, M., Drahor, M. G.; 2019: Geophysical techniques applied in archaeology. Archaeogeophysics: State of the art and case studies, Springer, 1-25.

Everett, M.E.; 2013: Near-Surface Applied Geophysics. Pp.209.

Corresponding author: angelica.capozzoli@unina.it

A novel approach for the assessment of the deterioration of RC structures by means of non-invasive tests supported by numerical models

L. Capozzoli[1], G. De Martino[1], S. Imperatore[2], F. Nerilli[2], L. Telesca[1], E. Vasanelli[3]

[1] Institute of Methodologies for Environmental Analysis, National Research Council of Italy (IMAA CNR), C. da S. Loja—Zona Industriale, Tito Scalo, 85050 Potenza, Italy
[2] Department of Civil Engineering, "Niccolò Cusano" University of Rome, 00166, Italy
[3] Institute of Heritage Science, National Research Council (ISPC- CNR) via per Monteroni, 73100 Lecce (LE), Italy

Economic, political, and social implications related to the safety of reinforced concrete structures and infrastructures pose significant and unavoidable challenges. As regards only the economic aspect, the global non-destructive testing market is projected to grow from $6,80 billion in 2022 to $16.66 billion by 2029, at a CAGR of 13,66% [Report, online resource].

Deterioration phenomena affecting concrete and/or reinforcements cause physicochemical and mechanical variations, difficult to detect and localize by using conventional diagnostic tools and methods, which are often low-resolution, invasive, cost, and time-consuming. Moreover, numerical models can support the safety condition assessment of reinforced concrete structures but to date, there isn't a consolidated approach for deteriorated materials.

It is evident how coupled with semi-destructive and destructive tests and/or other well-known non-destructive tests, geophysical methodologies can play a fundamental role in RCS corroded RC structures inspecting and monitoring [Vasanelli et al.]. For this reason, the development of innovative strategies for corrosion diagnosis based on a combined and integrated use of geophysical and other NDT methodologies is strongly required [Maierhofer et al., 2010; Capozzoli and Rizzo, 2017; Capozzoli et al., 2021]. Nowadays, protocols for the diagnosis of deteriorated RCS are not fully established, as they depend on the specificity of the case studies under investigation. Moreover, the potentialities of geophysical methodologies, alone or integrated, are not fully unleashed.

From a structural point of view, a lot of efforts in performing experimental tests and in assessing theoretical models on corroded RC members are still needed, due to the amount of random parameters governing the physical problem and the chemical processes. In detail, a lack of well-established formulations to employ in FEM-based structural analyses of aged structures is emerged, even if some statistically assessed formulations are available [Coccia et al. 2016; Imperatore et al., 2017; Imperatore and Rinaldi, 2019; Benenato et al., 2022; Imperatore, 2022].

In this framework the two CNR Institutes ISPC (Institute of Heritage Science) and IMAA (Institute of Methodologies for Environmental Analyses) and UNICUSANO University are working on the two-year Research Project of National Relevance (PRIN-2022) ICARUS which aims at exploring the contribution that geophysical methodologies can give for detecting and monitoring the main degradation phenomena affecting RCS, considering both the concrete and the reinforcements deterioration.

ICARUS proposes the development of an innovative multiscale and multisensor geophysical methodology based on integrating empirical relationships between physical and mechanical parameters in different deterioration conditions. The project's objective will consist of developing an innovative strategy based on integrating geophysical analyses, conventional NDT and DT, and advanced statistical analyses to identify the material decay evolution and upgrade existing corrosion damage models. In addition, novel structural assessment approaches for deteriorated RCS will be proposed. At this aim, improved bond-slip and tension-stiffening laws will be developed to assess how corrosion affects the steel-to-concrete interaction at both local and global levels. The outcomes, coupled with empirical relationships based on geophysical measurements for cracked concrete and corroded reinforcements and proper finite element approaches, will allow the evaluation of the structural behaviour of deteriorated reinforced concrete structures.

ICARUS will try to accomplish mainly two goals:

1. Development of a non-invasive and multiscale approach for the geophysical characterization and monitoring of degradation, and development of damage empirical models, through the analysis of correlations between geophysical parameters and mechanical properties of concrete and RC elements with damage progression.

2. Modelling of the mechanical response of RCS at different damage levels due to deterioration phenomena. In detail, the attention will be focused on the decay of the mechanical properties of the concrete and the steel-to-concrete interaction using experimental, analytical, and numerical approaches.

In order to accomplish its mission, ICARUS will analyze the degradation mechanisms occurring in concrete and their simulation in small-scale samples with different geophysical methodologies, DT and NDTs will be applied to degraded samples, accurately selected on the basis of aging procedures and specimens' dimensions. The accuracy of each geophysical methodology in defining the degradation level will be step-by-step analyzed by laboratory measurements, at different damage levels starting from the sound conditions of the material. Microstructural, physical, chemical, and mechanical characterization tests at different stages of decay will support the tests.

Further, damage assessment of corroded RC members by means of destructive tests and geophysical methodologies will be accurately evaluated through a step-by-step laboratory procedure; then the variations of the geophysical response due to the artificial corrosion of rebars will be analyzed. The microstructural/physical properties of the corroded samples and their mechanical response will be examined to characterize the degradation phenomena. Artificial corrosion degradation of RC elements to obtain different crack patterns and/or corrosion levels will

be implemented for evaluating the mechanical performance of the corroded steel-concrete elements subjected to different corrosion levels.

Fig. 1 - The innovative multi-scale and multi-sensor based approach of ICARUS

The outcomes of ICARUS have economic potential as its activities may reduce the costs of restoration and rehabilitation interventions. Moreover, the approach is focused on the extension of the service life of structures by providing a more accurate diagnostic of the RC buildings and infrastructure conditions according to Cluster 5 of Horizon Europe 21-27 Program.

References

Benenato, A., Ferracuti, B., Imperatore, S., & Lignola, G. P. (2022). Corrosion level estimation by means of the surface crack width. Construction and Building Materials, 342, 128010.

Capozzoli L. and E. Rizzo, Combined NDT techniques in civil engineering applications: Laboratory and real tests, Constr Build Mat, 154, pp 1139-1150, 2017

Capozzoli L. et al., Multi-Sensors Geophysical Monitoring for Reinforced Concrete Engineering Structures: A Laboratory Test, Sensors, 21(16):5565, 2021

Coccia S. et al, Influence of corrosion on the bond strength of steel rebars in concrete. Mater Struct, 49(1), 537-551,2016

Imperatore S. and Z. Rinaldi, Experimental behavior and analytical modeling of corroded steel rebars under compression. Constr Build Mat, 226,126-138,2019

Imperatore S. et al., Degradation relationships for the mechanical properties of corroded steel rebars. Constr Build Mat, 148, 219-230,2017

Imperatore, S. (2022). Modelling Strategies for Reinforced Concrete Elements under Corrosion Degradation. Materials, 15(13), 4601.

Maierhofer C. et al., Non-Destructive Evaluation of Reinforced Concrete Structures: Non-Destructive Testing Method, Elsevier,2010

NDT and Inspection Market by Technique (Visual Testing, Magnetic Particle, Liquid Penetrant, Eddy-Current, Ultrasonic, Radiographic, Terahertz Imaging, Acoustic Emission), Method, Service, Application, Vertical and Region-Global Forecast, report, online resource, last access 2023

Vasanelli E. et al, Combining non-invasive techniques for reliable prediction of soft stone strength in historic masonries, Constr Build Mat, 146, 744-754,2017

corresponding author: luigi.capozzoli@cnr.it

A Dynamic and Multi-Source Hydrogeophysical Model to Remediate a Complex Hydrocarbon-Contaminated Site

P.Ciampi[1], G.Cassiani[2], G.P.Deidda[3], C.Esposito[1], G.Scarascia Mugnozza[1], M. Petrangeli Papini[4]

[1] Department of Earth Science, Sapienza University of Rome
[2] Department of Geosciences, University of Padua
[3] Department of Civil, Environmental Engineering and Architecture, University of Cagliari
[4] Department of Chemistry, Sapienza University of Rome

Contaminated sites pose intricate challenges in characterization and remediation planning due to the complex interplay of contaminants and hydrogeological properties, often resulting in under-sampling issues at the site-specific scale. This study introduces a dynamic multi-source approach to address the challenges of characterizing and remediating a hydrocarbon-contaminated site. A comprehensive dataset is compiled from diverse sources, including stratigraphic boreholes, laser-induced fluorescence surveys (LIF), electrical resistivity tomography (ERT), and groundwater hydrochemical monitoring. These data are integrated into an interactive big-data package, enabling real-time 3D modeling throughout the characterization and remediation phases. The study yields a comprehensive conceptual hydrogeophysical model that captures hydrogeological and geophysical structures, as well as the spatial and temporal dynamics of contamination. By combining knowledge from multiple sources, the multi-source hydrogeophysical clone provides qualitative-quantitative indicators to reduce uncertainties associated with subsurface interpretation by separating signatures of geologic material in the absence of light non-aqueous phase liquids (LNAPL) and the local increase in electrical conductivity associated with petroleum hydrocarbon biodegradation. It reveals the real characteristics of the pollutant, contamination mechanisms, and residual hydrocarbon sequestration influenced by hydrogeological dynamics and on-site remediation actions. The emerging hydrogeophysical conceptual site model (CSM) serves as a dynamic interface for designing enhanced remediation actions, specifically targeting LNAPL and involving reagent injections into the subsurface to stimulate the desorption and oxidation of residual hydrocarbons. Geophysical monitoring, utilizing ERT, reveals subsurface dynamics and variations in electrical conductivity during injection, extraction, and subsequent pumping activities. The study underscores the importance of collecting diverse data for a reliable and high-resolution reconstruction of the conceptual framework. The dynamic multi-source model explains contamination/decontamination dynamics based on the variation of electrical properties in space-time, also induced by the application of remediation processes at the field scale. Data-driven model discriminates geophysical evidence on the basis of lithologic characteristics and

contamination effects, providing considerable qualitative-quantitative insights into both the distribution of products in a highly heterogeneous medium and the hydraulic perturbations associated with the pumping operated by traditional physical extraction wells. This research enhances our understanding of contaminant remediation dynamics, emphasizing the need for integrated, multi-source approaches in addressing the complexities of heterogeneous geoenvironments.

References

Ciampi, P., Esposito, C., Cassiani, G., Deidda, G. P., Rizzetto, P., Petrangeli Papini, M. (2021): A field-scale remediation of residual light non-aqueous phase liquid (LNAPL): chemical enhancers for pump and treat. Environmental Science and Pollution Research, 28(26), 35286-35296. https://doi.org/10.1007/s11356-021-14558-2.

Ciampi, P., Esposito, C., Cassiani, G., Deidda, G. P., Flores-Orozco, A., Rizzetto, P., Chiappa, A., Bernabei, M., Gardon, A., Petrangeli Papini, M. (2022). Contamination presence and dynamics at a polluted site: Spatial analysis of integrated data and joint conceptual modeling approach. Journal of Contaminant Hydrology, 248, 104026. https://doi.org/10.1016/j.jconhyd.2022.104026.

Orozco, A.F., Ciampi, P., Katona, T., Censini, M., Petrangeli Papini, M., Deidda, G.P., Cassiani, G. (2021). Delineation of hydrocarbon contaminants with multi-frequency complex conductivity imaging. Science of the Total Environment, 768, 144997. https://doi.org/10.1016/j.scitotenv.2021.144997.

Corresponding author: paolo.ciampi@uniroma1.it

The audio and electrical monitoring of the Mefite area in ELF band

G. Cianchini[1], C. Fidani[1,2], A. Piscini[1], M. Soldani[1], A. De Santis[1], L. Perrone[1] , M. Orlando[1], D. Sabbagh[1]

[1] Istituto Nazionale di Geofisica e Vulcanologia, Roma, Italy
[2] Central Italy Electromagnetic Network, Fermo, Italy

A multi-parameter station came into operation last year near the Mefite site, a CO_2-rich vent located in Irpinia, province of Avellino, Campania Region. The aim of studying fluid migration in relation to tectonic activity at this particular site falls within the scope of the FURTHER (the role of FlUids in the pReparaTory pHase of EaRthquakes in Southern Apennines) project. In this station there are two magnetometers for continuous monitoring, two electrodes for electrical variations, a microphone, and occasionally other instruments for limited intervals of time. The Very Low Frequency band of the electric field sampled at Mefite in relation to moderate and strong seismic events in the Mediterranean region was previously reported (Cianchini et al., 2023). The Extremely Low Frequency band concerns both the electric and acoustic fields. Electric field in this band are monitored by an instrument of the Central Italy Electromagnetic Network, and near the earth's surface contains information about several phenomena both far and close to the electrode sensors (Fidani, 2011). They are natural and anthropogenic phenomena. Anthropogenic signatures of electric phenomena are regular shapes on spectrograms. For example, the horizontal lines of Figure 1 top represent the everywhere emission by the electrical power distribution network. The main frequency of this emission occurs at 50 Hz and a series of harmonics at multiple frequencies. Such anthropogenic emissions occur around the electrodes up to hundreds of m. Instead, the horizontal bands on the black background barely appearing in grey and blue of the spectrum under 50 Hz, are a natural phenomenon known as Schumann Resonances. These are eigenfrequencies of the cavity between the earth's surface and the ionosphere that behave like conductors. They are global phenomena of radiation sustained by lightning activity and selected by interference at 8, 14, 19, 25, 31 Hz, and more, that are little affected by small and local causes within 100 km. Spectrograms shown in Figure 1 are 147-minute records in the evening of December 22, 2022, with stable meteorological conditions indicated by a low density of vertical coloured lines, which are more evident at the low part of the spectra. Vertical lines are electrical discharges occurring in the atmosphere mainly generated by meteorological activity and partially generated by anthropogenic activity. Lightning can be detected at hundreds of km, as in this case, up to thousands of km. While anthropogenic switching of utilizers can be recorded up to one km from electrodes. Finally, a very evident local phenomenon is observed in the electrical ELF spectrogram (Top). It was appearing only on the E-W electrode, that is the electrode oriented towards the

Mefite lake. It appears as a well defined red-coloured band that develops irregularly in the central part of the recording between 50 and 200 Hz. It is a local oscillation of the electric field because it does not appear at both electrodes, and it was demonstrated to have a source not longer than some tenths of m large (Fidani and Martinelli, 2015). This is the phenomenon that we are searching to observe in connection with the fluid escaping from the ground to study some kind of link between them.

From the theoretical approach (Fidani and Martinelli, 2015; Fidani et al., 2020), this signal should be generated by charged oscillating clouds whose dimensions would be from tenths of cm to a few meters dimension. The charged cloud is a stable structure as the pressure force is supposed to balance the electric force. It was mathematically demonstrated that such a physical system is able to oscillate, and the charge magnitude balancing slight pressure holes was estimated to depend on the oscillation frequency. Charges from 10^{-4} to 10^{-5} Coulombs were associated with the measured frequencies. Being pressure variations hypothesized for this kind of electrical sources, a comparison was made between the most intense electric oscillation and acoustic recordings. searching for possible mechanical effects of oscillating cloud transduction in pressure waves or thinking of fluid emission changes possibly related to electric oscillation triggers. The comparison was made between respective spectrograms. Being the acoustic signal initially sampled at 27 kHz, the spectral overlap with the electric ELF (up to 2 kHz) spectra was problematic, also due to the logarithm scale for ELF with respect to the linear for audio. The acoustic recording is reported in Figure 1 bottom, for the same time interval on December 12, 2022. No connections appeared between intensities nor in shapes. Higher audio frequency recordings seem to be related to wind, whereas the corresponding frequencies of the electrical oscillation were restricted in the violet band of Figure 1 bottom. A reduction of audio sampled frequency was first decided to reduce the wind influence, and a plot in the logarithm scale was realized for a better comparison with the electric recording.

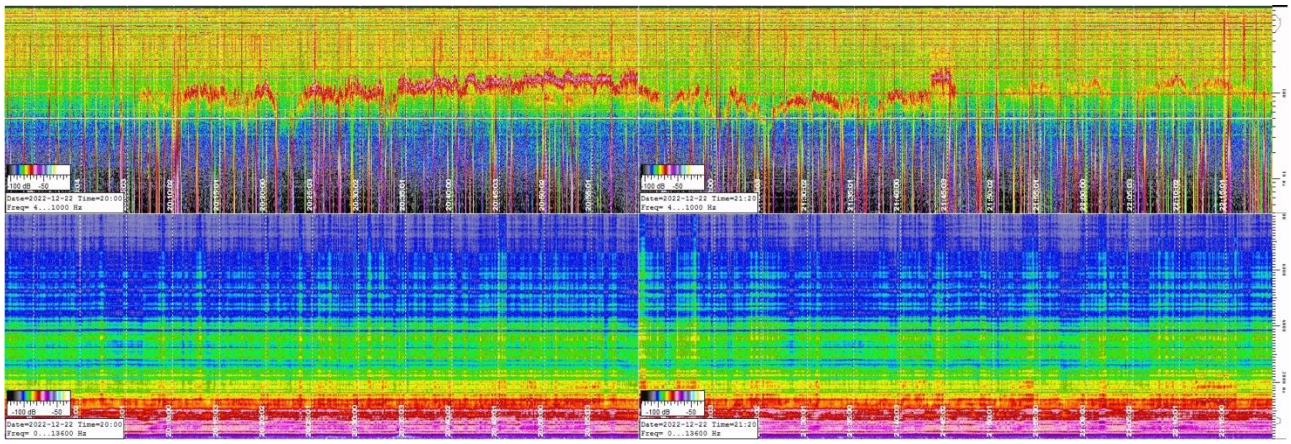

Fig. 1 – Spectrograms recorded on December 22, 2022, from 19:52 to 22:19 LT; the time is marked every 5 minutes by the vertical dotted lines. Frequency was reported in the logarithm scale on the y-axis and power of signals in dB by a colour legend. Two bands are related to the electrode E-W on the top, and to the microphone recording below. Labels on the left and in the middle referred to the power spectra intensities and times of the spectrograms.

From the beginning of April 2023 the audio sample frequency was reduced to 16 kHz, and the vertical frequency axis scale was set logarithmic covering the interval between 10 Hz and 8 kHz. In this way, spectrograms become comparable with the ELF ones for the electric field, and the spectral content in the lower part of the audio sound becomes more intelligible. During the Mefite station maintenance, it was possible to verify the good state of the microphone after several months of audio recording despite its continuous exposure to the corrosive emissions at Mefite. Indeed, the device was protected by a hood that was put on to shield it from gusts of wind for land audio recordings. While, the copper wires, although covered by sheath, were corroded perhaps due to small cracks in the sheath. Thus, a further comparison was momentarily not possible between electric and acoustic signals.

The spectral content of the lower part of the audio band, now visible by logarithmic scale, immediately evidenced a rich variety of eigenfrequencies. Furthermore, their amplitudes presented non-constant intensities both in a collective sense and in a singular sense. Some acoustic resonances appeared sporadically during the intense increase of the Mefite's blow. The Fourier analysis was particularly investigated at the time of small seismic events that occurred a few tenths of km away from the site. An example is shown in Figure 2, where more than 30 hours of audio recording have been reported starting from the day before the Mirabella M=2.1 earthquake occurred at the beginning of April 19, 2023. Hypocentre depth occurred at less than 10 km at a distance of around 20 km. The seismic event was preceded by a sensible noise increase that started about 11 hours before and was maintained for about 6 hours, then slowly faded over many hours. The noise increase was in turn preceded by two puff dampening lasting approximately one hour each, one immediately before the noise increase and the other around 4 hours before it. The earthquake time was indicated by a cyan vertical arrow and the colour legend permitted the evaluation of a noise increase of about 10 dB during the most intense emission, and audio suppressions of up to 10 dB during the dampening. Three sudden puffs with a 10 dB noise increase were evidenced. Moreover, the frequency band between 100 and more than 1000 Hz also showed an evident increase during the maximum noise manifestation.

The main eigenfrequencies of Figure 2 are at 45 and 65 Hz. They maintain constant intensity for a long time before the seismic event. Other less apparent horizontal bands occur at 103 Hz, and 125 Hz, other two bands at 300-400 Hz and 700-800 Hz, and many weak horizontal bands above 1000 Hz. More detailed observation of the power spectra in Figure 2 shows the entire series of 19, 45, 65, 103, 125, and 170 Hz, which appear more clearly during the damping hour preceding the significant increase of the audio noise of Figure 3 middle. Instead, longer periods of audio noise modulation whose durations were between 5 and 10 minutes are shown in Figure 3 left. Details of the third puff are shown in Figure 3 right, where a noise increase lasting two minutes between 10 and 40 Hz was accompanied by a well-defined audio note at 55-80 Hz with frequency increased in less than 2 minutes. It could be thought of as a resonance excitation of the final conduct due to the sudden intensification of the flux.

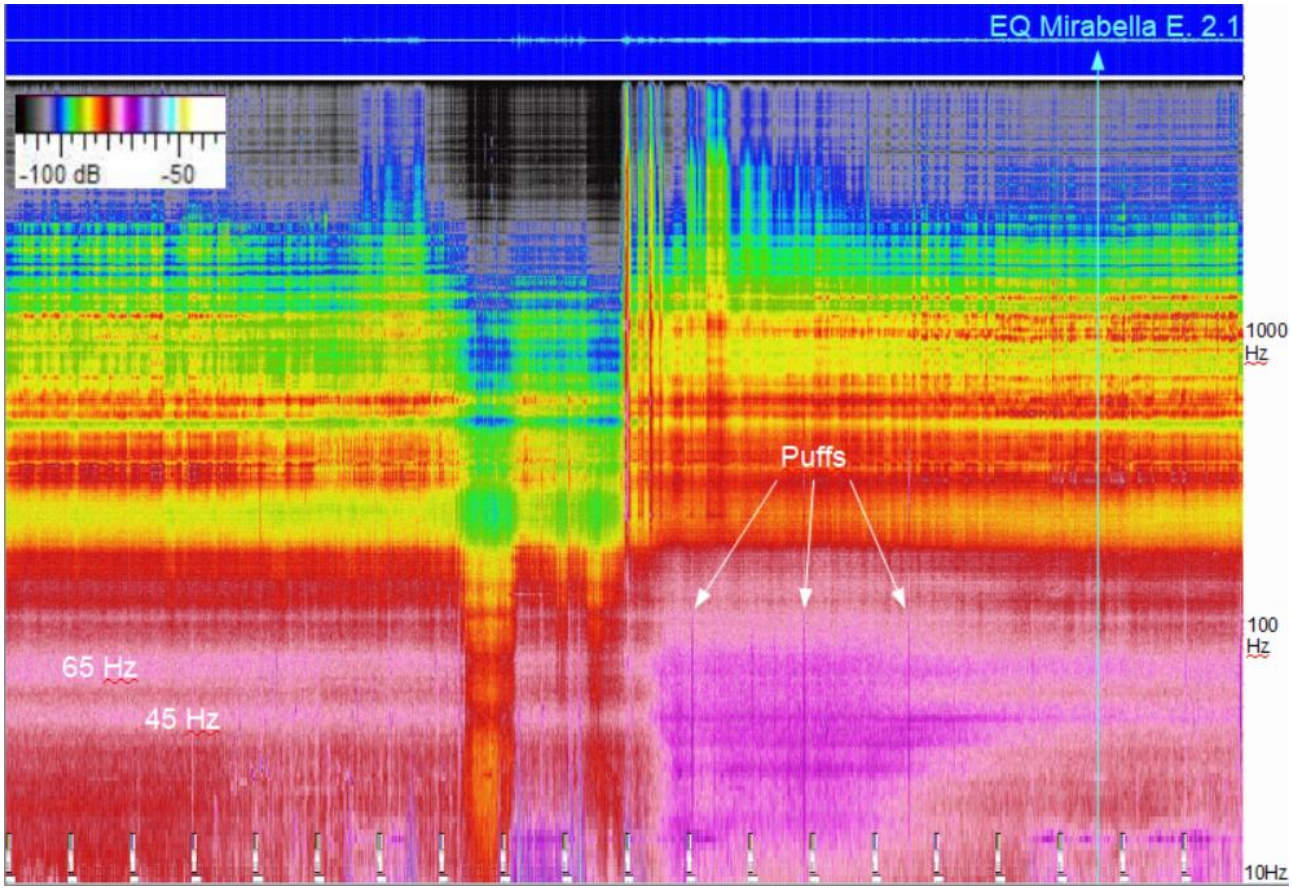

Fig. 2 – The acoustic spectrogram recorded on April 18 and the morning of 19, 2023, includes the moment of a small seismic event that occurred at Mirabella, M=2.1, about 20 km from Mefite. The Mirabella earthquake time is indicated by a vertical cyan arrow. Main eigenfrequencies and sudden puffs on the power spectra are indicated.

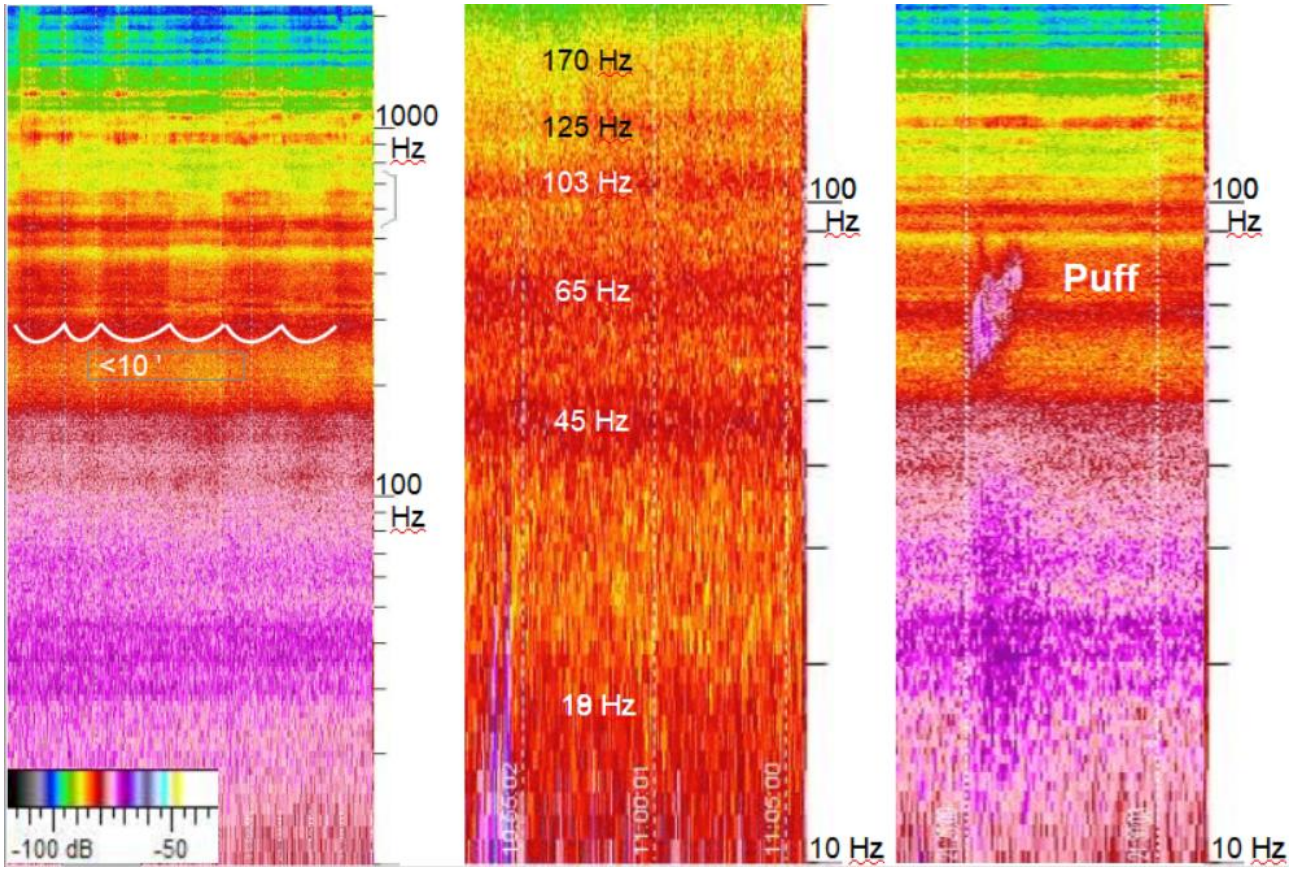

Fig. 3 – Details of the power spectrum relative to three moments (of less than 10 minutes to one hour) hours before the Mirabella M=2.1 earthquake. Periodic modulations of the noise of less than 10 minutes were evidenced between 200 and 800 Hz, on the left. The entire series of resonances from 19 to 170 Hz appeared during the damping interval at the centre. A detail of one of the three puffs is reported on the right where the sudden increase followed by a gradual fading that lasted two minutes is shown. The right plot also shows an unexpected growth of sound in a well-defined range between 55 and 80 Hz.

Acknowledgements

The authors thank the Limadou Scienza + (ASI), FURTHER (MUR) and Pianeta Dinamico (INGV-MUR) Projects for their financial support.

References

Cianchini G., et al.; 2023: A month of VLF detection at Mefite, Valle D'Ansanto, Italy. 41th GNGTS. February 7-9, Bologna.

Fidani C.; 2011: The Central Italy electromagnetic network and the 2009 L'Aquila earthquake: observed electric activity. Geosciences, 1 (1), 3–25.

Fidani C., and Martinelli G.; 2015: A possible explanation for electric perturbations recorded by the Italian CIEN stations before the 2012 Emilia earthquakes. Boll. Geofis. Teor. Appl. 56, 211–226.

Fidani C., et al.; 2020: Electric and Magnetic Recordings by Chieti CIEN Station During the Intense 2016–2017 Seismic Swarms in Central Italy. Front. Earth Sci., 8:536332.

Detecting fault geometries through electrical methods along some active faults of Mount Etna

F. D'Ajello Caracciolo[1], I. Nicolosi[1], V. Sapia[1], V. Materni[1], G. Tusa[1], M. Paratore[1], R. Azzaro[1]

[1] *Istituto Nazionale di Geofisica e Vulcanologia (INGV)*

Introduction

The Mt. Etna region is characterized by several active faults that play a significant role in local geodynamic processes (Azzaro et al., 2013a). Simultaneously, these faults exert a profound impact on the lives of local communities, strongly influencing land use across a substantial portion of the Etnean territory. The primary issue arising from the tectonic activity of these faults is related to seismic hazard, with many of them capable of generating strong earthquakes (Azzaro et al., 2013a). In the realm of earthquake geology, numerous studies have been conducted to map these active tectonic features and characterize their seismotectonic behavior (Azzaro et al., 2012).

Increasingly, local government authorities and professionals are considering the results of these research efforts for urban planning and infrastructure design, particularly in the aftermath of strong earthquakes causing significant damage to the building stock in the most densely populated areas of the volcano. This was evident in 2002 (Azzaro et al., 2010) following a flank eruption accompanied by an intense seismic crisis on the eastern flank of Etna. More recently, in 2018, a similar situation unfolded after the last eruption and a destructive earthquake (Azzaro et al., 2022).

In 2022, the regional Civil Protection Department initiated a new project for the seismic microzonation of 3rd level at Etna, with the aim of providing a detailed characterization of issues related to the interaction among active faults and urban planning. The goal is to improve and adapt to the Etnean territory, criteria and guidelines previously defined at a national level (Gruppo di lavoro MS, 2008). Currently, the scientific community involved in the project is focused on the characterization of the "active and capable faults" (hereinafter FAC), from both geological and geophysical points of view. Precise mapping and detection of active deformation lines by indirect methods, is the common target of all the participants.

In this framework, the INGV working group started a series of geophysical surveys in the eastern flank of Mount Etna in June 2023 (Fig.1). Specifically, electrical tomography and capacitive geoelectrical surveys were carried out along the Pernicana Fault, S. Leonardello Fault, and Fiandaca Fault. Geoelectrical methods, as demonstrated by Porreca et al. (2016), Civico et al.

(2017), Villani et al. (2015, 2017), have proven to be to be effective in revealing subsurface structures and fault geometries for this kind of applications.

Methods

Electrical tomography (ERT) is effectively employed in investigating geological horizons characterized by strong contrasts in electrical resistivity, often linked to lithological and structural variations. Measurements can be made using different arrays to maintain a good compromise between the vertical and horizontal shape of the recovered anomalies (Loke and Barker, 1996). An algorithm based on a least-squares deconvolution method is employed for the inversion of apparent resistivity, allowing 2D sections to be obtained through finite element calculation modules, also considering topographic corrections. A 10-channel, 72-electrode IRIS Syscal Pro was used for resistivity measurements, and the spatial coordinates of the electrodes were acquired through a Stonex S900 differential GPS with correction through the Italpos network.

This study focuses on the analysis and interpretation of two-dimensional electrical resistivity tomography profiles; each profile was primarily acquired using both Wenner and dipole-dipole (DD) electrode arrays. The electrical tomography profiles were acquired with a sampling interval of 1 m to achieve higher detail and, where possible, at 5 m intervals to reach greater depths of investigation.

Interpretative models are based on the inversion of a set of mixed apparent resistivity data from the two different arrays. To derive accurate true resistivity values from the measured apparent resistivity data, the smoothness-constrained least-squares method was employed. This method considers models with infinite perpendicular extension along the profile strike, as outlined in studies by Constable et al. (1987), deGroot-Headlin and Constable (1990), and Morelli and Labrecque (1996).

Preliminary results

The inversion models reveal the alternation of resistive and conductive layers, whose geometry and potential displacement highlight the presence of lateral discontinuities associated with recognized faults exposed at the surface. In a volcanic environment with volcanic and volcano-clastic products, electrical tomography reveals resistivity values ranging from medium-high to very high, consistently exceeding 300 Ohm/m. The dynamic range of resistivity values is characterized by the presence of more conductive layers with resistivity up to 1000 Ohm/m and more resistive layers with significantly higher values. These values align with the study area's characteristics, marked by lava flows and volcano-clastic products (Chiancone Formation).

In general, electrical tomography and capacitive geoelectrics reveal the presence of strong lateral discontinuities, whose geometry can be attributed to the existence of faults. Further studies, together with the integration of data from all the participants to the project, will provide indication for selecting the most suitable method/approach compared to different geological settings. The final goal is to compile guidelines for professionals, to be adopted as best-practise for future geophysical investigations.

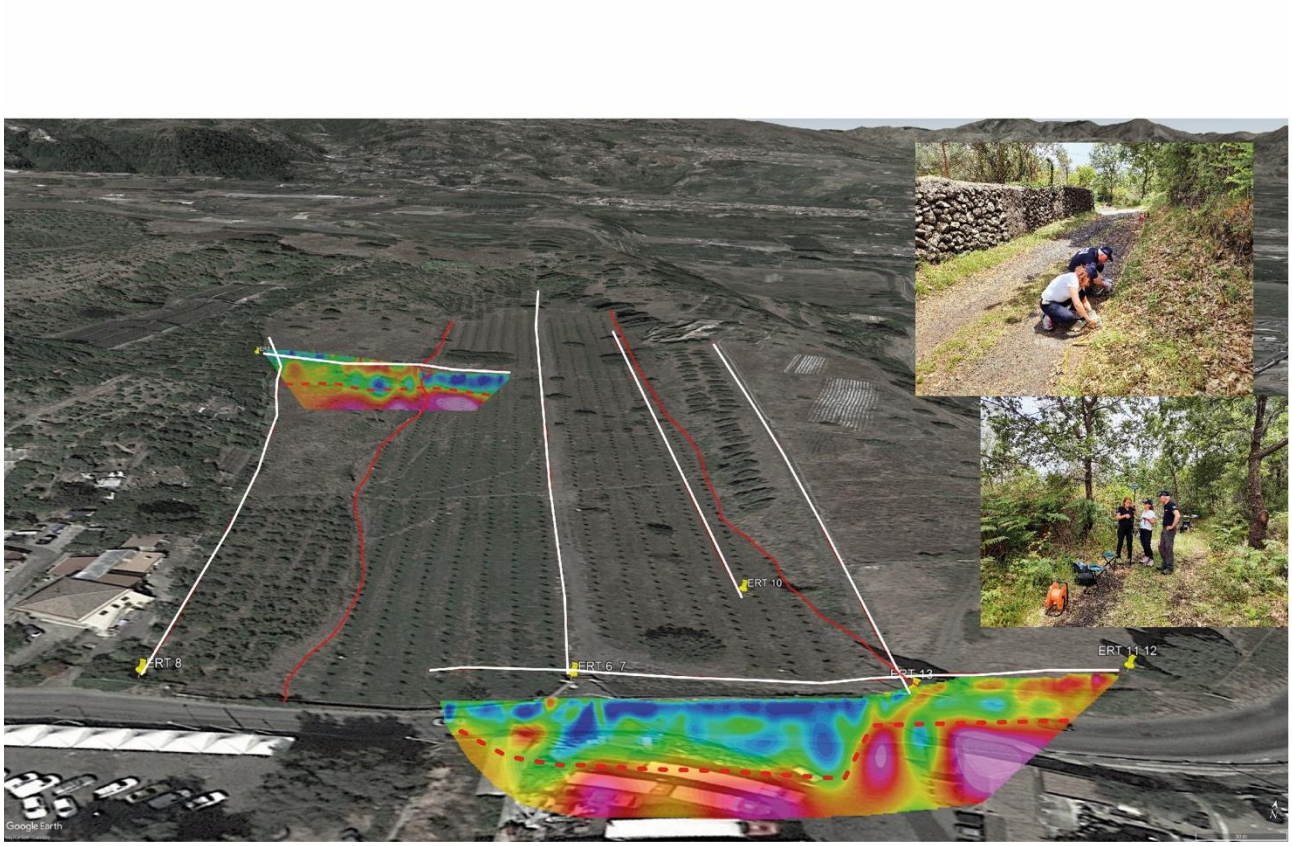

Figure 1: Perspective view of a measurement site along the S. Leonardello fault with traces of geoelectric profiles (in white), fault scarps (in red), and resulting 2D electrical tomography sections.

References

Azzaro R., Carocci C., Maugeri M. and Torrisi A. (Ed.); 2010: *Microzonazione sismica del versante orientale dell'Etna: studi di primo livello*. Regione Siciliana, Dipartimento della Protezione Civile, Le Nove Muse, Catania, 181 pp., 1 DVD-Rom, ISBN 978-88-87820-45-4.

Azzaro R., Branca S., Gwinner K. and Coltelli M.; 2012: *The volcano-tectonic map of Etna volcano, 1:100.000 scale: morphotectonic analysis from high-resolution DEM integrated with geologic, active faulting and seismotectonic data*. It. J. Geosciences (Boll. Soc. Geol. It.), 131 (1), 153-170.

Azzaro R., Bonforte A., Branca S. and Guglielmino F., 2013a: *Geometry and kinematics of the fault systems controlling the unstable flank of Etna volcano (Sicily)*. J. Volc. Geotherm. Res., 251, 5-15.

Azzaro R., D'Amico S., Peruzza L. and Tuvè, T.; 2013b: *Probabilistic seismic hazard at Mt. Etna (Italy): the contribution of local fault activity in mid-term assessment*. Journal of Volcanology and Geothermal Research, 251, 158-169.

Azzaro R., Pucci S., Villani F., Civico R., Branca S., Cantarero M., De Beni E., De Martini P.M., Cinti F.R., Caciagli M., Cucci L. and Pantosti D.; 2022: *Surface faulting of the 26 December 2018, Mw5 Mt. Etna earthquake (Italy): geological source model and implications for the seismic potential of the Fiandaca fault*. Tectonics, 41, DOI: 10.1029/2021TC007182.

Civico, R., Sapia, V., Di Giulio, G., Villani, F., Pucci, S., Baccheschi, P., et al. (2017). Geometry and evolution of a fault-controlled Quaternary basin by means of TDEM and single-station ambient

vibration surveys: The example of the 2009 L'Aquila earthquake area, central Italy. Journal of Geophysical Research: Solid Earth, 122, 2236–2259. doi.org/10.1002/2016JB013451.

Constable S.C., Parker R.L.and Constable C.G., (1987). Occams' inversion: A practical algorithm for generating smooth models from electromagnetic sounding data. Geophysics Vol. 52. N.3, 289-300.

De Groot-Hedlin, C., Constable, S., 1990. Occam's inversion to generate smooth, two dimensional models form magnetotelluric data. Geophysics 55, 1613-1624. doi.org/10.1190/1.1442813.

Gruppo di lavoro MS; 2008: *Indirizzi e criteri per la microzonazione sismica*. Conferenza delle Regioni e delle Provincie autonome – Dip. Della Protezione Civile, Roma, 3 vv. e DVD.

Loke, M.H., Barker, R.D., 1996. Rapid least-squares inversion of apparent resistivity pseudosections using a quasi-Newton method. Geophys. Prospect. 44, 131-152..

Morelli G. and Labrecque D., (1996). Advances in ERT inverse modeling European Journal of Environmental and Engineering Geophysics 1(2):171-186.

Porreca, M., Smedile A., Speranza F., Mochales T., D'Ajello Caracciolo F., Di Giulio G., Vassallo M., Villani F., Nicolosi I., Carluccio R., Amoroso S., Macrì P., Buratti N., Durante F., Tallini M. & Sagnotti L., (2016). Geological reconstruction in the area of maximum co-seismic subsidence during the 2009 Mw=6.1 L'Aquila earthquake using geophysical and borehole data, Italian Journal of Geosciences 135(2):1-33, doi:10.3301/IJG.2015.37.

Villani, F., Pucci, S., Civico, R., De Martini, P.M., Nicolosi, I., D'Ajello Caracciolo, F., Carluccio, R., Di Giulio, G., Vassallo, M., Smedile, A., Pantosti, D., 2015, Imaging the structural style of an active normal fault through multidisciplinary geophysical investigation: a case study from the Mw 6.1 L'Aquila earthquake region (central Italy). Geophys. J. Int. (2015) 200, 1676-1691.

Villani, F., & Sapia, V. (2017). The shallow structure of a surface-rupturing fault in unconsolidated deposits from multi-scale electrical resistivity data: The 30 October 2016 Mw 6.5 central Italy earthquake case study. Tectonophysics, 717(16), 628– 644. doi.org/10.1016/j.tecto.2017.08.00.

Corresponding author: francesca.caracciolo@ingv.it

Combining active and passive methods to understand the seismic velocity distribution in a thick Quaternary succession of the Po Plain. (Terre del Reno, Ferrara, Italy)

G. Di Giulio[1], L. Minarelli[1], M. Stefani[2], G. Milana[1], G. Tarabusi[1], M. Vassallo[1], S. Amoroso[1,3], A. Affatato[4], L. Baradello[4], L. Petronio[4]

1 Istituto Nazionale di Geofisica e Vulcanologia (Rome, Italy)

2 Università degli Studi di Ferrara (Ferrara, Italy)

3 Università degli Studi di Chieti-Pescara (Pescara, Italy)

4 Istituto Nazionale di Oceanografia e Geofisica Sperimentale – OGS (Trieste, Italy)

Introduction

To properly evaluate the local effects of earthquakes and improves the seismic profiles inversion, a good knowledge of the seismic velocity depth distribution is needed. Acquiring such a distribution is however a challenging issue in fast-subsiding alluvial sedimentary basins, with thick unlithified, low-velocity successions, and reduced seismic impedance contrasts, as in the Po Plain (Mascandola *et al*., 2021). Passive acquisition techniques, based on stand-alone stations and focused on the estimation of resonance frequency, can provide only raw information on the local velocity profile and are not particularly effective, by themselves, in areas as the lower Po Plain. Their proper interpretation needs independent stratigraphic data on the subsurface. Other passive techniques, based on array configurations of seismic stations, with varying geometries and apertures, increase the frequency band of analysis. Recent technology improvements and the advances in the array processing of three-component ambient-vibration recording further constrains the inversion process, generating a reliable shear-wave velocity profile, and supporting the extraction of the Rayleigh-wave ellipticity (Whatelet *et al*., 2018). HVSR and array methods however produce the most reliable results only in presence of sharp seismic contrasts, developed at a relatively shallow depth (approximately < 200 m), which is not the case of the study area. An effective approach to the reconstruction of deep velocity profiles, in similar sedimentary basins, consists in the combination of passive and active methods. Downhole and seismic reflection prospecting can provide reliable S and P velocity profiles. Petronio *et al*. (2023) shows an example of a successful application of such active methods in a case study from the Po Plain area, about 25 km west to our investigation site. The authors derived shear-wave (Vs) and compressional (Vp) velocity tomography models down to a depth of about 300 and 700 m respectively; Vs never exceed 600 m/s. Our study combines multiple geophysical techniques to define the seismic wave propagation model in a site at the south-west of Ferrara, near San Carlo (Fig. 1A), affected by the 2012 earthquakes. We acquired one of the deepest down-hole measurements so far available in the Po Plain, providing a rare opportunity to calibrate the velocity models produced by surface geophysical investigations. The Quaternary succession was drilled to the depth of almost 400 m,

cuttings were analysed, and a continuous spontaneous emission gamma log was measured. Accurate down-hole velocity measurements of both V_P and V_S were acquired, from the surface to the depth of 370 m, providing results in good match with a previous investigation, which was limited in depth (Minarelli *et al*. 2016). The down-hole recordings were compared with the results of the vertical seismic profile and of surface investigation we performed on site, consisting of a seismic reflection profile, passive seismic arrays, and single-station vibration measurements. The various sources of information were combined to generate a reliable Vs profile and an interdisciplinary image of the subsurface properties.

Geology and Stratigraphy Framework

The research region belongs to the external buried portion of the Apennines, dominated by active thrust-fold structures (Martelli *et al.*, 2017), developed through Plio-Pleistocene times (Ghielmi *et al*., 2013). The investigated site is placed on a broad syncline (Fig. 1A), part of the tectonic Ferrara Arc. The active faults generate a significant seismic activity, including that of May 2012. The strong synsedimentary deformation largely influenced the Plio-Quaternary stratigraphic architecture. The older unit involved in the research consists of Pliocene deep-marine terrigenous turbidites (P2, Fig. 3A). The interruption of the turbidite sedimentation in the study area (Porto Garibaldi Fm top) corresponds to the tectonic rising of submarine anticline bulges in western areas (e.g. Mirandola), preventing the currents from reaching eastern regions (Ghielmi *et al.* 2010, 2013). The following Marine Quaternary unit records the evolution from deep-water argillaceous deposits (QM2) to delta sediments (QM1). The combination of tectonics, eustasy, and climate fluctuations induced the unconformity surfaces supporting the subdivision of the following Quaternary successions into allostratigraphic units (Regione Emilia-Romagna *et al.*, 1998). A phase of deformation induced the unconformity base of the Emilia-Romagna Supersynthem, which is bipartite into the Lower (AEI) and Upper (AES) Emilia-Romagna Synthems by a surface associated with a gentler phase of structural reorganization and marine lowstand (Martelli, 2021). At the study site, the lowermost portion of AEI still records marine influences, associated with interglacial highstand phases. The upper part of AEI and in AES record purely continental conditions. The synthems in turn frame several subsynthems, each corresponding to an individual glacio-eustasy fluctuation, in the 100,000-year frequency band, as in the upper three Subsynthems (AES 6, 7, 8). The research well crossed the whole of the Emilia-Romagna Supersynthem and penetrated a large portion of QM1. The properties of the underlying units, down to the Pliocene turbidites (P2), were indirectly interpreted from the seismic investigation we performed.

Research methods and results

In the research site, multiple geophysical techniques were combined to achieve a reliable seismic wave propagation model. The site was selected because placed in the epicentral area of the 2012 seismic sequence, and because of the availability of an accessible deep well, where a previous down-hole investigation (Minarelli *et al.*, 2016) already measured both Vp and Vs velocities, to the depth of 265 m. We performed new accurate downhole measurements (Fig. 1B), to the depth of 370 m, together with passive and active seismic surveys at the surface. Active methods, performed by OGS authors, involved the data-acquisition, in the S-waves mode, by geophones and hydrophones in the deep borehole, using a Mini-Vibratory (MiniVib) as source. First-break arrivals and reflected waves were analysed to generate a 1D shear-wave velocity profile, analysed together with the reflection signals recorded by a linear pattern of horizontal geophones, placed at the surface. Passive methods were also applied, through a high-resolution frequency-wavenumber

beamforming (f-k) and spatial autocorrelation (SPAC) analysis (Hailemikael *et al.*, 2023), using a 2D array of seismic stations, with a maximum aperture of about 880 m (Fig. 1B). We computed the Rayleigh (R) and Love (L) dispersion curves (DC) from both (*i*) the linear array of geophones, using the f-k method, and the MiniVib as active source, and (*ii*) from the 2D array of seismic stations, using ambient vibration three-component data, though f-k and SPAC methods. The observed dispersion and H/V curves were jointly inverted with the Geopsy tool (Wathelet et al. 2020) to obtain the 1D shear-wave velocity (Vs) profiles (Fig. 2).

The main result of the work is a consistent mono-dimensional Vs profile, generated by the synthesis the active and passive methodologies, supporting the seismic stratigraphy interpretation of the subsurface to a depth of about 700 m (Fig. 3). The regional unconformity surfaces, supporting the stratigraphic subdivision of the Quaternary successions, are associated with discrete layers of sharp increase of the seismic velocity. The strongest velocity increase is associated with the top of the P2 turbidites, at about 680 m, in perfect match with the base of the Marine Quaternary (QM) illustrated by the Emilia-Romagna Region study, as visible in Fig. 3. The 1D seismic velocity model, developed at the study site, can be extrapolated to similar syncline areas in a wider Po basin area in the finality of seismic response analysis and microzonation analyses.

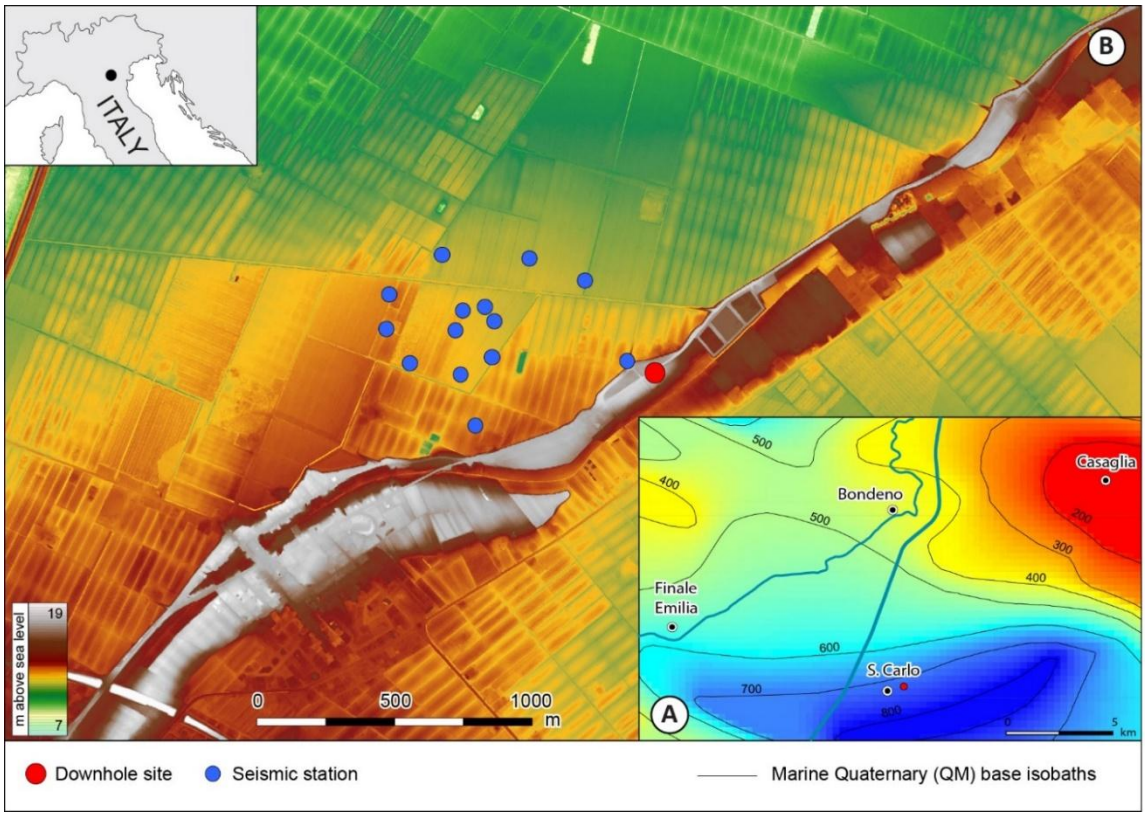

Fig. 1. (A) Depth of the Marine Quaternary top, which has been largely deformed by the ongoing compressional deformation (map produced by the Emilia-Romagna Region Geology Survey). The investigations site is placed on the syncline, at the south of the Casaglia High. (B) Location of the down-hole and of the array of seismic stations. A MiniVib as source was applied for the down-hole acquisition, whereas the seismic stations recorded ambient vibration data. The image background shows the Lidar generated elevation model, depicting the depositional fluvial ridge of the river Reno.

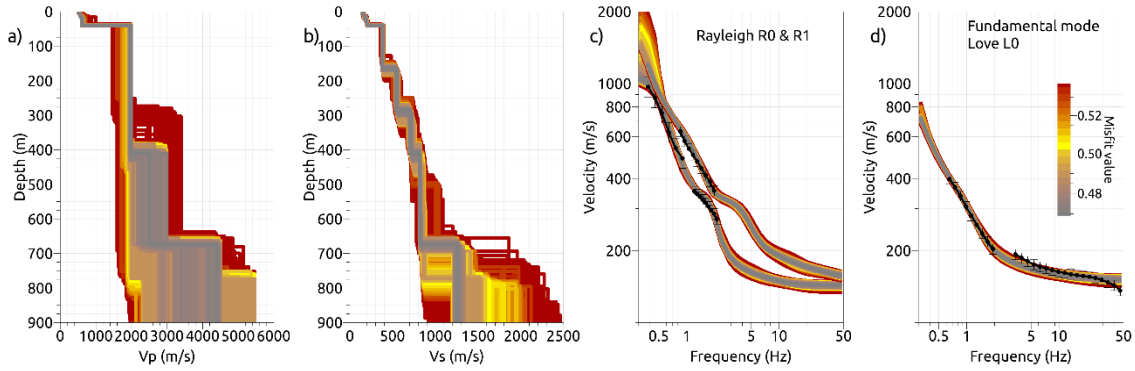

Fig. 2. Inversion results with the rainbow scale proportional to the misfit value. a) Vp models; b) Vs models; c) DCs of the fundamental Rayleigh (R0) and the first higher (R1) mode; d) DCs of the fundamental Love (L0) mode. The field DCs are overlaid in black.

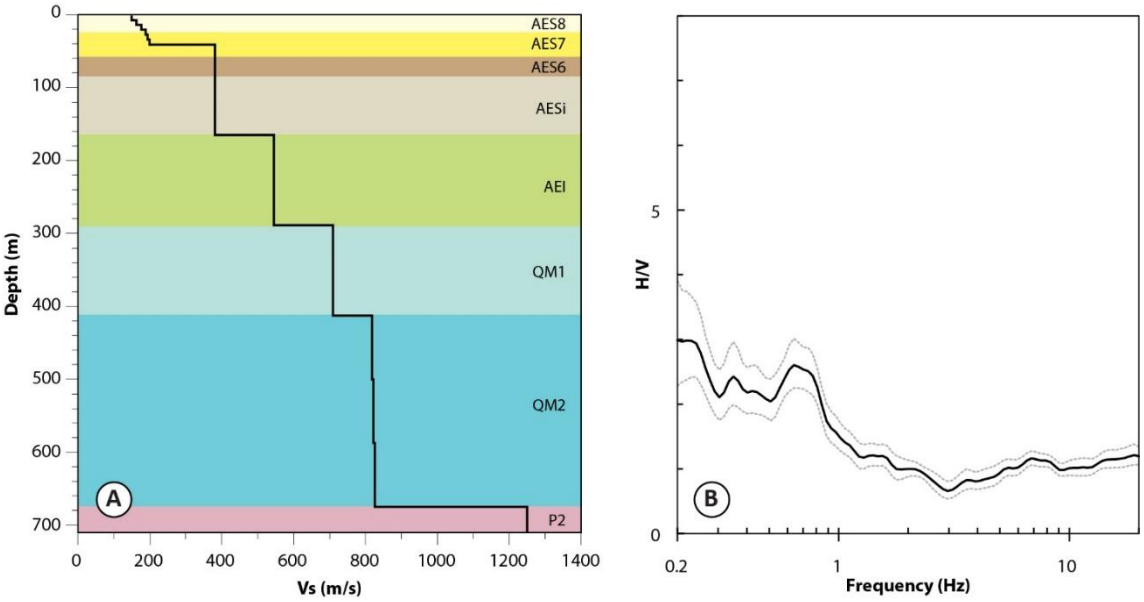

Fig. 3. (A) Average distribution of the S waves velocity with depth, generated by the synthesis of the active and passive methods data, correlated with the stratigraphic units described in the text. Sharp increases in velocity, of the best fitting model extracted from Fig. 2, are normally matched with the main discordance surfaces and stratigraphic boundaries. (B) H/V noise spectral ratios in proximity of the downhole site, derived from many hours of ambient vibration data acquired in November 2018.

Acknowledgements

This work is dedicated to and in memory of Lorenzo Petronio.

References

Ghielmi M., Minervini M., Nini C., Rogledi S. and Rossi M.; 2013: Late Miocene–Middle Pleistocene sequences in the Po Plain - Northern Adriatic Sea (Italy): The stratigraphic record of modification phases affecting a complex foreland basin. Mar. Pet. Geol., SI 42, 50–81.

Hailemikael S., Di Giulio G., Milana G., Vassallo M. and Bordoni P.; 2023: From ambient vibration data analysis to 1D ground-motion prediction of the Mj 5.9 and the Mj 6.5 Kumamoto earthquakes in the Kumamoto alluvial plain, Japan. Earth, Planets and Space, 75(1), p.105.

Mascandola C., Barani S., Massa M. and Albarello D.; 2021: New insights into long-period (> 1 s) seismic amplification effects in deep sedimentary basins: A case of the Po Plain basin of northern Italy. Bulletin of the Seismological Society of America, 111(4), pp.2071-2086.

Martelli L., Bonini M., Calabrese L., Corti G., Ercolessi G., Molinari F.C., Piccardi L., Pondrelli S., Sani F., Severi P.; 2017: Carta sismotettonica della Regione Emilia- Romagna e aree limitrofe, scala 1:250.000 (ed. 2016). Con note illustrative. Regione Emilia-Romagna, SGSS; CNR, IGG sez. FI; Università degli Studi di Firenze, DST; INGV sez. BO. D.R.E.AM. Italia.

Martelli L.; 2021: Assessment of Seismic Bedrock in Deep Alluvial Plains. Case Studies from the Emilia-Romagna Plain. Geosciences, 11(7), p.297.

Minarelli L., Amoroso S., Tarabusi G., Stefani M. and Pulelli G.; 2016: Down-hole geophysical characterization of middle-upper Quaternary sequences in the Apennine Foredeep, Mirabello, Italy. Annals of Geophysics, 59(5), p. S0543, https://doi.org/10.4401/ag-7114.

Petronio L., Baradello L., Poggi V., Minarelli L., Böhm G., Affatato A., Barbagallo A., Cristofano G., Sorgo D., Martelli L. and Lai C.G.; 2023: Combining SH-and P-wave seismic reflection survey to support seismic response analysis. A case study from Cavezzo (Italy) after the 2012 Emilia earthquake. Engineering Geology, 313, p.106916. https://doi.org/10.1016/j.enggeo.2022.106916.

Wathelet M., Guillier B., Roux P., Cornou C. and Ohrnberger M.; 2018: Rayleigh wave three-component beamforming: signed ellipticity assessment from high-resolution frequency-wavenumber processing of ambient vibration arrays. Geophysical Journal international, 215(1), pp.507-523.

Wathelet M., Chatelain J.L., Cornou C., Di Giulio G., Guillier B., Ohrnberger M. and Savvaidis A.; 2020: Geopsy: A user-friendly open-source tool set for ambient vibration processing. Seismological Research Letters, 91(3), pp.1878-1889.

Corresponding author: giuseppe.digiulio@ingv.it

Inductive Induced Polarization Effects: the Loupe EM synthetic case study

F. Dauti[1], A. Viezzoli[2], G. Fiandaca[1]

[1] The EEM Team for Hydro & eXploration, Dep. of Earth Sciences A. Desio, Università degli Studi di Milano, Milano (Italy)
[2] Emergo s.r.l., Cascina (Italy)

Introduction

The Loupe electromagnetic profiling system (Street et alii, 2018) is a two-operator, portable, time-domain electromagnetic system mounted on backpacks, designed to image electrical conductivity in the near-surface at high spatial and vertical resolution. This particular configuration (visible in *figure 1*), as well as drastically speed up the acquisition procedure, allows to acquire data where the topography and logistic are too complex for a standard EM loop. This extends the EM application to a great number of environments.

Figure 1. Loupe EM system configuration for an acquisition in the Val Sabbia (BS) mountainous area.

For the Loupe system, a quick transmitter waveform turn-off (10 μs) allows to get a good resolution in the near surface while the of 20 A of peak current and 13 turns in the coil allow to reach a good depth of investigation, exceeding 50 m.
With this work we aim to assess if and how the system is sensitive to Induced Polarization (IP) effects.
IP effects on EM data have been studied since the early '80s (e.g. Spies, 1980; Lee, 1981), and have re-gained attention in recent years thanks to the ability to invert for IP effects on EM data in terms of Cole-Cole models (e.g. Viezzoli et al., 2017; Lin et al, 2019; Couto et al., 2020; Grombacher et al., 2021). However, the importance of IP modelling in EM data is still often overlooked, and false structures (incorrect conductivity-thickness parameters) may be recovered when IP is not properly modelled (Viezzoli et al. 2017). In order to study the IP effect on the Loupe system, we focused on a simple but representative case: a two-layer model with a chargeable cover over a resistive bedrock. This case may represent targets suitable for the Loupe system: mine wastes; permafrost; weathered covers over bedrock on mountainous areas. The study is performed varying the electrical properties of the cover layer, and its thickness, in order to highlight quantitatively the significance of the IP effect.

Method

In order to define how the Induced Polarization affects the Loupe electromagnetic response, we compute the forward response (following Auken et al., 2015) from a large amount of two-layer models, consisting of a chargeable cover over a resistive bedrock. The model space is defined in terms of the Cole-Cole resistivity model, as defined by Pelton et al. (1978):

$$m_{IP} = \{\rho_j, m_{0_j}, c_j, thk_j\}, \quad j = 1,2 \qquad \text{(eq. 1)}$$

Table 1 contains the Cole-Cole parameters used for simulating the first chargeable layer, in all combinations. The second layer instead has been always considered a purely resistive layer at 1000 Ω*m. For each Cole-Cole two-layer model, we calculate a corresponding purely resistive two-layer model (using the DC resistivity value of the Cole-Cole model), and we compare the responses.

Chargeable first layer				
Rho [Ω*m]	**m0** [mV/V]	**Tau** [s]	**C**	**Thk** [m]
1	5	1e-04	0.5	5
2	8	3e-04		20
3	13	1e-03		
4	20	3e-03		
6	30	1e-02		
10	50	3e-01		

15	80	1e-01		
25	125	1		
40	199			
65	315			
100	500			

Table 1. Parameter values of the first layer.

The amount of distortion produced by IP for each forward response is computed as the mean absolute percentage difference over the entire response, as follows:

$$Distortion = \sum_{j=1}^{n} \frac{100}{n} \left\| \frac{fwr_{NOIP_j} - fwr_{IP_j}}{fwr_{NOIP_j}} \right\| \bullet \qquad \text{(eq.2)}$$

Where n represents the number of gates above the noise floor, set to 1e-12 V/Am^4 at 1 ms, in order to quantify only detectable IP effects; fwr_{NOIP_j} represents the jth gate of the forward response computed disregarding IP; fwr_{IP_j} is the jth forward response computed with IP.

Results

An example of comparison of forward responses with/without IP for the X and Z components of the Loupe system is shown in *figure 1*. The model, described in the textbox, represent a simplified but common geology, with a thin conductive, slightly chargeable cover that overlies a resistive second layer. As clearly evident, the transients affected by IP are heavily distorted, both for the X and for the Z component, culminating in the change of sign of the modelled signal.

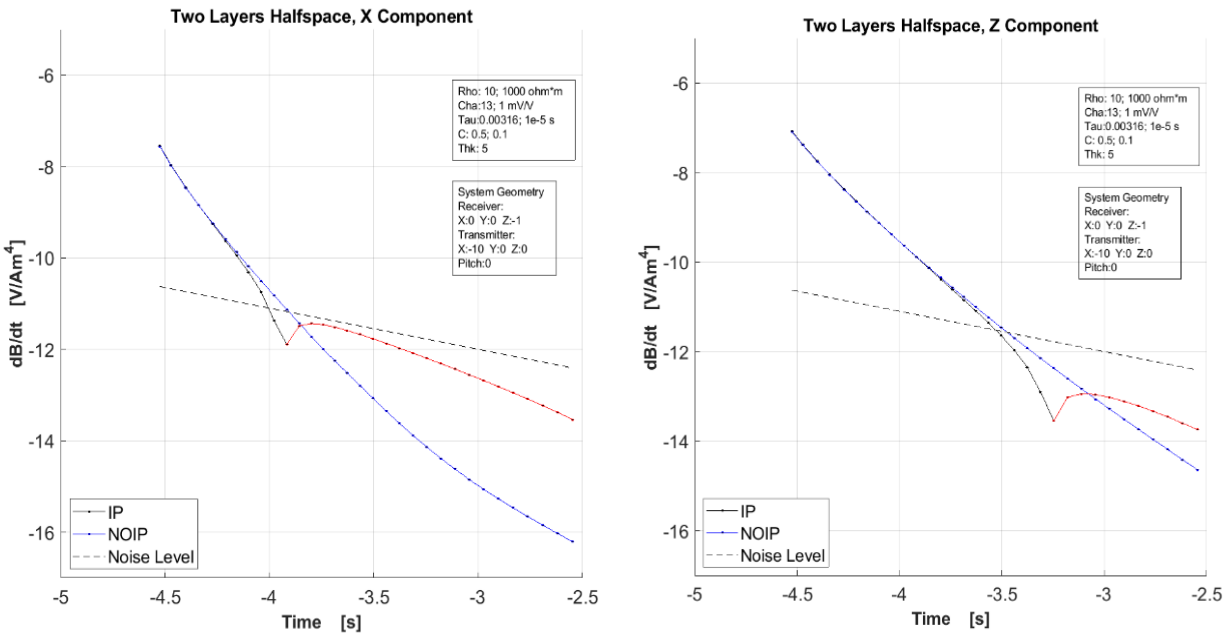

Below, *in figure 3*, follows an example of representation of the results in a 2D map, representing in color the distortion, as computed following equation 2, as a function of chargeability and resistivity of the first layer.

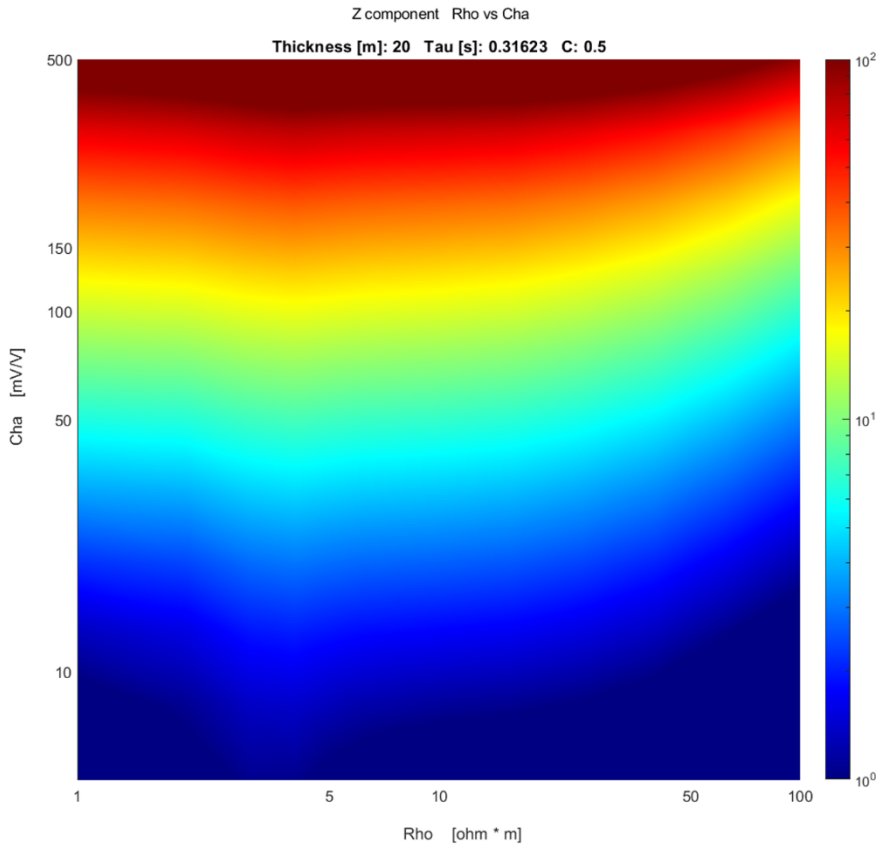

Figure 3. Representation of the IP Distortion (eq.2) for the Loupe Z component, for two layers models. The first layer thickness, Tau and C parameters are kept fixed in the title, while the Resistivity and Chargeability vary along the axes. The colorscale represents the difference, in percentage, between the IP affected halfspace and the purely resistive halfspace forward responses.

IP affects significantly the forward response even with low values for chargeability and high values for the time constant. The increase of the distortion follows the increase in chargeability, and already from 10 mV/V an error higher of 5% is reached. This spread of IP effects is linked to the two-layers configuration with resistive bedrock: the IP EM vortex currents, which flow in opposite direction of the eddy currents, propagate slowly in the second layer and dominate the current flow. In this configuration it is also interesting to see how even for a time constant of 0.3 ms it is possible to detect the IP effects above the noise level, also with a 75 Hz instrument.

Conclusions

The results presented in this study are surprising: in a two-layer environment with a chargeable cover over a resistive bedrock, even small chargeability values (e.g. 10 mV/V) creates significant effect in the responses measurable with the portable Loupe System, also with detectable data change of sign. Furthermore, these effects are not confined to low values of the time constant of the Cole-Cole model (e.g. below 1 ms), but persist also for tau values in the range of seconds. These results imply that the IP effect cannot be overlooked when operating with the Loupe system, for instance in surveys involving mine wastes, permafrost and weathered covers over bedrock on mountainous areas.

References

Auken E., Christiansen A.V., Kirkegaard C., Fiandaca G., Schamper C., Behroozmand A.A., Binley A., Nielsen E., Efferso F., Christensen N.B., Sorensen K., Foged N. & Vignoli G., 2015. An overview of a highly versatile forward and stable inverse algorithm for airborne, ground-based and borehole electromagnetic and electric data, Exploration Geophysics, 46, 223-235. 10.1071/eg13097

Couto Junior, M. A., Fiandaca, G., Maurya, P. K., Christiansen, A. V., Porsani, J. L., & Auken, E. (2020). AEMIP robust inversion using maximum phase angle Cole–Cole model re-parameterisation applied for HTEM survey over Lamego gold mine, Quadrilátero Ferrífero, MG, Brazil. Exploration Geophysics, 51(1), 170-183.

Grombacher, D., Auken, E., Foged, N., Bording, T., Foley, N., Doran, P. T., ... & Tulaczyk, S., 2021. Induced polarization effects in airborne transient electromagnetic data collected in the McMurdo Dry Valleys, Antarctica. Geophysical Journal International, 226(3), 1574-1583.

Lee, T., 1981. Transient electromagnetic response of a polarizable ground. Geophysics, 46,7, 1037-1041.

Lin, C., Fiandaca, G., Auken, E., Couto, M. A., & Christiansen, A. V., 2019. A discussion of 2D induced polarization effects in airborne electromagnetic and inversion with a robust 1D laterally constrained inversion scheme. Geophysics, 84(2), E75-E88.

Pelton, W. H., Rijo, L., & Swift Jr, C. M., 1978. Inversion of two-dimensional resistivity and induced-polarization data. Geophysics, 43(4), 788-803.

Spies, B.R., 1980. A field occurrence of sign reversals with the transient electromagnetic method. Geophysical Prospecting, 28, 620-632.

Street, G., Duncan, A., Fullagar, P., Tresidder, R., 2018. LOUPE – A Portable EM Profiling System. System, ASEG Extended Abstracts, 2018:1, 1-3, DOI: 10.1071/ASEG2018abW10_3G.

Viezzoli, A., Kaminski, V., Fiandaca, G., 2017. Modeling induced polarization effects in helicopter TEM data: Synthetic case studies. Geophysics, (82-2) E31-E50.

Reference Author: Francesco Dauti, francesco.dauti@unimi.it

Comparing various seismic equipment for H/V and dispersion measurements in three sites near Ferrara (Po Plain, Italy)

G. Di Giulio[1], L. Minarelli[1], G. Milana[1], M. Vassallo[1], G. Tarabusi[1], M. Stefani[2]

1 Istituto Nazionale di Geofisica e Vulcanologia (Rome, Italy)
2 Università degli Studi di Ferrara (Ferrara, Italy)

H/V spectral ratios and surface-wave analysis are very popular techniques in the engineering-seismology community to extract near-surface properties processing data of ambient seismic vibrations (Foti *et al*., 2018). The H/V ratios provide the fundamental resonance of a site (f0), the value of which is related to both the depth of the main impedance contrast and the shear-wave velocity (Vs) of the soft deposit (Molnar et al., 2022). Surface-wave analysis is largely used for the extraction of Rayleigh and Love dispersion curves, using several sensors, deployed in mono (1D) or bi-dimensional (2D) field geometry, for recording ambient vibrations (passive case). Surface-wave analysis computes dispersion curves for Rayleigh and Love waves (R and L, respectively), through frequency-wavenumber (f-k) and spatial autocorrelation (SPAC) methods (for methodology details see Hailemikael et al., 2023). Recent advances in the technology of seismic equipment make it possible to use many seismic sensors, different in properties and cost, for measurements the H/V and dispersion curves.

In this work, the research aim is to test the performance of different equipment in the estimation of the field curves (i.e. H/V and surface-wave dispersion). We show H/V and surface-wave curves (Rayleigh and Love), acquired with different sensors and field geometry, in three case studies from the Ferrara area, Po Plain (Italy). The Po sedimentary basin is the largest of Italy and is characterized by tick, soft terrigenous deposits and low-frequency resonance (Mascandola *et al*., 2021).

One of the selected sites is within the Ferrara city wall, near the Jewish cemetery, one in the village of Casaglia, about 9 km north-east of the city centre, one in the Pieve di Cento municipality, 20 km south-west of Ferrara town (Fig. 1). At each of the three sites, in October 2020, the following equipment for recording ambient vibrations was used: i) twelve seismic 24-bit dataloggers (Reftek 130) coupled with Lennartz three-components velocimeter (Le3D) with eigen-frequency of 0.2 Hz, ii) seven all-in-one three-components Terrabot stations produced by Sara Electronics, with an eigen-frequency of 4.5 Hz, iii) twenty-four vertical geophones with eigen-frequency of 4.5 Hz connected to a multi-channel station (Geode manufactured by Geometrics).

All the above equipment was deployed in 2D configuration, following nearly circular geometry, depending on the local logistic. Fig. 1 show an example of installation, at the Casaglia site. The Le3D and Terrabot velocimeters were arranged in the field with a maximum aperture varying from about 200 to 300 m (depending on site). The vertical geophones, which are constrained by cables, were deployed in a circular ring of 50 m of aperture. All the data were processed with similar parameters, using the Geopsy tool (Wathelet *et al*. 2020).

The comparison of the H/V curves (Fig. 2) shows that Le3D and Terrabot provide the same H/V spectral ratios, at the three selected sites, even if the f0 is well below the Terrabot eigen-frequency of 4.5 Hz. At the Casaglia site, the H/V curves show a consistent narrow and strong peak at 0.7 Hz, resulting from both Le3D and Terrabot instruments. The good agreement between Le3D and Terrabot is also verified at the Ferrara site, where the f0 is at about 0.2 Hz. A good fit is also observed for the last site at Pieve di Cento, where the H/V curves do not show a clear peak, but rather a bump between 0.2 and 0.3 Hz (Fig. 2).

Concerning the dispersion curves, we also observed a good fit between the three equipment typologies, taking into account the different geometry and number of receivers giving dispersion curves in different frequency bands. However, the resulting dispersion curves from Le3D, Terrabot and geophones show a good match in the nearly overlapping frequency band.

For the Casaglia site, corresponding to a structural high zone of the Po Plain (Tarabusi and Caputo, 2017), we also present a joint inversion of the dispersion and H/V curves (Fig. 3). The Vs profile shows a main interface at about 140 m deep, corresponding to the angular unconformity, erosive top of the marine Miocene marls. The overlying Quaternary succession largely consists of alluvial plain deposits, showing a downward Vs increase from 120 to 450 m/s.

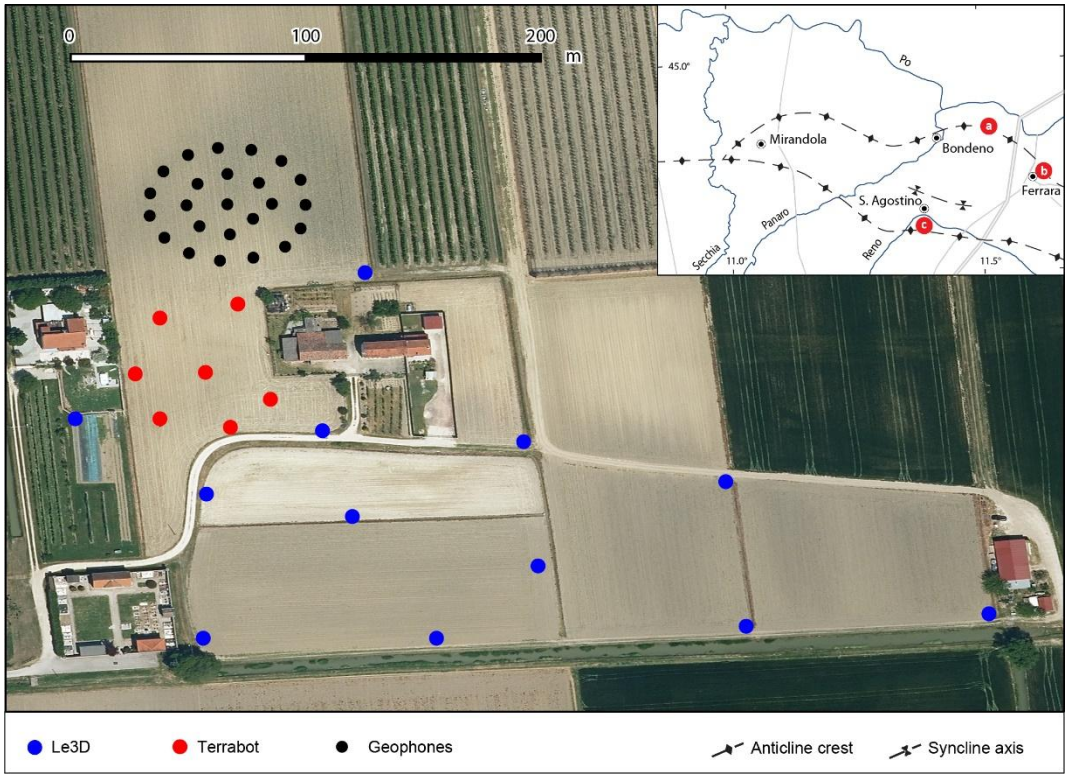

Fig. 1. Sensors array geometry for the Casaglia site. The seven Terrabot are shown as red dots (maximum aperture of 50 m), the twelve Le3D5s velocimeters are shown by blue colour (maximum aperture of about 300 m), the twenty-four vertical 4.5 Hz geophones are shown by black colour (maximum aperture of 60 m). The inset shows the position of the three investigated sites (Casaglia, Ferrara and Pieve di Cento).

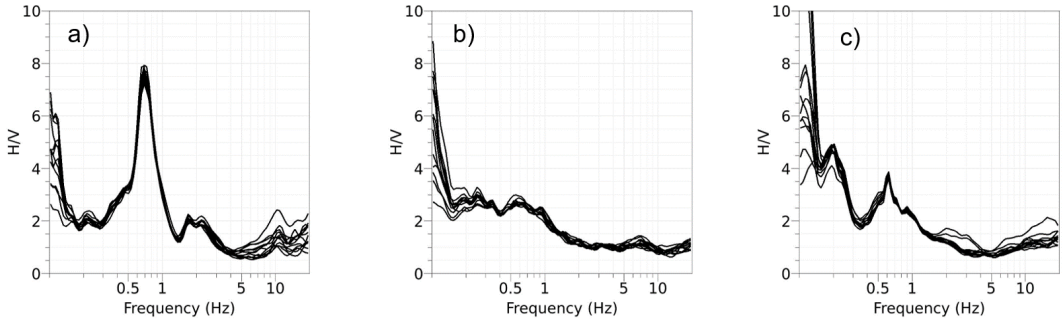

Fig. 2. H/V noise spectral ratios for Casaglia (a), Pieve di Cento (b), and for the northern sector of the city of Ferrara (c).

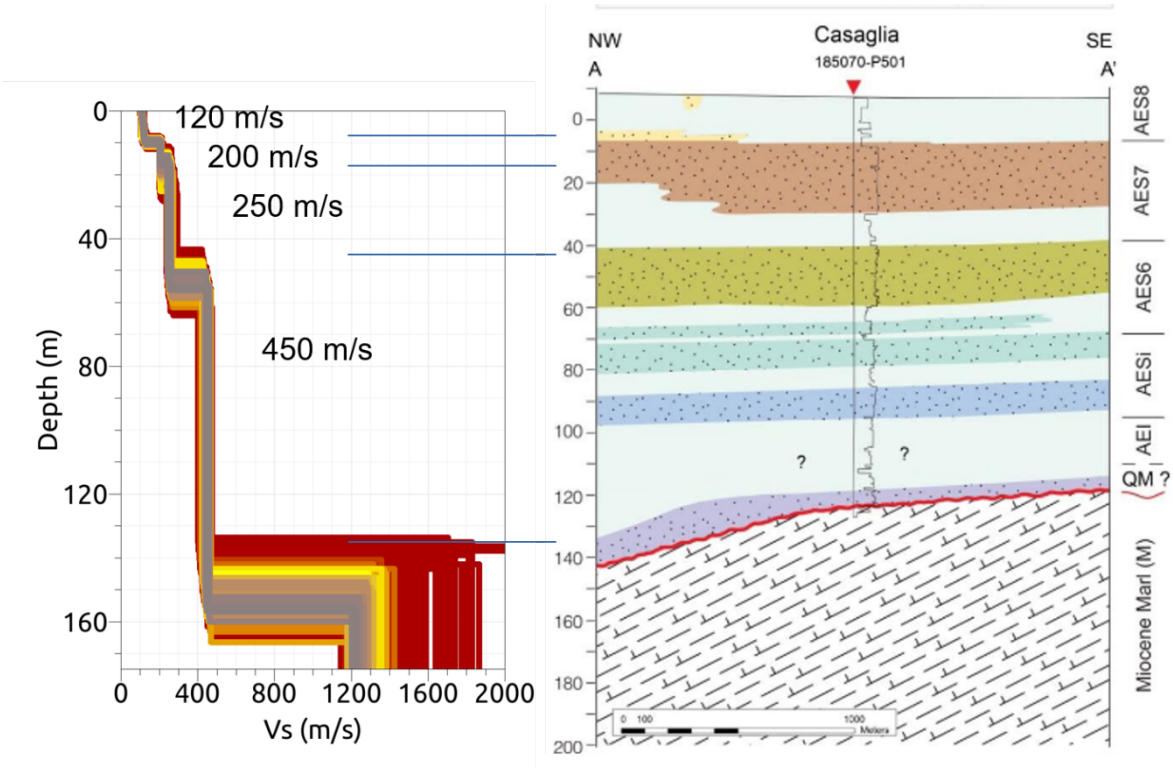

Fig. 3. Casaglia site. Shear-wave velocity profile derived from surface-wave inversion (the colour is proportional to the misfit value), together with stratigraphic interpretation of the Quaternary succession. The value of average Vs is also depicted in the profile.

References

Foti S., Hollender F., Garofalo F., Albarello D., Asten M., Bard P.Y., Comina C., Cornou C., Cox B., Di Giulio G. and Forbriger T.; 2018: Guidelines for the good practice of surface wave analysis: a product of the InterPACIFIC project. Bulletin of Earthquake Engineering, 16(6), pp.2367-2420

Molnar S., Sirohey A., Assaf J., Bard P.Y., Castellaro S., Cornou C., Cox B., Guillier B., Hassani B., Kawase H. and Matsushima S.; 2022: A review of the microtremor horizontal-to-vertical spectral ratio (MHVSR) method. Journal of Seismology, pp.1-33

Hailemikael S., Di Giulio G., Milana G., Vassallo M. and Bordoni P.; 2023: From ambient vibration data analysis to 1D ground-motion prediction of the Mj 5.9 and the Mj 6.5 Kumamoto earthquakes in the Kumamoto alluvial plain, Japan. Earth, Planets and Space, 75(1), p.105.

Mascandola C., Barani S., Massa M. and Albarello D.; 2021: New insights into long-period (> 1 s) seismic amplification effects in deep sedimentary basins: A case of the Po Plain basin of northern Italy. Bulletin of the Seismological Society of America, 111(4), pp.2071-2086.

Tarabusi G. and Caputo R.; 2017: The use of H/V measurements for investigating buried tectonic structures: The Mirandola anticline, Northern Italy, as a case study, Int. J. Earth. Sci. 106, no. 1, 341–353

Wathelet M., Chatelain J.L., Cornou C., Di Giulio G., Guillier B., Ohrnberger M. and Savvaidis A.; 2020: Geopsy: A user-friendly open-source tool set for ambient vibration processing. Seismological Research Letters, 91(3), pp.1878-1889.

Corresponding author: giuseppe.digiulio@ingv.it

Non-Destructive Testing for the conservation of a cultural heritage: GPR surveying on masonry walls at the Castellina Museum (Norcia, Italy).

M. Ercoli[1*], N. Cavalagli[2], M. Barchi[1], C. Pauselli[1], M. Porreca[1], R. Lupi[3].

1 Università degli Studi di Perugia, Dip. Fisica e Geologia, Italy.
2 Università degli Studi di Perugia, Dip. Ingegneria Civile ed Ambientale, Italy.
3 Università degli Studi di Perugia, Dip. di Scienze Politiche, Italy.

The conservation of historical masonry constructions represents one of the major challenges for scientific research, especially in the case of monumental buildings with high artistic and cultural values in areas characterized by high seismic hazard. Here, historical buildings are periodically shacked and damaged by strong earthquakes, and have been subjected to restorations and changes of their original configuration. By a mechanical point of view, in the last decades the research has been continuously involved in the development of advanced and effective methodologies, conventionally invasive, focused to derive a mechanical evaluation of their static and dynamic behaviour, as well as on the characterisation of masonry materials. At the same time, Non-Destructive Testing (NDT) techniques can be also very useful when the preservation of such cultural heritages needs to be ensured by reducing the invasive interventions (Santos-Assuncao et al., 2014). GPR is one of the non-invasive techniques providing high-resolution images of the subsurface, founding wide application in archaeological and civil engineering studies on ancient walls (Ercoli et al., 2016), as well as for masonry wall diagnostics (Lombardi et al., 2021; Negri and Aiello, 2021).

In this work, we have used a Ground Penetrating Radar (GPR) to obtain non-destructive information on the internal structure of a historic masonry wall of the Castellina Museum in Norcia city centre, which is currently unusable after the serious damaging caused by the long-lasting seismic sequence occurred in 2016-2017 (Norcia earthquake sequence, mainshock Mw=6.5, Porreca et al., 2018). We have investigated a wall located at the ground floor of the building, known to be part (the facade) of a previous edifice, the Palazzo del Podestà. On such a masonry wall, standard sonic tests (ST) have been formerly performed on localized areas to investigate the homogeneity degree of the masonry and, to identify the presence of possible voids, cracks and degraded areas. Such measures aimed to measure the propagation velocity of sonic waves on a regular grid, in order to obtain velocity maps able highlighting velocity variations, to be correlated with degraded areas.

Based on such pre-existing data, n°25 Common Offset GPR profiles have been collected across the same grid using high frequency antennas (1 GHz and 1.5 GHz), and later processed, aiming to

integrate and validate the existing data. Additionally, extensive profiling has been accomplished across a wider area, extending horizontally and vertically the initial grid. The first results show the internal structure of the wall, suggesting the presence of heterogenous material and possible internal issues, in agreement with ST maps. Such extensive GPR mapping also evidences the GPR signature sharply changing its reflectivity across the surveyed area, generally showing a significant decrease in reflectivity due to high signal attenuation (high electrical conductivity) particularly in the lower sectors but not without important lateral variations, possibly suggesting moisture variation and degraded sectors (Šťastný et al., 2021). Such behaviour needs further investigations using other NDT techniques (e.g. ERT, De Donno et al., 2017) and chemical analysis to verify the preliminary hypothesis and to assess the general state of conservation of the masonry, mandatory to program suitable remediation interventions in the near future.

References

De Donno, G., Di Giambattista L., Orlando L., 2017: High-resolution investigation of masonry samples through GPR and electrical resistivity tomography, Construction and Building Material, 154, 1234-1249.

Ercoli M., Brigante R., Radicioni F., Pauselli C., Mazzocca M., Centi G., Stoppini A., 2016: Inside the polygonal walls of Amelia (Central Italy): a multidisciplinary data integration, encompassing geodetic monitoring and geophysical prospections. J. Appl. Geophys., 127, 31-44.

Lombardi, F., Lualdi, M., Garavaglia, E., 2021: Masonry texture reconstruction for building seismic assessment: Practical evaluation and potentials of Ground Penetrating Radar methodology, Construction and Building Materials, 299, 124189.

Negri S., Aiello M.A., 2021: High-resolution GPR survey for masonry wall diagnostics, Journal of Building Engineering, 33, 101817.

Porreca, M., Minelli, G., Ercoli, M., Brobia, A., Mancinelli, P., Cruciani, F., Giorgetti, C., Carboni, C., Mirabella, F., Cavinato, G., Cannata, A., Pauselli, C., Barchi, M.R., 2018: Seismic reflection profiles and subsurface geology of the area interested by the 2016–2017 earthquake sequence (Central Italy). Tectonics 37, 1–22.

Santos-Assunçao S., Perez-Gracia V., Caselles O., Clapes J., Salinas V., 2014: Assessment of Complex Masonry Structures with GPR Compared to Other Non-Destructive Testing Studies. Remote Sens., 6, 8220-8237.

Šťastný P., Gašparík J., Makýš O.; 2021: Analysis of moisture and salinity of historical constructions before and after the application of REMEDIATIONS, Journal of Building Engineering, 41, 102785.

Acknowledgements

This project is founded by the Università degli Studi di Perugia, Finanziamento di Progetti di Ricerca di Ateneo Anno 2021, project “Un percorso di ricerca interdisciplinare nel Patrimonio Culturale materiale e immateriale: l’Umbria come laboratorio di indagine” (P.I. Prof.ssa Carla Falluomini), WP 2.4 - Conoscenza, valorizzazione e conservazione del patrimonio materiale e immateriale (Sottogruppo ‘‘Un’eredità fragile: per una rinascita dei patrimoni culturali in area sismica’’). The authors thanks the Municipality of Norcia for their kind support and collaboration.

*Corresponding author: maurizio.ercoli@unipg.it

Mapping surface/ground water interactions and embarkment composition along the Po river with transient electromagnetics

G. Fiandaca[1], A. Signora[1], S. Galli[1], J. Chen[1], C. Compostella[1], M. Gisolo[2], A. Viezzoli[3]

[1] The EEM Team for Hydro & eXploration, Department of Earth Sciences "Ardito Desio", Università degli Studi di Milano, Milano (Italy)
[2] A2A ciclo idrico s.p.a., Brescia (Italy)
[3] EMergo S.r.l. , Cascina (Italy)

In the last week of July 2023 the MapPo dimostrative survey has been carried out along the Po river and its embarkments with waterborne and ground-based electromagnetic methods, for more than 120 km of acquired data, as well as along 350 line km of airborne EM lines, across Lombardia, Veneto and Emilia Romagna (Fig. 1). The MapPo project aimed at mapping groundwater resources, and in particular, with its waterborne and ground-based acquisition, at studying the surface watwer/groundwater interaxctions and at mapping the internal composition of the embarkments.

The ground-based and waterborne acquisition have been carried out twith the tTEM (Auken et al., 2019) and FloaTEM (Maurya et al., 2022) systems, respectively (Fig. 2), while the airborne EM data have been acquired with the SkyTEM306HP system. Furthermore, 1.9 km of time-domain direct-current and induced polarization (DCIP) data have been measured, with the ABEM Terrameter LS2 instrument.

All data have been processed in EEMstudio, an opensource and freeware processing tool for electric and electromagnetic data (Sullivan et al., 2024; Fig. 1), and inverted with EEMverter (Fiandaca et al., 2024). Fig. 3 presents the tTEM and FloaTEM inversion models along 20 km of acquisitions, reaching more than 100 m of depth of investigation, together with the comparison of the DCIP inversion. The FloaTEM inversions allow to discriminate the interactions between river and groundwater, thanks to the ability to map the impermeable (conductive) areas below the river, whicle the tTEM inversions are able to image the thickness of the clays in the embarkment, evidencing the filtration areas mapped by the Po river basin authority. Furthermore, the presence of fossil saline water close to Ferrara, as well as sea water intrusion close to the Po di Goro are well imaged.

The tTEM and FloaTEM inversions are also well comparable with the airborne EM inversions, thank also to the possibility to invert both ground-based, waterborne and airborne EM data in a unique inversion kernel, i.e. EEMverter.

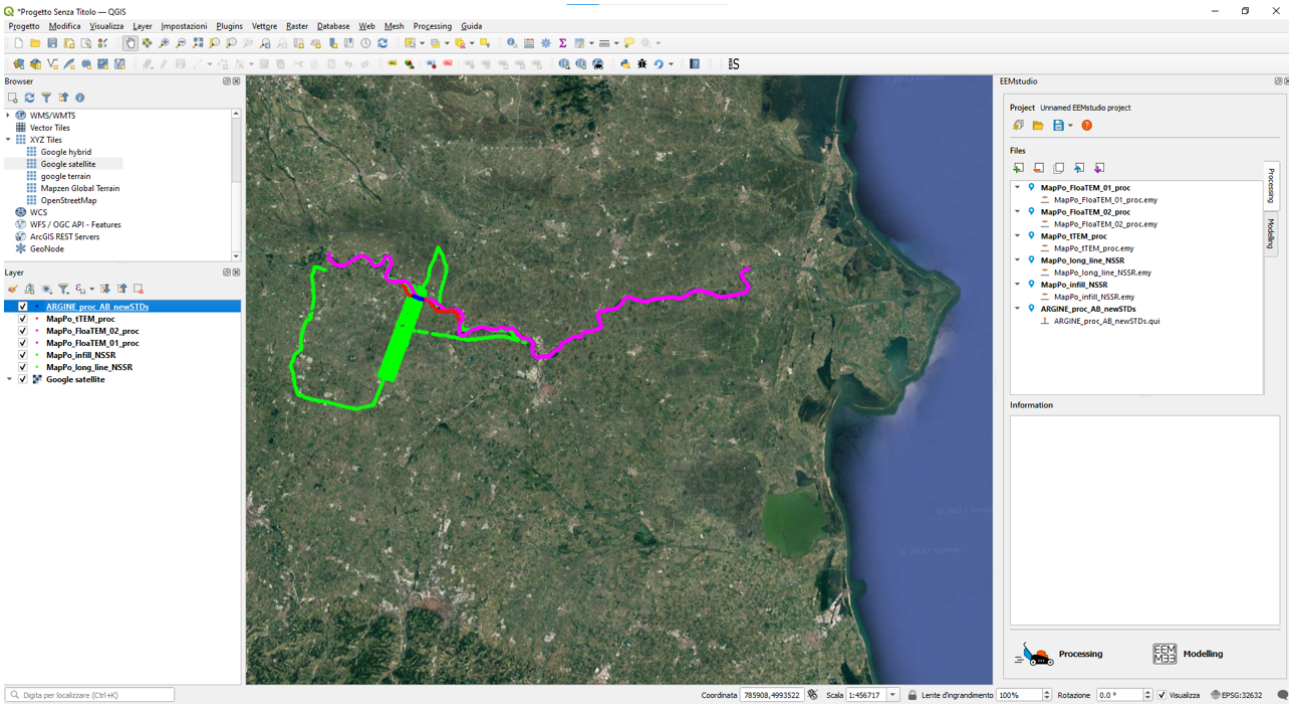

Figure 1. Acquisition lines of the MApPo project visualized in EEMstudio (Sullivan et al., 2024). Magenta line: FloaTEM acquisition. Red line: tTEM acquisition. Blue line: DCIP acquisition. Green lines: SkyTEM acquisition.

Figure 2. Images of the tTEM and FloaTEM acquisitions in the MapPo project.

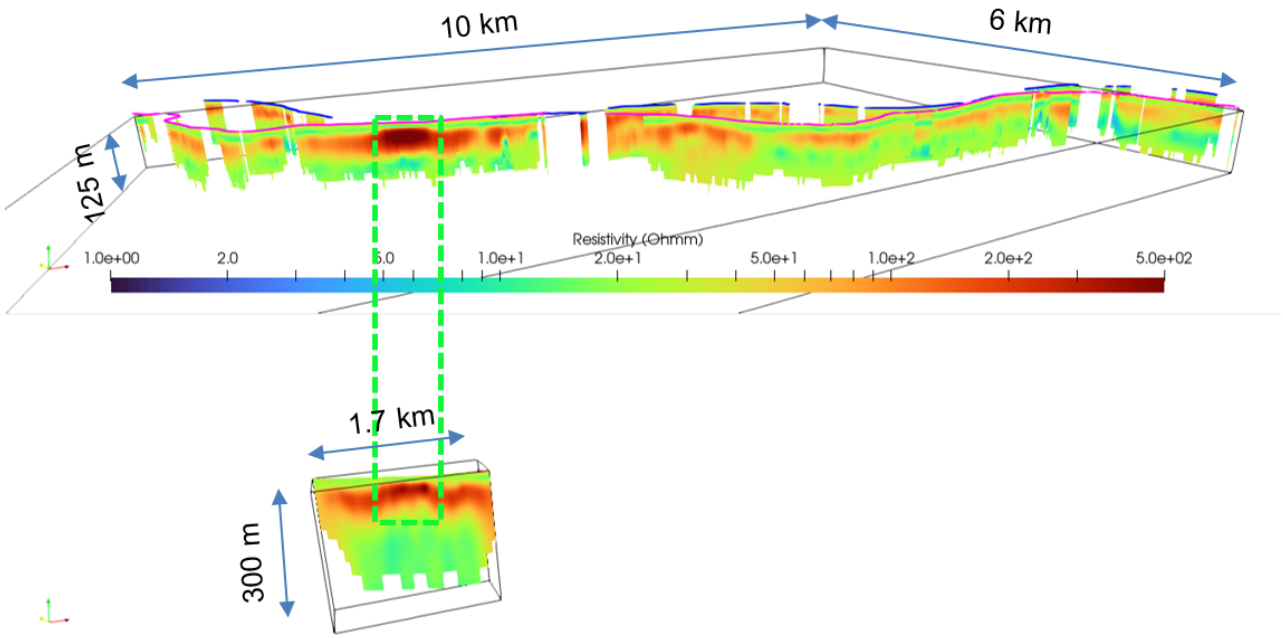

Figure 3. Inversion models of tTEM, FloaTEM and DCIP data along the Po river and its south embarkment. Dashed green line: filtration zone of the embarkment, mapped by adbpo.

Acknowledgments

This study has been funded by A2A ciclo idrico s.p.a., Emergo s.r.l. and The EEM Team for Hydro & eXploration.

References

Auken E., Foged N., Larsen J.J., Trøllund Lassen K.V., Maurya P.K., Dath S.M., Eiskjær T.T (2019). tTEM — A towed transient electromagnetic system for detailed 3D imaging of the top 70 m of the subsurface. Geophysics, 84 (1), E13-E22.

Fiandaca, G., Zhang, B., Chen, J., Signora, A., Dauti, F., Galli, S., Sullivan, N.A.L., Bollino, A., Viezzoli, A. (2024). EEMverter, a new 1D/2D/3D inversion tool for Electric and Electromagnetic data with focus on Induced Polarization. GNGTS 2024, 13-16 February 2024, Ferrara, Italy.

Maurya, Pradip Kumar, et al. "Efficient imaging of hydrological units below lakes and fjords with a floating, transient electromagnetic (FloaTEM) system." Hydrology and Earth System Sciences 26.11 (2022): 2813-2827.

Sullivan, N.A.L., Viezzoli, A., Fiandaca, G. (2024). EEMstudio: processing and modelling of electric and electromagnetic data in a QGIS plugin. GNGTS 2024, 13-16 February 2024, Ferrara, Italy.

Corresponding author: gianluca.fiandaca@unimi.it

Waterborne electromagnetics: two case studies

S. Galli[1], A. Signora[1], J. Chen[1], F. Schaars[2], M. Grohen[3], G. Fiandaca[1]

[1] The EEM Team for Hydro and eXploration, Dep. of Earth Sciences A. Desio, Università degli Studi di Milano, Milano (Italy)
[2] Artesia Water, Schoonhoven (The Netherlands)
[3] Wiertsema & partners, Tolbert (The Netherlands)

Introduction

Interactions between surface water and groundwater are the key for a good understanding of the hydrologic system (Harvey and Gooseff, 2015). In order to describe the hydrologic system, it's mandatory to have a good knowledge of hydrogeological settings below the water column of water. Non-invasive geophysical methods provide spatial information on subsurface properties, but on water bodies has always been difficult (Sheets and Dumouchelle, 2009) or impossible. Electrical and electromagnetic (EM) methods are among the most used geophysical techniques for hydrology (Christiansen et al., 2006; Siemon et al., 2009). Among the electrical methods, electrical resistivity tomography (ERT) has been used a lot for aquatic applications (Manheim et al., 2004). ERT surveys can be performed in many different configurations: with a towed floating cable, with still floating cables or with cables placed on the bottom of the water body. Transient electromagnetic (TEM) and frequency domain EM methods have been used too for hydrology (Ong et al., 2010) and exploration (Munk et al., 2016). Airborne methods have proved themselves reliable at mapping beneath water bodies (Fitterman and Deszcz-Pan, 1998), but they are expensive and have lower vertical and lateral resolution than ground-based methods (Hatch et al., 2010). The tTEM system (Auken et al., 2018), developed in Aarhus University, provided the necessary framework for adapting it to a floating EM system. The waterborne version of the tTEM system is referred to as FloaTEM (Maurya et al., 2022). In Lane et al. (2020) the FloaTEM system was used, in tTEM configuration without modifications, on rivers to characterize the hydrological systems. In this abstract, two applications of FloaTEM mapping carried out in freshwater lakes are presented, in very different geological environments: the southern shore of the Iseo lake in the Brescia province (Italy) and the artificial Ijsselmeer lake in the Netherlands.

Methods and results

For the data acquisition it was used a tTEM system adapted to work on water: the instrument is mounted on a boat made of plastic (to avoid spurious EM coupling in the measurements) that pulls other two smaller plastic boats carrying transmitter loop and receiver loop. To adapt the system for the waterborne survey, plastic supports were built to accommodate the instrumentation and to avoid cables to touch the propeller. Furthermore, an echo sounder synchronized with a GPS were

added in order to record bathymetry. Data were processed using an in-house developed open source and freeware QGIS plug-in, EEMstudio (Sullivan et al., 2024).

Figure 1 shows the acquisition layout and the inversion model of the data acquired in the southern shore of the Iseo lake and in the *Torbiere del Sebino* in the Brescia province (Italy).

In the Iseo lake area the goal is understanding the interactions between surface water and

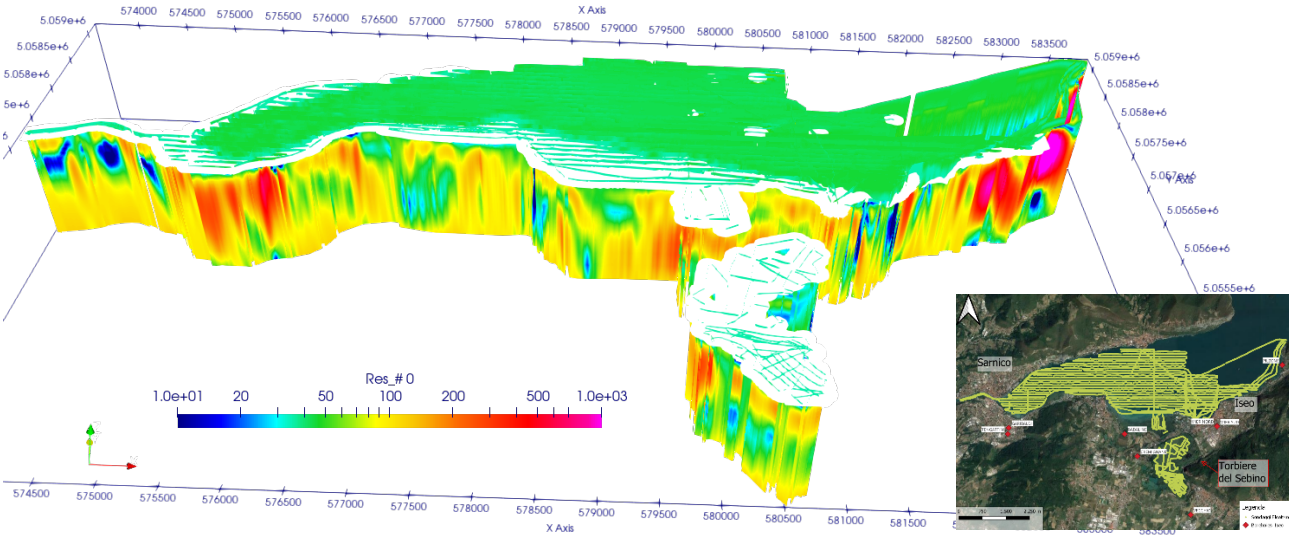

groundwater. In order to achieve this goal, over a five days campaign, 180 km of FloaTEM data were acquired in the Iseo lake and 20 km data were acquired in the Torbiere del Sebino, with a sounding every 5 meters.

The data were inverted in the EEMverter inversion suite (Fiandaca et al., 2024) using a 1D forward mesh interpolated to a 2D model mesh. Bathymetry was incorporated in the inversion breaking the vertical constraints at the bathymetric interface and forcing a narrower resistivity range in the water column (30-50 Ohm m).

Figure 2 shows a comparison between a standard inversion and the inversion that incorporates bathymetry: the bathymetry incorporation avoids overshooting/undershooting of resistivities in the shallowest layer.

Interesting features can be inferred from the inversion model presented in fig. 1: below the water column, in the eastern-most area, a very resistive anomaly (magenta) represents the mountain dipping directly in the lake. In the southern area, below the bottom of the lake, the discontinuous resistive anomaly represents the aquifer underlying the lake. These are the target bodies to understand how lacustrine water interacts with groundwater.

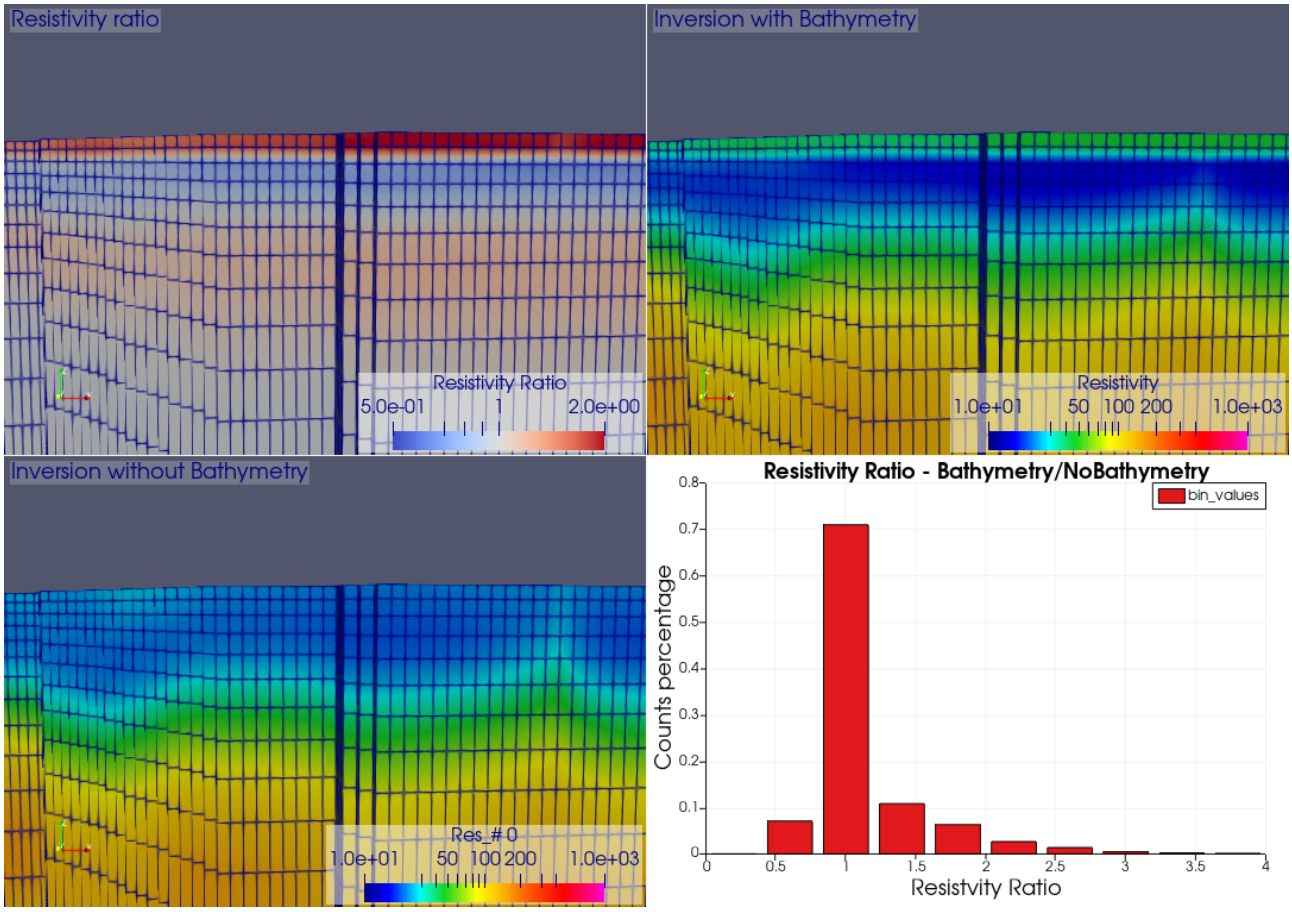

Figure 2: Comparison of standard inversion and bathymetric inversion of FloaTEM data. Top right: bathymetry incorporated in the inversion; Bottom left: standard inversion, without bathymetry incorporation; Top left: ratio between inversion with/without bathymetry incorporation; Bottom right: histogram of the ratio of the resistivity values of the two inversions.

In the Ijsselmeer survey (fig. 3) the geological setting was different and so was the goal: the IJsselmeer was part of the North Sea, but ì in 1932 a 32 km long damn was built, which separated the IJsselmeer from the North Sea; thus, the water gradually freshened, but salty water pockets remain below the lake, separated by a few meters thick discontinuous clay layer.

To map the clay layer and understand the interaction between saltwater and freshwater, over 65 km of FloaTEM data were acquired in a 3-day-long campaign in the western shore of the lake, close

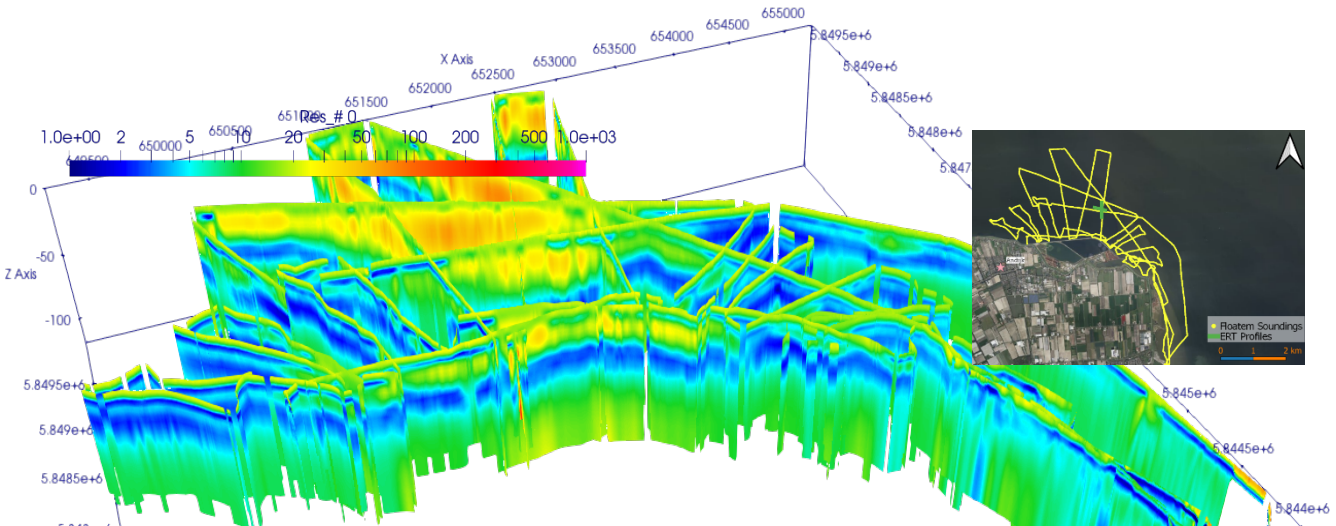

to PWN (a Dutch water management company) facilities in Andijk. Also, to validate data acquired in a new geological setting, a more established geophysical method was used: two underwater ERT profiles, 400 m long each, were acquired close to the FloaTEM soundings acquired in the previous days. The North-South profile was acquired with a Wenner array, the East-West was acquired with a Wenner-Schlumberger array. It was used one 400 m long cable with electrode spacing of 5 meters in the central 200 m and 10 meters on the sides, for a total of 61 electrodes.

Using this system, it was possible to identify areas where the continuity of the clay layer (more conductive) was interrupted and, therefore, it can be seen a freshwater bubble (more resistive) seeping downward from the lake.

Conclusions

Mapping geological heterogeneities below water bodies is mandatory to study interactions between surface waters and groundwater. The FloaTEM system can be a fast, reliable and efficent solution for acquiring data above rivers, lakes and other water bodies. This system offers a good lateral and vertical resolution that can help in mapping small-scale heterogeneities, crucial to correctly depict hydrologic frameworks. Furthermore, the FloaTEM results compare well with more established geophysical methods, such as ERT, but can be acquired with a much higher productivity. In this study the FloaTEM mapping was successfully used to identify interesting underground features in different hydrogeological environments, impossible to infer from ground-based data only.

References

Auken, E., Foged, N., Larsen, J., Lassen, K., Maurya, P., Dath, S., and Eiskjær, T.: tTEM – A towed transient electromagnetic system for detailed 3D imaging of the top 70 m of the subsurface, Geophysics, E13–E22, https://doi.org/10.1190/geo2018-0355.1, 2018.

Christiansen, A. V., Auken, E., and Sørensen, K. I.: The transient electromagnetic method, in: Groundwater Geophysics. A tool for hydrogeology, 1st Edn., edited by: Kirsch, R., Springer, 179–224, https://doi.org/10.1007/3-540-29387-6_6, 2006.

Danielsen, J. E., Auken, E., Jørgensen, F., Søndergaard, V., and Sørensen, K. I.: The application of the transient electromagnetic method in hydrogeophysical surveys, J. Appl. Geophys., 53, 181–198, 2003.

Fiandaca, G., Zhang, B., Chen, J., Signora, A., Dauti, F., Galli, S., Sullivan, N.A.L., Bollino, A., Viezzoli, A. (2024). EEMverter, a new 1D/2D/3D inversion tool for Electric and Electromagnetic data with focus on Induced Polarization. *GNGTS 2024, 13-16 February 2024, Ferrara, Italy.*

Fitterman, D. V. and Deszcz-Pan, M.: Helicopter EM mapping of saltwater intrusion in Everglades National Park, Florida, Explor. Geophys., 29, 240–243, https://doi.org/10.1071/EG998240, 1998.

Farquharson, C.G. & Oldenburg, D.W., (1998). Non-linear inversion using general measures of data misfit and model structure, Geophysics, 134, 213–227.

Harvey, J. and Gooseff, M.: River corridor science: Hydrologic exchange and ecological consequences from bedforms to basins, Water Resour. Res., 51, 6893–6922, https://doi.org/10.1002/2015WR017617, 2015.

Hatch, M., Munday, T., and Heinson, G.: A comparative study of in-river geophysical techniques to define variations in riverbed salt load and aid managing river salinization, 75, WA135–WA147, https://doi.org/10.1190/1.3475706, 2010.

Lane, J. W., Briggs, M. A., Maurya, P. K., White, E. A., Pedersen, J. B., Auken, E., Terry, N., Minsley, B., Kress, W., LeBlanc, D. R., Adams, R., and Johnson, C. D.: Characterizing the diverse hydrogeology underlying rivers and estuaries using new floating transient electromagnetic methodology, Sci. Total Environ., 740, 140074, https://doi.org/10.1016/j.scitotenv.2020.140074, 2020.

Manheim, F. T., Krantz, D. E., and Bratton, J. F.: Studying Ground Water Under Delmarva Coastal Bays Using Electrical Resistivity, Groundwater, 42, 1052–1068, https://doi.org/10.1111/j.1745-6584.2004.tb02643.x, 2004.

Maurya, P. K., Christensen, F. E., Kass, M. A., Pedersen, J. B., Frederiksen, R. R., Foged, N., Christiansen, A. V., and Auken, E.: Technical note: Efficient imaging of hydrological units below lakes and fjords with a floating, transient electromagnetic (FloaTEM) system, Hydrol. Earth Syst. Sci., 26, 2813–2827, https://doi.org/10.5194/hess-26-2813-2022, 2022.

Munk, L., Hynek, S., Bradley, D. C., Boutt, D., Labay, K. A., and Jochens, H.: Lithium brines: A global perspective: Chapter 14, Econ. Geol., 18, 339–365, https://doi.org/10.5382/Rev.18.14, 2016.

Ong, J. B., Lane, J. W., Zlotnik, V. A., Halihan, T., and White, E. A.: Combined use of frequency-domain electromagnetic and electrical resistivity surveys to delineate near-lake groundwater flow in the semi-arid Nebraska Sand Hills, USA, Hydrogeol. J., 18, 1539–1545, https://doi.org/10.1007/s10040-010-0617-x, 2010.

Pihlainen, S., Zandersen, M., Hyytiäinen, K., Andersen, H. E., Bartosova, A., Gustafsson, B., Jabloun, M., McCrackin, M., Meier, H. M., and Olesen, J. E.: Impacts of changing society and climate on nutrient loading to the Baltic Sea, Sci. Total Environ., 731, 138935, https://doi.org/10.1016/j.scitotenv.2020.138935, 2020.

Siemon, B., Christiansen, A. V., and Auken, E.: A review of helicopter-borne electromagnetic methods for groundwater exploration, Near Surf. Geophys., 7, 629–646, 2009.

Sullivan N. A. L., Viezzoli. A., Fiandaca, G.; 2024: EEMstudio: processing and modelling of electric and electromagnetic data in a QGIS plugin, *GNGTS 2024, 13-16 February 2024, Ferrara, Italy.*

Corresponding author: Stefano.galli2@unimi.it

Seismic noise surveys in the area of Etna volcano (southern Italy).

S. Hailemikael[1], D. Famiani[1], G. Milana[1], G. Tusa[2], M. Paratore[2], G. Brunelli[3], R. Azzaro[2]

[1] Istituto Nazionale di Geofisica e Vulcanologia, Rome, Italy.
[2] Istituto Nazionale di Geofisica e Vulcanologia, Catania, Italy.
[3] Istituto Nazionale di Geofisica e Vulcanologia, Milan, Italy.

In 2022 the regional Civil Protection Department started a new project for 3rd level seismic microzonation at Etna, coordinated under the umbrella of the Centro per la Microzonazione Sismica e le sue applicazioni (CentroMS). In the wide range of activities scheduled in the project, one of the targets is the dynamic characterization of the subsurface structure through seismic noise measurements. In this framework, a working group of the Istituto Nazionale di Geofisica e Vulcanologia (INGV) in July 2023 started a campaign of seismic acquisition in the eastern flank of the volcano, the most exposed in terms of seismic hazard due to a number of highly seismogenic faults crossing a very densely urbanised territory (Azzaro et al., 2012, 2013).

In general, the main scientific issue is to characterise subsurface structures related to very different geological and tectonic conditions. In fact, the volcanic environment is highly heterogeneous in terms of lithology for the presence of soft (pyroclastics) and hard (basalts) units determining strong lateral and vertical discontinuities. In addition, the tectonic activity contributes to complicate the geophysical interpretation, since the bedrock is extremely fractured near the fault zone. This also implies a significant role of subsurface fluids circulations.

The first surveys were carried out at 4 selected sites belonging to the national permanent seismic monitoring networks (Nicolosi-ENIC, Sant'Alfio-ESAL; Santa Venerina-EVRN and -SVN). Passive seismic surveys were also carried out at 3 additional sites to investigate the effect of active faults on the noise signals (polarization, see Di Giulio et al., 2009 and references herein).

For each investigated site (Fig. 1), noise data were recorded by nodal seismic sensors in array configuration adapting the experimental setup to environmental conditions. Each sensor is composed of a data recorder, which contains a battery, a 24-bit digitizer, 32 Gb solid-state memory, GPS and GLONASS receiver in a sealed case connected with a three-component geophone sensor with 4.5 Hz eigen-frequency.

In particular, the following parameters varied across sites:

i) number of sensors, ranging from 11 to 46;

ii) acquisition layout;

iii) maximum array aperture, ranging from 100 to 200 m;

iv) recording durations, ranging from 1.5 to 15 hours.

Single station data have been analysed by Horizontal-to-vertical spectral ratio method (H/V), considering also its azimuthal amplitude variation, while Rayleigh wave 3-component beamforming method (RTBF) has been adopted for array data processing.

Preliminary results obtained at seismic monitoring sites showed spatially consistent results across each array in terms of H/V functions, but only in the low frequency range, where low resonance frequency peaks ($f_0<2$ Hz) were often observed. Such resonance peaks displayed large amplitude variations, up to 50 %, as a function of the considered horizontal direction (Fig. 2). In the high frequency range ($f>2$ Hz), individual H/V functions across each array showed large differences in terms of amplitudes and secondary resonance frequencies (f_1), which suggests a large variability in the shallow elastic properties distribution within a short area.

In few cases, H/V functions calculated across active tectonic structures showed significant variations in terms of amplitude and shape, which are interpreted as correlated to the shallow sedimentary structure of the subsurface caused by such faults.

RTBF analysis performed on data acquired at seismic monitoring sites, showed clear dispersion curve (DC) images both for Rayleigh and Love wave, within a variable frequency range (2-10 Hz). While Love DC data appear dominated by the fundamental mode, Rayleigh-wave dispersion images showed a significant contribution of higher modes (Fig. 3), which support the idea of a complex subsurface model characterised by inverse dispersive properties with depth.

Such preliminary findings suggest a rather complex subsurface structure at the investigated sites on Etna volcano, whose reconstruction should be supported by advanced array processing and carefully considering all available geological information.

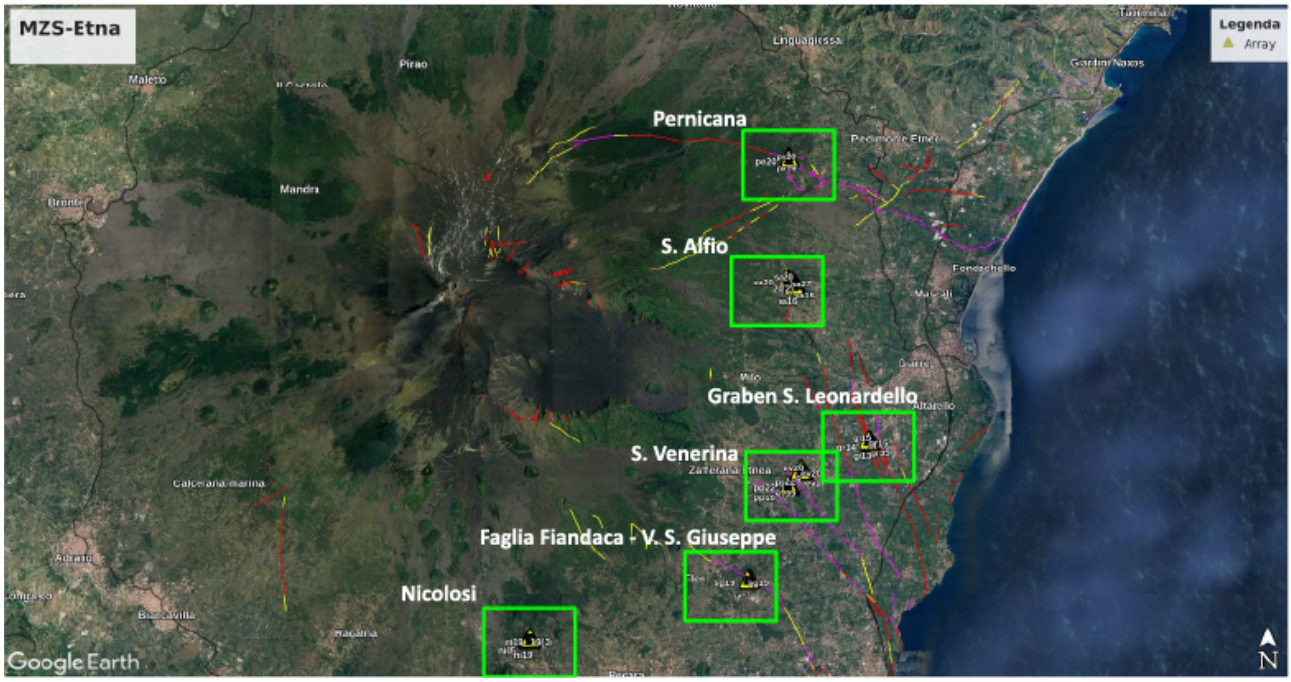

Fig. 1 Map of investigated sites

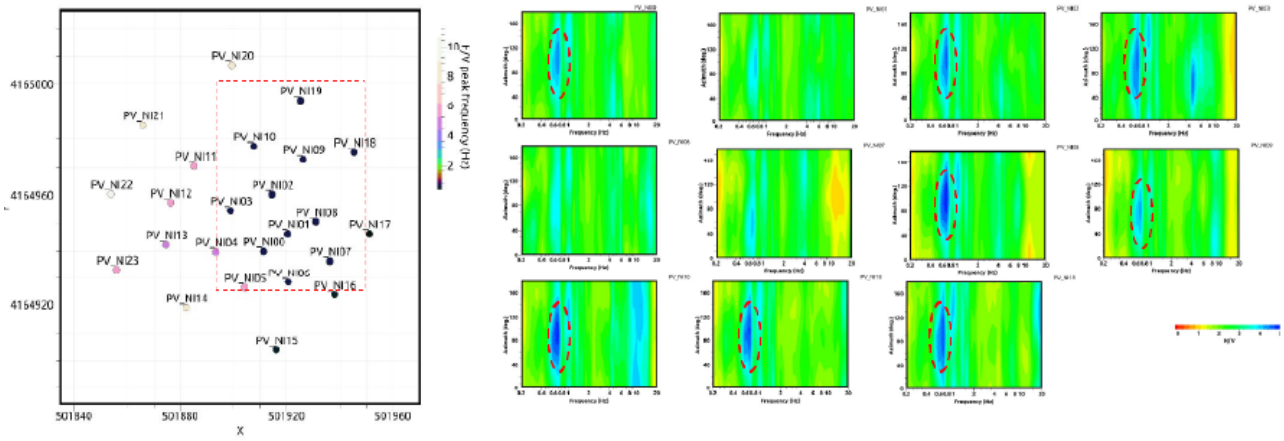

Fig. 2 Azimuthal variation of H/V functions at selected nodal stations of the passive array survey carried out at Nicolosi (ENIC) monitoring site.

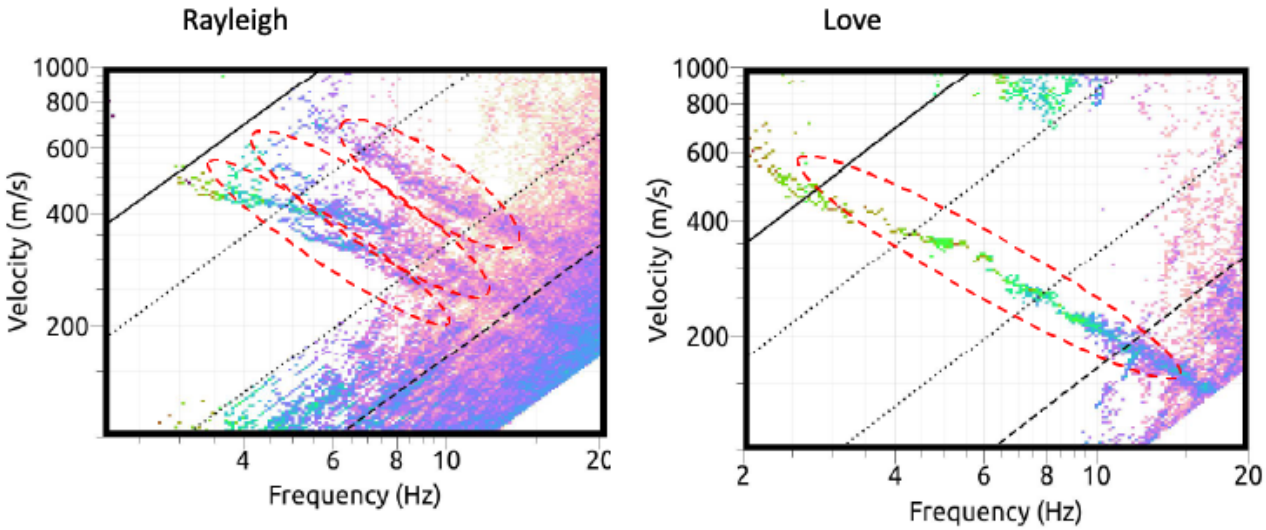

Fig. 3 Rayleigh and Love wave dispersion curves from RTBF analysis of the passive array data collected at Nicolosi (ENIC) seismic monitoring site.

References

Azzaro R., Branca S., Gwinner K. and Coltelli M.; 2012: The volcano-tectonic map of Etna volcano, 1:100.000 scale: morphotectonic analysis from high-resolution DEM integrated with geologic, active faulting and seismotectonic data. It. J. Geosciences (Boll. Soc. Geol. It.), 131 (1), 153-170.

Azzaro R., D'Amico S., Peruzza L. and Tuvè, T.; 2013: Probabilistic seismic hazard at Mt. Etna (Italy): the contribution of local fault activity in mid-term assessment. Journal of Volcanology and Geothermal Research, 251, 158-169.

Cultrera G., Cornou C., Di Giulio G., Bard P.Y.; 2021: Indicators for site characterization at seismic station: recommendation from a dedicated survey. Bull Earthquake Eng 19, 4171–4195.

Di Giulio G., Cara F., Rovelli A., Lombardo G., Rigano R.; 2009: Evidences for strong directional resonances in intensely deformed zones of the Pernicana fault, Mount Etna, Italy, J. Geophys. Res., 114, B10308, doi:10.1029/2009JB006393.

Di Giulio G., Cultrera G., Cornou C., Cornou C., Bard P.Y., Al Tfaily B.; 2021: Quality assessment for site characterization at seismic stations. Bull Earthquake Eng 19, 4643–4691.

Garofalo F., Foti S., Hollender F., Bard P.Y., Cornou C., Cox B.R., Ohrnberger M., Sicilia D., Asten M., Di Giulio G., Forbriger T., Guillier B., Hayashi K., Martin A., Matsushima S., Mercerat D., Poggi V., Yamanaka H.; 2016: InterPACIFIC project: comparison of invasive and non-invasive methods for seismic site characterization. Part I: Intra-comparison of surface wave methods. Soil Dyn Earthq Eng 82:222–240.

Molnar S., Cassidy J.F., Castellaro S. et al.; 2018: Application of Microtremor Horizontal-to-Vertical Spectral Ratio (MHVSR) Analysis for Site Characterization: State of the Art. Surv Geophys 39, 613–631.

Wathelet M., Guillier B., Roux P., Cornou C., Ohrnberger M., 2018: Rayleigh wave three-component beamforming: signed ellipticity assessment from high-resolution frequency-wavenumber processing of ambient vibration arrays. Geophysical Journal International 215 (1) 507–523.

Corresponding author: salomon.hailemikael@ingv.it

Geophysical surveys to detect buried archaeological remains in an area near the Dioscuri Temple (Valley of Temples, Agrigento, Italy)

S. Imposa[1], S. Grassi[1], G. Morreale[1], C. Pirrotta[1], L. Cavalier[2], A. Gilotti[3], D. Giuliano[4], E. Cayre[5], L.M. Caliò[6]

[1] Department of Biological, Geological and Environmental Sciences, University of Catania, Catania, Italy
[2] Unité mixte de Recherche Ausonius (UMR 5607), Université Bordeaux-Montaigne, Pessac, France
[3] Greensol S.R.L., Syracuse, Italy
[4] Department of Cultures and Society, University of Palermo, Palermo, Italy
[5] Post-doc researcher, Grand Programme de Recherche Human Past, Université de Bordeaux, Talence (France)
[6] Department of Human Science, University of Catania, Catania, Italy

Introduction

In the last few decades, geophysical prospections have been considered a fundamental tool for archaeological research due to their ability to expeditiously investigate large areas and identify buried targets in the subsoil without directly interacting with it (Witten, 2006; Grassi et al., 2021). These techniques enable more precise planning of excavation operations, enhancing their efficiency and cost-effectiveness, preserving the integrity of the subsoil and minimizing the risk of damaging potential discoveries (Cella et al., 2015). In this work, an extensive geophysical field survey was carried out, in which the Electromagnetic Method (EM) and Electrical Resistivity Tomography (ERT) were used in an unexplored area near the Dioscuri Temple (Valley of Temples, Agrigento, Sicily, Italy) (Fig. 1a,b). By integrating the data obtained from both geophysical methods, several underground anomalies attributable to buried structures were identified, due to their shape and physical attributes.
A preliminary archaeological dig carried out in one of the areas where the geophysical anomalies were located, revealed the existence of a wall built using local calcarenites blocks.
Subsequently, the wall was scanned using photogrammetric techniques to obtain a detailed 3D reconstruction. Preliminary analysis suggests that this wall is part of a building possibly dating to the Hellenistic or Classical period. This discovery probably represents only a very small portion of a larger and more complex structure. This structure may have played a key role in the religious topography of Akragas since it is located near the entrance to the sanctuary of the "circular altars".

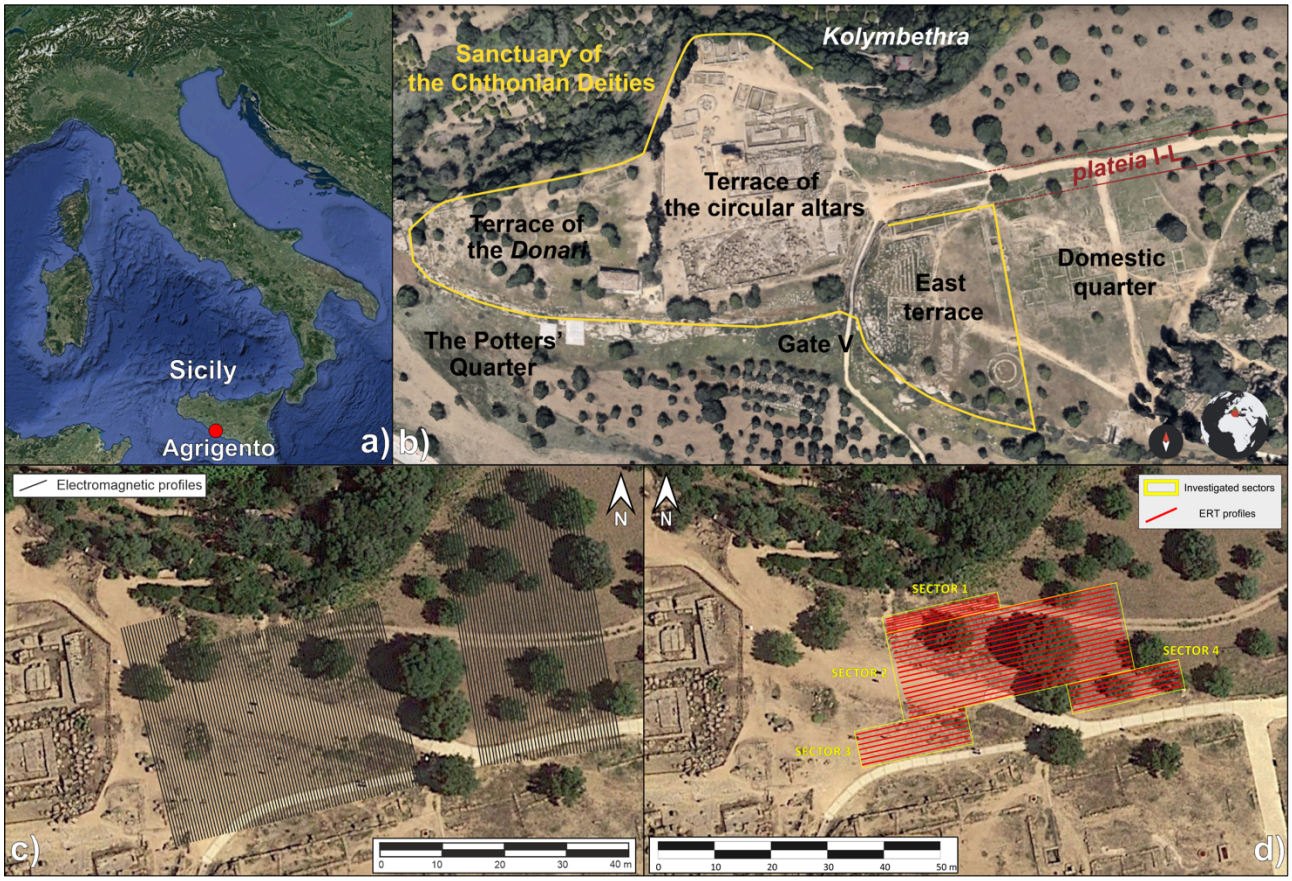

Fig. 1 – a) Location of the Valley of the Temples; b) aerial view of the Sanctuary of Chthonian deities; c) location of EM surveys and d) location of ERT surveys.

Methods and Data Collection

The electromagnetic survey method is one of the widely used techniques in archaeological research. It can identify the contrast of magnetic and electrical properties between buried structures and surrounding lithotypes (Bigman, 2012). This method is used to measure the electric currents produced in the subsurface by electromagnetic field induction using transmitting and receiving coils in the frequency domain (FDEM) (Di Maio et al. 2016).

The EM survey was performed on an area of about 3000 m², with an acquisition step of 0.5 m (Fig. 1c). Along each profile, the data were collected using a sampling step of 0.50 m. The equipment used is an AEMP14 multifrequency electromagnetometer, which consists of three coils: one transmitting and two receiving coils. The distance between the transmitting coil and the first receiving coil is 1.5 m, and the distance to the second receiving coil is 2.5 m. The device is capable to operate at 14 frequencies ranging from 2.5 kHz to 250 kHz.

Electrical resistivity tomography (ERT) is a geophysical method with a wide range of applicability. It allows to obtain 2D sections and 3D models showing the distribution of the resistivity in the subsoil (Tong and Yang, 1990; Sasaki, 1992). The investigated area was divided into 4 sectors, investigated by 38 ERT surveys spaced 0.50 m apart in sector 1, while the spacing increased to 1 m in sectors 2, 3 and 4 (Fig. 1d). The acquisitions were performed with two quadripolar configurations for each linear array: DD (Dipole-Dipole) and MGA (Multiple Gradient Array).

Results

For the data acquired by the EM method, the analysis focused on the quadrature component derived from the highest frequency antenna (250 kHz) to derive the trend of electrical resistivity. The resistivity map obtained reveals the presence of numerous electrical anomalies within the study area (Fig. 2a). These anomalies are characterized by high electrical resistivity values, ranging from 150 to 180 Ohm*m. The primary anomalous sector is characterized by a pronounced alignment of high electrical resistivity values. This sector extends into the central portion of the area, following an almost NNW-SSE direction. Another alignment is observed in the southern boundary of the study area, extends in E-W direction. Moreover, two minor alignments of outliers are observed in the northeastern and northwestern sectors, both of which follow a NW-SE direction.

Concerning ERT surveys, resistivity mapping was obtained for each sector. Low resistivity values, ranging from 1.25 to 1.95 log_Res (Ω*m), indicate the presence of loose or poorly consolidated sediments, suggesting the presence of overburden soils. On the other hand, high resistivity values above 1.95 log_Res (Ω*m) are indicative of more consolidated and cemented rock materials. Anomalies, mainly observed in sectors 1, 2 and 4 (Fig. 2b), consist of abrupt changes in resistivity values from low to high. Sector 3, on the other hand, does not show the presence of anomalies but is entirely characterized by high resistivity values, attributable to the geological characteristics of the site. All high resistive anomalies show a fairly regular pattern and shape. Based on these results, a preliminary archaeological excavation was performed, limited to the area highlighted in Figure 2b within the green circle (Sector 4).

Discussion and Conclusion

Electromagnetic (EM) surveys and ERT electrical resistivity tomographies, performed in the Temple Valley, show the presence of several portions characterized by high resistivity values, surrounded by areas with low resistivity values. The high resistivity anomalies suggest the existence of low conductivity bodies, which, considering the lithologies observed in the study area, are probably attributable to Pleistocene calcarenites. In contrast, areas characterized by higher conductivity values may indicate the presence of poorly consolidated filled soils resulting from the erosion process of blue-gray marly clays. Previous studies on archaeological sites, such as those by Di Maio et al. (2016), have shown that similar values of resistivity anomalies may be indicative of buried rock walls. Based on these evidences, along with the elongated and narrow shape of the alignment of anomalies, as well as their direction and location, it is plausible to assume that these anomalies represent remains of walls from buildings.

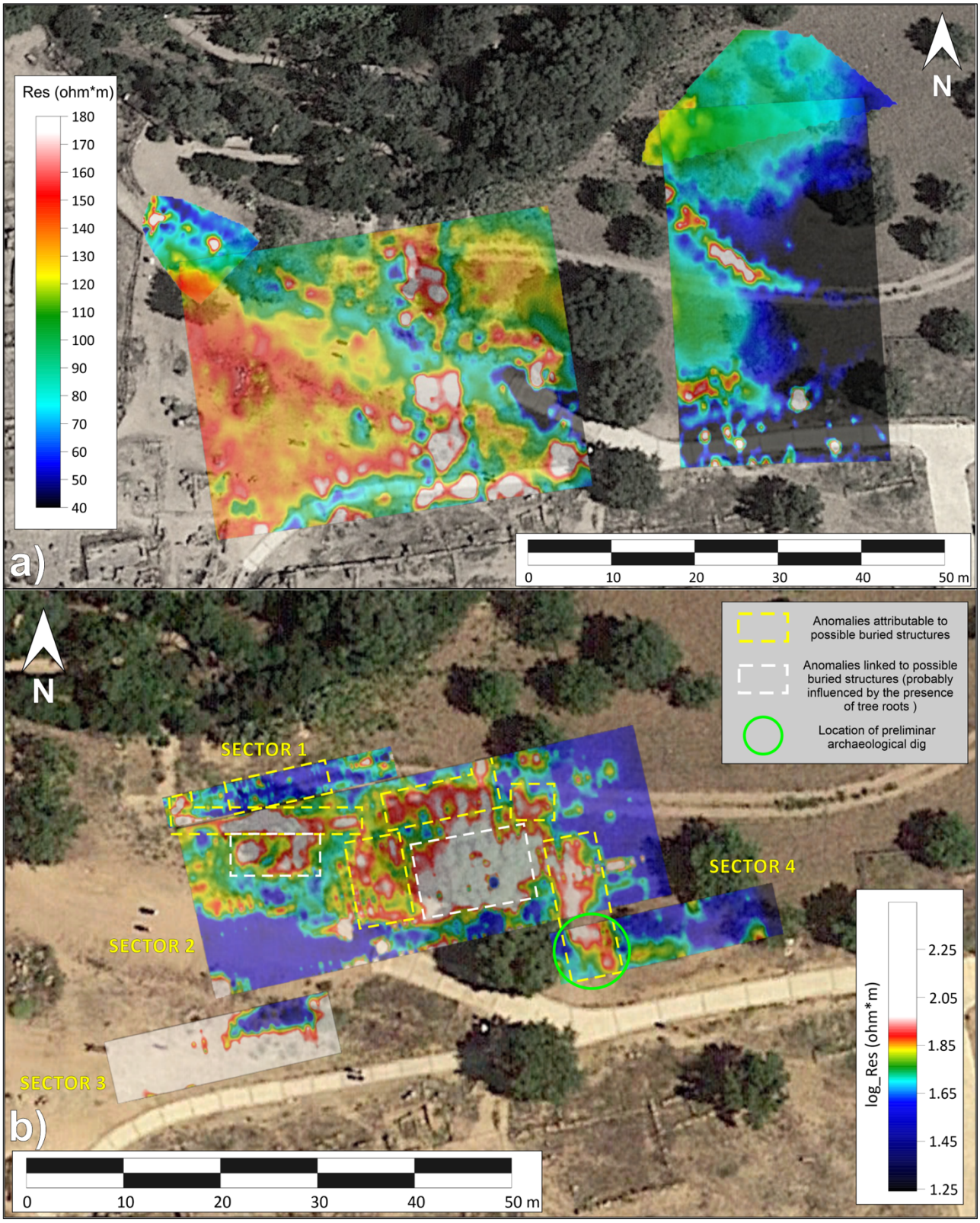

Fig. 2 – a) Electromagnetic resistivity map of the surveyed area and b) Electrical Resistivity map of the study area obtained from ERT surveys.

The archaeological dig performed where the geophysical surveys had identified anomalies revealed a 3.65-m-long wall section, SE-NW orientation, consisting of a single course of 5 preserved blocks of varying height (Fig. 3). The southernmost two blocks of this wall rest on fill, while the other 3 blocks rest partially on another, probably earlier wall with the same orientation,

it consists of large blocks (about 1.30 m long). The wall rests on a layer of clay in which flint fragments were found. The northern part of the wall was completed with coarse rubble mixed with soil. The pottery associated with these remains is currently being studied and should allow for an accurate dating and phase for the discovered building. This monument is located at the edge of the *plateia IL*, near the entrance to the sanctuary "of the circular altars." Given its properties and location, the significance of this monument is of crucial importance for the complete understanding of the religious topography of Akragas. Since the excavation is still in the early stages, further investigation is needed.

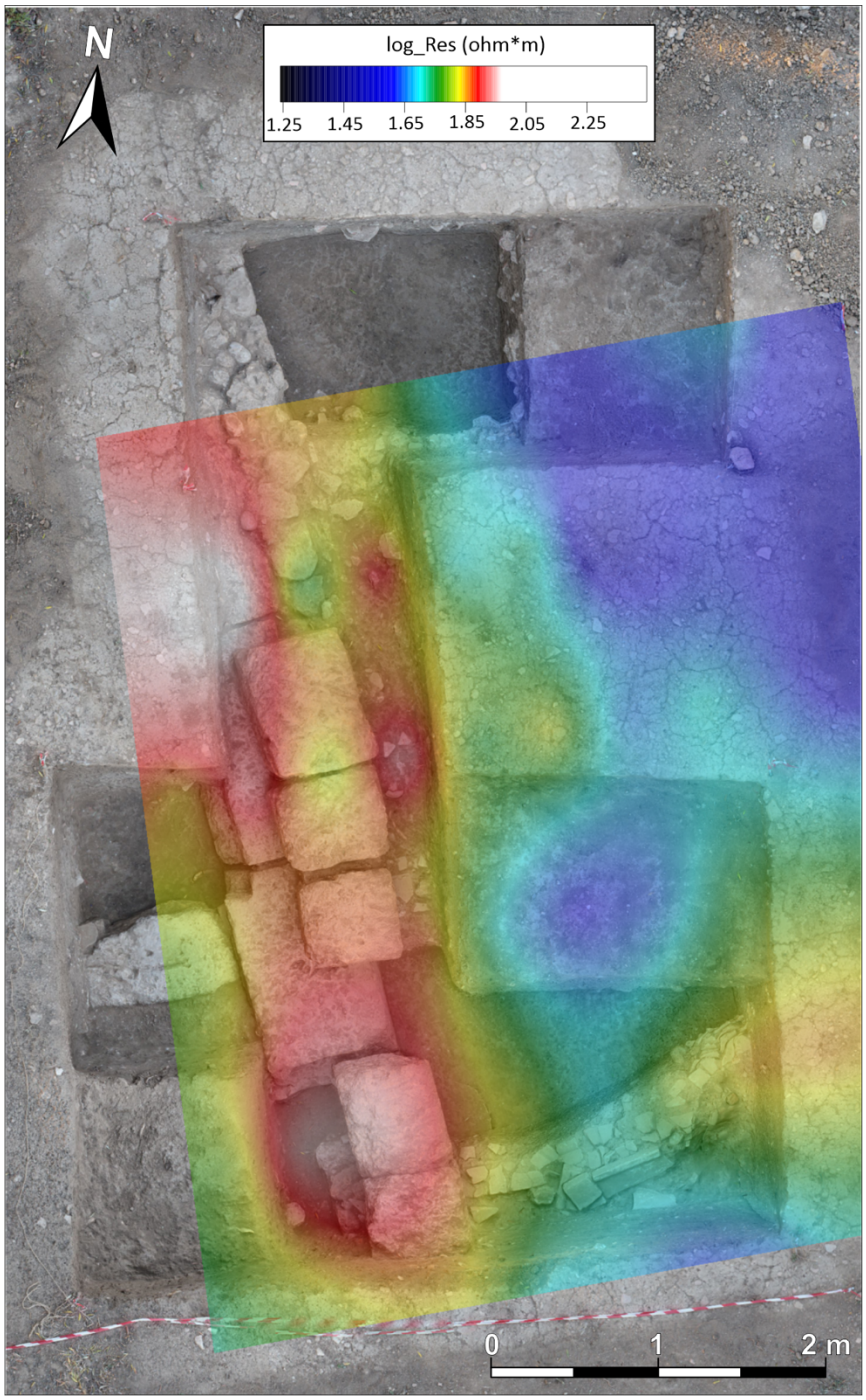

Fig. 3 - Resistivity map obtained from ERT data processing overlaid on the 3D reconstruction of the archaeological excavation.

EM and ERT techniques has proven to be an essential tool in guiding archaeological digs to discover buried remains, at the Akragas site. The processing of the data acquired have identified anomalies in the subsurface characterized by significant variations in physical parameters. Given their physical and geometrical characteristics, such anomalies were attributed to buried structures of anthropogenic origin. Based on the results obtained by ERT surveys, an initial test excavation was conducted in one of the areas identified by the geophysical surveys. Excavation revealed the presence of an unknown building of potentially crucial importance to the religious topography of the area under investigation.

The integration of geophysical techniques with traditional archaeological methods contributes to a more efficient, cost-effective, and informed approach to archaeological research and preservation.

References

Bigman D.P.; 2012: The use of electromagnetic induction in locating graves and mapping cemeteries: An example from Native North America. Archaeological Prospection. 19, 31–39. https://doi.org/10.1002/arp.1416.

Cella F., Fedi M. 2015: High-resolution geophysical 3D imaging for archaeology by magnetic and EM data: The case of the iron age settlement of Torre Galli, Southern Italy. Survey in Geophysics,36, 831–850.

Di Maio R., La Manna M., Piegari E.; 2016: 3D reconstruction of buried structures from magnetic, electromagnetic and ERT data: Example from the archaeological site of Phaistos (Crete, Greece). Archaeological Prospection. 23, 3–13. https://doi.org/10.1002/arp.1516.

Grassi S., Patti G., Tiralongo P., Imposa S., Aprile, D.; 2021: Applied geophysics to support the cultural heritage safeguard: A quick and non-invasive method to evaluate the dynamic response of a great historical interest building. Journal of Applied Geophysics. https://doi.org/10.1016/j.jappgeo.2021.104321

Sasaki Y.; 1992: Resolution of resistivity tomography inferred from numerical simulation 1. Geophysical Prospecting. 40(4):453–463

Tong L.T., Yang C. H.; 1990: Incorporation of topography into two-dimensional resistivity inversion. Geophysics, 55(3), 354-361.

Witten A.J.; 2006: Handbook of Geophysics and Archaeology, Equinox Pub: London, UK.

Corresponding author: gabriele.morreale@phd.unict.it

Characterizing groundwater springs in the Italian Alps: an integrated geological, geophysical, and hydrogeological approach

A. Lucchelli[1], A. Signora[1], F. Dauti[1], S. Galli[1], M. Gisolo[2], G. Fiandaca[1]

[1] The EEM Team for Hydro & eXploration, Department of Earth Sciences "Ardito Desio", Università degli Studi di Milano, Milano, Italy
[2] a2a Ciclo Idrico s.p.a., Brescia, Italy

Spring water is one of the major sources of drinking water for local communities throughout the Italian Alps and in mountain areas worldwide (ISTAT, 2020; United Nations, 2022). As water demand and pressure on groundwater resources increase in a context of fast-changing climate, there is a growing commitment to assess groundwater availability and develop sustainable water supply strategies.

The proper management of groundwater resources requires the characterization of the aquifer systems. In this regard, karst terrains pose unique challenges due to their complex and heterogeneous nature. This study focuses on the assessment of an aquifer system in a karst-fissured mountain environment, by employing an integrated approach based on three pillars: geology, geophysics, and hydrogeology. The study area, located in the Brescia Prealps (northern Italy), is characterized by a Lower-Middle Triassic succession with a fold-and-thrust architecture, typical of the Southern Alps domain, complicated by the presence of faults (Boni & Cassinis, 1973).

The geological pillar is based on a 3D geological-structural model developed using both bibliographic data and field observations. This model serves as the foundation for understanding the spatial distribution of geological formations and the major tectonic lineaments.

The geophysical pillar is built on both ground-based geophysics (classic electrical tomography, ERT, and innovative transient EM methods, i.e. Loupe TEM (Street et al., 2018)) and on densely-spaced airborne electromagnetics (AEM) (Fig. 1).

The hydrogeological pillar consists of spring discharge data, groundwater chemical analysis, and stable isotope analysis of Oxygen, Hydrogen, and Carbon (Fig. 1).

Where geological data is sparse, 3D geological modeling can be used to derive a homogeneous, realistic representation of geological features over the entire study area. In this study it was performed using the GeoModeller software by Intrepid Geophysics (Calcagno et al., 2008). Geophysical surveys, on the other hand, play a key role in capturing the subsurface heterogeneity and identifying preferential flow paths within the rock volumes. Together, these methods provide the information needed to understand aquifer architecture.

To model the electric and electromagnetic data the EEMverter inversion software has been used (Fiandaca et al., 2023). For the mutual calibration of geological and geophysical data, two rules

Fig. SEQ Figure * ARABIC 1 - Geophysical surveys tracks and location of the springs with their relative data.

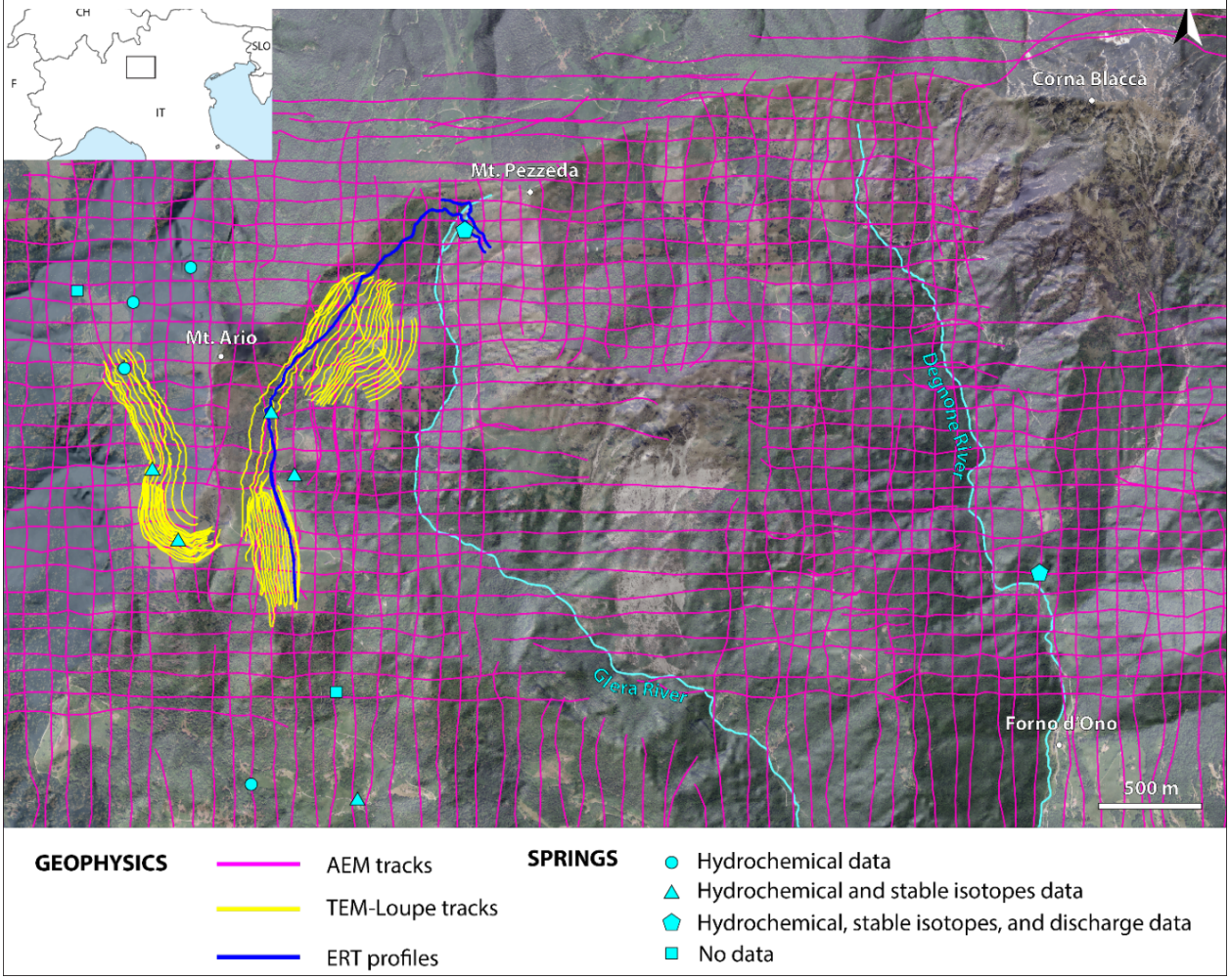

have been introduced in EEMverter. In the first rule, the basal boundaries of the geological formations are treated as barriers that separate different regions: the vertical constraints on the electrical resistivity parameter can be broken at these barriers. This rule accounts for the fact that adjacent geological formations can have significantly different electrical properties. The second rule takes allows to specify different resistivity ranges in each region.

The integration and mutual calibration of geophysical data with the 3D geological model allows for the refinement and validation of the model parameters, ensuring a more realistic representation of the aquifer system. This iterative process enhances the precision of the model and provides valuable insights into the hydrogeological characteristics of the investigated system (Fig. 2). Hydrogeology, and particularly the isotope analysis, helped to identify the origin of the groundwater and to determine an approximate elevation for the main recharge areas of the aquifer system (Longinelli & Selmo, 2003).

The results reveal the existence of different rock volumes with similar electrical behavior, within which heterogeneities in resistivity distribution are recognized. In addition, the integration of 3D geological modeling and geophysical surveys provides a comprehensive and accurate representation of subsurface structures (Fig. 3).

In conclusion, this research offers practical insights for the sustainable management of groundwater springs in complex geological settings and is the first step in the development of a

numerical flow model. This is essential for the assessment of groundwater availability as a function of climate change scenarios.

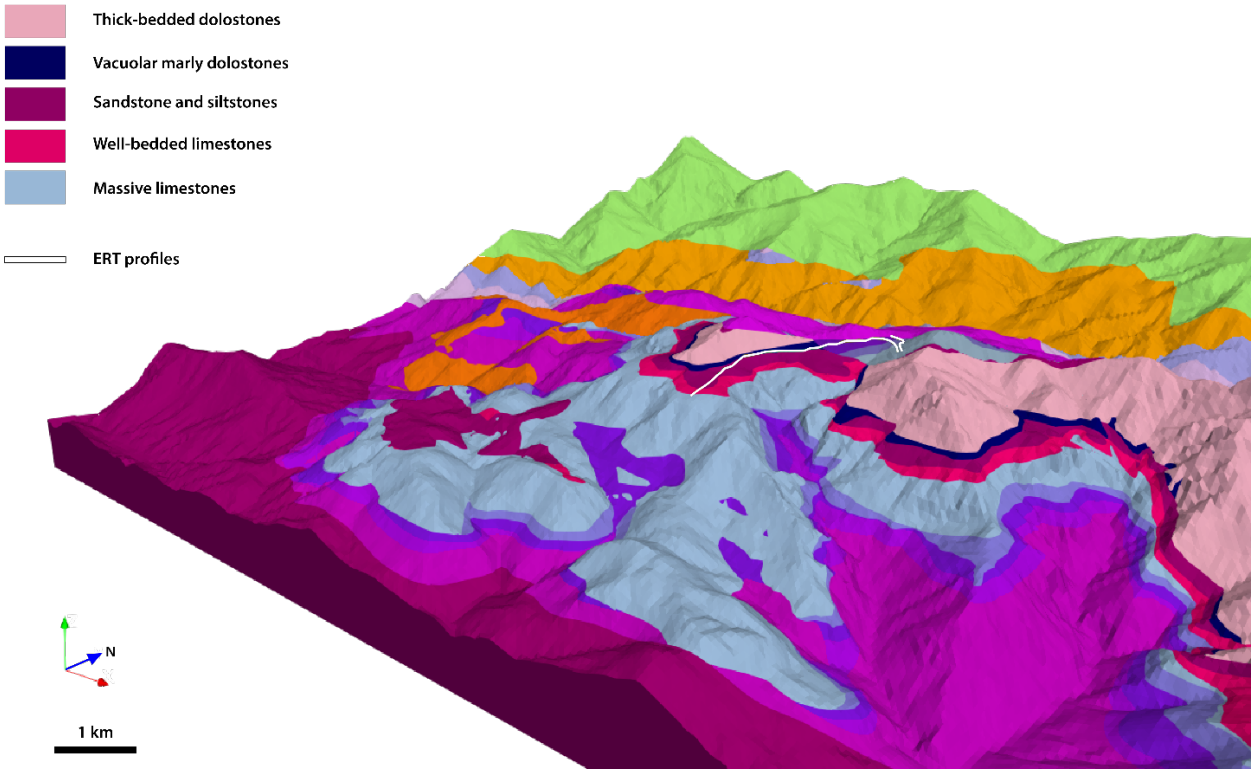

Fig. 2 – 3D geological model of the study area with the ERT track.

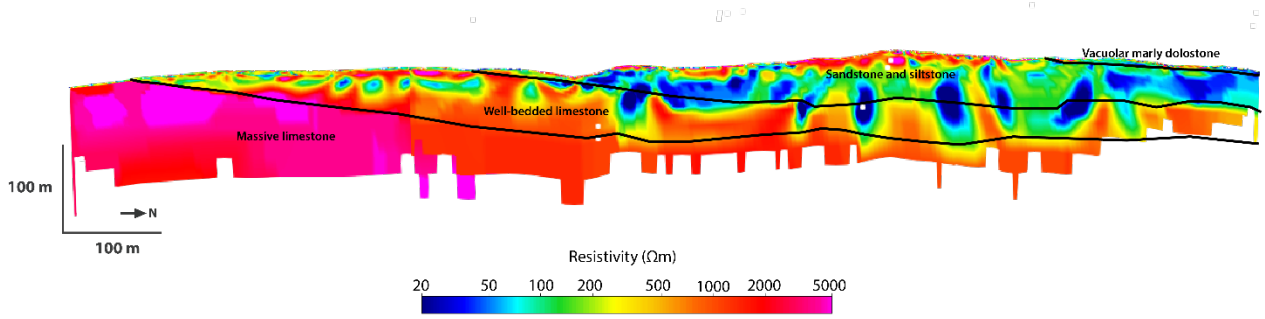

Fig. 3 – ERT profile integrated with geological boundaries exported directly from the 3D geological model.

Acknowledgments

This study has been carried out within the projects MountainHydro and HydroEEMaging, funded by a2a Ciclo Idrico S.p.A.

References

Boni A. & Cassinis G.; 1973: Carta geologica delle Prealpi Bresciane a sud dell'Adamello. Tipografia del libro.

Calcagno P., Chilès J.P., Courrioux G. & Guillen, A.; 2008: Geological modelling from field data and geological knowledge – Part I. Modelling method coupling 3D potential-field interpolation and geological rules. Physics of the Earth and Planetary Interiors 171, 147-157.

Fiandaca G., Zhang B., Chen J., Signora A., Dauti F., Galli S., Sullivan N.A.L., Bollino A., Viezzoli A.; 2023: Closing the gap between galvanic and inductive methods: EEMverter, a new 1D/2D/3D inversion tool for Electric and Electromagnetic data with focus on Induced Polarization. AEM2023 -8th International Airborne Electromagnetics Workshop.

ISTAT; 2022: Censimento delle acque per uso civile. https://www.istat.it/it/archivio/279363

Longinelli A., Selmo E.; 2003: Isotopic composition of precipitation in Italy: a first overall map. Journal of Hydrology 270, 75-88.

Street G., Duncan A., Fullagar P. & Tresidder R., 2018. Loupe – A portable EM profiling system. ASEG Extended Abstracts 1, 1-3.

United Nations; 2022: The United Nations World Water Development Report 2022 – Groundwater: Making the invisible visible. UNESCO, Paris.

Corresponding author: alice.lucchelli@unimi.it

Quantitative integration of geoelectrical data for mapping of leachate plumes: application to a MSW landfill in Central Italy

D. Melegari[1], G. De Donno[1], E. Piegari[2]

[1] DICEA (Sapienza - University of Rome, Rome, Italy)
[2] DISTAR (Federico II - University of Naples, Naples, Italy)

Introduction

Waste management is one of the main challenges for contemporary society, as highlighted by the United Nations SDGs (Target 12.4). Specifically, the uncontrolled accumulation of leachate in municipal solid waste (MSW) landfills represents a potential risk for the environment, since leachate is a liquid with a high pollutant content that can contaminate aquifers (Assamoi B., Lawryshyn Y.; 2012) and affect the stability of landfills. Therefore, mapping and monitoring the waste mass down to significant depths is required for an appropriate management of the landfill sites. Among the geophysical techniques, electrical resistivity tomography (ERT) and induced polarization (IP) methods are perfectly suited for this purpose given the electrical properties of leachate (highly conductive and chargeable) compared to the unsaturated waste mass (Soupios P., Ntarlagiannis D.; 2017).

In the present study we present an application of a machine learning-based approach for a quantitative integration of ERT and IP data for imaging of leachate levels in a MSW landfill located in Central Italy. The quantitative interpretation of resistivity, chargeability and normalized chargeability data is provided by using the Fuzzy C-means clustering algorithm which allows for the identification of the leachate accumulation zones and for assessing the reliability of the reconstruction by means of the membership value. The results of the cluster analysis are validated by the computation of the Silhoutte coefficient and supported by well data.

Study area, data acquisition and processing

The landfill is located in Central Italy on a steep slope, in which the leachate accumulation can trigger instability phenomena (Fig. 1a). We focused our investigation on four selected terraced steps with four electrical lines (L1-L4) 300 to 500 meters long (Fig. 1b), using a multi-parameter reconstruction through electrical resistivity tomography (ERT) and time-domain induced polarization (TDIP) methods. Experimental datasets were acquired through the Syscal Pro resistivity-meter (IRIS Instruments) with stainless steel electrodes spaced 5 m apart, using the dipole-dipole (DD) array and a roll-along configuration. For IP acquisition, we used a current

injection time of 2 s with 4 stacks, a time delay of 40 ms and a logarithmic sampling of the IP decay curve using 20 gates. We also logged leachate levels in five different piezometers along L2 and L3.

We inverted ERT/TDIP data for resistivity and integral chargeability using the VEMI software (De Donno G., Cardarelli E.; 2017), which employs the finite element method for solving the forward problem and a Gauss-Newton inversion algorithm, while the linear approach (Method I after Oldenburg D. W., Li Y.; 1994) is adopted for chargeability forward modelling. After inversion we added to the resistivity (ρ) and integral chargeability (M) models also the normalized chargeability (M_n) to emphasize the contribution of surface conductivity, derived by normalizing chargeability by the resistivity.

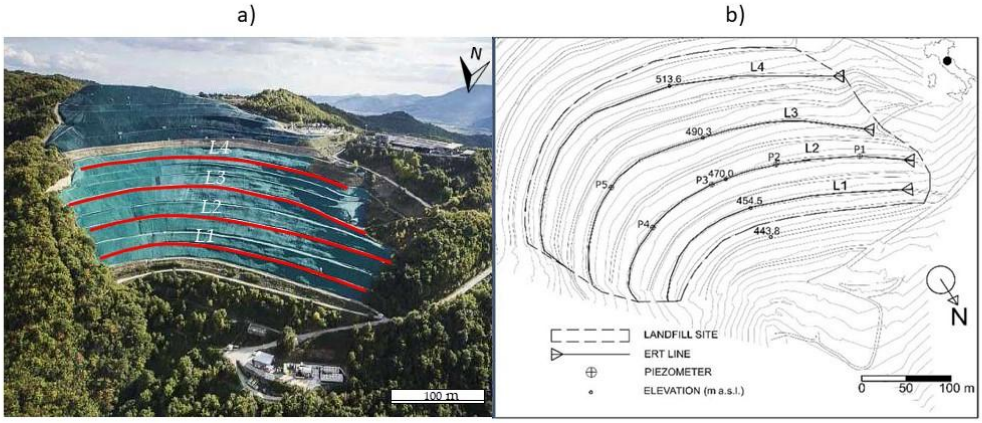

Fig. 1 – Aerial image (a) and plan (b) of the municipal solid waste landfill in Central Italy, with the location of the four investigated ERT/IP lines (L1-L4) and of the five piezometers (P1-P5)

To integrate information from electrical inverted models, we applied a machine learning-based approach (Piegari E. et al.; 2023), which is based on a cluster analysis in the parameter model space defined by the inverted values of ρ, M and M_n. However, instead of the widely-used K-means, we performed the cluster analysis by using the Fuzzy C-Means algorithm (Bezdek J. C.; 2013). This algorithm is a soft clustering approach, which allows data points to belong to multiple clusters with a degree of membership μ that is a function of the distance to the closest centroids. This makes the algorithm more robust to noise and outliers in the data compared to K-means and we can also have an assessment of the reliability of the clustered section by means of the degree of membership section. The optimal number of clusters was assessed by the Elbow method applied to the explained variance, while the quality of the results was finally evaluated by calculating the Silhouette value (Rousseeuw P. J.; 1987).

At the end of the clustering procedure, we achieved a single model that integrates all geoelectrical information providing an accurate identification of leachate accumulation zones through a color-based scale, where dark red color is associated to the fully saturated zones.

Results

The results are shown in Figure 2 for the L2 line, where is also available the direct information. The three inverted models resulting from inversion process (Fig 2a-c) are compared to the clustering models, with the leachate levels logged superimposed. The models from traditional approach (without clustering) show three main layers in agreement with the expected stratigraphy of a landfill: i) a shallow layer (thickness less than 10 m) showing high resistivity (ρ > 20 Ωm) and low chargeability (M < 2 mV/V), related to the presence of unsaturated waste and covering soil; ii) an intermediate layer with low resistivity (ρ < 20 Ωm) and high chargeability (M > 2 mV/V), which reflects the presence of leachate. This layer seems quite heterogeneous, with lateral changes due to a different degree of saturation inside the waste mass; iii) a deeper layer, extended down to the maximum depth of investigation (~ 50 m) with very high values of resistivity (ρ >> 20 Ωm) and low chargeability (M < 2 mV/V), associated to the presence of HDPE bottom liner, which does not allow current to flow outside the landfill. However, the electrical models still leave ambiguities on the identification of leachate accumulation zones, as confirmed by the mismatch between the high values of normalized chargeability and the leachate levels logged in P4.

The results of Fuzzy C-Means analysis are shown in terms of clustered (Fig. 2d) and membership sections (Fig. 2e), resulting from an optimal number of clusters equal to 8 computed by the Elbow method. The clustered section shows a less ambiguous and more accurate identification of the leachate accumulation, validated by direct information from P4, which is in good agreement with the cluster no. 8 (lowest ρ and highest M and M_n), while the other wells do not show significant leachate levels according to the clustering reconstruction. In addition, thanks to membership section we can evaluate the reliability of the reconstruction achieved by the clustering. Given the high values (μ > 0.75) displayed in the dark red cluster, we can validate the final reconstruction.

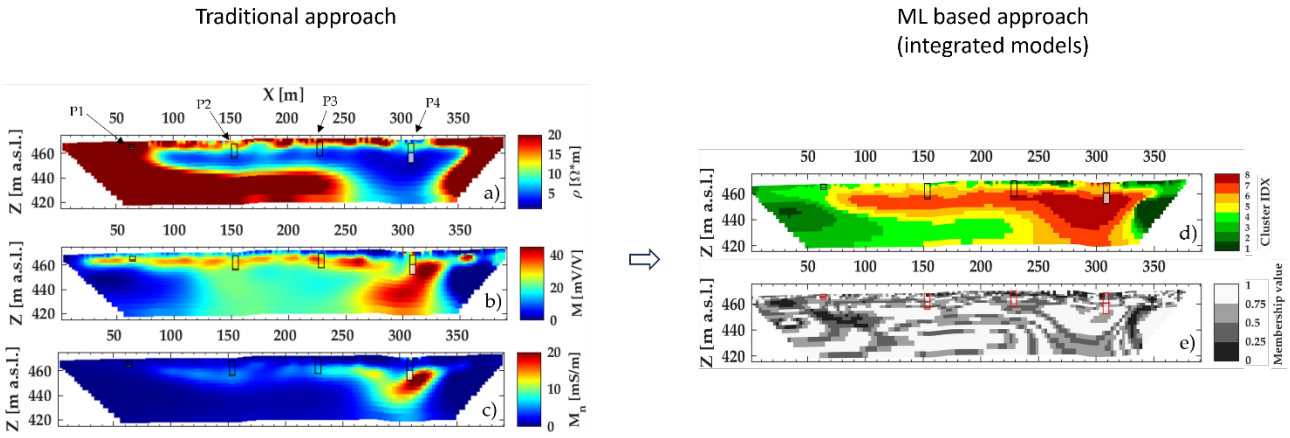

Fig. 2 – ERT/TDIP data inversion and clustering analysis on the L2 line: resistivity model (a), chargeability model (b), normalized chargeability model (c), clustered section (d) and membership section (e). The leachate levels logged in piezometers P1-P4 are marked with a white area.

Conclusions

In this work, we presented a machine-learning based approach to upgrade leachate identification in municipal solid waste landfill trough geoelectrical data. This approach supplies a promising method to reduce the residual ambiguities arising from ERT or TDIP standalone applications. We demonstrated two advantages: i) integrating ERT and IP data through clustering analysis can be effective for mapping the leachate accumulation zones with more accuracy compared to a traditional approach; ii) the membership section derived by using soft clustering can provide a quantitative validation of the final landfill clustered model, in addition to the available direct information. These development over the traditional approach represents an important step to improve landfill's drainage operations, particularly during the maintenance of MSW landfills. Future work will be focused on application of this method to other landfill sites in order to validate the parameters selected during the cluster analysis, especially with regard to the optimal number of clusters.

References

Assamoi B., Lawryshyn Y.; 2012: The environmental comparison of landfilling vs. incineration of MSW accounting for waste diversion. Waste management, 32(5), 1019-1030.

Bezdek J. C.; 2013: Pattern recognition with fuzzy objective function algorithms. Springer Science & Business Media.

De Donno G., Cardarelli E.; 2017: VEMI: a flexible interface for 3D tomographic inversion of time- and frequency-domain electrical data in EIDORS. Near Surface Geophysics, 15(1), 43-58.

Oldenburg D. W., Li Y.; 1994: Inversion of induced polarization data. Geophysics, 59(9), 1327-1341.

Piegari E., De Donno G., Melegari D. & Paoletti, V.; 2023: A machine learning-based approach for mapping leachate contamination using geoelectrical methods. Waste Management, 157, 121-129.

Rousseeuw P. J.; 1987: Silhouettes: a graphical aid to the interpretation and validation of cluster analysis. Journal of computational and applied mathematics, 20, 53-65.

Soupios P., Ntarlagiannis D.; 2017: Characterization and monitoring of solid waste disposal sites using geophysical methods: Current applications and novel trends. Modelling trends in solid and hazardous waste management, 75-103.

Corresponding author: davide.melegari@uniroma1.it

Mixed-dimensional forward-problem solver for the geoelectrical analysis of highly resistive liners in landfills

L. Panzeri[1,2], A. Fumagalli[2], L. Longoni[1], M. Papini[1], L. Zanzi[1], D. Arosio[3]

[1] Department of Civil and Environmental Engineering, Politecnico di Milano, Italy
[2] Department of Mathematics, Politecnico di Milano, Italy
[3] Dipartimento di Scienze Chimiche e Geologiche, Università degli studi di Modena e Reggio Emilia, Italy

To avoid the diffusion of the leachate in the subsoil and the possible contamination of aquifers, a thin liner of high-density polyethylene (HDPE) is placed underneath the waste in municipal solid waste landfills (MSWLFs). The conditions of the plastic membrane are of paramount relevance but, unfortunately, they are difficult to be assessed due to the location of the liner. A 3D code based on a mixed-dimensional mathematical model has been developed to simulate the flow of the current injected in the geoelectrical surveys to allow a non-destructive analysis of the highly resistive liner (Aguzzoli et al. 2020, Aguzzoli et al. 2021, Fumagalli et al., 2023, Panzeri et al., 2023)).

The peculiarity of our approach is to consider the problem as mixed-dimensional. This means that elements of different dimensions coexist in the same mesh (Fig.1). Due to their reduced dimension along x and y with respect to z, electrodes have been simulated as 1D elements (Peacemean 1978), while the liner is simulated as a 2D element because of its limited thickness (typically a few millimetres). The new code defines parallelepipedal boxes around the electrodes and exploits the finite volume Multipoint Flux Approximation method (MPFA). These conditions need to be mathematically expressed in the formulation of the forward problem also including the interface/ coupling conditions between the elements with different dimensions.

In this work, the results obtained with our Python code based on Porepy (Keilegavlen et al. 2021) have been compared, first, with two analytical solutions. One represents two horizontal layers with different conductivity (Sheriff et al., 1990), and the other is characterized by the presence of a conductive sphere in an infinite horizontal space (Aldridge and Oldenburg, 1989). After that, the results were compared with the outcomes of an open-source library for multi-method modelling and inversion in geophysics named pyGIMLi (Rücker et al. 2017). Finally, to further validate our modelling code, tests were performed with different settings in the laboratory on a homogeneous material (water) placed in a plastic box.

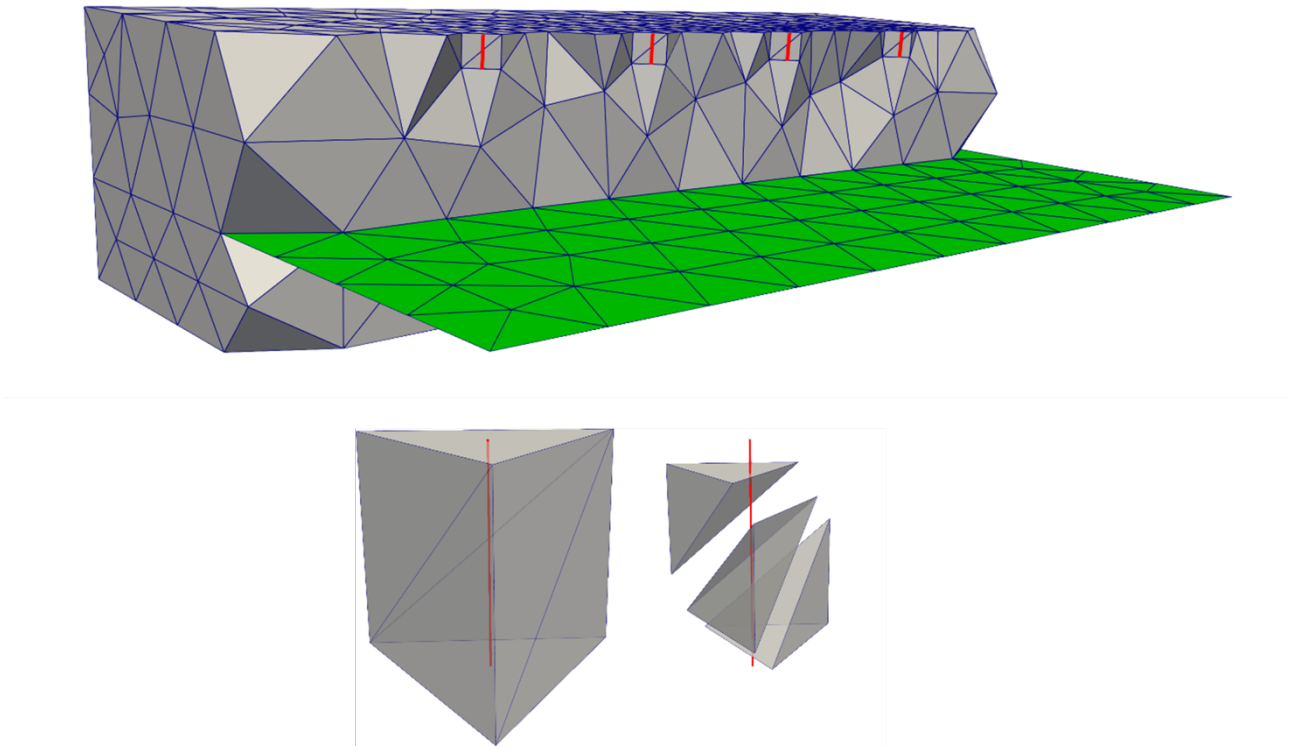

Fig. 1 – Mixed-dimensional mesh scheme. Graphical representation of the domain (grey), the liner in green and the electrodes in red. Below, a detail about the construction of cells around an electrode is shown (Fumagalli et al., 2023).

Particular attention has been given to mesh creation, which is very similar on one side, while on the other has a different structure due to the different approaches considered. In particular, pyGIMLi represents the electrodes as points and considers the nodes of the mesh as the degrees of freedom of the problem. This differs from the proposed approach in which the degrees of freedom are the elements of the mesh (tetrahedra). To make the results comparable, different meshes almost equal in terms of the number of nodes and elements have been created. Gmsh defines a characteristic length of the mesh which has been set equal to 0.5 cm in the region close to the electrodes and equal to 5 cm elsewhere. To have the same structure in pyGIMLi, a series of nodes with distances equal to 0.5 cm along the three dimensions have been defined in the area close to the electrodes.

Once the forward problem solver was validated, we were interested in the ability of our modelling code to obtain meaningful information about the liner in situ. A widespread issue for this type of analysis regards having satisfactory sensitivity far from the deployed electrodes. What types of arrays, how many measurements, and what electrode positions should we consider to best investigate the area where the membrane is located? To solve this problem, an analysis was performed with the aim of highlighting the areas with higher and lower sensitivity by paying special attention to the 2D elements of the membrane. The aim was to optimize the acquisition by following different strategies to reduce the number of measurements that would later be implemented in situ.

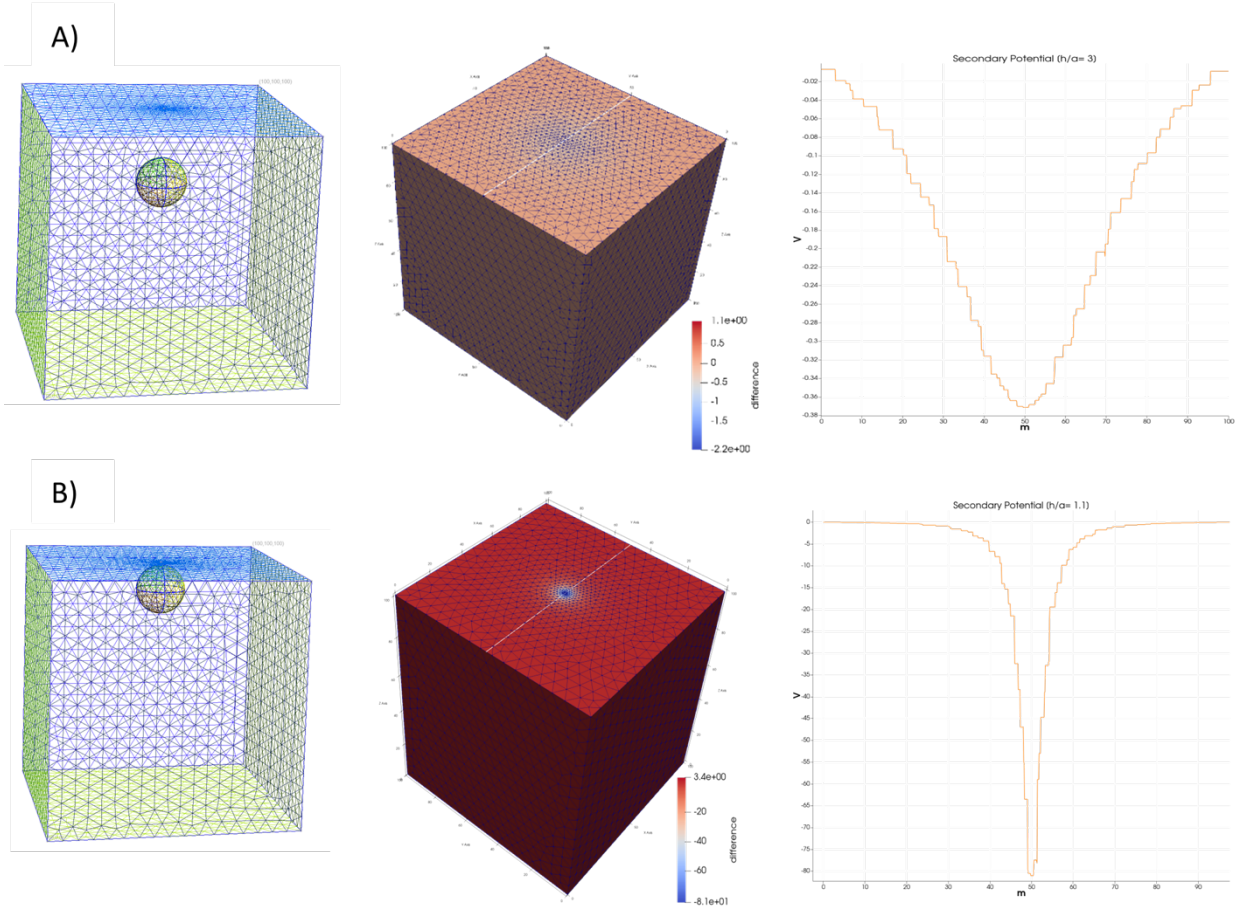

Fig. 2 – Simulation related to a conductive sphere (ρ2 = 10 Ωm) in a resistive background (ρ1= 1000 Ωm). A) Modelled mesh (left), computed secondary potential (centre) and computed secondary potential along a line of electrodes at the surface (right); the ratio between the depth of the sphere centre and its radius is 3 (depth = 30 m, radius = 10 m). B) same as A) with the ratio between the depth of the sphere centre and its radius equal to 1.1 (depth = 11 m, radius = 10 m).

References

Aguzzoli, A., Hojat A., Zanzi L., Arosio, D.;2020: Two Dimensional ERT Simulations to Check the Integrity of Geomembranes at the Base of Landfill Bodies. In 26th European Meeting of Environmental and Engineering Geophysics, 2020, p.1 – 5.

Aguzzoli, A., Fumagalli, A., Scotti, A., Zanzi, L., Arosio, D.;2021: Inversion of Synthetic and Measured 3D Geoelectrical Data to Study the Geomembrane below a Landfill. In 4th Asia Pacific Meeting on Near Surface Geoscience & Engineering, 2021, p.1 - 5.

Aldridge, D. F., & Oldenburg, D. W. ;1989: Direct current electric potential field associated with two spherical conductors in a whole-space 1. *Geophysical prospecting*, *37*(3), 311-330.

Fumagalli, A., Panzeri, L., Formaggia, L., Scotti, A., Arosio, D.; 2023: A mixed-dimensional model for direct current simulations in presence of a thin high-resistivity liner. *Journal for Numerical Methods in Engineering,* doi: 10.1002/NME.7407.

Keilegavlen, E., Berge, R., Fumagalli, A., Starnoni, M., Stefansson, I., Varela, J., and Berre, I.;2021: Porepy: An open-source software for simulation of multiphysics processes in fractured porous media. *Computational Geosciences*, *25*(1), 243-265.

Panzeri, L., Fumagalli, A., Aguzzoli, A., Zanzi, L., Longoni, L., Papini, M. Arosio, D.; 2023: Lab and modelling DC Resistivity Tests to Analyse the Response of a High Resistivity Liner. In 5th Asia Pacific Meeting on Near Surface Geoscience & Engineering, 2023, p.1 - 5.

Peaceman, D. W.; 1978: Interpretation of well-block pressures in numerical reservoir simulation (includes associated paper 6988). *Society of Petroleum Engineers Journal*, *18*(03), 183-194.

Rücker, C., Günther, T., & Wagner, F. M.;2017: pyGIMLi: An open-source library for modelling and inversion in geophysics. Computers & Geosciences, 109, 106-123.

Sheriff, R.E. Telford, W.M., Geldart, L.P.;1990: Applied Geophysics. Cambridge University Press, 2nd edition.

Corresponding author: lorenzo.panzeri@polimi.it

Application of conductive textile sachets as electrodes for electrical resistivity tomography measurements collected on debris and coarse-blocky surfaces

M. Pavoni [1], J. Boaga [1], A. Bast [2,3], Lichtenegger [2,3], J. Buckel [4]

[1]Department of Geosciences, University of Padova, Padova, Italy.
[2]WSL Institute for Snow and Avalanche Research SLF, Davos Dorf, Switzerland.
[3]Climate Change, Extremes and Natural Hazards in Alpine Regions Research Center CERC, Davos Dorf, Switzerland.
[4]Institute for Geophysics and Extraterrestrial Physics, Technische Universität Braunschweig, Braunschweig, Germany.

1. Abstract

Electrical resistivity tomography surveys are commonly applied in geophysical investigations performed in high mountain environments where debris and coarse-blocky surfaces can be found, e.g. landslide or rockfall deposits, blocky slopes and rock glaciers. In this harsh situation, obtaining acceptable contact resistances between the electrodes, usually composed of stainless-steel spikes, and the ground surface is challenging. The electrodes must be steadily coupled between the boulders (e.g. by hammering them) and, to improve the galvanic contact, sponges soaked in salt water are typically inserted among the spike and the rock surface (Hauck and Kneisel, 2008). Considering all this, it is clear that deploying ERT arrays in these environments is particularly time-consuming. To decrease this time effort, recently Buckel et al. (2023) applied conductive textile sachets as electrodes in ERT surveys performed on rock glaciers. To verify the reliability of this new electrodes approach, in this work we intensively tested the conductive textile sachets electrodes in different envinroments with debris and corse-blocky surfaces.

2. Introduction

It is well known in the geophysical community that collecting a high-quality ERT dataset requires a good galvanic contact between the electrodes and the ground surface (Day-Lewis, 2008). The parameter that represents the electrical contact area of two materials is defined as contact resistance. Low values of contact resistance allow to easily inject the electrical current and consequently to acquire ERT datasets with higher signal to noise ratio (Pavoni et al., 2022). This condition is particularly challenging to be achieved in envinroments with debris and corse-blocky surfaces. Coupling the electrodes with sponges soaked in salt-water is an efficient solution to minimize the contact resistance (Hauck and Kneisel, 2008). Despite this, the approach requires a significant amount of time to deploy the entire electrodes array, and a considerable amount of salt water to wet the sponges. Considering this, Buckel et al. (2023) proposed an alternative electrodes system to facilitate the preparation of ERT arrays in rock glacier envinroments. Instead of the traditional steel spikes, conductive textile sachets (wet with salt-water) are used as electrodes. In

this way, the electrodes don't need to be hammered between the boulders, but we can simply push them, and, compared to the sponges, we can use lower quantity of salt-water to wet them. To evaluate the performance of the conductive textile sachets, we compared the ERT measurements performed with this new electrode approach with the ERT measurements collected with the traditional steel spikes and sponges, considering common investigation lines. This comparative test has been carried out in three sites, which present different lithologies and size of the debris/boulders on the surface, and using different electrodes spacing. The collected datasets have been compered in terms of contact resistances, injected electrical current, measured apparent resistivities, reciprocal error, and inverted resistivity values.

3. Sites description

We tested the conductive textile sachets electrodes in three different envinroments that presents a debris and coarse-blocky surface: i) the Marocche di Drò landslide deposit, ii) the inactive rock glacier of Sadole, and iii) the active rock glacier of Flüelapass.

Marocche di Drò is a landslide deposit located in the lower part of Sarca Valley (Trento, Italy). Among the various landslide deposits in the area, we selected the Kas deposit, which is composed of calcareous debris, angular blocks, and limited vegetation cover (Martin et al., 2014). The comparative test was realized with 40 electrodes spaced 3 meters.

Sadole inactive rock glacier is located in the Sadole Valley (Trento, Italy). Steep rock walls and sharp crests, composed of magmatic ignimbrites rocks, surround the rooting area of the rock glacier. The rock glacier surface is composed of large size boulders, and widespread vegetation cover. The ERT survey line for the comparative test was realized with 43 electrodes spaced 5 meters, in a position with a coarse-blocky surface without vegetation, and where a discontinuos frozen layer was found in previous ERT investigations (Pavoni et al., 2023).

The Flüelapass active rock glacier is located in the eastern Swiss Alps (Engadin). The rooting area is surrounded by steep rock walls consisting of metamorphic amphibolite and paragneiss. Its surface is composed by a various granulometric size of debris and boulders, and isolated areas with finer sediment. The comparative test was carried out with an array of 48 electrodes spaced 2 meters.

4. Conductive textile sachets electrodes

Conductive textile sachets electrodes are realized with a commercial fabric (Holland Shielding Systems BV) made of polyester (65±5%) metallized with copper (20±2 %) and Nickel (15±2 %). Each sachet was realized with square pieces of 30 cm x 30 cm (the textile can be easily cut with sewing scissors), which were filled with 300 g of fine sand. The sachet is sealed with thin zip ties in such a way to leave a flake at the top where is possible to link the ERT cord clips. The cost to produce one conductive textile sachet electrode is about 15 euros, mainly due to the value of the metallic fabric, and the manufacturing of one sachet takes few minutes.

5. Data acquisition

In each test site, the ERT measurements have been collected with the same acquisition parameters and georesistivimeter (Syscal Pro, Iris Instruments). The datasets have been acquired with a dipole-dipole acquisition scheme with multiple dipole length, a stacking range between 3-6 (standard deviation threshold 5%), and with direct-reciprocal configuration to obtain a reliable estimation of the data error (Binley et al., 2015). Firstly, we collected the measurements with steel-spikes

electrodes hammered between the rocks and coupled with sponges soaked in salt water (e.g. Figure 1A). Subsequently, the same ERT array was measured using the conductive textile sachets electrodes pushed between the boulders and moistened with salt water (e.g. Figure 1B).

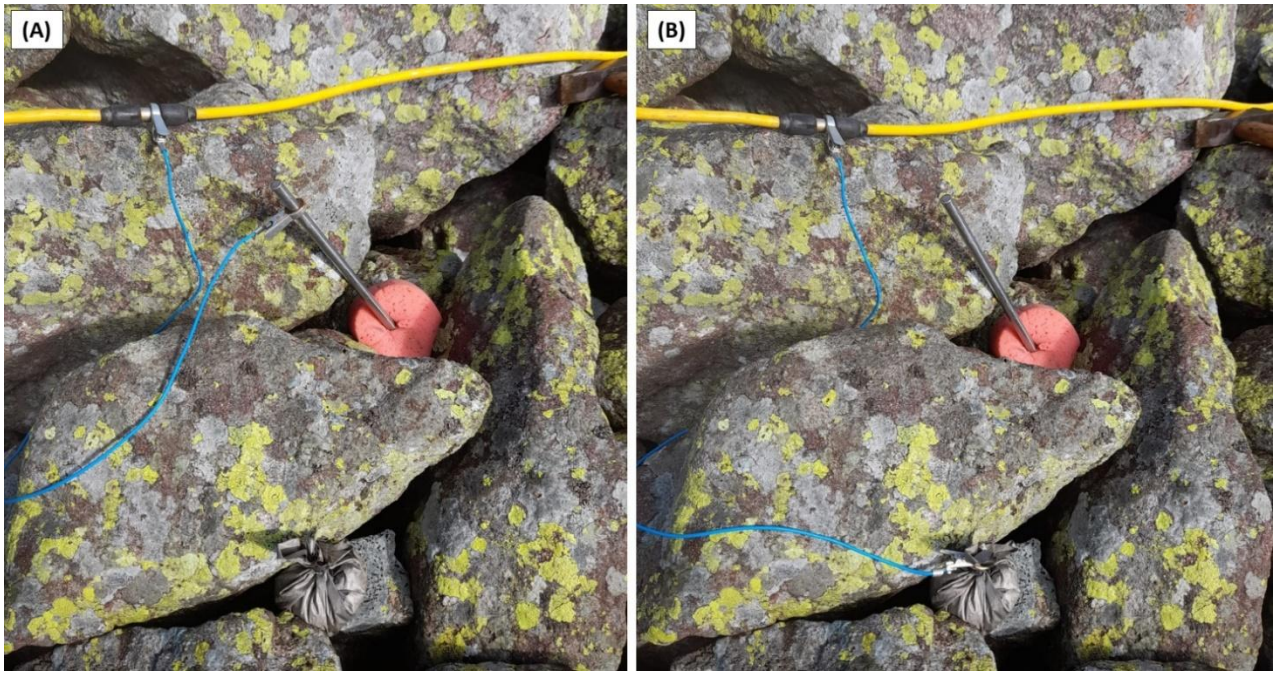

Figure 1. A) Example of measurements collected with steel-spike electrodes hammered between the boulders and coupled with sponges soaked in salt-water. B) Example of measurements collected with conductive textile sachets electrodes pushed between the boulders and wet with salt-water. Pictures realized during the comparative test performed on the inactive rock glacier of Sadole.

6. Data processing

To evaluate the reliability of the conductive textile sachets we compared the contact resistances, the injected electrical current, the measured apparent resistivities, the quadrupoles reciprocal error, and the inverted resistivity models obtained with the measurements collected with the different electrode's approaches. A statistical analysis was carried out following the approach proposed by Bast et al. (2015), using R (R-core-Team, 2022). Violin plots have been used for the data exploration, which include both the density distribution of the data and notched box plots. The robust Spearman correlation coefficient was calculated for each of the five variables.

To statistically compare the results obtained with steel-spikes electrodes and conductive textile sachets electrodes, for each site and variable, we fitted a robust linear regression model with an extended MM estimator (using the R package *robustbase* - Rousseeuw et al., 2009). Diagnostic regression plots were realized to verify that the model assumptions were met. Finally, the inverted resistivity models (inversion modelling performed with ResIPy – Blanchy et al. (2020)) are plotted and compared to evaluate the differences.

Discussion

The obtained results, which will be presented during the 42nd National Conference of the GNGTS 2024 in Ferrara (Italy), clearly demonstrate that conductive textile sachets electrodes can be successfully used to collect reliable ERT datasets in environments with debris and coarse-blocky surface, decreasing the time requested to deploy the investigation line. Consequently, applying this alternative electrode approach in future ERT measurements performed on rock glaciers, would allow to acquire measurements more rapidly, and the opportunity to collect more survey lines (e.g. realization of pseudo-3D geometries) extending the characterization of the investigated mountain permafrost area.

eferences

Bast, A., Wilcke, W., Graf, F., Lüscher, P., and Gärtner, H.; 2015: A simplified and rapid technique to determine an aggregate stability coefficient in coarse grained soils, CATENA, 127, 170-176, https://doi.org/10.1016/j.catena.2014.11.017.

Binley, A.; 2015: Tools and Techniques: Electrical Methods, in: Treatise on Geophysics (Second Edition), edited by: Schubert, G., Elsevier, Oxford, 233-259, https://doi.org/10.1016/B978-0-444-53802-4.00192-5.

Blanchy, G., Saneiyan, S., Boyd, J., McLachlan, P., and Binley, A.; 2020: ResIPy, an intuitive open source software for complex geoelectrical inversion/modeling, Computers & Geosciences, 137, 104423, https://doi.org/10.1016/j.cageo.2020.104423.

Buckel, J., Mudler, J., Gardeweg, R., Hauck, C., Hilbich, C., Frauenfelder, R., Kneisel, C., Buchelt, S., Blöthe, J. H., Hördt, A., and Bücker, M.; 2023: Identifying mountain permafrost degradation by repeating historical electrical resistivity tomography (ERT) measurements, The Cryosphere, 17, 2919–2940. https://doi.org/10.5194/tc-17-2919-2023.

Day-Lewis, F.D., Johnson, C.D., Singha, K., Lane, J.W.J.; 2008: Best practices in electrical resistivity imaging: Data collection and processing, and application to data from Corinna, Maine. In: An Administrative Report for the United States Environmental Protection Agency Region, p. 1.

Hauck, C. and Kneisel, C.; 2008: Applied Geophysics in Periglacial Environments, Cambridge University Press, ISBN 9780521889667.

Martin, S., Campedel, P., Ivy-Ochs, S., Viganò, A., Alfimov, V., Vockenhuber, C., ... & Rigo, M.; 2014: Lavini di Marco (Trentino, Italy): 36Cl exposure dating of a polyphase rock avalanche. Quaternary Geochronology, 19, 106-116.. https://doi.org/10.1016/j.quageo.2013.08.003.

Pavoni, M., Carrera, A., Boaga, J.; 2022: Improving the galvanic contact resistance for geoelectrical measurements in debris areas: a case study. Near Surf. Geophys. https://doi.org/10.1002/nsg.12192.

Pavoni, M., Boaga, J., Carrera, A., Zuecco, G., Carturan, L., & Zumiani, M.; 2023: Brief communication: Mountain permafrost acts as an aquitard during an infiltration experiment monitored with electrical resistivity tomography time-lapse measurements. The Cryosphere, 17(4), 1601-1607. https://doi.org/10.5194/tc-17-1601-2023.

Rousseeuw, P., Croux, C., Todorov, V., Ruckstuhl, A., Salibian-Barrera, M., Verbeke, T., Koller, M., and Maechler, M.; 2009: Robustbase: basic robust statistics, R package version 0.4-5, URL http:// CRAN. R-project. org/package= robustbase.

R-core-Team (2022): A Language and Environment for Statistical Computing, R Foundation for Statistical Computing. https://www.R-project.org (4.2.2) [code].

Corresponding author: mirko.pavoni@phd.unipd.it jacopo.boaga@unipd.it

Integrating cross-gradient joint inversion of ERT and SRT data and unsupervised machine learning on structured meshes incorporating topography

G. Penta de Peppo[1], M. Cercato[1], G. De Donno[1]

[1] *"Sapienza" University of Rome – DICEA*

Introduction

Among the geophysical methods applied for Civil and Environmental Engineering, the combined use of electrical resistivity tomography (ERT) and seismic refraction tomography (SRT) has shown to be effective for investigating the hydrogeological framework where civil structures and infrastructures are located, since these high-resolution methods are highly sensitive to different physical properties of the subsurface. Combining them in a coupled inversion scheme can significantly improve model reconstruction, so that the resulting subsurface models are more consistent and reliable than those obtained by comparing the results of individual inversions (Doetsch et al., 2010). During the last decades coupled inversions have become increasingly popular, in particular those involving one or more common additional terms in the objective function to be minimized, even though their practical implementation can be complex.

The structural gradient-based joint inversion approach is valid when changes in the geophysical properties are aligned, which is a reasonable assumption in a wide range of scenarios. The huge number of real-world case studies suggests that the cross-gradient joint inversion introduced by Gallardo and Meju (2004) is presently one of the most robust approaches. Currently, there are many applications of cross-gradient joint inversion on structured meshes with flat topography, but such algorithms are usually unable to manage non-flat surfaces. Jordi et al. (2020) developed a novel scheme on unstructured meshes, which can obviously adapt also to not-flat topographies, but for this purpose they modified the original cross-gradient method, which considers the direct neighbourhood of a single cell. We developed a new cross-gradient joint inversion routine in Python to process apparent resistivity and travel-time data incorporating topography, without modifying the original approach from Gallardo and Meju (2004) whose effectiveness is well demonstrated. In order to assess the impact of the coupled inversion scheme in both qualitative and quantitative terms a new standardization of the cross-gradient parameter is proposed ("Normalized cross-gradient", NCG). After the joint inversion procedure, an unsupervised machine learning algorithm is applied for improving the final interpretation by integrating the two output models into a single cross-section. Our approach is applied to both synthetic and field examples related to the application of ERT and SRT techniques to Civil and Environmental Engineering.

Individual inversions are carried out through the open-source pyGIMLi package (Rücker et al., 2017) properly adapted to work with the newly implemented structured mesh, and, for better comparison between separate and joint inversion results, the same inversion parameters, including regularization settings, initial model and forward modelling are used during each inversion step.

Method

Gallardo and Meju (2004) developed a structural procedure for two-dimensional simultaneous joint inversion in which the cross-gradient penalty function is applied to improve the resolution of common boundaries. This dimensionless function, which defines the geometrical similarity of two models as a distribution of gradients, is defined as:

$$t_{CG}(x,y,z) = m_r(x,y,z)m_v(x,y,z) \tag{1}$$

where $\mathbf{m}_r$ and $\mathbf{m}_v$ are resistivity and seismic velocity models, in our work variable in a two-dimensional space.

Adding the term in Eq.1 to the objective function, we obtain:

$$(m_r, m_v) = \left\| \frac{D_r\left(f(m_r) - d_r\right)}{D_v\left(f(m_v) - d_v\right)} \right\| + \frac{\lambda_r}{\lambda_v} \left\| \frac{C_r m_r}{C_v m_v} \right\| + \lambda_{CG} \left\| t_{CG}(m_r, m_v) \right\| \rightarrow min \tag{2}$$

In Eq.2 $\mathbf{D}_r$ and $\mathbf{D}_v$ are data weighting matrices, f($\mathbf{m}_r$) and f($\mathbf{m}_v$) the forward responses, $\mathbf{d}_r$ and $\mathbf{d}_v$ the observed data vectors, λ_r and λ_v weighting factors, $\mathbf{C}_r$ and $\mathbf{C}_v$ regularization matrices and λ_{CG} the cross-gradient weighting term. The objective function is nonlinear, since forward problems as well as the cross-gradient constraint are nonlinear, so to minimize it we used a first-order Taylor expansion (i.e. the Gauss-Newton method) and consequently solved the resulting system using the conjugate gradient algorithm.

The visual representation of the unchanged cross-gradient is rather complex, as it varies by several orders of magnitude and very differently from case to case, preventing a consistently accurate mode. Gallardo and Meju (2004) represented this quantity setting a minimum and maximum threshold. Observing that the unvaried cross-gradient always showed a Gaussian distribution, we defined a new standardization of it shown in Eq.3:

$$NCG = \frac{\left| t_{CG} \right|}{\left| t_{CG} \right|_{68}} \tag{3}$$

where $|t_{CG}|_{68}$ is the sixty-eighth percentile (a standard deviation threshold) of cross-gradient's absolute value distribution and the previous ratio is calculated for each cell of the mesh. This term, plotted between 0 and 10 compressing the variation between 1 and 10 showed the ability to well represent any case, overcoming the bottleneck of the unchanged cross-gradient visualization.

As an auxiliary tool we applied a fuzzy c-means (FCM) algorithm (Bezdek, 1981) to both individually and jointly inverted models yielding quantitative integrated cross-sections which resemble both models. FCM minimizes within-cluster variances (squared Euclidean distances) through an iterative process that assigns points to clusters in a probabilistic way (Paasche et al., 2010) reducing the objective function:

$$J = \sum_{i=1}^{c} \sum_{j=1}^{n} (u_{ij})^f \left\| d_j - v_i \right\|^2 \quad (4)$$

In Eq.4 n is the number of data points, c the number of clusters, u_{ij} the degree of membership of data point $\mathbf{d}_j$ to cluster i defined by its center $\mathbf{v}_i$ and f is the weighting exponent, set as 2. Finally, the output of fuzzy clustering is arranged in a unique plot developed by modifying the approach after Paasche et al. (2010), where primary colors denote different clusters while color saturation is proportional to the degree of membership to the assigned cluster.

Synthetic example

The synthetic example (Fig.1a) simulates a road embankment, in which a surface layer (ρ = 10 Ωm, v_P = 600 m/s) overlays an harder stabilising high-resistivity base (ρ = 1000 Ωm, v_P = 1800 m/s), both lying over a lower-resistivity and stiffer bedrock (ρ = 100 Ωm, v_P = 3000 m/s). Synthetic ERT dataset was generated by using 48 electrodes spaced 0.5 m apart in a dipole-dipole array with a maximum dipole length a_{max}=5 and a maximum dipole separation n_{max}=6. The resulting 945 apparent resistivity data points were contaminated with a zero-mean 3% Gaussian error. Analogously, for SRT geophones were located at the same electrode positions, simulating a shot every two geophones. A zero-mean Gaussian noise having a 0.1 ms standard deviation (median travel-time is about 5 ms) was added to the 1128 traveltime measurements. Results from separate inversions are shown in Fig.1b. The surface between superficial and intermediate layers, as well as the lateral extent of the latter are well defined in resistivity section, while the transition from the base to the bedrock is not well reproduced. Structural joint inversion (Fig.1c) highly improves the resistivity model, so that the base is properly placed where modelled with a significant upgrading in vertical reconstruction; jointly inverted velocity model exhibits an enhancement in a sharper transition from the superficial layer to the deeper ones. The NCG values (Fig.1d) from individual inversions are generally higher compared to those from the joint inversion, particularly in the area below the middle layer and in the transition between surface layer and bedrock. Finally, cluster analysis (Fig.1e) from jointly inverted models shows a better reconstruction, especially for the middle cluster (cluster no. 3) which is properly reconstructed within its real boundaries, and the bottom

layer (cluster no. 2) looks uniformed toned, improving the reconstruction compared to that achieved by individual inversion.

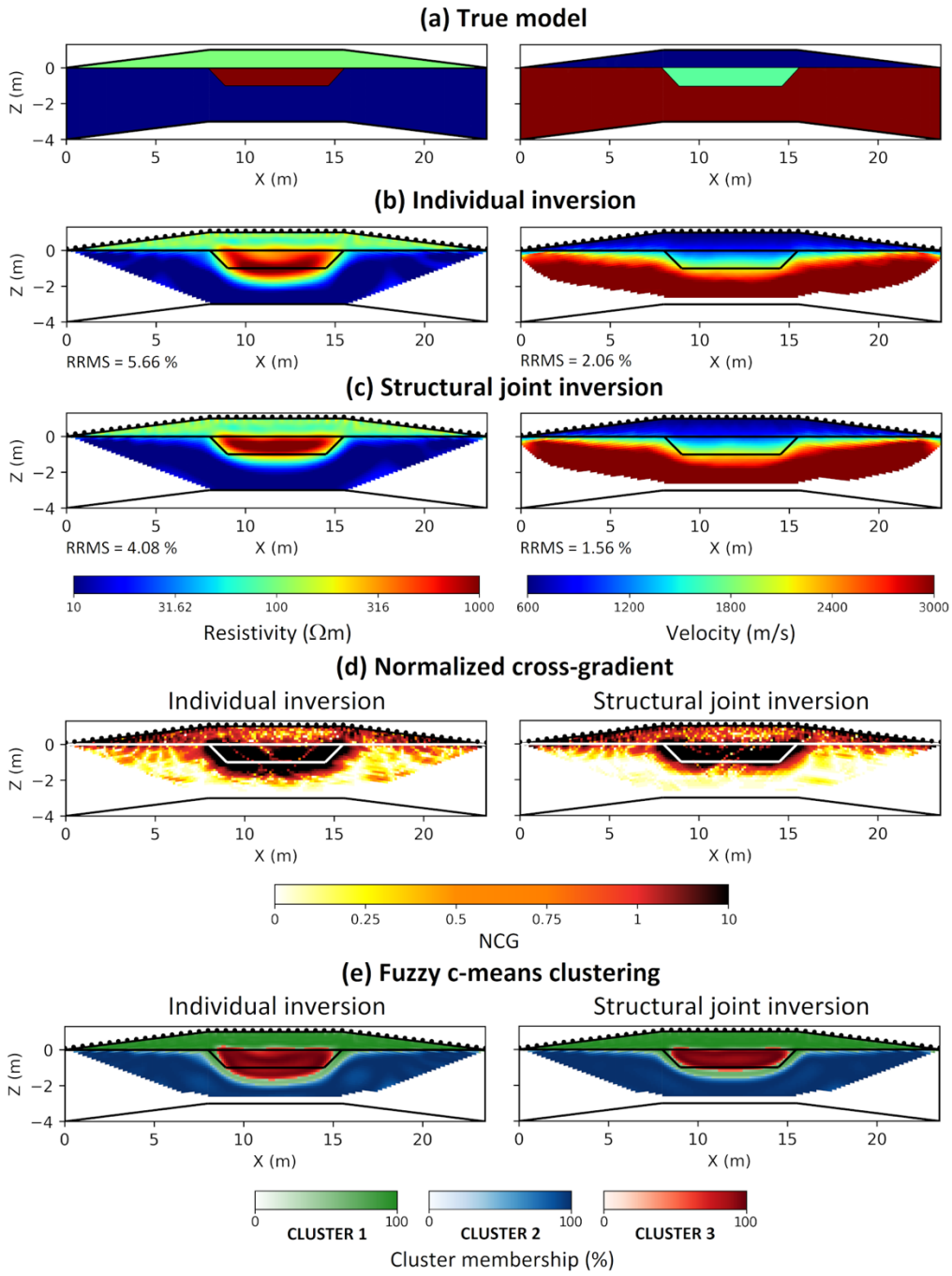

Figure 1. Synthetic example: (a) true model, (b) individual inversion, (c) cross-gradient joint inversion, (d) normalized cross-gradient, (e) fuzzy c-means clustering.

Field case study

The field case study is the Penne concrete dam located in central Italy (around 130 km east of Rome) and built in the second half of the sixties as a reservoir for irrigation (Fig. 2a). The hydro-geological layout of the site consists of Pliocene marly flysch having low permeability (hydraulic conductivity $K < 10^{-6}$ m/s), covered by Holocene ancient and recent alluvial deposits of the Tavo River. The alluvium is subdivided into a fine-grained shallower unit (clay and sandy silt) and a

coarse-grained high-permeable (K > 10^{-2} m/s) deeper one (sand and gravel). The dam was operating with a maximum water level well below the originally designed working conditions (256 m a.s.l.), since seepage phenomena occurring at the right abutment of the reservoir were confirmed by piezometric measurements that showed an increase of groundwater level downstream, which occurred when the reservoir level was higher than 250 m a.s.l. (Fig. 2b). Therefore, assessing the thickness and lateral extension of the coarse-graded highly permeable unit is pivotal for a correct design of the planned rehabilitation intervention (cut-off wall).

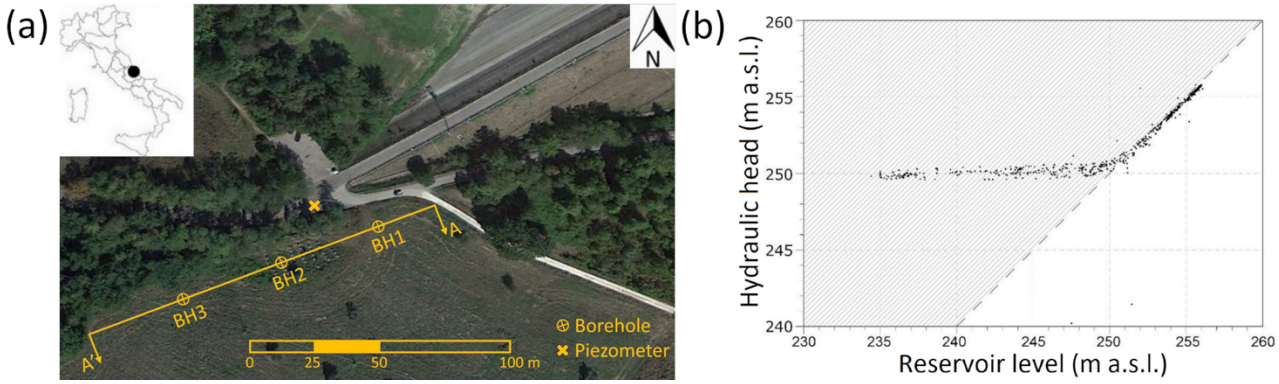

Figure 2. Penne case study (Central Italy): (a) aerial view with location of the ERT/SRT line and of the three boreholes; (b) hydraulic head logged as a function of the reservoir level (after Cardarelli, Cercato and De Donno, 2018).

Both ERT e SRT were performed along a 142 m alignment (Fig. 2a), with equally 2 m spaced sensor points (electrodes and geophones locations). ERT profile was acquired using the IRIS Instruments Syscal Pro resistivity-meter with 48 stainless steel electrodes in a pole-dipole array configuration, while P-wave seismic data were recorded employing a 48-channel system of 8 Hz vertical geophones by running a shot every two geophones using an 8-gauge Minibang shotgun. Three boreholes spaced 40 m apart along the geophysical line were drilled down the alignment for validating the geophysical surface investigations (Fig.2a). Results from individual inversion (Fig.3a) exhibit a three-layer geometry: low resistivity and P-wave velocity values (10-40 Ωm, 400-800 m/s) at shallow depths indicate the presence of the fine-grained alluvial deposits, followed by a less conductive formation (ρ = 100-300 Ωm, v_P = 1000-1800 m/s) that can be linked to the coarse-graded alluvial material and by a deep low-resistivity stiffer medium (ρ = 5-10 Ωm, v_P > 1800 m/s) revealing the presence of the flysch unit. Resistivity model clearly shows the thickness of the sand and gravel layer (about 7-10 m), but its lateral extent cannot be accurately determined in an area of lower resolution, even if it seems to vanish in the second part of section. Boreholes clarify the geometry of this layer: it has a thickness of 7 m (from 253 to 246 m a.s.l.) in BH1 (x = 23.5 m) and 8 m (at the same elevation) in BH2 (x = 63.5 m) confirming it has a sub-horizontal trend, but it was not detected in BH3 (x = 103.5 m), so we can deduce it ends between 63.5 and 103.5 m. The jointly inverted resistivity model (Fig.3b) displays a similar thickness of the coarse-graded material but its lateral extent is significantly reduced, ending around 80-85 m in good agreement with borehole data. Conversely, the P-wave velocity model remains nearly unchanged. The NCG index (Fig.3c) shows a decrease in the higher values at the central zone of the section, where the joint approach conspicuously impacts in better describing the termination of the sand and gravel unit. Finally, the quantitative integration of geophysical models through the results of cluster analysis is able to well

reconstruct the three main geological units of the study area (Fig.3d) and highlights the benefit of the joint approach, as cluster no. 3 ends abruptly at x = 81 m rather than extending endlessly towards last part of the section.

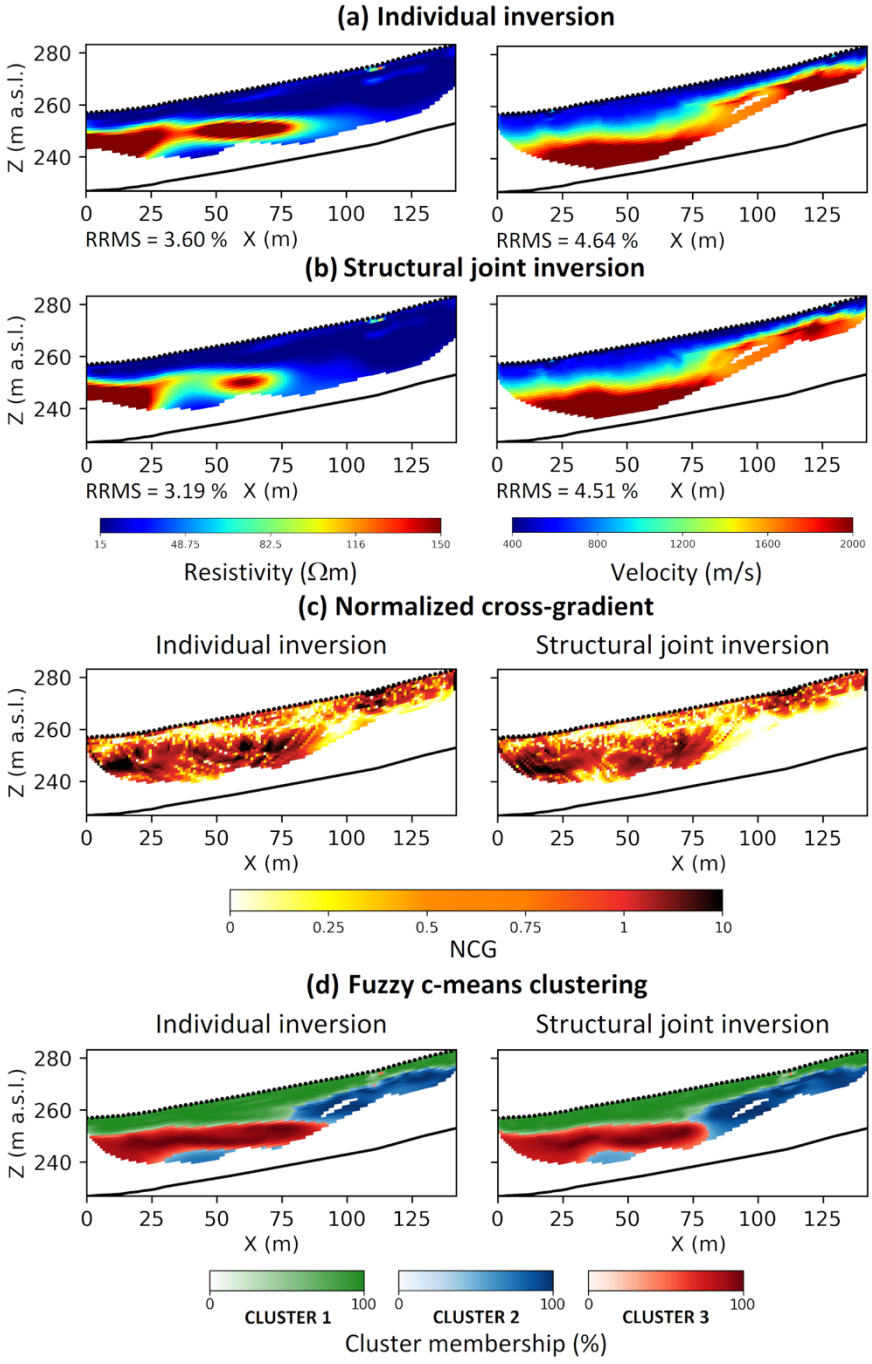

Figure 3. Field case study at the Penne dam (Central Italy): (a) individual inversion, (b) cross-gradient joint inversion, (c) normalized cross-gradient, (d) fuzzy c-means clustering.

Conclusions

A cross-gradient algorithm to jointly inverted ERT an SRT data on structured mesh incorporating topography was presented. The benefit of the proposed approach was quantitatively evaluated in terms of a new standardization of the cross-gradient parameter to assess the impact of the coupled scheme and a fuzzy c-means analysis to improve the final interpretation phase. A synthetic

example showed the reliability of the proposed algorithm for improving accuracy in model reconstruction in comparison to individual inversions. Then, the application to a field case study (investigation of the lateral abutment of a concrete dam) revealed the benefit of such an algorithm in a complex hydrogeological scenario, where the jointly inverted models are in better agreement with boreholes information, compared to individual inversions. The improvement provided by the coupled procedure with respect to single inversions is also strengthened by the lower root-mean-square errors and NCG values especially in the low-sensitivity deep zones and close to the interfaces between different layers. Finally, the fuzzy c-means analysis can allow for a final quantitative interpretation which resembles the effective layering of the case study, giving also an assessment of the reliability of the reconstruction by means of the membership values. Therefore, the proposed approach can be effective in improving the geophysical reconstruction for complex cases, where resistivity and P-wave velocities are expected to have sharp lateral and vertical changes.

References

Bezdek J. C.; 1981: Pattern recognition with fuzzy objective function algorithms. Plenum Press.

Cardarelli E., Cercato M. and De Donno G.; 2018: Surface and borehole geophysics for the rehabilitation of a concrete dam (Penne, Central Italy). Engineering Geology.

Doetsch J., Linde N., Coscia I., Greenhalgh S. A. and Green A. G.; 2010: Zonation for 3D aquifer characterization based on joint inversions of multimethod crosshole geophysical data. Geophysics.

Gallardo L. A. and Meju M. A.; 2004: Joint Two-Dimensional DC Resistivity and Seismic Travel Time Inversion with Cross-Gradients Constraints. Journal of Geophysical Research.

Jordi C., Doetsch J., Günther T., Schmelzbach C., Maurer H. and Robertsson J. O. A.; 2020: Structural joint inversion on irregular meshes. Geophysical Journal International.

Paasche H., Tronicke J. and Dietrich P.; 2010: Automated integration of partially colocated models: Subsurface zonation using a modified fuzzy c-means cluster analysis algorithm. Geophysics.

Rücker C., Günther T. and Wagner F. M.; 2017: pyGIMLi: An open-source library for modelling and inversion in geophysics. Computers and Geosciences.

Corresponding author: guido.pentadepeppo@uniroma1.it

In situ geophysical techniques for the hydrogeological hazard assessment in urban area: the Gorgoglione (Basilicata region, Southern Italy) case study

A. Perrone[1], J. Bellanova[1], G. Calamita[1], F. Falabella[2], M.R. Gallipoli[1], E. Gueguen[1], A. Pepe[2], S. Piscitelli[1], V. Serlenga[1], T.A. Stabile[1]

[1] Consiglio Nazionale delle Ricerche, Istituto di metodologie per l'analisi ambientale (IMAA) - Italy

[2] Consiglio Nazionale delle Ricerche, Istituto per il Rilevamento Elettromagnetico dell'Ambiente (IREA) - Italy

The geomorphological fragility of the Basilicata territory (southern Italy) and, in particular, the vulnerability to landslides can be considered the result of various causes such as the lithology of the outcropping terrain, the morphology of the reliefs, neotectonics, seismicity, climate and vegetation.

Since the 17th century, landslides have been recognized and recorded as a problem for the Lucanian territory (Boenzi, 1974; Stuart, 1993). In the 18th century, the changes in land use significantly increased the number of landslides. Subsequently other factors such as the experience of poorly designed and poorly constructed urban settlements, the defective disposal of water and wastewater, the limited consolidation against landslides and the progressive abandonment of land around inhabited centers territory, have contributed in accelerating the occurrence of landslides (Stuart, 1993; Vita-Finzi, 1969). Climate change and the incidence of extreme rainfall events in an already very fragile landscape have also played an important role in this acceleration into the 20th and 21st centuries.

Currently all 131 municipalities in Basilicata Region are involved by landslides (Inventory of Landslide Phenomena in Italy, IFFI Project 2020) and in 83 of them the landslides have affected the continuous and discontinuous urban fabric as well as industrial or commercial areas. In many cases, as for example in the Gorgoglione test site, the state of emergency has been declared with evacuation orders for residential buildings and commercial activities and, where necessary, also with the demolition of historic buildings (Perrone et al., 2021; Calamita et al., 2023).

Traditional direct techniques, such as geotechnical boreholes, offer point-specific information but can be highly invasive, leading to potential damage to economic and cultural resources such as archaeological sites and underground utilities, especially in the upper layers of the subsoil. In the

context of investigating landslides in urban areas, alternative approaches may be more suitable. A significant contribution can be achieved through the combined utilization of remote sensing and in situ geophysical techniques (Perrone et al., 2006; de Bari et al., 2011).

In this work, ground based SAR (GB-SAR) interferometry, electrical resistivity tomography (ERT) and passive seismic techniques have been integrated for investigating the phenomenon affecting the Gorgoglione urban area, located in the south-western part of Matera Province (Basilicata Region, southern Italy) on a hilly area at about 800 m a.s.l. (Fig.1). The GB-SAR results provided information on the activity status of the phenomenon. The ERT and the single-station seismic ambient noise measurements allowed the reconstruction of the subsoil geological setting, the identification of physical discontinuities correlated with lithological boundaries and sliding surfaces and the location of high water content areas.

This information was used to assess the landslide residual risk, to plan and implement the risk mitigation actions and to correctly design the remediation works.

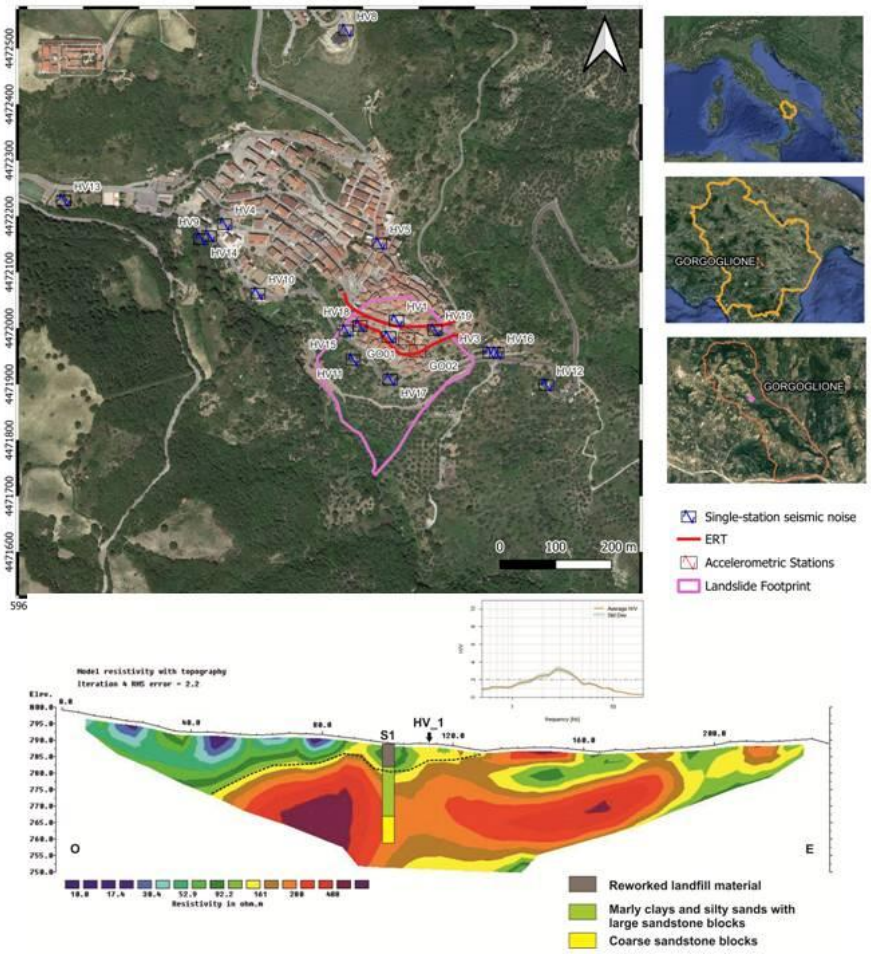

Fig. 1 – Map of Gorgoglione test site (Basilicata region, southern Italy) with location of the in-situ geophysical measurements carried out in the urban area.

References

Boenzi F.; 1974: Il dissesto idrogeologico in Basilicata dalla fine del 1600 ad oggi. Pages 23-28 in Atti del IV Simposio Nazionale sulla Conservazione della Natura, I, Bari.

Calamita G., Gallipoli M.R., Gueguen E., Sinisi R., Summa V., Vignola L., Stabile T.A., Bellanova J., Piscitelli S., Perrone A.; 2023: Integrated geophysical and geological surveys reveal new details of the large Montescaglioso (southern Italy) landslide of December 2013. Engineering geology 313 , pp. Art.n.106984-1–Art.n.106984-16.

de Bari C., Lapenna V., Perrone A., Puglisi C., Sdao F.; 2011: Digital photogrammetric analysis and electrical resistivity tomography for investigating the Picerno landslide (Basilicata region, southern Italy). Geomorphology 133, 34–46

IFFI Project (Inventario dei Fenomeni Franosi in Italia). ISPRA, Dipartimento Difesa del Suolo, Servizio Geologico d'Italia. Available online: http://www.progettoiffi.isprambiente.it/cartanetiffi/ (accessed on May 2020)

Perrone A., Canora F., Calamita G., Bellanova J., Serlenga V., Panebianco S., Tragni N., Piscitelli S., Vignola L., Doglioni A., Simeone V., Sdao F., Lapenna V.; 2020: A multidisciplinary approach for landslide residual risk assessment: the Pomarico landslide (Basilicata Region, Southern Italy) case study. Landslides 18, 353–365.

Perrone A., Zeni G., Piscitelli S., Pepe A., Loperte A., Lapenna V., Lanari R.; 2006: Joint analysis of SAR interferometry and electrical resistivity tomography surveys for investigating ground deformation: the case-study of Satriano di Lucania (Potenza, Italy). Engineering Geology 88, 260–273.

Stuart O.; 1993: 20-th century urban landslides in the Basilicata Region of Italy. Environmental Management 17 (4), 433-444.

Vita-Finzi C.; 1969: The Mediterranean valleys: geological changes in historical times. Cambridge University Press, Cambridge, UK

Corresponding author: angela.perrone@cnr.it

Geophysical-based approach for studying the submarine groundwater discharge: the SUBGEO Project

G. Romano[1], L. Capozzoli[2], V. Lapenna[2], M. Polemio[3]

[1] Department of Earth and Geo-Environmental Sciences, University of Bari Aldo Moro, Piazza Umberto I, 70121 Bari, Italy
[2] Institute of Methodologies for Environmental Analysis, National Research Council of Italy (IMAA CNR), C. da S. Loja—Zona Industriale, Tito Scalo, 85050 Potenza, Italy
[3] Research Institute for Hydrogeological Protection, National Research Council of Italy (IRPI CNR) 70126 Bari, Italy

The problem of water supply represents a priority for not only the Mediterranean Area but for the World if we consider the age-old problem of the drought exacerbated by the climate change events that are constantly seen [Jiao and Post, 2019]. Coastal aquifers are fundamental for water supply and innovative strategies are strongly required to detect and preserve water resources under increasing pressure. Developing new knowledge and innovative solutions for a systemic and inclusive approach of water management represents a big challenge for the scientific community.

Indeed, delineating coastal hydrogeologic structures, or hydrostratigraphy, is a crucial step for the characterization of groundwater flow and management of groundwater resources. Furthermore, hydrostratigraphic complexities play a fundamental role in the interactions occurring between coastal aquifers and marine ecosystems and influence the transport of solutes to coastal waters, and the response to climate change [Befus et al., 2014]. However, as coastal groundwater investigations are addressed to characterize and monitor the onshore resources and coastal fringe processes, the interactions between fresh groundwater within submarine aquifers remain poorly explored [Post et al., 2013; Knight et al., 2019]. The increasing water demand on the global scale because of per capita demand and population increases causes a strongly increasing exploitation of the available high-quality water resources, increasing the risk of salinization via mixing for seawater intrusion. These trends can be further worsened in large areas by the enduring effects of climate change. All these conditions are causing stress on the water resources of coastal aquifers. The management efforts require more knowledge of coastal springs and submarine groundwater discharge (SGD), to preserve residual fresh resources and to find the freshest possible groundwater for desalination [Polemio et al., 2020]. However, coastal areas, are challenging places for the application of geophysical methods due to their being highly dynamic and fragile systems and because they are constituted by two different operational conditions: land onshore and sea offshore. At present time, the relatively few surveys aimed to characterize the coastal areas are usually performed by joint together land and marine surveys. This practice, whereas of simple applications, has a relevant limit. The boundary area between the sea and the land, the area close

to the shore, remains poorly or not investigated either by the land surveyor by the marine one. Consequently, missing information on the area where seawater and groundwater start to interact, the reconstruction of the hydrogeological processes in the coastal area may be inaccurate or incomplete.

In this framework, the University of Bari (UNIBA) and the two CNR Institutes, IMAA and IRPI, have proposed the two-year Research Project of National Relevance (PRIN PNRR 2022) SUBGEO (Submarine groundwater discharge analysis with an innovative and integrated geophysical approach) addressed to develop and employ an innovative strategy based on the integrated multiscale and multiresolution geophysical investigation approach for the coastal underground freshwater reservoir non-invasive characterization.

SUBGEO aims to setup an innovative investigation strategy able to furnish continuous information from the land to the sea useful to define the water fluxes dynamics. A two-level strategy is proposed. In the first level, the investigations will provide an expeditious and not expensive overall characterization of the geophysical framework of the investigated area). The second investigation level will include a more complex integration of electrical and electromagnetic geophysical methodologies and will be more informative. The expected results will consist of a multiscale and multiresolution subsoil characterization from land to sea, that crossing the shoreline, will not have any spatial informational gap. The outcome of the second investigation level will support the creation of optimized hydrogeological models of the investigated area and can also be directly used by the decision-maker to implement sustainable water resources management strategies.

SUBGEO is addressed to gain useful tools for the optimal and sustainable management of the coastal areas and resources, operating on the largest Italian coastal aquifer, the Apulia region where the coastal aquifers fed the highest concentration of submarine springs and SGD [Polemio, 2016]. The project will develop an innovative geophysical approach based on the integrated use of aerial, land, land-marine and marine geophysical electric and electromagnetic techniques to provide spatially continuous and high-resolution information on the subsoil structure from the offshore areas, where the outward fluxes mix with the seawater, to the onshore ones. Finally, SUBGEO will be tuned by small-scale laboratory experiments and numerical simulations to define the best acquisition procedures and check the sensitivity of the strategy for different subsurface conditions.

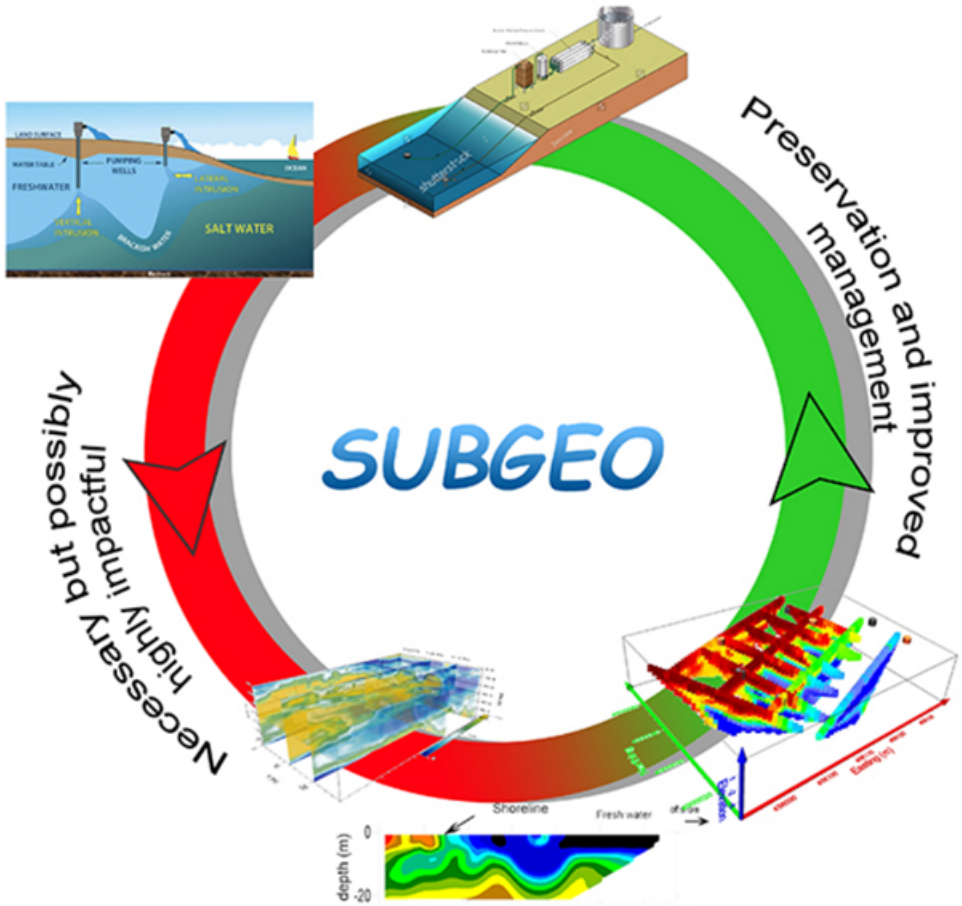

Fig. 1 - The proposed geophysical approach for characterizing coastal areas of SUBGEO

References

Befus et al., 2014, Geoelectrical signals of geologic and hydrologic processes in a fringing reef lagoon setting, J. Hydrol, 517, 10.1016/j.jhydrol.2014.05.070.

Jiao J., and V. Post, Coastal hydrogeology. Cambridge University Press, 2019.

Knight et al., 2019.Combined geophysical and analytical methods to estimate offshore freshwater extent, J. Hydrol, 576, 10.1016/j.jhydrol.2019.06.059

Polemio M., 2016, Monitoring and Management of Karstic Coastal Groundwater in a Changing Environment (Southern Italy) A Review of a Regional Experience. Water, 8, 10.3390/w8040148

Polemio, M. et al. 2020, Review of Utilization Management of Groundwater at Risk of Salinization. J. Water Resour. Plan. Manag, 146

Post et al., 2013, Offshore fresh groundwater reserves as a global phenomenon. Nature, 504, 10.1038/nature12858

Corresponding author: gerardo.romano@uniba.it

Integrated GPR and FDEM to detect brines pockets in Continental Antarctica

I. Santin[1], E. Forte[1], M. Guglielmin[2]

[1] Department of Mathematics, Informatics and Geosciences (University of Trieste, Italy)
[2] Department of Theoretical and Applied Science (University of Insubria, Italy)

Introduction

The extreme environmental condition of Antarctica and the presence of subcryospheric saline waters makes it one of the most relevant planetary analogues for Mars, especially since hypersaline brines were found on the red planet (*Martínez and Renno, 2013*). As a consequence, the interest on Antarctic brines have increased, especially to determine the lifeforms in these environments and their adaptability to extreme environmental conditions. From the geophysical point of view, brines are peculiar materials whose characteristics are strictly correlated with their salinity, density, temperature and pressure. Considering that, at liquid state, brines are hypersaline and therefore high-conductive solutions, electromagnetic (EM)-based methods, such as Ground Penetrating Radar (GPR) can be successfully exploited to detect and image brines pockets, although their EM signature on GPR data is not unequivocally defined (*Forte et al., 2020*). However, recently also Frequency-Domain Electromagnetic (FDEM) inductive methods are increasing their applications to glaciology, even though their effectiveness is not always fully demonstrated and, up to now, no applications to Antarctic brines detection have been reported.
We focus on Boulder Clay Glacier area (Victoria Land, East Antarctica), i.e. a coastal zone characterized by a glacier, its moraines and some perennially frozen lakes (*Guglielmin et al., 2009*). The area is located about 6 km SW from the Italian Antarctic Station (MZS in FIG.1A), close to the southern side of a gravel landing strip, built in 2019. Several boreholes have been dug both on the moraine, the glacier and some lakes, and at least three detected brines pockets have been sampled to study their prokaryotic (*Azzaro et al., 2021*) and fungal (*Sannino et al., 2020*) communities. In particular, Lake n.16 is neighbour with a CALM permafrost grid (FIG.1B), which is part of the CALM program aiming at the observation of the response of the active layer to climate change over multi-decadal time scales (*Guglielmin et al., 2009*). Such a grid has been relocated in its actual position in 2019 due to the landing strip building, and now it lies near a borehole discussed in *Sannino et al., 2020*. In this work, starting from the borehole dug in 2014 in which a liquid brine pocket was discovered, we proposed an integrated geophysical approach to define the EM signature of brine pockets, combining GPR and FDEM induction surveys. The geophysical characterization of brines pockets allows to deepen the investigation about the complex geomorphological settings of the area, providing a more constrained methodology to optimize the

position of future boreholes while developing and approach that can be exploited even in other geological, geomorphological, and glaciological situations.

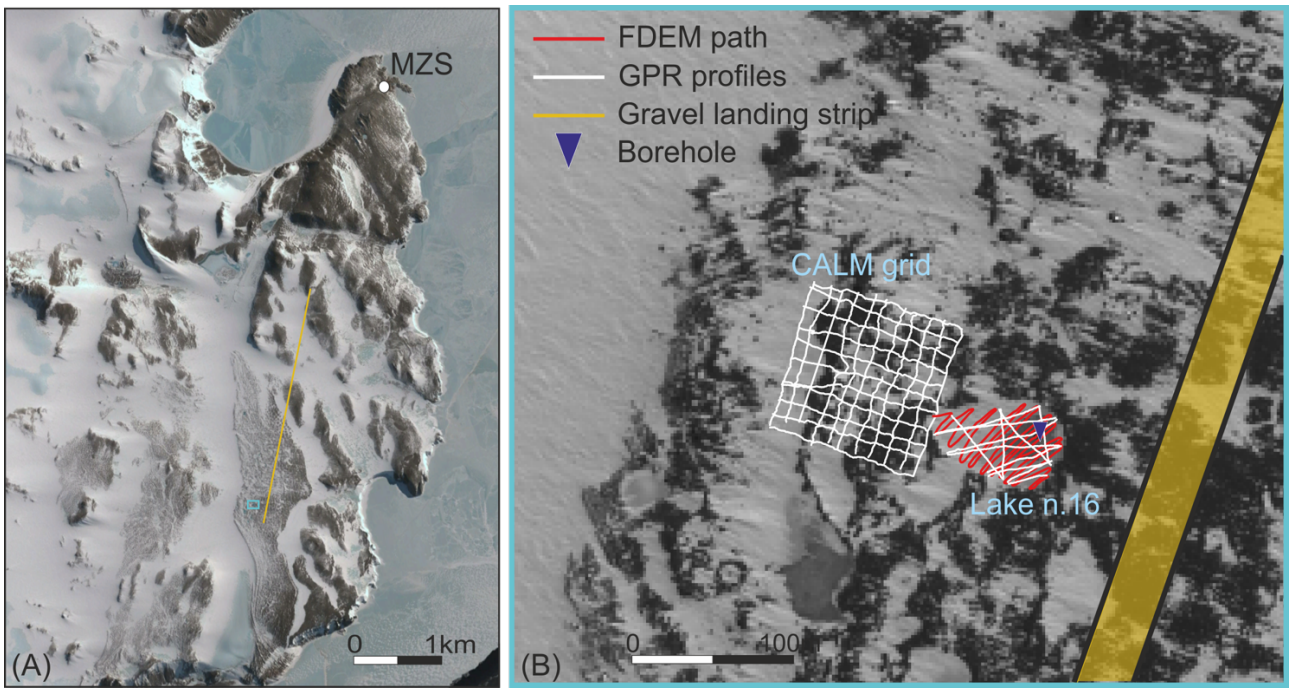

Fig. 1 – (A) Location map of CALM grid and Lake n.16 (light blue square) in Boulder Clay Glacier area (MZS: Mario Zucchelli Italian Station). (B) Ortophoto with superimposed the GPR profiles, in white, and the FDEM survey, in red. Yellow lines mark the position of the gravel landing strip.

Methods

During the XXXVIII Italian Expedition in Antarctica (November 2022), two GPR surveys were performed on the CALM grid and the neighbouring Lake n.16. On the latter, an FDEM survey was also collected. The 880 m-long FDEM dataset (red line in FIG.1B) was acquired with a CMD-2 probe (GF-Instruments), recording the mean conductivity value every 0.5 s, down to a maximum nominal depth of 2.5 m. The dataset is characterized by a high overall quality, with minimum and maximum values of 0.05 mS/m and 12 mS/m, respectively. The conductivity values were interpolated on a regular grid (2 m by 2 m) with a Kriging algorithm, obtaining the apparent conductivity map, shown in FIG.2. As far as the GPR surveys (white lines in FIG.1B), they were both performed with a ProEx GPR system (Malå Geoscience), equipped with 500 MHz shielded antennas. A basic processing flow was applied, including zero-time correction, band-pass filtering, amplitude recovery, depth conversion and topographic correction, considering a constant velocity of 0.17 m/ns (I.e. the typical value for pure clean glacial ice). To improve the EM characterization of brines pockets, the interpretation of CALM grid GPR dataset was supported by GPR attribute analysis, which already demonstrated their effectiveness in glacial environments (e.g. *Zhao et al., 2016*). We specifically focused on frequency-, phase- and texture-related attributes, integrating them during data interpretation.

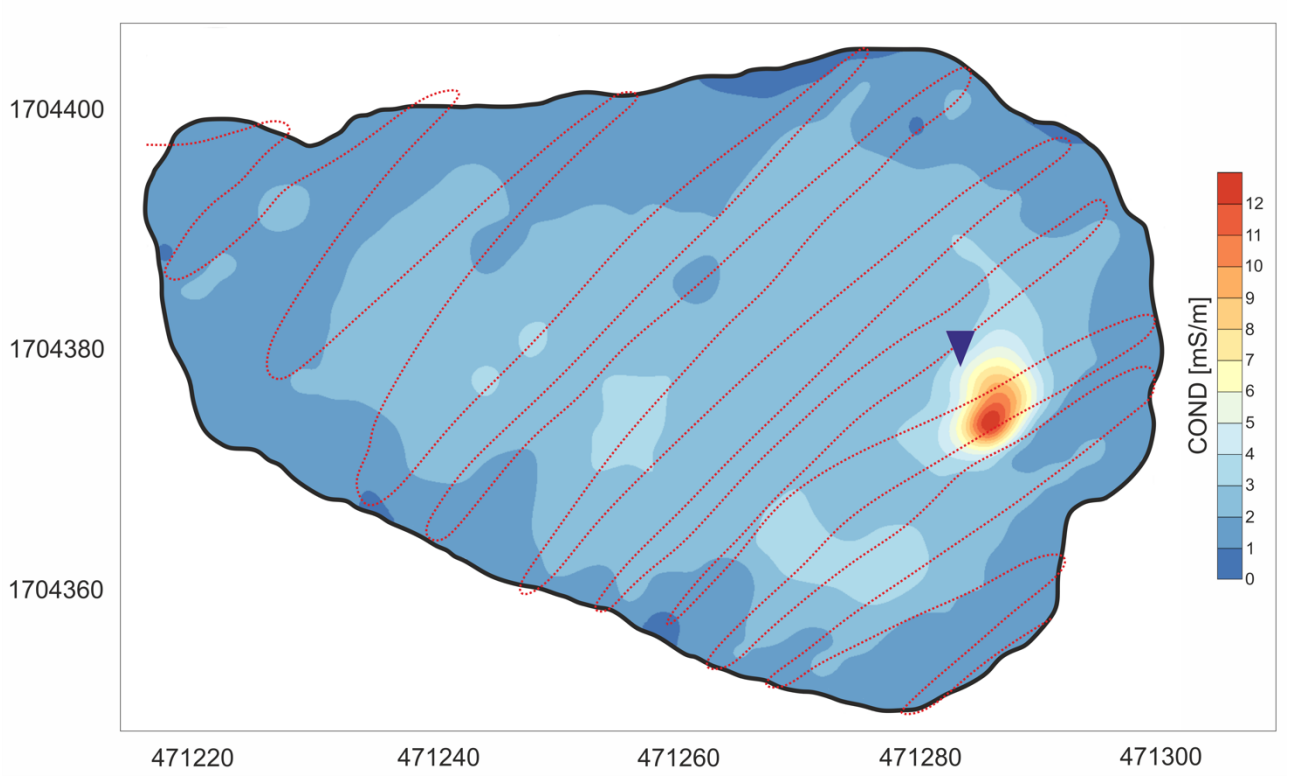

Fig. 2 – Apparent conductivity map down to a nominal depth of 2.5 m on Lake n.16. Red dotted line marks the path of the FDEM survey, while the blue triangle the location of borehole BC1 (taken from *Azzaro et al., 2021*).

Results and discussion

FIG.2 shows the mean apparent conductivity map of the Lake n.16 down to a maximum depth of about 2.5 m. It is characterized by a very low conductivity close to 0 mS/m, typical of the ice, however, a high conductivity spot is apparent, reaching a maximum value of more than 12 mS/m. In *Azzaro et al., 2021*, the borehole named BC1 whose location is marked in FIG.2 revealed the saltiest brines pocket of this lake at a depth of about 2.5 m; it is very close to the high conductivity spot highlighted by FDEM. It is interesting to note the accurate correlation between the information provided by the borehole and by the FDEM survey, both indicating the target depth at about 2.5 m, even considering the temporal interval of 8 years between the two surveys (2014 for the borehole and 2022 for the FDEM). GPR profiles in FIG.3A-3B cross close to the high conductivity spot and the borehole BC1 of *Azzaro et al., 2021.* On the two almost perpendicular GPR sections, it can be recognized the base of the lake as a high amplitude reflection at the bottom of the mainly transparent facies of the lake ice. However, the continuity of such horizon is interrupted near the BC1 borehole location, where the amplitude of the EM signal is strongly attenuated. Such extremely high attenuation is most likely produced by the high conductivity of the brines pocket, which limited the propagation of the EM signal. Such peculiar setting was found also on the GPR dataset of the neighbour CALM grid. FIG.3C shows the same high EM signal attenuation with the horizon interruption deepening, as described for Lake n.16. The spectral behaviour of the EM signal reveals a rapid decrease of frequency content, moving towards lower frequencies, corresponding to the transparent and high attenuated facies (red colour in FIG.3C'). In addition, the texture-related attributes highlight a more chaotic facies (FIG.3C''), possibly

suggesting fluids upwelling, while the phase-related attribute makes more evident the interruption of the continuity of all horizons across the highly attenuated facies.

It is remarkable to point that the GPR signature and response to the attributes analysis we performed on the GPR profiles of CALM grid, find a match with the outcomes described in *Forte et al., 2016* for other Antarctic coastal lakes. As a matter of fact, the accuracy of the match in terms of spectral behaviour and EM facies further validate the applicability of GPR as a low-time consuming method to identify hidden brines pockets. However, it is essential to point out that in some cases the signal is so attenuated that prevents the application of attributes analysis. Such situation occurs for instance on the GPR profiles of Lake n.16 where attributes analysis gave no remarkable results. Therefore, the integration of FDEM and GPR, allows to be more accurate and favourable about the presence of buried brines pockets.

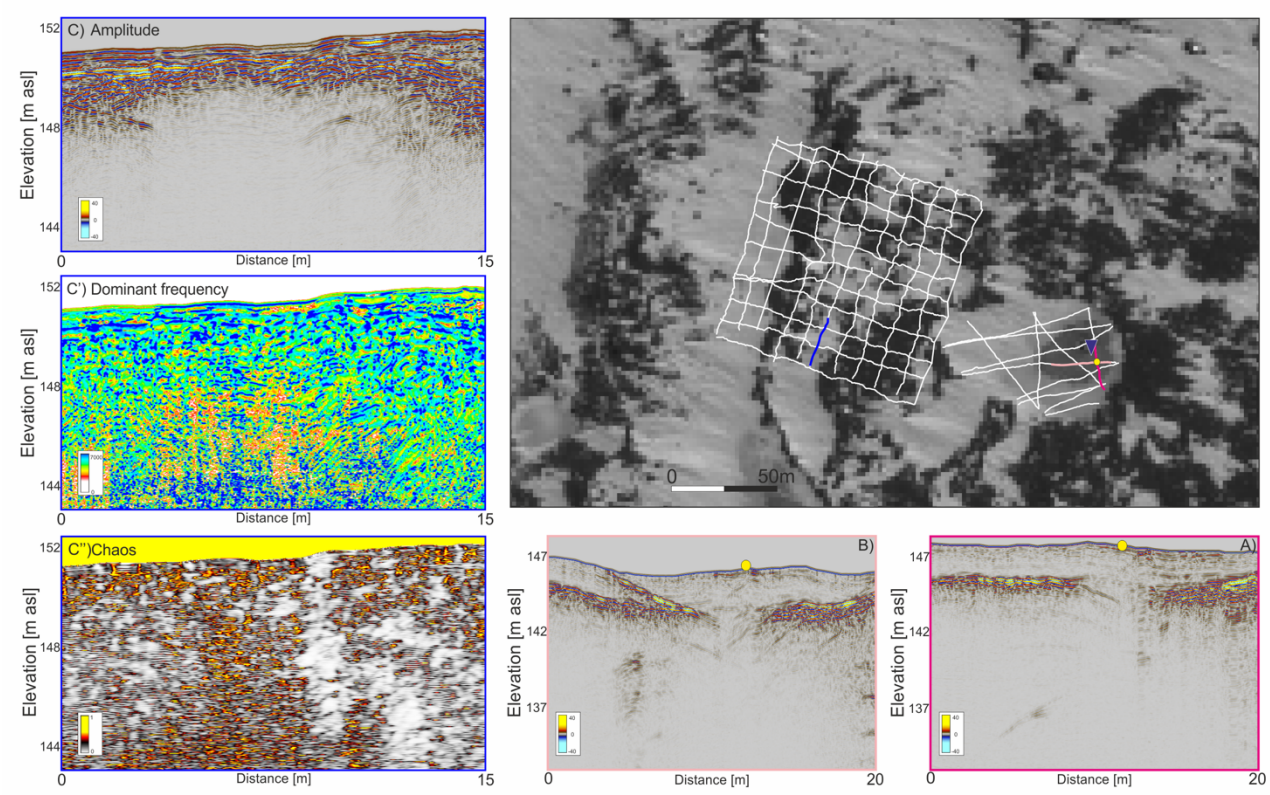

Fig. 3 – Exemplary GPR profiles on Lake n.16 (A, B) and on CALM grid (C, C', C''), both represented with white lines. C' and C'' display dominant frequency and chaos attributes, respectively, of profile C. Yellow dot marks the crossing point between A and B. Location of each GPR profile is highlighted by a coloured line: C, C', C'' with a blue line, while A and B with pink and magenta lines, respectively. Pink triangle marks the location of BC1.

Conclusion

We proposed a detailed analysis of the geophysical signature of Antarctic brines pockets, validated through boreholes. The integration of FDEM and GPR surveys allowed to characterize brines pockets in terms of high electrical conductivity and a peculiar EM facies, respectively. The high conductivity (up to more than 12 mS/m in the investigated area) related to the brines strongly affects the propagation of the EM wave generating an attenuated EM facies which is characterized, in addition to the low reflectivity, by a spectral shift to lower frequencies, horizons continuity

interruptions and an overall chaotic texture. The integrated peculiar and clear geophysical response of brines pockets can be exploited to effectively determine the presence of brines pockets and their approximated depth, thus resulting in a helpful strategy to map even large areas in which drill possible future boreholes for brines sampling.

Acknowledgements

This work was supported by grants CRYOVEG and IPECA from the National Antarctic Research Program (PNRA18_00288-D; PNRA18_00186-E). We gratefully acknowledge Schlumberger through the University of Trieste Petrel® interpretation package academic grant.

References

Azzaro M., Maimone G., La Ferla R., Cosenza A., Rappazzo A.C., Caruso G. et al.; 2021: The prokaryotic community in an extreme Antarctic environment: the brines of Boulder Clay lakes (Northern Victoria Land). Hydrobiologia, 848(8), 1837-1857. doi: 10.1007/s10750-021-04557-2

Forte, E., Dalle Fratte, M., Azzaro, M., Guglielmin, M.; 2016: Pressurized brines in continental Antarctica as a possible analogue of Mars. Scientific Reports, 6, 33158. doi: 10.1038/srep33158

Forte E., Dossi M., Guglielmin M.; 2020: The search for brines: GPR markers, proxies, and challenges. SEG Global Meeting Abstracts, 73-76. doi: 10.1190/gpr2020-020.1

Guglielmin M., Lewkowicz A.G., French H.M., Strini, A.; 2009: Lake-ice blisters, Terra Nova Bay area, Northern Victoria Land, Antarctica. Geografiska Annaler, 91, A(2), 99-111. doi: 10.1111/j.1468-0459.2009.00357.x

Martínez, G.M., Renno, N.O.; 2013: Water and Brines on Mars: Current Evidence and Implications for MSL. Space Science Reviews, 175, 29–51. doi: 10.1007/s11214-012-9956-3

Sannino C., Borruso L., Mezzasoma A., Battistel D., Zucconi L., Selbmann L. et al.; 2020. Intra- and inter-cores fungal diversity suggests interconnection of different habitats in an Antarctic frozen lake (Boulder Clay, Northern Victoria Land). Environmental Microbiology, 22(8), 3463-3477. doi: doi:10.1111/1462-2920.15117

Zhao W., Forte E., Colucci R.R., Pipan M.; 2016. High-resolution glacier imaging and characterization by means of GPR attribute analysis. Geophysical Journal International, 206(2), 1366–1374. doi: 10.1093/gji/ggw208

Seafloor morphology and very shallow stratigraphic information from acoustic data processing

C. Sauli and L. Baradello

Istituto Nazionale di Oceanografia e di Geofisica Sperimentale – OGS, Trieste.

Acoustic data acquired in Antarctica in 2006 and 2017 (PNRA projects Vild and Glevors) with the hull-mounted Chirp II DataSonics system aboard the N/R OGS Explora have been subjected to seismic processing to obtain a truly high-resolution data set, providing metric and sub-metric resolution, from which information on the very shallow stratigraphy can be obtained and increasing the possibility of correlation with sediment cores of the order of a few meters.

In particular, the processing of the 2006 data, originally stored in envelope mode (classical approach with Hilbert transform, Henkart, 2006), was possible after waveform recovery (Baradello et al., 2021), unlike the 2017 data, which were already stored in full-wave mode (only cross-correlation with the pilot sweep).

With the full-wave signal, the chirp data can be treated with traditional seismic processing, resulting in a significant improvement in signal-to-noise ratio (Quinn et al., 1997; Baradello, 2014) and an increase in lateral and vertical resolution. Ocean wave effects were attenuated by applying a non-surface-consistent static correction, while the true amplitude was recovered by applying the amplitude decay inversion function after spherical divergence. Predictive deconvolution (second zero of autocorrelation as gap length, 9 ms as operator length and 0.1 % white noise content) was applied for ripple attenuation.

The processing made the necessary changes to the sub-bottom profiles to overcome the noise problems due to the very rough sea during the recording phase and consequently improve the resolution and penetrability of the acoustic data. The possibility of visualizing with a certain continuity some internal reflectors in the first meters of the seabed, as well as the attempted correlation with the lithostratigraphic data derived from the core holes, allows us to analyze the geomorphology of some glacial landforms, even in the interior, and the acoustic facies.

Seafloor reflectivity mapping confirms the presence of some areas of greater hardness due to the possibly different lithology and physical/mechanical properties (i.e. greater compaction, dewatering) of glacial and glaciomarine sediments).

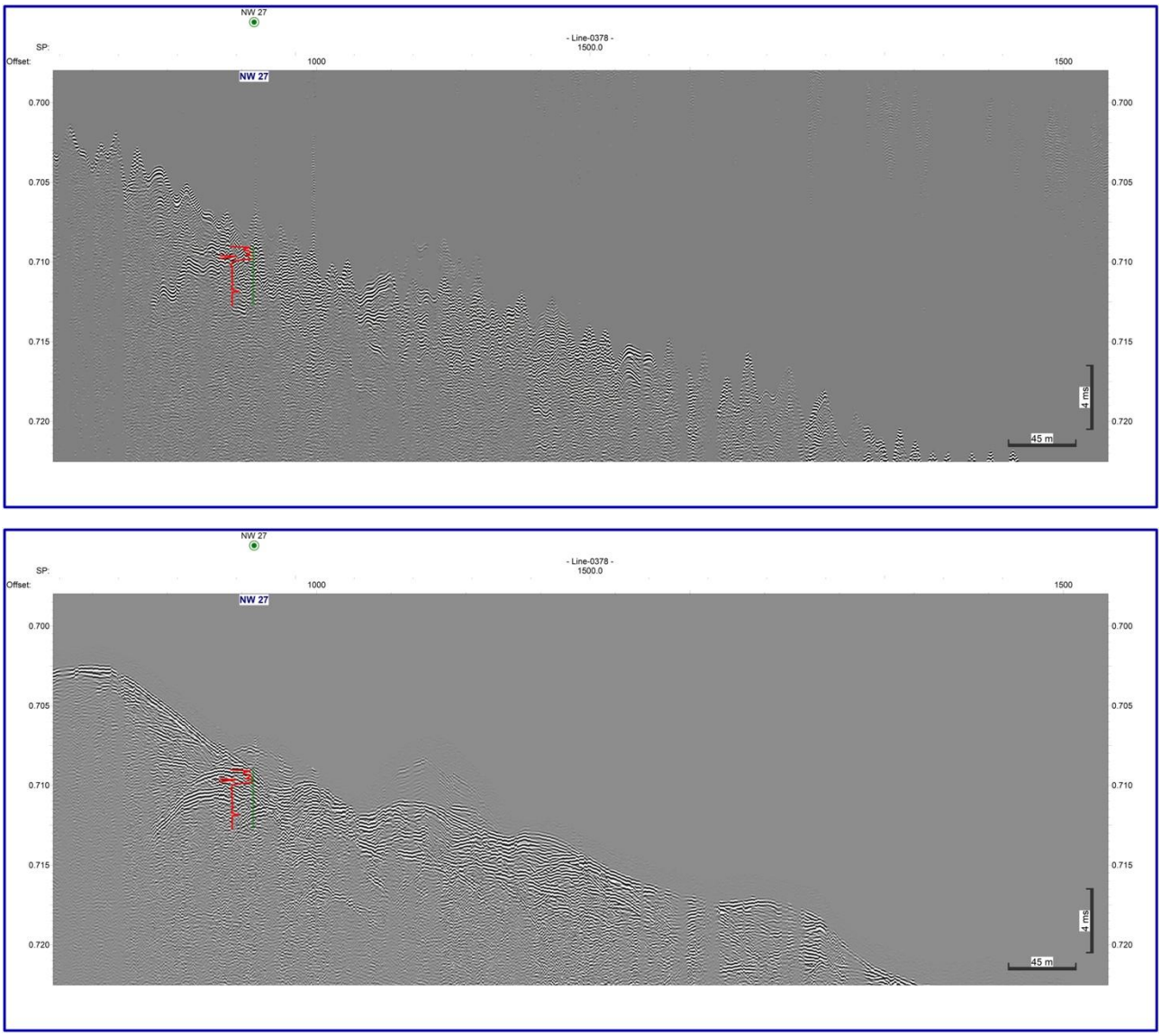

Fig.1 - Sub-bottom profile before(a) and after processing(b). Time/depth and susceptibility curve of a PNRA sediment core NW27, projected onto both profiles.

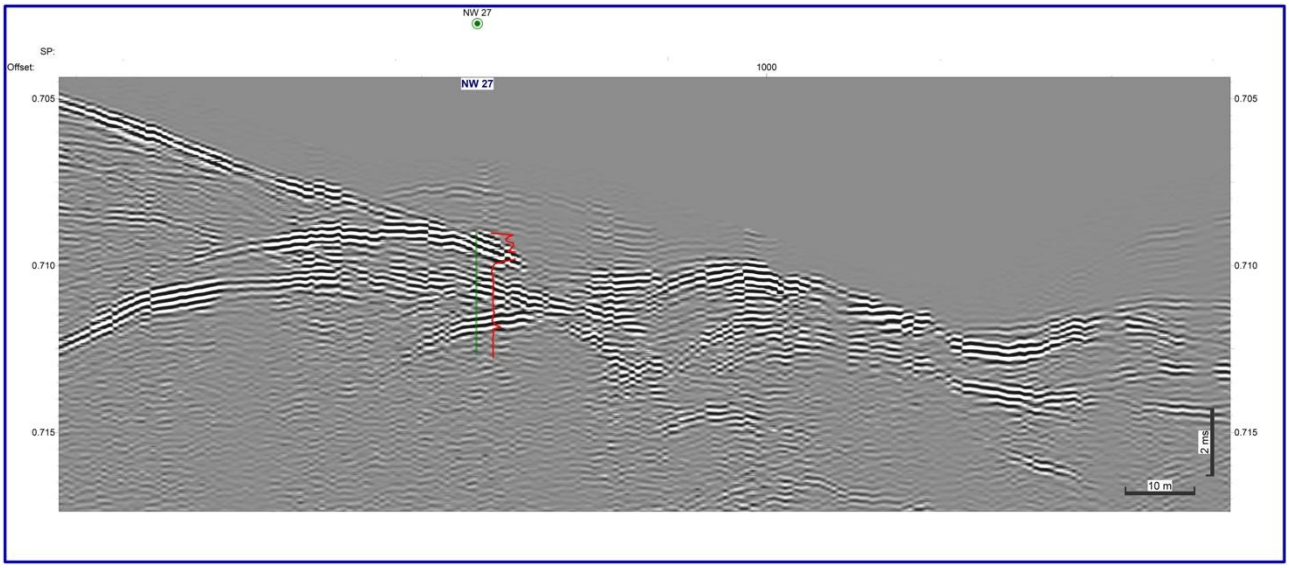

Fig.2 - Zoom section of the sub-bottom profile shown in Fig.1

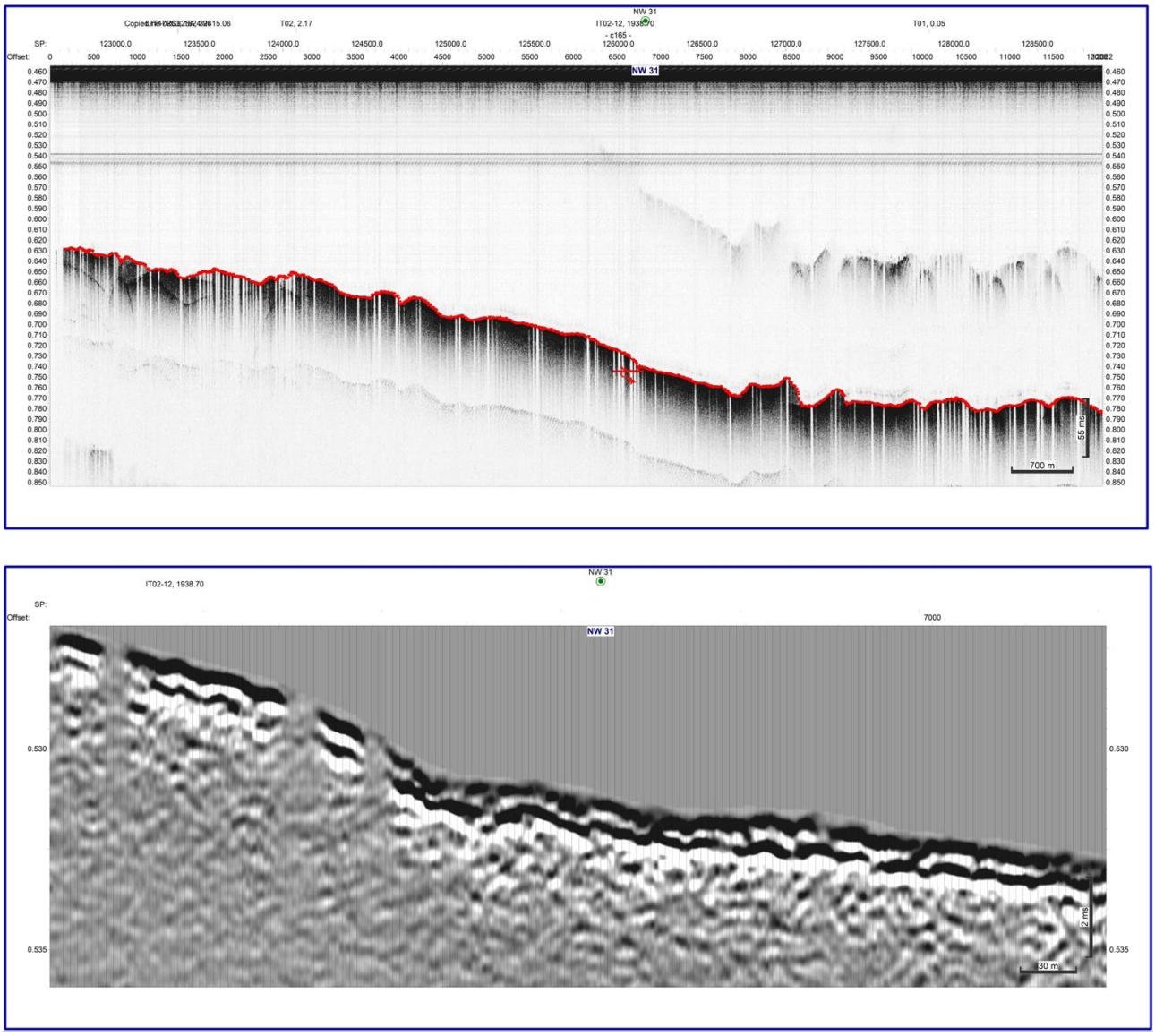

Fig. 3 - Sub-bottom profile originally stored in envelope mode(a) and below a zoom pseudo-seismic section(b) (Baradello et al. 2021) near the sediment core NW31 projection onto the profile.

References

Baradello L (2014) An improved processing sequence for uncorrelated Chirp sonar data. Marine Geophys Res 35(4):337–344

Baradello L., Battaglia F., Vesnaver A. (2021) Fast method to transform chirp envelope data into pseudo-seismic data. Marine Geophys Res 42:14 https://doi.org/10.1007/s11001-021-09436-y

Henkart P (2006) Chirp Sub-Bottom profiler processing – a review. Sea Technol 47(10):35–38

Quinn R, Bull JM, Dix JK (1998) Optimal processing of marine high resolution seismic reflection (Chirp) data. Marine Geophys Res. 20:13–20

Corresponding author: csauli@ogs.it

The Italian calibration and reference site for E & EM geophysical methods: The HydroGeosITe

A. Signora[1], S. Galli[1], F. Dauti[1], A. L. Sullivan[1], A. Lucchelli[1], M. Gisolo[2], G. Fiandaca[1]

[1] The EEM Team for Hydro & eXploration, Department Of Earth Sciences "Ardito Desio", Università degli Studi di Milano, Milano (Italy)
[2] A2A Ciclo Idrico S.p.a. , Brescia (Italy)

1. The HydroGeosITe project

From the spring of 2021 to July 2023 over 20000 line-km of airborne electromagnetic (AEM) data have been acquired for mapping and managing groundwater resources in the entire plain of Brescia province and a mountainous sector, over an area of approximately 1800 km^2 (Figure 1). Within this AEM campaign, the largest ever carried out in Italy for groundwater mapping and management, the water management company A2A Ciclo Idrico S.p.A. financed the HydroGeosITe project, which aims at establishing the first calibration and reference site for galvanic methods and for ground and airborne electromagnetic methods, for hydrogeological purposes. The need for calibration sites of EM systems derives by the sensitivity of EM data to system characteristics, such as receiver transfer function, transmitter current waveform, and transmitter-receiver synchronization and geometry, which if neglected lead to significant bias in the retrieval of the electrical properties (Christiansen et al., 2011). For instance, the Lyngby Danish reference site has been established for ensuring the calibration of both airborne and ground-based EM systems (Foged et al., 2013), while the Menindee Australian test range (Brodie and Cooper, 2018) focuses only on airborne systems, but covers a much longer stretch (more than 35 km). In both cases, calibrated systems are expected to retrieve satisfactory resistivity models, the eventual calibration consisting in adjusting the system characteristics until the inversion model compares well enough with the reference model.

Within the HydroGeosITe we have characterized the electrical properties of the subsurface with an unprecedented density of measurements, both in terms of conduction and polarization. This effort aims also to test a new inversion scheme where both inductive and galvanic (EM) and galvanic (DCIP) are incorporated into the same inversion framework. To validate the HydroGeosITe both in terms of calibration and reference, three boreholes are expected to be drilled, the first of which has been completed in December 2023, reaching the depth of 350 m from the surface. Accurate lithological description, along with future borehole-logging, is expected as well, likely positioning the HydroGeosITe as a key reference point in interpreting the future AEM campaign.

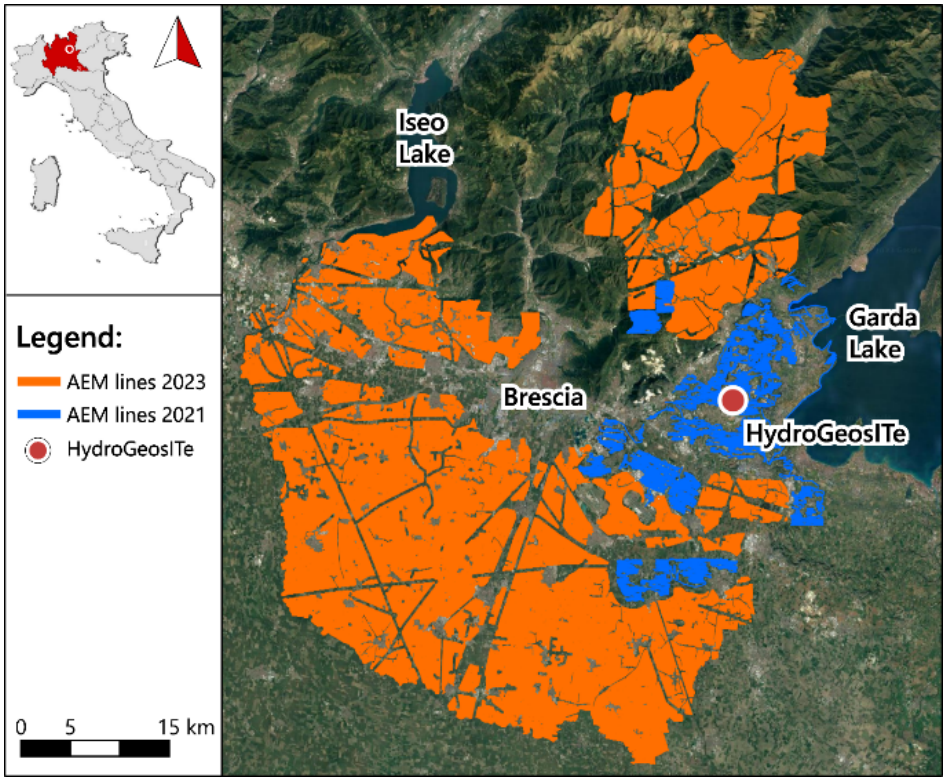

Figure 1 - Flight lines of 2021 and 2023 AEM campaigns in Brescia province. Blue lines represent the 2000 line-km of data flown in 2021; orange lines represent the 20000 line-km of the 2023 survey. The red dot shows the position of the HydroGeosITe.

2. Site characterization

The HydroGeosITe is located in northern Italy, close to the southern margin of the Italian Alpine chain (Fig. 1), within a fluvioglacial and glacial depositional environment which lays on bedrock, supposedly Pliocene marine bedrock. Therefore, the near surface deposits expect the complex superimposition and interdigitation of morain and fluvial deposits due to the repeated advance and retreat of the glacial system (Plesitocene) followed by the quaternary alluvial deposit of Chiese river's alluvial plain (Conti et al., 2009). The comprehensive geophysical measurements carried out to characterized this spot in such complex geological settings are presented in the following section and displayed in Figure 2. These involve both AEM acquisition and ground EM surveying with four different systems, along with galvanic acquisition of DCIP data.

2.2. AEM acquisitions

Concerning the AEM data (Fig. 2, bottom-left map), the SkyTEM312 system was employed in 2021 to survey the HydroGeosITe. The site has been surveyed again in summer 2023 using the new SkyTEM306HP. The 2023 AEM data were collected, overlapping with each other and with the geophysical ground measurements, at three different flight heights to ensure the absence of system bias, and with the aim of setting a quality standard for future AEM surveys.

2.3. Ground TEM acquisitions

Several ground transient electromagnetic (TEM) soundings have been measured with the ABEM WalkTEM 2 instrument in central-loop configuration, with two different transmitter units (TX-20 and TX-60, with 20 ampere and 60 ampere peak-to-peak maximum current, respectively) and three transmitter sizes (Fig. 2, top right map):

- Thirty 40x40 m^2 Tx-20 soundings, with 30 minutes of stacking time and 10 ms of acquisition time;
- Five 100x100 m^2 Tx-60 soundings, with 60 minutes of stacking time and 30 ms of acquisition time;
- One 200x200 m^2 Tx-60 sounding, with 100 minutes of stacking time and 30 ms of acquisition time.

All soundings were measured with two different receivers, RC5 and RC200, with 5 m^2 and 200 m^2 effective area, respectively. The 40x40 m^2 soundings reached approximately 300 m of depth of investigation (Christiansen and Auken, 2012), while the 100x100 m^2 went down to ≈400 m and the 200x200 m^2 down to ≈700 m.

2.4. tTEM and Loupe acquisitions

The tTEM system (Auken et al., 2019) has been employed to acquire more than 55 km of data (Fig. 2, bottom right) through a 3x3 m^2 transmitter with receiver in offset configuration. This system allows to carry out continuous TEM measurements when pulled by an ATV vehicle at the max speed of 20 km/h, to retrieve subsoil models up to ≈100 meters of depth. Almost the same area was surveyed with the Loupe portable system (Street & Duncan 2018) with 20 km of lines.

2.5. DCIP acquisitions

The DCIP data have been measured with the ABEM Terrameter LS2 system in 100% duty cycle (Olsson et al., 2015) with full waveform acquisition, and gated after harmonic denoising and drift removal following Olsson et al. (2016). As shown in Fig. 2, top right panel, approximately 4 km of data have been measured with 10 m electrode spacing, and another 4 km with 5 m electrode spacing. The gradient protocol has been used for acquisition, with 12 seconds of acquisition time and two stacks per quadrupole, with mean injected current of approximately 0.5 Amperes. The number of quadrupoles acquired among the different profiles ranges between 1400 and 2700 ca., depending on the profile length and the electrode spacing.

2.6.Drillings

Three boreholes few hundred meters deep (100 m, 190 m, 350 m) are being drilled, with lithological description and resistivity log; the 200 m deep borehole was completed in December 2023, while the other two will be completed within Spring 2024.

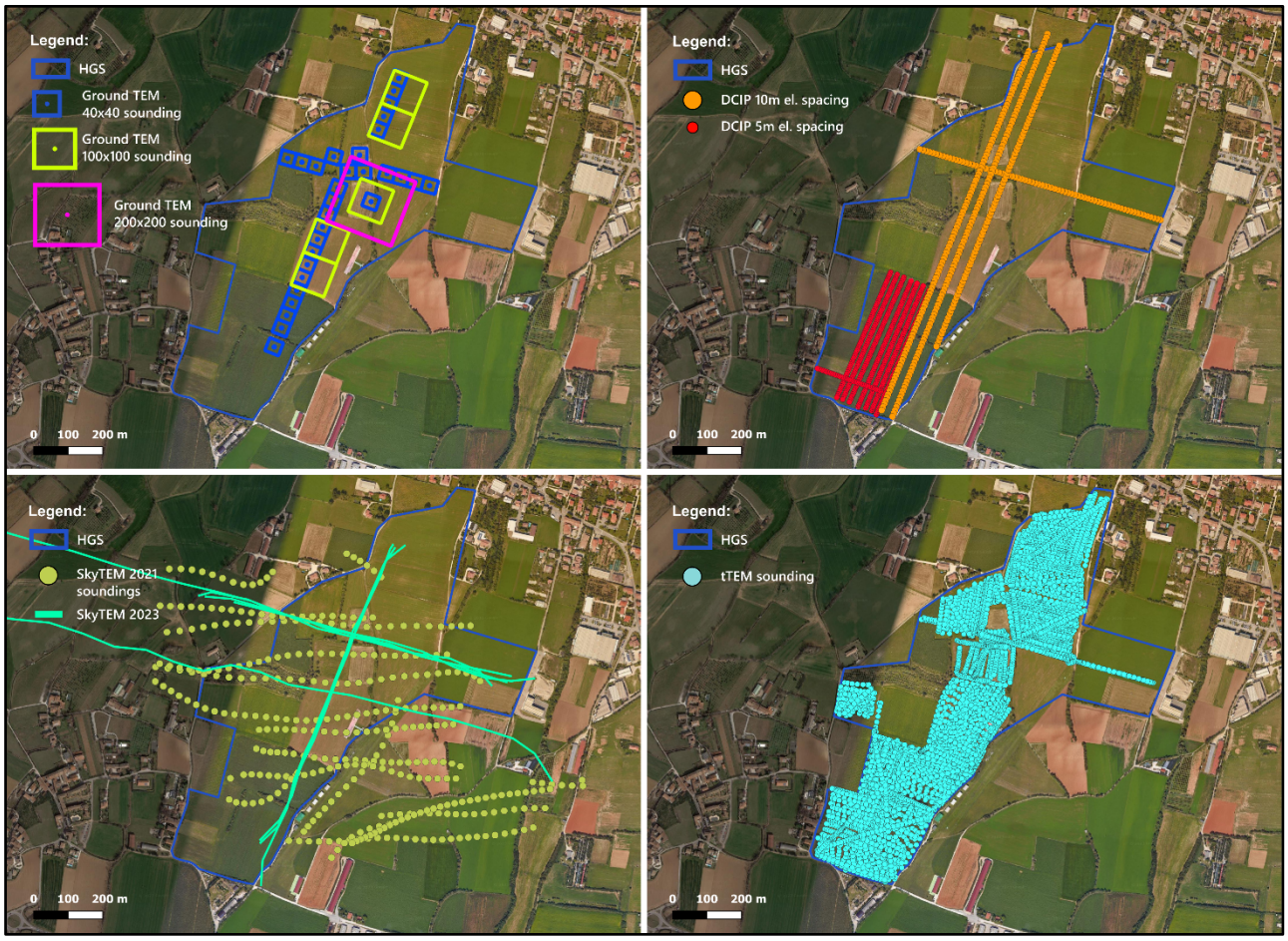

Figure 2 - Maps of the geophysical surveys carried out at the HydroGeosITe, with the perimeter of the area always accessible indicated in blue (HGS in the legend). Top left – Ground TEM soundings with 40x40 m² (blue squares) 100x100 m² (yellow) and 200x200 m² (magenta square) loop sizes. Top right – DCIP profiles with 10 m spacing (dotted orange lines, ≈ 4 km) and 5 m spacing. Bottom left – SkyTEM312 2021 soundings displayed by green-dots, while SkyTEM306HP 2023 soundings are displayed with marine-green lines for all the three different flight heights. Bottom right – tTEM soundings; approximately the same area has been covered with the Loupe system

3. Data Modelling and Joint inversion

Inductive and galvanic data give usually significantly different inversion models, due to their different sensitivity to the resistivity distribution. Often resistivity anisotropy is used to justify the lack of accordance between the two methods (e.g. Christiansen et al., 2007), even if recent publications have shown compatibility between AEM and galvanic data (Christensen, 2022), but without considering the induced polarization effect. However, Fiandaca et al. (2022) have shown that the IP phenomenon has a strong effect on inductive data also in environmental applications, with significant dependence of the effect on the system characteristics.

Following these findings, we propose first a comprehensive interpretation of the independent models, then the employment of joint inversion scheme to retrieve a unique model from both galvanic and inductive data taking into induced polarization. In particular, all the inversions are carried out following Fiandaca et al. (2024) with EEMverter, a software specifically designed for modelling IP in joint inductive/galvanic inversions. EM data are modelled in 1D, while the galvanic

DC and full-decay IP data are modelled in 2D (Fiandaca et al., 2013) in terms of the maximum phase angle (MPA) Cole-Cole re-parameterization (Fiandaca et al., 2018). The objective function of the inversion is defined as:

$$Q = \left[\frac{1}{N_d + N_r} \left(\sum_{i=1}^{N_d} \frac{\left(d_{obs} - d_{forward} \right)^2}{\sigma_{d_i}^2} \; ++ \; \sum_{i,j}^{N_r} \frac{\left(m_i - m_j \right)^2}{\sigma_{r_{i,j}}^2} \right) \right]^{\frac{1}{2}} \quad (1)$$

Where N_d and N_r are the numbers of data d_{obs} (both inductive and galvanic) and roughness constraints (on the unique joint model m), respectively, and the balance between inductive and galvanic data is achieved through their standard deviation σ_d^2. The independent inversions have been carried out with the same forward schemes of the joint inversion, but using only one data type at once. All data have been processed in EEMstudio (Sullivan et al., 2024) for culling outliers out before inversion. Both the geophysical galvanic and inductive models exhibit concordance with each other and display features likely consistent with the geological-stratigraphic characteristic of the area. The joint models derived from incorporating both E & EM data within a unified inversion framework, not only confirm the primary structures defined by the independent models but also significantly enhance the resistivity model resolution, as shown in Figure 3.

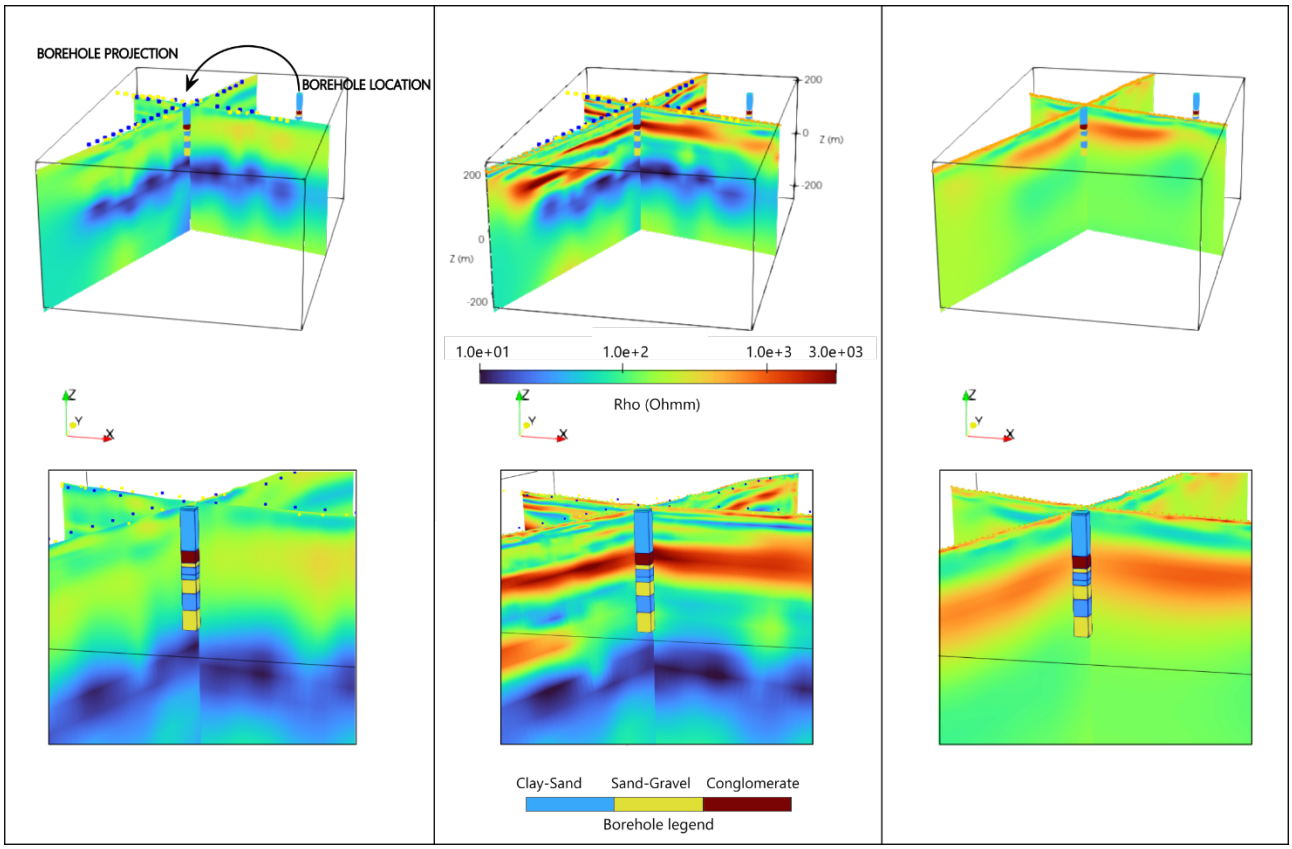

Figure 3: Inversion models of the crossing North-South and West-East profiles obtained through inductive-only AEM and ground TEM data (left), joint AEM-Ground EM-tTEM-DCIP data (center) and galvanic-only DCIP data (right), with full profile view in the top panels and zoom-in close to the crossing point in the bottom panels. The lithological description of a borehole near to the profiles is shown in color bars; for helping the comparison between borehole information and inversions, the borehole has been projected from its true position to the crossing point of the profiles. Ground EM, SkyTEM, tTEM sounding positions and electrodes are indicated with the same color coding of Figure 2

Acknowledgments

The HydroGeosITe project is funded by A2A Ciclo Idrico S.p.A. We acknowledge Emergo S.r.l for the support with AEM data.

References

Auken E., Foged N., Larsen J.J., Trøllund Lassen K.V., Maurya P.K., Dath S.M., Eiskjær T.T; 2019: tTEM — A towed transient electromagnetic system for detailed 3D imaging of the top 70 m of the subsurface. Geophysics, 84 (1), E13-E22.

Brodie R. C., Cooper, Y.; 2018: Spatially and conductivity Log constrained AEM inversion. AEGC2018 – 1st Australian Exploration Geoscience Conference, 18-21 February 2018, Sydney, Australia.

Christensen, N. B; 2022: Joint inversion of airborne TEM data and surface geoelectrical data. The Egebjerg case. Journal of Applied Geophysics, 196, 104511.

Christiansen, A. V., Auken, E., Foged, N., & Sørensen, K. I.; 2007: Mutually and laterally constrained inversion of CVES and TEM data: a case study. Near Surface Geophysics, 5(2), 115-123

Christiansen, A. V., Auken, E., & Viezzoli, A.; 2011: Quantification of modeling errors in airborne TEM caused by inaccurate system description. Geophysics, 76(1), F43-F52.

Christiansen, A.V. & Auken, E.; 2012: A global measure for depth of investigation. Geophysics, 77(4), WB171-WB177.

Conti M. and Conti A.; 2009: Tech. Rep. Comune di Bedizzole

Fiandaca, G., Ramm, J., Binley, A., Gazoty, A., Christiansen, A. V., & Auken, E;. 2013: Resolving spectral information from time domain induced polarization data through 2-D inversion. Geophysical Journal International, 192(2), 631–646.

Fiandaca, G., Madsen, L. M., & Maurya, P. K.; 2018: Re-parameterisations of the Cole–Cole model for improved spectral inversion of induced polarization data. Near Surface Geophysics, 16(4), 385-399.

Fiandaca, G. Dauti, F., Signora A.; 2022: Effect of induced plarization on galvanic and inductive data: where is it stronger? Near Surface Geoscience Conference, 18-22 September 2022, Belgrade, Serbia

Fiandaca, G., Zhang, B., Chen, J., Signora, A., Dauti, F., Galli, S., Sullivan, N.A.L., Viezzoli, A.; 2024: EEMverter, a new 1D/2D/3D inversion tool for Electric and Electromagnetic data with focus on Induced Polarization, GNGTS 2024, 13-16 February 2024, Ferrara, Italy.

Foged, N., Auken, E., Christiansen, A. V., & Sørensen, K. I.; 2013: Test-site calibration and validation of airborne and ground-based TEM systems. Geophysics, 78(2), E95-E106.

Olsson, P. I., Dahlin, T., Fiandaca, G., & Auken, E.; 2015: Measuring time-domain spectral induced polarization in the on-time: decreasing acquisition time and increasing signal-to-noise ratio. Journal of Applied Geophysics, 123, 316-321.

Olsson, P. I., Fiandaca, G., Larsen, J. J., Dahlin, T., & Auken, E.: 2016: Doubling the spectrum of time-domain induced polarization by harmonic de-noising, drift correction, spike removal, tapered gating and data uncertainty estimation. Geophysical Journal International, 207(2), 774–784.

Street, G., Duncan, A., Fullagar, P., & Tresidder, R.; 2018: Loupe-a portable EM profiling system. ASEG Extended Abstracts.

Sullivan N. A. L., Viezzoli. A., Fiandaca, G.; 2024: EEMstudio: processing and modelling of electric and electromagnetic data in a QGIS plugin, GNGTS 2024, 13-16 February 2024, Ferrara, Italy.

Corresponding author: alessandro.signora@unimi.it

EEMstudio: processing and modelling of electric and electromagnetic data in a QGIS plugin

N.A.L. Sullivan[1], A. Viezzoli[2], G. Fiandaca[1]

[1] The EEM Team for Hydro & eXploration, Department of Earth Sciences "Ardito Desio", Università degli Studi di Milano, Milano, Italy
[2] EMergo S.r.l., Cascina (PI), Italy

Introduction

In electric and electromagnetic (EM) methods, the typical workflow is acquisition, processing and modelling. The processing part is where we evaluate the data in order to exclude outliers from the inversion, and prevent the generation of artifacts in the models that do not reflect geology. EM and IP measurements are particularly affected by coupling with man-made metal structures and random noise, which alter the response of the ground, causing the presence of buried conductors in the model and spotted appearance (Viezzoli et al., 2013). It is therefore important to identify these interferences and remove these data from the dataset in order to obtain reliable models. Besides automatic processing, the preferred method for this refining is the manual culling of data, supported by a georeferenced map to remove coupling effects.

At the moment, many software and tools are available for the inversion of electric and electromagnetic data: for instance, there are AarhusInv (Auken et al., 2015), SimPEG (Cockett et al., 2015), the GA AEM programs (Brodie, 2016) and EMagPY (McLachlan et al., 2021) for inductive data and RES2DINV/RES3DINV (Loke, 2004), ResIPy (Blanchy et al., 2020) and pyGIMLi (Rücker et al., 2017) for galvanic data. However, focusing on data processing, the choice is restricted to less options. The most comprehensive one, with an integrated GIS for data georeferencing is the commercial software Aarhus Workbench (Auken et al., 2009), with AarhusInv for inversions (Auken et al., 2015).

EEMstudio is a QGIS plugin that allows to process electric and electromagnetic data, always keeping the link with the georeferenced map. It is freeware and open source, under license EUPL 1.2, and available for academic, teaching and professional use. It is going to be distributed together with EEMverter (Fiandaca et al., 2024), a modelling tool for electric and electromagnetic data with focus on induced polarization, which will be distributed freely as well for most of the ground-based applications.

In the following sections, all parts that constitute the plugin will be presented.

QGIS Widget

Locating the data and checking the acquisition surroundings during processing is essential to ensure a good quality analysis. Choosing QGIS as the base of EEMstudio means embedding a powerful Geographic Information System (GIS), the most widespread software available with this purpose, to the processing and modelling tools. This results in having just one workspace to work with and the possibility to use data files among other georeferenced layers.

EEMstudio plugin starts as a docked widget in the QGIS main window (Fig. 1). Here there is the possibility to organize data and modelling files, and open them for processing or visualization of the results, loading automatically the acquisition points.

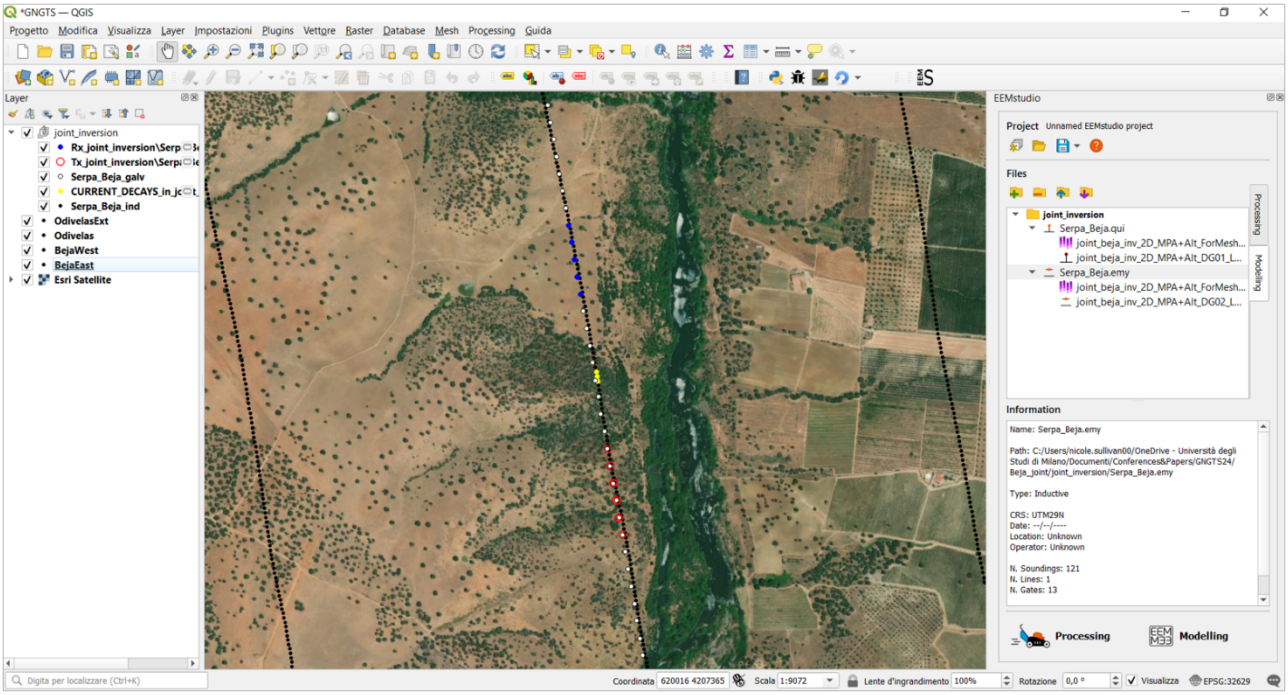

Fig. 1 – QGIS main window with EEMstudio widget on the right, used for management of processing and modelling files. Once uploaded, the coordinates of the acquisition points are automatically added to the QGIS layer, among eventual other layers in the QGIS project. In this figure, two types of data are shown: galvanic and inductive (airborne). White dots are the electrodes, red circles and blue points are the positions of the quadrupoles used in the soundings selected in the galvanic processing app (Figure 2a). Black dots are the inductive soundings and yellow points are the soundings highlighted in red in the inductive processing app (Figure 2b).

Processing

A separate window is dedicated to data processing and visualization of forward and model. Regarding processing, this graphic interface allows to select data to refine the dataset, to clean it from coupling effects and noise, using a vast range of shortcuts to optimize the process. Moreover, all the soundings that are shown and selected in this window are also plotted as georeferenced points in the QGIS map, to locate them instantly.

Two different types of this interface have been developed to fit various kinds of data: one for galvanic data and time-domain induced polarization (Fig. 2a) and one for transient EM data (airborne or ground-based, in Fig. 2b).

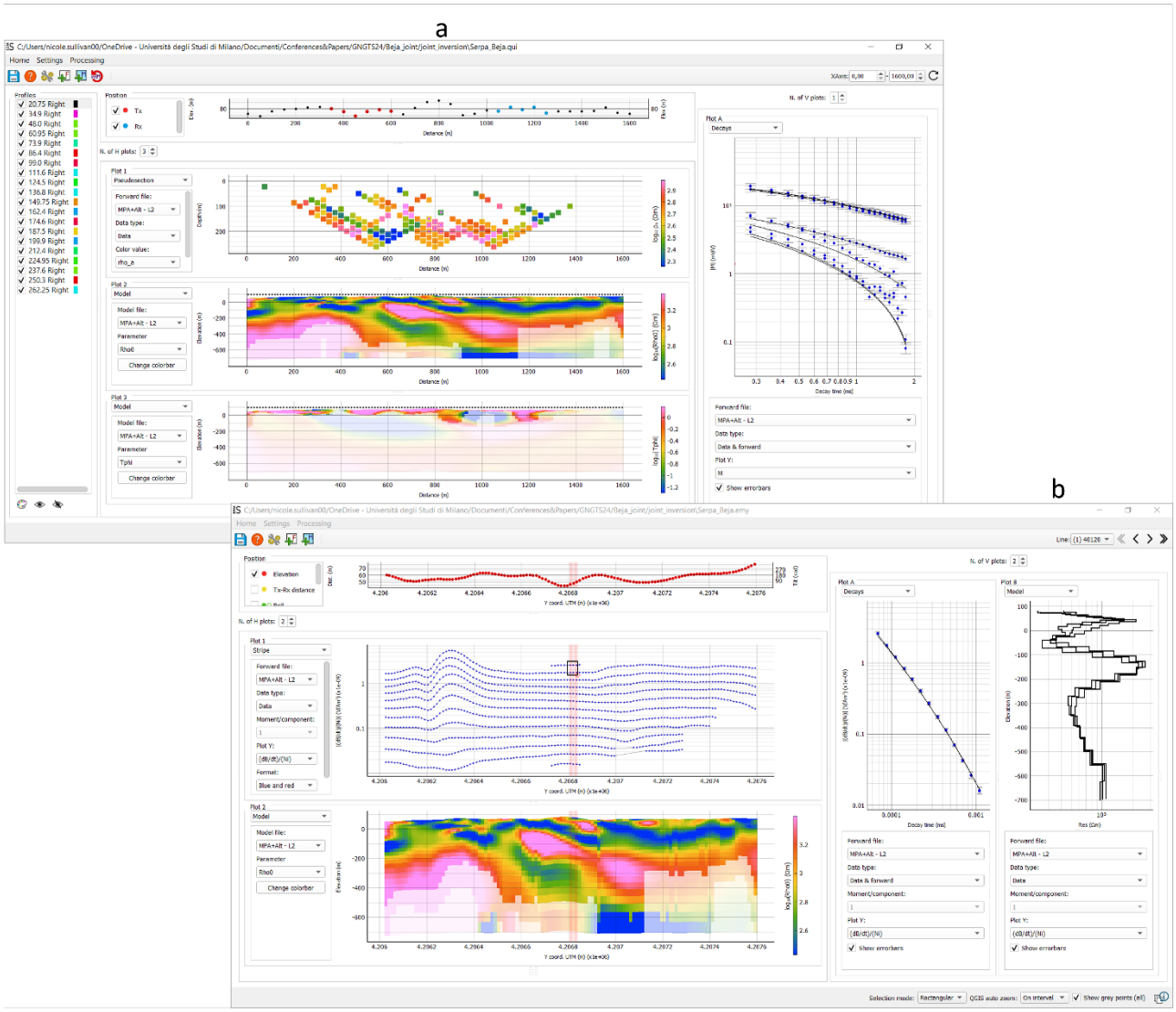

Fig.2 – Processing window supporting a) galvanic data visualization b) inductive data visualization. In galvanic window, first section: electrode position; second section: data pseudosection; third section: model of rho0; fourth section: model of phi; right panel: IP decay for the selected quadrupoles in the pseudosection. In inductive window, first section: flight altitude; second section: data (blue dots); third section: model of rho0; first left panel: decay in correspondence of the red highlights in the sections; models of rho0 in correspondence of the red highlights in the sections.

Both windows include many plots to show information of different nature, including pitch, roll and yaw for AEM data and electrode positions for galvanic data. As for measured data, for galvanic and IP data the user can choose between apparent resistivity and chargeability (gate by gate or integral chargeability in the pseudosection), as well as the full IP decay for selected quadrupoles, while for inductive data between apparent resistivity or every dB/dt normalization. It is also possible to

upload one or more forward models and model sections to compare easily data and results in a post-processing phase.

Modelling

Within EEMstudio it is also possible to manage easily modelling, with two different interfaces. The first one (Fig. 3a) has been developed to organize and prepare all necessary files with the desired configuration to launch 1D/2D/3D inversions, also in time-lapse and/or jointly among galvanic and inductive data using EEMverter (Fiandaca et al., 2024), the inversion kernel developed by the EEM Team for Hydro & eXploration, freeware for most ground-based applications. The other interface (Fig. 3b) has the purpose of building 1D/2D/3D synthetic models from scratch, which can be used as starting models or for forward computation.

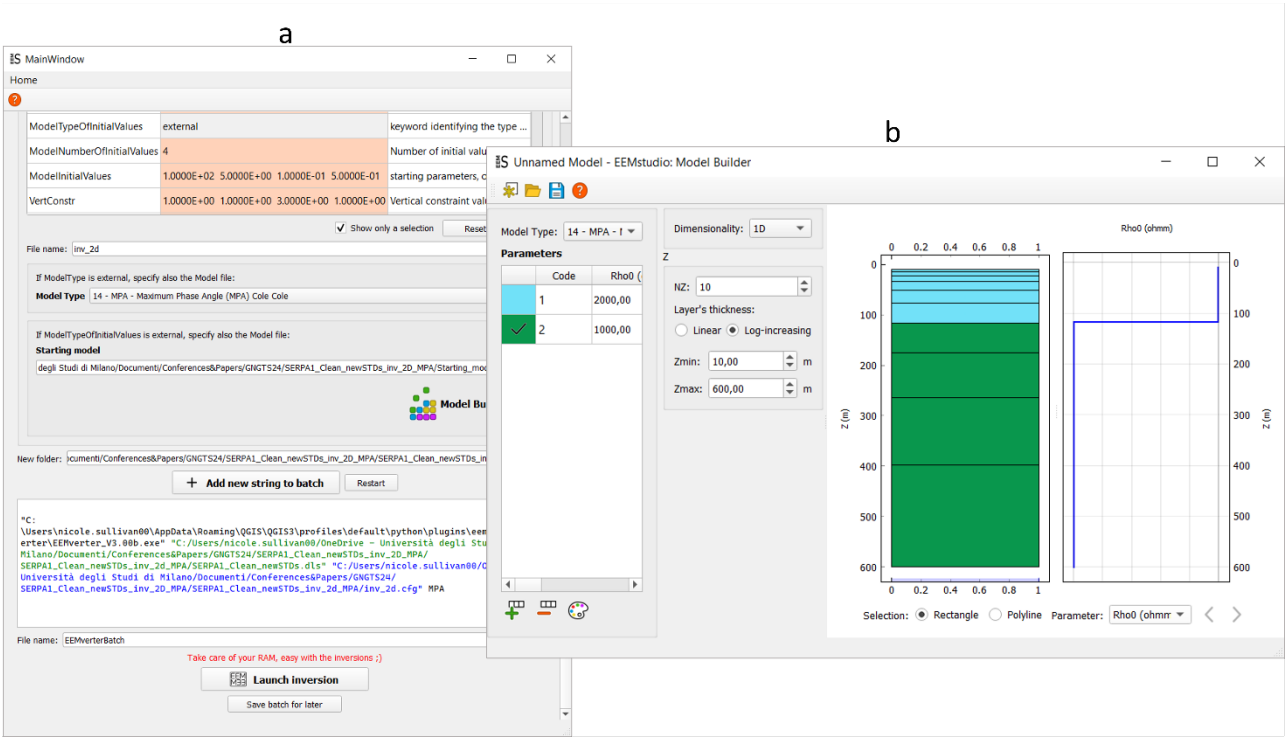

Fig3 – Modelling windows. a) Interface to gather all necessary files to launch easily inversions with EEMverter (Fiandaca et al. 2024). b) Model Builder, to build synthetic models. From left to right: table with the parameters and the associated colors, widgets to change the grid, grid where it's possible to select the cells and assign a color, 1D model of the row marked in blue on the bottom of the grid.

Conclusions

EEMstudio is a tool where it is possible to visualize, process and model electric and electromagnetic data, all within the QGIS environment, taking advantage of its potentiality. Moreover, QGIS is the most widespread open-source GIS software, used by geophysicists but especially by geologists, therefore having a common workspace to be confident with.

EEMstudio is also a freeware tool, available for everyone, from students to professionals, and have an open-source code, so that there is the possibility to modify and improve it to fit everyone necessity.

Acknowledgments

This study has been partially carried out within the Horizon Europe project SEMACRET.

References

Auken, E., Viezzoli, A., & Christensen, A. (2009). A single software for processing, inversion, and presentation of AEM data of different systems: The Aarhus Workbench. ASEG Extended Abstracts, 2009(1), 1-5.

Auken, E., Christiansen, A. V., Kirkegaard, C., Fiandaca, G., Schamper, C., Behroozmand, A. A., ... & Vignoli, G. (2015). An overview of a highly versatile forward and stable inverse algorithm for airborne, ground-based and borehole electromagnetic and electric data. Exploration Geophysics, 46(3), 223-235.

Blanchy, G., Saneiyan, S., Boyd, J., McLachlan, P., & Binley, A. (2020). ResIPy, an intuitive open source software for complex geoelectrical inversion/modeling. Computers & Geosciences, 137, 104423.

Brodie, R. C., 2016, User Manual for Geoscience Australia's Airborne Electromagnetic Inversion Software. Online: https://github.com/GeoscienceAustralia/ga-aem.git.

Cockett, R., Kang, S., Heagy, L. J., Pidlisecky, A., & Oldenburg, D. W. (2015). SimPEG: An open source framework for simulation and gradient based parameter estimation in geophysical applications. Computers & Geosciences, 85, 142- 154.

Fiandaca, G., Zhang, B., Chen, J., Signora, A., Dauti, F., Galli, S., Sullivan, N.A.L., Bollino, A., Viezzoli, A. (2024). EEMverter, a new 1D/2D/3D inversion tool for Electric and Electromagnetic data with focus on Induced Polarization.GNGTS 2024, 13-16 February 2024, Ferrara, Italy.

Loke, M. H. (2004). Tutorial: 2-D and 3-D electrical imaging surveys.

McLachlan, P., Blanchy, G., & Binley, A. (2021). EMagPy: Open-source standalone software for processing, forward modeling and inversion of electromagnetic induction data. Computers & Geosciences, 146, 104561.

Rücker, C., Günther, T., & Wagner, F. M. (2017). pyGIMLi: An open-source library for modelling and inversion in geophysics. Computers & Geosciences, 109, 106-123.

Viezzoli, A., Jørgensen, F., & Sørensen, C. (2013). Flawed processing of airborne EM data affecting hydrogeological interpretation, Groundwater, 51, 191–202.

Corresponding author: nicole.sullivan@unimi.it

Statistical analysis between the experimental and theoretical HVSR curves using different models.

Tanzini[1], E. Paolucci[2], D. Albarello[1,3]

[1]University of Siena, Italy
[2]University of Bologna, Italy
[3]CNR-IGAG, Montelibretti (Rome), Italy

Abstract
The ambient vibration Horizontal to Vertical Spectral Ratios (HVSR) (Nakamura, 1989) is a widely used technique to identify the seismic resonance phenomena induced by the presence of seismic impedance contrasts at depth. Moreover, the HVSR curve can be used to constrain the shear wave velocity (Vs) profile in numerical inversion procedures: to this purpose, different HVSR forward modeling were developed in the last decades, which differ from each other both for the basic theoretical assumptions related to the ambient vibration wavefield simulation and for the phases of the involved seismic waves. In order to explore if significant differences between these modeling exist, Paolucci et al. (2022) and Albarello et al. (2023) performed some comparisons using the results of large sets of numerical simulations obtained by considering realistic Vs profiles. These studies show that strong similarities between the resulting simulated curves exist.

In view of these conclusions, in this work, a comparison of the different theoretical HVSR modeling with experimental HVSR curves has been performed. HVSR measurements were carried out at test sites belonging to VEL (Valutazione Effetti Locali) down-hole database of the Tuscany Region (https://www.regione.toscana.it/-/banca-dati-vel).

Tanzini et al. (2023) described the procedure performed and information associated with the acquisition of experimental data, and the analyzed sites were implemented from 50 to 116 DHs. The experimental HVSR measurement obtained was compared with the various theoretical HVSR models used in Albarello et al. (2023). A minimum frequency threshold (MFT) was considered for each site, which corresponds to the maximum frequency that is reasonable to have with the Vs available from the DHs. The HVSR curves (experimental and theoretical) were therefore compared and a statistical analysis was performed, in particular the Pearson coefficient and the Goodness-of-fit Index S (GoF) proposed by Anderson (2004) were calculated taking into account consideration of the maximum peak of the curve in term of frequency (F_d) and amplitude (A_d). Finally, a global Similarity Index ($I_{\_Sim}$) was calculated to relate Pearson's coefficient and Index S (F_d and A_d) using different weights.

$$I_{\_Sim} = (\text{Pearson Coefficient}*0.2)+(F_d*0.5)+(A_d*0.3) \quad [1]$$

Out of 116 sites, only in 91 cases the numerical outcomes satisfactory reproduce the empirical HVSR curves. Moreover, the better agreement is not obtained by the same model. As concerns the remaining 25 cases, no correlation with the respective geological context or geographical position has been found. The same holds as concerns $V_{s,eq}$ or V_{s30} values, or the presence of anisotropy in the ambient vibration wavefield. Some inversion procedures were considered to evaluate at what extent unknown variable or possible experimental uncertainty relative to down-hole measurements. This analysis revealed that the lack of similarity cannot be explained by considering these aspects.

References

Albarello D., Herak M., Lunedei E., Paolucci E., Tanzini A.; 2023: Simulating H/V spectral ratios (HVSR) of ambient vibrations: a comparison among numerical models. Geophysical Journal International, Volume 234, Issue 2, August 2023, Pages 870–878, https://doi.org/10.1093/gji/ggad109

Anderson J.G.; 2004: Quantitative estimate of the goodness of fit synthetic seismogram. Proceedings of the 13thWorld Conference on Earthquake Engineering, B.B., Canada, August 1–6 2004, Paper n.243.

Nakamura Y.; 1989: A method for dynamic characteristics estimation of subsurface using microtremor on the ground surface. QR Railway Technical Research Institute, 30, 25 - 33.

Paolucci E., Tanzini A., Albarello D.; 2022: From HVSR to site SH response function: Potentiality and pitfalls inferred by 1D physical modelling. Soil Dynamics and Earthquake Engineering https://doi.org/10.1016/j.soildyn.2022.107703

Regione Toscana - VEL database: https://www.regione.toscana.it/-/banca-dati-vel

Tanzini A., Paolucci E., Albarello D.; 2023: Preliminary comparison between experimental and theoretical HVSR curves using different models. Gruppo Nazionale di Geofisica della Terra Solida, Atti del 41°Convegno nazionale, Trieste – sessione 2.2.

Corresponding author: Anna Tanzini tanzinianna@gmail.com

Imaging the buried Mirandola and Casaglia anticlines in the Po Plain, northern Italy, based on HVSR frequencies and amplitudes analysis

G. Tarabusi[1], G. Sgattoni[1], R. Caputo[2,3]

[1] Istituto Nazionale di Geofisica e Vulcanologia, Italy
[2] Dept. of Physics and Earth Sciences, Ferrara University, Italy
[3] CRUST, UR-UniFE, Italy

The Mirandola and Casaglia anticlines are two buried fault-propagation folds that started forming during Quaternary due to the seismogenic activity of blind segments belonging to the broader Ferrara Arc (Po Plain, Italy, Fig. 1). The last reactivation of segments of this Arc was during the May 2012 Emilia sequence (20 May, Mw 6.1 and 29 May, Mw 5.9 earthquakes, Pondrelli et al. 2012).

On top of these structures the thickness of the marine and continental deposits of the Po Plain foredeep is particularly reduced.

The results of a previous study carried out in correspondence of the Mirandola anticline area (Tarabusi and Caputo, 2017) represent the starting point of this research, in which we largely increased the dataset and extended the method to the area of the Casaglia anticline, where the stratigraphy and the relationships between the subsoil units are similar though partly different (Fig. 1). Indeed, in Casaglia, as in Mirandola, in correspondence with the structural culminations of the fault-propagation anticlines, the thickness of the continental Quaternary deposits is generally reduced and they directly overlay the Miocene units. As a consequence, a high impedance contrast occurs due to the abrupt increase of material density and hence of the seismic waves velocity.

For the purpose of the present research, numerous passive seismic measurements were carried out for obtaining the horizontal-to-vertical spectral ratios (HVSR) to identify resonance frequencies (Fig. 1). This approach has a twofold target: to supplement the existing data in the Mirandola region in order to enhance and extend the existing subsoil model, and to develop an analogous detailed subsoil model of the Casaglia area, which had not been explored previously.

A detailed image of the anticline structures was successfully obtained (Fig. 1), confirming the strong correlation between the HVSR outcomes, such as peak frequencies and amplitudes, and the available stratigraphic data primarily obtained from boreholes. We obtained high resolution resonance frequency and HVSR peak amplitude maps and a 3D reconstruction of both anticlines (Fig. 2).

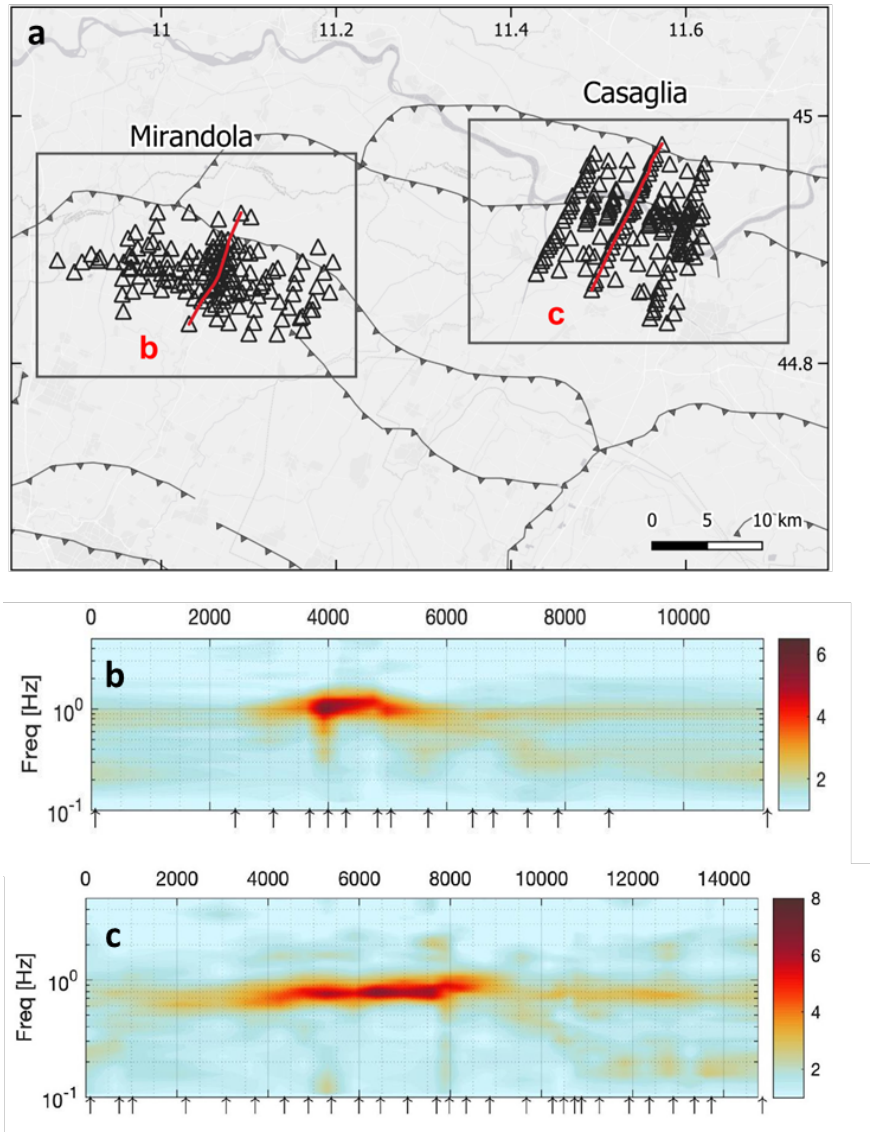

Fig. 1 - (a) Location of the HVSR measurements (triangles) within the two focus areas. Red lines indicate the traces of the transects represented in b) and c) showing absolute HVSR amplitudes.

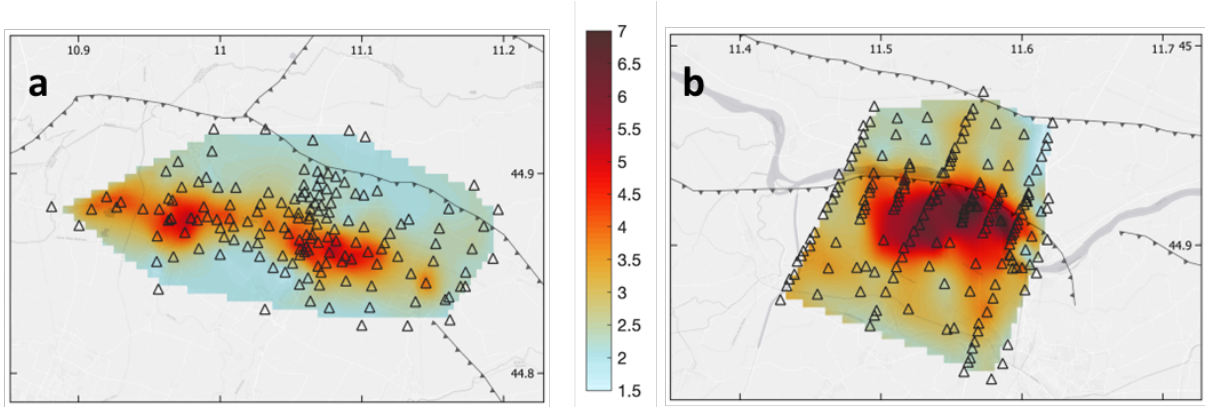

Fig. 2 - HVSR peak amplitude distributions at the Mirandola (a) and Casaglia (b) areas. The triangles are the single-station microtremor measurements used in the interpolation.

Furthermore, by assuming a power-law relation between Vs and depth, a peak frequency versus depth empirical relationship could be derived by fitting measured resonance frequencies with the

substrate depths identified in the nearby boreholes. This empirical relationship is valid for the shallow subsurface within the depth range used for the regression analysis (say, from -60 to -230 m), which allows the conversion from the frequency to the depth domain of the HVSR curves.

These results have several practical applications: firstly, they help identifying areas that are likely to experience greater ground motion amplification during an earthquake; secondly, they enable the development of empirical formulas for estimating the depth of the seismic bedrock based on HVSR outcomes (Martelli, 2021) with high accuracy; and thirdly, they highlight significant stratigraphic and structural differences between the Mirandola and Casaglia areas.

References

Martelli, L. (2021). Assessment of Seismic Bedrock in Deep Alluvial Plains. Case Studies from the Emilia-Romagna Plain. Geosciences 11(7):297. https://doi.org/10.3390/geosciences11070297

Pondrelli, S., Salimbeni, S., Perfetti, P., Danecek, P. (2012). Quick regional centroid moment tensor solutions for the Emilia 2012 (northern Italy) seismic sequence. Annals of Geophysics 55(4):615–621, doi: https://doi:10.4401/ag-6146

Tarabusi, G., Caputo, R. (2017). The use of HVSR measurements for investigating buried tectonic structures: the Mirandola anticline, Northern Italy, as a case study. International Journal of Earth Sciences 106(1), doi: https://doi.org/10.1007/s00531-016-1322-3.

Denser is better? Spatial sampling vs trace stacking in multichannel GPR data to improve sections and depth-slices readability for archaeological prospections.

A. Vergnano[1], C. Comina[1]

[1] *Università degli Studi di Torino, department of Earth Sciences; Torino, Italy*

Introduction

Among the geophysical indirect methods to preliminary assess the presence of underground structures for archaeological studies (and for many other applications), multichannel GPR systems have been under the spotlight for more than a decade (Corradini et al., 2022; Trinks et al., 2009; Viberg et al., 2020). Their peculiarity is to be composed of several radar antennas, both transmitter and receiver, placed one aside the other, in order to produce a spatially dense amount of data, which easily allows for full 3D surveys, with a logistical effort "similar" to that of a standard GPR single-channel system (Novo et al., 2012). This means that very high resolutions, usually of the order of few centimeters, can be easily achieved, making it possible to detect smaller targets (Linck et al., 2022), and making more reliable the interpolation process to produce horizontal depth-slices. Nevertheless, the data processing of multichannel GPR data can be significantly different (Trinks et al., 2018) and more time consuming, from traditional GPR systems, given the large amount of data created. Also, in some situations, the increased density of spatial sampling does not correspond to an increased quality of depth-slices given that small anomalies and wave scattering can disturb the data and reduce the visibility of more relevant targets of archaeological interest (i.e. walls or structures). Moreover, notwithstanding the benefits of new multichannel GPR systems, they are still subject to limitations intrinsic to the GPR wave propagation, for example the difficulty of penetrating for more than a few meters into the soil, and the data quality degradation in the presence of even small quantities of clay materials. This makes the data processing of multichannel GPR dataset an interesting research topic and various studies are available in recent literature, which include Principal Component Analysis (Linford, 2023), studies on the signal polarization and orientation (Lualdi and Lombardi, 2014), studies on various filters for artifact reduction (Verdonck et al., 2013), studies on positioning accuracy (Gabryś and Ortyl, 2020).
In this context, this work aims to assess the variation of depth-slices quality with the variation of between-channels resolution, and proposes an alternative processing step for noise reduction of GPR multichannel datasets. It focuses on two objectives connected one to each other:

• Which is the optimal resolution of multi-channel GPR data for archaeological applications, i.e. the minimum space sampling below which there is not a great improvement in the data?

• Can the data acquired by adjacent channels be stacked to improve the signal-to-noise ratio, and if so, in which cases this processing step can give substantial advantages?

Instrument and data processing

The GPR multichannel system used in this study is the Stream C manufactured by IDS and available at Officina della Ricerca e della Didattica of University of Torino. It has 34 antennas, 24 of which have the dipoles oriented vertically, and 10 horizontally, with respect to the acquisition direction. A total of 23 traces with both the transmitter and the receiver oriented vertically ("VV" with an horizontal separation of about 4 cm) and 9 horizontally ("HH" with an horizontal separation of about 10 cm) are therefore available for each acquisition (i.e. each swath). The central frequency band is 600 MHz; however, frequency distributions centered at about 250-300 MHz were observed in most test sites. This system was adopted in different case studies of archaeological interest in the past few years. Two example test sites are reported in the following to test the working objectives.

For both test sites the data were processed, using the Reflexw software, according to the following processing flow: 1. subtract-mean (dewow) filter with 4 ns timewindow; 2. automatic time-zero correction; 3. background removal; 4. energy decay (an automatic gain function); 5. meanfilter (a 1D moving average filter over a 10-sample window); 6. bandpass filter (100-1000 MHz); 7. subtracting average over 100 traces (= 5m); 8. fk migration with velocity estimated from hyperbola analysis; 9. energy decay; 10. Envelope; 11. normalize profiles (to better compare the depth-slices). Optionally, between step 3 and step 4, an additional processing step consisting in the stacking of an on purpose defined number of adjacent channels was adopted. After those processing steps, the 2D sections are combined to produce a 3D GPR data volume, which is then "cut horizontally" to produce depth-slices. The 3D GPR data volume was produced with a lateral resolution of 5 cm, and a interpolation distance of 50 cm (the interpolation was weighted on the squared distance between the data points and the output point).

First experiment: how the data quality of a GPR 3D data volume is dependent on the number of channels used.

The first dataset was acquired at the archaeological site of “Statio Ad Fines” in Malano in the municipality of Avigliana. Roman buildings and structures are attended at the test site. In this experiment, the 3D GPR data volume, and the consequent depth-slices, consider different subsets of the total 32 channels of the Stream C system. The results of this experiment, comparing the different subsets of channels, is reported in Fig. 1.

Looking at the upper panels of Fig. 1, one can notice the difference between VV and HH dipoles, which can detect different features of the subsoil: in particular, HH dipoles can "see" an elongated diagonal structure at the top of the picture, which VV dipoles struggle to detect. Conversely VV dipoles, can detect more clearly the rectangular features in the lower part of the area. This observation was expected, and it is in line with previous literature (Lualdi and Lombardi, 2014).

Moreover, looking at the HH and VV channels separately, the resulting images are clearer than the one with all the channels together.
Looking at the lower panels, one can appreciate the difference when using only a subset of the 32 VV dipoles: 8 dipoles (12 cm between-lines resolution), 4 dipoles (25 cm) and 2 dipoles (50 cm). In this test site, the 12-cm image and even the 25-cm one, do not differ too much from the all-VV (4cm) image. Instead, the 50-cm-resolution image, which have a resolution similar to surveys performed with single-antenna GPR systems, is much less clear, even if the major structures are still roughly detected.

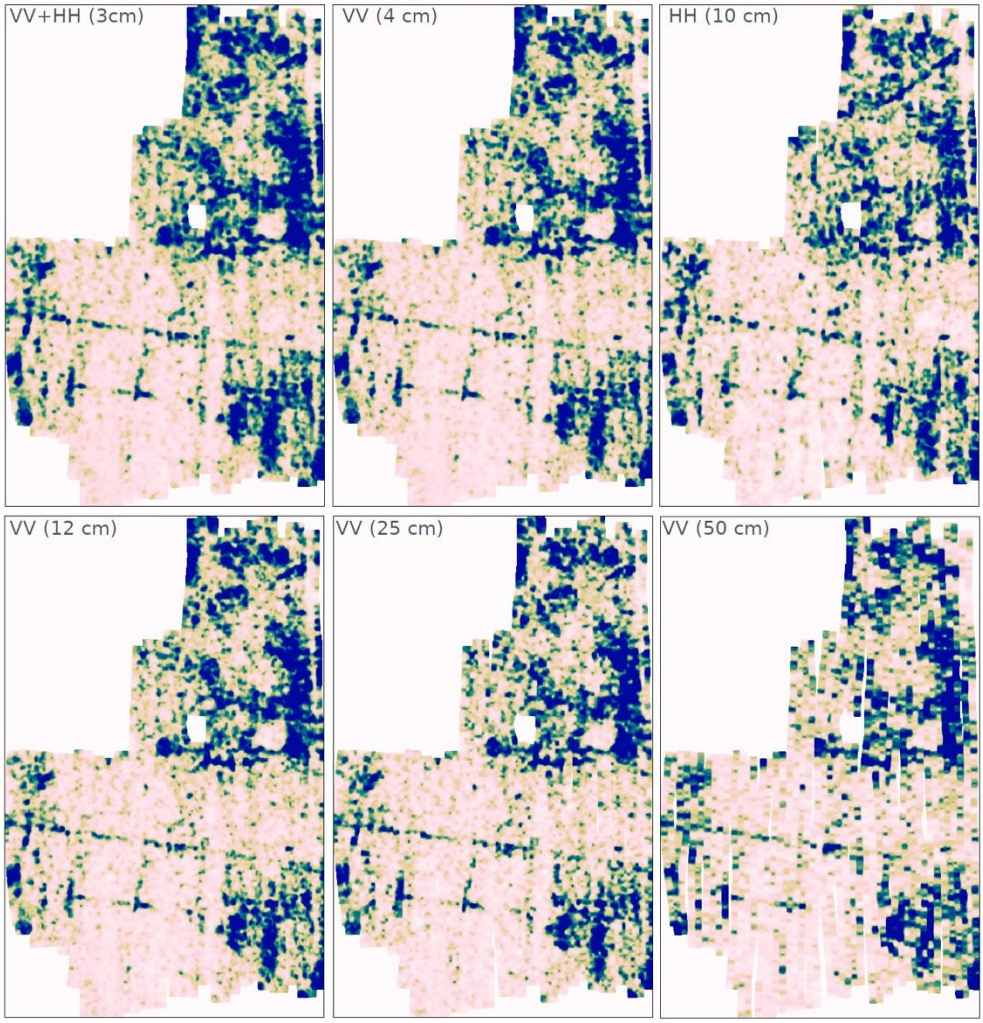

Fig. 1 – Comparison between 1.25 m depth-slices from 3D data volumes created using 6 different subsets of the total 32 channels of the Stream C: : upper panels) all the 32 channels, VV+HH (spacing about 3 cm), only the VV channels (spacing about 4 cm), only the HH channels (spacing about 10 cm); lower panels) different subsets of the VV channels with spacing of about 12, 25 and 50 cm respectively.

One can argue if the total amount of channels in the Stream C is really necessary to perform an archaeological investigation. Surely, the presence of both HH and VV dipoles seems important, and in the absence of both, the survey should be carried out in a grid shape, instead of a simpler boustrophedon path, to avoid missing some important targets. However, the depth-slice obtained using only 4 out of 23 channels is not much worse than the total one. Probably, lighter GPR multichannel systems including 4 VV channels and 4 HH channels could be an optimal compromise

between instrument cost and results. To fully review this statement, more test sites are expected to be analysed in such a way.

Second experiment: how the data quality of GPR 2D sections and 3D data volume may be improved by the stacking of adjacent channels.

The previous observations bring to the second experiment: since, in a typical test site, all the dipoles were not strictly necessary, an idea to make better use of them is to stack adjacent dipoles. This is meant to try to improve the signal-to-noise ratio, potentially useful at depth or when the data are noisy for various reasons. The second dataset was acquired at the archaeological park of Tindari in the municipality of Patti, Sicily, Italy. This site is recognized to be very challenging with respect to the GPR wave propagation given the high signal attenuation due to the presence of clay formations at the site (De Domenico et al., 2006).

Fig. 2 shows the improvement from non-stacked radargrams and radargrams obtained from the stacking of adjacent dipoles. The major improvements (red rectangles in Fig.2) were noticed in the 15-30 ns range, and this improvement is maintained in the 2D sections after the other processing steps (not shown here). The stacked 2D radargrams were then used to create 3D GPR data volumes, as in the first experiment.

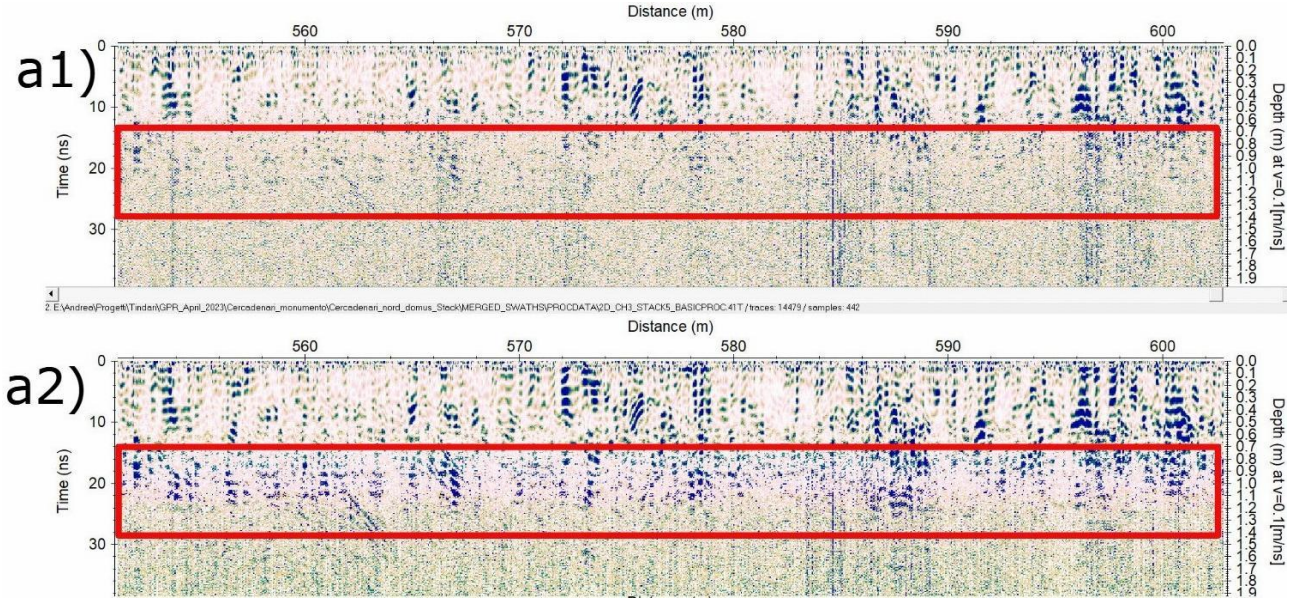

Fig. 2 – Comparison between GPR sections before and after stacking. **a1):** after dewow, move startime, and background removal. **a2)**: a1) + stacking of adjacent 5 channels. An energy decay gain filter was then applied to both sections to allow for meaningful visual readability.

In Fig. 3, the a-panels refer to a 60-cm depth-slice, while the b panels display a 40-cm depth slice. Looking at Fig. 3, it is possible to recognize that the stacking of adjacent radargrams can improve the overall quality of 3D data volumes, when sources of noise, or attenuation, or other problems, challenge the readability of depth-slices even at shallow depths. The noise gets reduced, which makes bigger features more visible.

In the data displayed and available, the improvement was still not able to clearly distinguish underground features which were not already visible without the stacking. In our opinion, the stacking of adjacent channels (or other processing steps based on this philosophy) is promising as

a tool to improve data readability in both 2D and 3D visualizations, but has still to be refined and tuned for different scenarios, and needs to be automatized in main GPR processing software. Moreover, while improving the signal-to-noise ratio at depth, it might affect the detection of smaller targets at shallow depths.

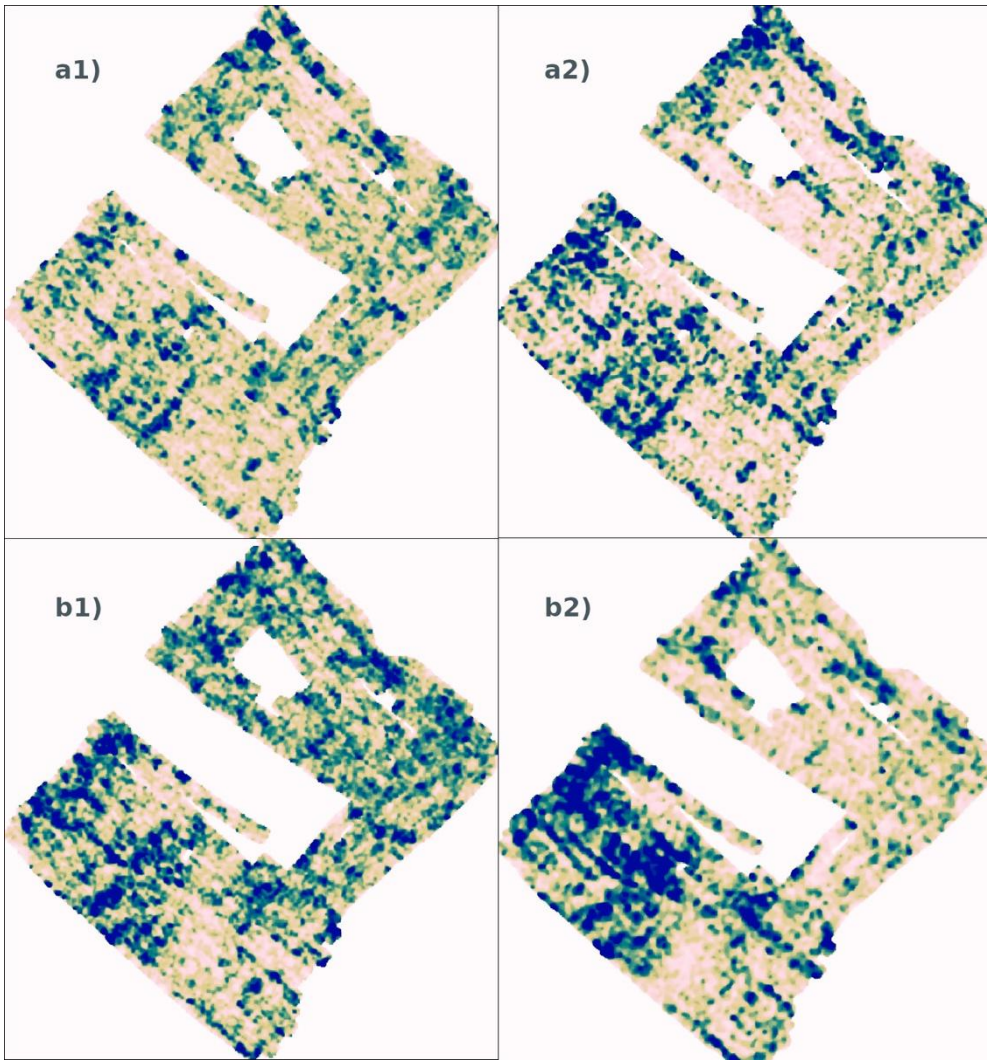

Fig. 3 – a) Comparison between a 60 cm depth-slice from Tindari test site, a1): non stacked, a2) stacked with 5 channels. b) as a), but at 40 cm depth.

Conclusions

The conclusion of this work is that denser is better if the data density is used in a proper way according to the exploration target. For simple explorative archaeological surveys, a multichannel GPR system that combines 4 VV and 4 HH channels could be sufficient in many situations. However, higher data densities allow performing the stacking of adjacent channels, which represents an interesting tool to improve the data quality at greater depths or in particularly challenging noisy sites.

Acknowledgements

Authors are indebted with Officina della Ricerca e della Didattica of University of Torino for the permission to use the GPR, with Prof. Rosina Leone of University of Torino and Parco Archeologico di Tindari for the work performed at the Tindari site and with Soprintendenza Archeologia Belle Arti e Paesaggio and A3 association for the work performed at the Malano site.

References

Corradini, E., Groß, D., Wunderlich, T., Lübke, H., Wilken, D., Erkul, E., Schmölcke, U., Rabbel, W., 2022. Finding Mesolithic Sites: A Multichannel Ground-Penetrating Radar (GPR) Investigation at the Ancient Lake Duvensee. Remote Sens. 14, 781. https://doi.org/10.3390/rs14030781

De Domenico, D., Giannino, F., Leucci, G., Bottari, C., 2006. Integrated geophysical surveys at the archaeological site of Tindari (Sicily, Italy). Journal of Archaeological Science 33 (2006) 961 – 970. https://doi.org/10.1016/j.jas.2005.11.004

Gabryś, M., Ortyl, Ł., 2020. Georeferencing of Multi-Channel GPR—Accuracy and Efficiency of Mapping of Underground Utility Networks. Remote Sens. 12, 2945. https://doi.org/10.3390/rs12182945

Linck, R., Stele, A., Schuler, H., 2022. Evaluation of the benefits for mapping faint archaeological features by using an ultra-dense ground-penetrating-radar antenna array. Archaeol. Prospect. 29, 637–643. https://doi.org/10.1002/arp.1870

Linford, N., 2023. Structure aware noise reduction of multi-channel ground penetrating radar data using Principal Component Analysis, in: Wunderlich, T., Hadler, H., Blankenfeldt, R. (Eds.), Advances in On- and Offshore Archaeological Prospection. Universitätsverlag Kiel | Kiel University Publishing, Kiel, pp. 427–429. https://doi.org/10.38072/978-3-928794-83-1/p87

Lualdi, M., Lombardi, F., 2014. Significance of GPR polarisation for improving target detection and characterisation. Nondestruct. Test. Eval. 29, 345–356. https://doi.org/10.1080/10589759.2014.949708

Novo, A., Dabas, M., Morelli, G., 2012. The STREAM X Multichannel GPR System: First Test at Vieil-Evreux (France) and Comparison with Other Geophysical Data. Archaeol. Prospect. 19, 179–189. https://doi.org/10.1002/arp.1426

Sandmeier, K.-J., 2021. Reflexw. Zipser Strasse 1, 76227 Karlsruhe, Germany. Available at: https://www.sandmeier-geo.de/index.html accessed on 6 December 2023.

Trinks, I., Gustafsson, J., Emilsson, J., Gustafsson, C., Johansson, B., Nissen, J., 2009. Efficient, large-scale archaeological prospection using a true 3D GPR array system. ArchéoSciences 367–370. https://doi.org/10.4000/archeosciences.1857

Trinks, I., Hinterleitner, A., Neubauer, W., Nau, E., Löcker, K., Wallner, M., Gabler, M., Filzwieser, R., Wilding, J., Schiel, H., Jansa, V., Schneidhofer, P., Trausmuth, T., Sandici, V., Ruß, D., Flöry, S., Kainz, J., Kucera, M., Vonkilch, A., Tencer, T., Gustavsen, L., Kristiansen, M., Bye-Johansen, L., Tonning, C., Zitz, T., Paasche, K., Gansum, T., Seren, S., 2018. Large-area high-resolution ground-penetrating radar measurements for archaeological prospection. Archaeol. Prospect. 25, 171–195. https://doi.org/10.1002/arp.1599

Verdonck, L., Vermeulen, F., Docter, R., Meyer, C., Kniess, R., 2013. 2D and 3D ground-penetrating radar surveys with a modular system: data processing strategies and results from archaeological field tests. Surf. Geophys. 11, 239–252. https://doi.org/10.3997/1873-0604.2013007

Viberg, A., Gustafsson, C., Andrén, A., 2020. Multi-Channel Ground-Penetrating Radar Array Surveys of the Iron Age and Medieval Ringfort Bårby on the Island of Öland, Sweden. Remote Sens. 12, 227. https://doi.org/10.3390/rs12020227

Corresponding Author: andrea.vergnano@unito.it